University of Glasgow

Zeng, Zhuoer (2026) *Engineering programmable isothermal amplification and CRISPR/Cas12a for nucleic acid detection.* PhD thesis.

https://theses.gla.ac.uk/86373/

Copyright and moral rights for this work are retained by the author

A copy can be downloaded for personal non-commercial research or study, without prior permission or charge

This work cannot be reproduced or quoted extensively from without first obtaining permission in writing from the author

The content must not be changed in any way or sold commercially in any format or medium without the formal permission of the author

When referring to this work, full bibliographic details including the author, title, awarding institution and date of the thesis must be given

Enlighten: Theses
https://theses.gla.ac.uk/
research-enlighten@glasgow.ac.uk

Engineering Programmable Isothermal Amplification and CRISPR/Cas12a for Nucleic Acid Detection



Zhuoer Zeng

Submitted in fulfilment of the requirements for the degree of Doctor of Philosophy

Division of Biomedical Engineering

School of Engineering

College of Science and Engineering

September 2026

Abstract

Rapid and multiplex nucleic acid detection remains limited by assay complexity and non-specific signals. This thesis investigated simplified, programmable strategies based on isothermal amplification and CRISPR/Cas12a. Different assay formats examined CRISPR-triggered amplification, in situ crRNA generation and promoter-independent self-transcription using human papillomavirus (HPV) and miR-21 as model targets.

An abstract model-based hairpin amplification system was first evaluated for HPV16 detection. Putative self-folding products were observed, but poor reproducibility and persistent non-specific amplification prevented reliable detection. A separate CRISPR/Cas12a-integrated loop amplification strategy was developed, in which two core primers initiated target recognition and staggered cleavage-based amplification. The strategy detected HPV16, HPV18 and HPV52 and produced amplification responses from mixed HPV16/18 samples and individually tested HPV targets under triplex primer conditions in both two-step and one-pot formats. The two-step triplex assay produced distinguishable melting peaks for the individually tested targets, while reliable genotype discrimination in mixed samples was not established.

In another strategy, extended recombinase polymerase amplification primers were designed so that the amplicons generated crRNA through transcription. Primer-derived transcription was identified as a major source of background and suppressed by reducing primer concentration. The three-step assay detected 10 copies of HPV16 per reaction, while the two-in-one format detected 100 copies and showed good specificity. An unexpected primer-derived signal was subsequently repurposed to establish Self-Transcribing Self-Recognition CRISPR (STSR-CRISPR). Designed ssDNA templates generated RNA-containing products through promoter-independent transcription and supported Cas12a activation without a conventional promoter or externally synthesised crRNA. However, mechanistic complexity and variation between independent transcription reactions prevented reliable analytical characterisation.

Together, these studies show how assigning additional functions to reaction components can simplify different assay formats and support multiplex detection. They also identify unintended pathways as a central design challenge for lower-complexity CRISPR-based detection.

Acknowledgements

Firstly, undoubtedly, I would like to give my deepest gratitude to my supervisors, Professor Jonathan Cooper and Professor Julien Reboud. Jon, your unwavering support and encouragement have accompanied me throughout this journey. Thanks for always trusting and having faith in me. Julien, thank you for your guidance, patience, and valuable suggestions, helping me find the right way when I'm lost. I feel incredibly fortunate to have worked with both of you.

I feel very lucky to have been part of such a warm and supportive AB group, where everyone has always been kind and willing to help. My special thanks go to Dr Pawel Jajesniak, who has always been willing to listen to my "weird" ideas and results, helping me sort things out. I am also grateful to Dr Andrew Glidle for his help with reagent ordering and laboratory management. Thanks to our collaborators in China, Gaolian, Yalin and Lijun, for providing valuable inspiration for the project. To everyone in the AB group, thank you for making the lab such a supportive and enjoyable place to work. I would also like to acknowledge the use of OpenAI's ChatGPT for language polishing and assistance with bioinformatics analysis.

I am also grateful to the many precious friends who have been with me throughout this period. Their company made this journey much easier, was often the best painkiller for the occasional stress, and gave me the comfort of knowing they were always there for me. All the laughter and tears we shared will become precious core memories in my life.

Thanks to my funder, the China Scholarship Council (CSC), for making all this possible.

Last but not least, I want to thank my Mom and Dad for their endless love, support and understanding.

This would never have happened without any of you. Thank you!

Author's Declaration

I hereby declare that, except where explicit reference is made to the contribution of others, this dissertation is the result of my own work and has not been submitted for any other degree or professional qualification at the University of Glasgow or any other institution.

Signed: Zhuoer Zeng

Date: September 2026

Contents

Abstract i

Acknowledgements ii

Author's Declaration iii

List of Figures viii

List of Tables xxvi

Abbreviations xxvii

1 Introduction 1

1.1 Nucleic Acid Isothermal Amplification in Diagnostics 1

1.1.1 Overview of isothermal amplification methods 1

1.1.2 Structure-driven isothermal amplification 4

1.1.3 Recombinase polymerase amplification 9

1.1.4 Challenges of isothermal amplification in multiplexing diagnostics . 10

1.2 CRISPR/Cas12a for nucleic acid detection 12

1.2.1 Cas12a target recognition and cleavage 12

1.2.2 Integration of Cas12a and isothermal amplification 14

1.2.3 Multiplex HPV Detection 16

1.3 Transcription-assisted CRISPR detection 17

1.3.1 T7 RNA polymerase and in vitro transcription 17

1.3.2 In situ generation of crRNA 19

1.3.3 microRNA detection 20
1.4 Aim and Objectives 20

2 Abstract model-based isothermal amplification assay for nucleic acid detection 22
2.1 Introduction 22
2.2 Material and Methods 23
2.2.1 Primer design 23
2.2.2 Reaction conditions 24
2.2.3 Gel extraction and sequencing 25
2.2.4 Data analysis 25
2.3 Results and discussion 26
2.3.1 Primer design and selection 27
2.3.2 Optimisation of ABM amplification 31
2.3.3 Sequencing analysis 38
2.4 Conclusion 41

3 Development of a CRISPR/Cas12a-integrated Loop Amplification Assay for multiplex HPV detection 43
3.1 Introduction 43
3.2 Material and Methods 45
3.2.1 Primer design 45
3.2.2 Template synthesis 48
3.2.3 Loop amplification assay 48
3.2.4 CRISPR/Cas12a cis- cleavage and verification 49
3.2.5 CRISPR/Cas12a-integrated loop amplification assay 49
3.3 Results and discussion 50
3.3.1 Primer design and selection 51
3.3.2 CRISPR/Cas12a cleavage verification 64
3.3.3 Development of CRISPR/Cas12a-integrated loop amplification assay 67
3.3.4 Development of multiplex detection assay 75

3.3.5 Analytical performance of CRISPR/Cas12a integrated loop amplification . . . 80
3.4 Conclusion . . . 82

4 An RPA-Based Self-Transcribing CRISPR/Cas12a Assay for HPV16 Detection 85
4.1 Introduction . . . 85
4.2 Material and Methods . . . 86
4.2.1 Primer design . . . 86
4.2.2 RPA assay . . . 87
4.2.3 Denaturing Urea polyacrylamide gel electrophoresis . . . 88
4.2.4 Three-step RPA–IVT–CRISPR assay . . . 88
4.2.5 Two-in-one RPA–(IVT–CRISPR) assay . . . 89
4.2.6 Data analysis . . . 89
4.3 Results and discussion . . . 90
4.3.1 Design principle of the self-transcribing RPA-CRISPR assay . . . 90
4.3.2 Validation of extended RPA primers . . . 91
4.3.3 Feasibility of the integrated RPA-IVT-CRISPR assay . . . 92
4.3.4 Analytical performance of the RPA-IVT-CRISPR assay . . . 102
4.4 Conclusion . . . 105

5 STSR-CRISPR: an amplification-free self-transcribing, self-recognition CRISPR-Cas12a for miRNA detection 108
5.1 Introduction . . . 108
5.2 Material and Methods . . . 109
5.2.1 Oligonucleotide design . . . 109
5.2.2 Oligonucleotide hybridisation . . . 113
5.2.3 In vitro self-transcribing crRNA and CRISPR assay . . . 113
5.2.4 Self-transcribing split crRNA assay . . . 113
5.2.5 Synthetic crRNA-based Cas12a assay . . . 114
5.2.6 DNase I digestion and template removal . . . 114
5.2.7 STSR-CRISPR assay for miR-21 detection . . . 114

5.2.8 Native PAGE gel analysis . . . 115
5.2.9 Bioanalyzer and smallRNA seq . . . 115
5.2.10 Bioinformatics . . . 115
5.3 Results and discussion . . . 115
5.3.1 Establishing the self-transcribing CRISPR platform . . . 115
5.3.2 Mechanistic investigation of STSR-CRISPR activation . . . 121
5.3.3 Direct TMSD-gated STSR-CRISPR for miR-21 detection . . . 134
5.3.4 Dragon hairpin-mediated target recycling for enhanced miR-21 detection . . . 139
5.3.5 Bioanalyzer and RNA-seq . . . 143
5.4 Conclusion . . . 153

6 Summary and future perspective **155**
6.1 Summary of key findings . . . 155
6.1.1 From programmable structure to controlled reaction initiation . . . 156
6.1.2 Expanding the functional role of CRISPR/Cas12a . . . 157
6.1.3 Unintended reaction as a source of mechanistic discovery . . . 158
6.1.4 Progress towards programmable and multiplex detection . . . 159
6.1.5 Overall contribution . . . 159
6.2 Limitations . . . 160
6.3 Future work . . . 161
6.3.1 Identification of amplification and transcription products . . . 161
6.3.2 Development of generalisable design rules . . . 162
6.3.3 Analytical and multiplex validation . . . 162

Bibliography **164**

Appendix A. Python scripts for RNA sequencing analysis **192**
A.1 Identification and ranking of the top 10 RNA products . . . 192
A.2 Classification of RNA products . . . 194
A.3 AgniAlign visualisation . . . 198

List of Figures

1-1 Publication trends for selected nucleic acid isothermal amplification methods from 2015 to 2025. Figure adapted from reference[1]. 2

1-2 Primer organisation and formation of the stem–loop intermediates that initiate loop-mediated isothermal amplification. Adapted from Ref.[2] 5

1-3 Schematic representation of asymmetric stem-loop-mediated isothermal amplification (ASLAMP). Adapted from Ref.[3] 6

1-4 Schematic representation of single-crossing cross-priming amplification (CPA). Adapted from Ref.[4]. 7

1-5 Abstraction-based representation and programmable design of structure-driven isothermal amplification. (a) Cross-priming amplification (CPA) and (b) loop-mediated isothermal amplification (LAMP) are represented using common reaction circuits based on functional single-stranded intermediates. (c) Introduction of a universal sequence (us) simplifies the amplification intermediate to us–1s–2s–ua while retaining the same basic amplification circuits. (d) Proposed amplification pathway of the simplified programmable system, in which complementary us/ua regions promote intramolecular folding, followed by primer extension and strand displacement to regenerate amplification intermediates. Adapted from Ref.[5]. 8

1-6 Schematic representation of recombinase polymerase amplification (RPA). Adapted from Ref.[6]. 9

1-7 Representative strategies for target-specific readout in multiplex LAMP. (a) DARQ-LAMP, in which amplification-driven strand displacement separates the fluorophore-labelled oligonucleotide from its quencher, generating a target-specific fluorescence signal. (b) QUASR-LAMP, where a fluorophore-labelled primer is incorporated into the amplification product, while unincorporated primers are quenched by a complementary quencher oligonucleotide after amplification. (c) Lateral-flow detection using DIG- and biotin-labelled primers to generate dual-labelled amplicons that are captured on antibody-functionalised test lines. (d) Multiplex lateral-flow detection using different antigen labels and corresponding antibodies to distinguish amplification products from different targets. Different fluorophores or capture labels can be assigned to individual targets to enable multiplex discrimination. Adapted from Ref.[7]. 11

1-8 Schematic illustration of CRISPR-Cas12a target recognition and cleavage mechanism. Figure adapted from Ref.[8]. 13

1-9 Representative strategies for integrating CRISPR/Cas12a with nucleic acid amplification. (a) DETECTR; (b) AIOD-CRISPR; (c) CASTSA. Adapted from Ref.[9–11] 15

1-10 Representative strategies coupling isothermal amplification, transcription and CRISPR-based detection. (a) Schematic of SHERLOCK. (b) UNIVERSE assay. Adapted from Ref.[12,13]. 18

1-11 Proposed mechanism and strand-displacement activity associated with DragonRNA synthesis. (a) Proposed model of DragonRNA formation. (b) DragonRNA extension on double-stranded DNA substrates by Rpo41. Adapted from Ref.[14]. 19

2-1 Interface of the Primer Designer software.[15] 23

2-2 Schematic of ABM isothermal amplification. Initially, primer us-2a hybridises to the 2s region of the target, followed by B3 binding to B3s and strand displacement. Subsequently, primers us-1s and F3 bind to the complementary strand, respectively, generating a single-stranded DNA product that can fold into a hairpin structure. The exposed loop regions (2s or 1a) provide binding sites for us-2a or us-1s, respectively, enabling further primer extension and duplex formation. The resulting duplex is proposed to regenerate hairpin structures, allowing repeated amplification cycles. 27

2-3 Screening of candidate primers for the ABM system. (a–c) Real-time amplification curves using three candidate primers (us-2aa, us-2ab, and us-2ac) together with F3, B3, and us-1s. (d) Conventional LAMP amplification using F3, B3, FIP, and BIP as a positive control for validating F3 and B3. NTC: non-template control. RFU: relative fluorescence unit. n=2. 28

2-4 Evaluation of the analytical performance of the ABM system using the us-2ac primer set. Time-to-positive (TTP) values obtained from reactions containing HPV16 DNA concentrations from 0.1 to 10^6 copies/µL and no-template controls (NTC). n=3. 29

2-5 Verification of the ABM amplification products. (a) Real-time amplification curve of different concentrations of target. (b) Melting curve of (a). n=2. (c) Agarose gel electrophoresis. The band shown at approximately 100 bp (red box) indicates a band migrating near the predicted size of the "us–1s–2s–ua" intermediate product. 30

2-6 Reproducibility test of ABM system. (a–d) Amplification curves obtained from four independent experiments using HPV16 DNA (10^3copies/µL) and no-template controls (NTC). n=3. 31

2-7 Optimisation of the ABM system. 33

2-8 Optimisation of primer ratios in the ABM system. (a) Initial screening of different primer ratios using HPV16 DNA (10^4copies/µL) and NTCs. (b) Reproducibility assessment of selected primer ratios based on multiple independent experiments. Each point represents one experimental replicate. . . 34

2-9 Heterodimer analysis of us-1s and us-2ac by Oligo Analyzer. 35

2-10 Evaluation of mismatch-modified primer sets, TTP values using different primer sets with intentional single-base mismatches designed to reduce primer-dimer formation. n=3. 36

2-11 Primer sequence optimisation. The positions of primer regions 1s and 2ac, together with the alternative designs (1s-short and 2d–2g), are indicated by horizontal lines along the target DNA sequence (5′–3′). Vertical dashed lines mark the boundaries of the primer-binding regions. Underlined, blue-coloured and yellow-highlighted sequences indicate repeated sequence motifs. 36

2-12 Alternative primer combination test. (a) Screening of different primer combinations using shortened Us+1s (Us+1s short) and alternative Us+2 primers, with full-length Us+1s combinations included for comparison. n = 2. (b) Repeat testing of the selected primer combinations (Us+1s short/Us+2ad and Us+1s short/Us+2af) across multiple independent experiments. Each point represents one experimental replicate and the horizontal line indicates the median TTP value. 37

2-13 The first Sanger sequencing results. The upper panel shows the expected ABM amplicon sequence, with the primer-derived regions (us, 1s, 2s and ua) and the target-specific region indicated. The lower panels show Sanger sequencing chromatograms and corresponding sequences of amplification products obtained using the 44 bp us-1s primer. Orange highlighting indicates sequences matching the expected 2s and ua regions. Both products contained these regions, whereas the expected target-specific sequence was not confirmed. 39

2-14 Agarose gel of the amplification product. The left panel shows the original gel, while the right panel indicates the fragments cut for Sanger sequencing. 40

2-15 The second Sanger sequencing of the cut band. Sanger sequencing analysis of gel-excised amplification products. Sanger sequencing chromatograms and corresponding sequences of products generated using the 22 bp us primer. 40

3-1 Comparison of primer design and target recognition between conventional LAMP (left) and the proposed CRISPR/Cas12a-integrated loop amplification assay (right) 46

3-2 Schematic of CRISPR/Cas12a integrated loop amplification assay and primer target region. In the presence of target DNA, Cas12a cleavage generates a free 5′ terminal on the non-target strand (NTS), enabling TSP binding and extension. Subsequent hairpin formation and primer extension by P1 or P2 support further amplification. In the absence of target DNA, the CRISPR and amplification pathway is not initiated. Different colours represent sequence domains, and asterisks indicate complementary sequences. 51

3-3 Comparison of different concentration ratios of core primers TSP1 and P1. (a) Real-time fluorescence amplification curves obtained using different TSP1:P1 concentration ratios (1:1, 0.5:1, and 1:0.5). (b) Melting curve analysis corresponding to the amplification products shown in (a). (c) Real-time fluorescence amplification curves obtained using the optimised TSP1:P1 ratio of 1:1. (d) Melting curve analysis of (c). T: with template; NTC: non-template control. RFU: relative fluorescence unit. n=2. 53

3-4 Comparison of different HPV18 core primer sets. (a) TSP1+P1. (b) TSP1.1+P1. (c) TSP3+P1. (d) TSP1+P2. (e) TSP1.1+P2. (f) TSP3+P2. T: with template; NTC: non-template control. n=2. 54

3-5 Comparison of different HPV 52 primer sets. (a) TSP1+P1. (b) TSP2+P2. n=2. 54

3-6 Schematic of amplification using the core primers (TSP1 and P1) (a) and the modified primers with extended TSP and additional loop primers (TSP3, b1, b3, f, a*-f) (b). 55

3-7 Evaluation of different primer combinations using the 78 bp mimic CRISPR cut product as template. (a) Screening of TSP1- and TSP3-based primer combinations and their corresponding amplification TTP. (b) Evaluation of additional primer designs based on the TSP3 primer set. Amplification efficiency was compared by time-to-positive (TTP) values using 10^7 copies of HPV18 dsDNA, the right panel. n=2. Statistical comparisons were not performed due to the limited number of replicates. 56

3-8 Effect of outer primer d. (a) schematic of primer target region. (b) TTP values of using TSP1+b1 and TSP1+P1 primer sets respectively. n=2. Statistical comparisons were not performed due to the limited number of replicates. . . 57

3-9 Schematic illustration of the proposed self-priming amplification mechanism using a phosphorothioate-modified primer (PS-TSP). Following primer binding and extension, the resulting DNA folds back to form a hairpin structure, enabling further extension and repeated self-priming. Cyan highlighting (e-f-e*) indicates phosphorothioate-modified DNA regions, and asterisks represent complementary sequence domains. 58

3-10 Comparison of PS-modified and unmodified TSP1 at different reaction temperatures using instrument-generated ΔRn and manually baseline-corrected fluorescence (ΔF). Panels (a, e, i) and (b, f, j) show the instrument-generated ΔRn curves for PS-TSP1 and unmodified TSP1 at 65, 68, and 72 °C, respectively. Panels (c, g, k) and (d, h, l) show the corresponding manually baseline-corrected fluorescence (ΔF) curves. Manual baseline correction was performed by subtracting the fluorescence of the first measurements from each individual Rn. Red and black lines represent reactions with target DNA (T) and no-template controls (NTC), respectively. Individual replicates are shown (n = 2). The negative-going ΔRn curves may result from the instrument's automatic baseline subtraction, whereas the manually corrected ΔF curves retain time-dependent background fluorescence changes. 59

3-11 Agarose gel electrophoresis of PS-TSP1 and TSP1 with or without target DNA at different temperatures. Lanes 1–6 represent PS-TSP1 incubated at 65, 68, and 72 °C in the presence (odd-numbered lanes) or absence (even-numbered lanes) of target DNA. Lanes 7 and 8 represent non-modified TSP1 incubated at 72 °C in the presence and absence of target DNA, respectively. 60

3-12 Real-time fluorescence curve for different target DNA concentrations using a PS-modified primer at 68 °C. Curves represent the mean of two replicate reactions per condition (n = 2). Target DNA concentrations are expressed as copies per reaction. 61

3-13 Optimisation of primer conditions. (a)-(b) the ratio of primer TSP and P2; n=2. (c) Effect of the second loop primer (LP) addition on Time-to-positive time (TTP); n=3. (d) Effect of loop primer capture length on TTP. n=3. T: with template, NTC: non-template control. N/A indicates no amplification detected during the experiment period. Due to the limited replicate numbers and the presence of reactions without measurable TTP values, the results were interpreted descriptively without statistical significance testing. 62

3-14 Optimization of amplification temperature (a) and magnesium ion concentration. Magenta circles represent reactions containing target DNA (n=3), while brown circles represent non-template controls (NTC, n=5). Individual data points are shown. N/A indicates reactions in which no amplification was detected within the experimental period. Horizontal bars and error bars represent the mean ± SD of reactions with measurable TTP values, where applicable. 63

3-15 Effect of betaine addition and evaluation of the OptiGene Mastermix. (a) Real-time fluorescence amplification curves obtained in the presence and absence of betaine. n=2. (b) Amplification performance using the OptiGene master mix with different primers in the absence of target DNA. Water was used as the negative control. n=3. 64

3-16 Verification of CRISPR/Cas12a cleavage efficiency by PCR amplification. (a). Two primers were designed to amplify the sequence adjacent to the CRISPR target region. (b). Denaturing PAGE gel electrophoresis of 120 bp template for identification of cis-cleavage. (c). Real-time fluorescence curves of PCR amplification for CRISPR-treated and untreated templates. Curves represent the mean of two replicate reactions per condition (n = 2). . 65

3-17 Denaturing PAGE gel electrophoresis of 307 bp template after CRISPR treatment. (a) Cis-cleavage of the 307 bp template at different digestion times (10, 15, 20, and 30 min). (b) Cleavage analysis of different amounts of template after 10 min and Cas12a inactivation methods. Lanes 1–3, 4–6, and 7–9 contained 26 ng, 13 ng, and 5.2 ng template, respectively. Lanes 2, 5, and 8 were treated with Proteinase K, whereas lanes 3, 6, and 9 were heat-treated. . . . 66

3-18 Evaluation of the feasibility and concentration-dependent amplification behaviour of the loop amplification system. (a) Real-time fluorescence amplification curves using the HPV16 "a-b1-b2-c" ssDNA template. (b) Real-time fluorescence curves at different target DNA concentrations (3.6×10^5–3.6×10^9 copies/reaction). (c) Time-to-positive (TTP) values for target concentrations ranging from 10^3 to 10^7 copies/reaction over a 90 min reaction period. (d) Linear regression of TTP against the logarithm of target concentration over the range of 10^5–10^9 copies/reaction during a 60 min reaction period. Individual measurements are shown in (c), and error bars represent mean ± SD (n = 3) in (c) and (d). 68

3-19 Time-to-positive (TTP) values for HPV18 ssDNA amplification at different target concentrations (10^2–10^9 copies/reaction). Individual data points are shown, with horizontal bars representing the mean and error bars indicating the range (n = 2). N/A indicates reactions in which no amplification was detected within the 90 min experimental period. 69

3-20 Time-to-positive (TTP) for HPV52 amplification at different target DNA concentrations with (b) and without (a) the d-outer primer. Individual data points represent replicate reactions (n = 3 for panel a and n = 2 for panel b). N/A indicates reactions in which no amplification was detected within the experimental period. 70

3-21 Comparison of amplification using intact (UNCUT), CRISPR-cleaved (CRISPR), and mimic cut-product templates (CUT1S1A). (a) Schematic of the 120 bp template showing the CRISPR/Cas12a cleavage site and primer-binding regions. (b) Schematic of the 78 bp mimic cut-product template and primer-binding regions. (c) TTP comparison using the TSP3+b1 primer set. Individual data points represent replicate reactions (n = 3), and bars and error bars represent mean ± SD. 71

3-22 Investigation of the delayed amplification observed following the addition of CRISPR/Cas12a reaction components. (a) Comparison of amplification-only, mock-CRISPR, original CRISPR, and spike-in CRISPR reactions. Amplification-only refers to reactions without CRISPR components. Mock-CRISPR refers to reactions using non-targeting HPV16/18 crRNA instead of HPV52 crRNA, while original CRISPR contains the target-specific HPV52 crRNA and Cas12a. In spike-in CRISPR reactions, the CRISPR mixture was pre-incubated without target DNA before the template was added. (b) Effect of reducing buffer and CRISPR/Cas12a components. Reduced r2.1 buffer refers to a lower contribution of Mg^{2+} from the CRISPR buffer, while reduced CRISPR refers to a reduced volume of the CRISPR reaction mixture added to the amplification system. (c) Effect of individual buffer components on amplification, including Tris-HCl, BSA, NaCl, and $MgCl_2$. (d) Comparison of commercial and handmade r2.1 buffer formulations, including a formulation with reduced Mg^{2+} concentration. Individual fluorescence traces represent duplicate reactions for each condition (n = 2). 73

3-23 Optimisation of total Mg^{2+} concentration in the CRISPR/Cas12a-integrated loop amplification assay. Time-to-positive (TTP) values were compared at total Mg^{2+} concentrations of 6, 8, and 9.5 mM. Individual data points represent replicate reactions (n = 3), and horizontal bars indicate the mean TTP. . 74

3-24 Comparison of the TTP values obtained by amplification-only, two-step, and one-pot detection formats at different target DNA concentrations (9.6×10^3–9.6×10^6 copies/reaction). Individual data points represent replicate reactions (n = 3 per condition), and horizontal bars indicate the mean TTP. 75

3-25 Duplex HPV16/18 amplification using the loop amplification system. (a) Real-time fluorescence curves for individual HPV16 and HPV18 targets, their mixture (HPV16+18), and the no-template control (NTC). (b) Melting curve analysis of the amplification products, showing melting peaks at approximately 86 °C for HPV16, 89 °C for HPV18, and an intermediate peak at 88 °C for the mixed sample. Each target was tested at 10^7 copies/reaction. Three replicate reactions were performed per condition (n = 3). 76

3-26 Multiplex HPV16 and 18 detection using CRISPR-integrated loop amplification. (a) Real-time fluorescence amplification curves and (b) melting curve for the two-step assay. (c) Real-time fluorescence amplification curves and (d) melting curve analysis for the one-pot assay. Each target was tested at 10^5 copies/reaction. HPV16+18 represents reactions containing both HPV16 and HPV18 targets, while NTC represents the no-template control. Three replicate reactions were performed per condition (n = 3). The mixed HPV16/18 samples exhibited overlapping or intermediate melting peaks rather than two clearly resolved peaks, indicating a limitation of melt-based discrimination. 77

3-27 Detection of HPV16, HPV18 and HPV52 using a triplex CRISPR-integrated loop amplification assay. (a) Real-time fluorescence amplification curves and (b) melting curve analysis for the two-step assay. (c) Real-time fluorescence amplification curves for the one-pot assay. The colored numbers in (b) indicate the melting temperatures (Tm) of the corresponding amplicons. Each target was tested at 10^7 copies/reaction. n=3. Melting curve analysis was performed for the two-step assay, while the one-pot assay was evaluated using real-time fluorescence measurements only. 78

3-28 Evaluation of primer concentration for triplex loop amplification. (a) TTP values of no-template controls (NTCs) at different primer concentrations. (b) TTP values for HPV16, HPV18 and HPV52 at 10^6 and 10^5 copies/reaction, using a primer concentration of 700 nM. The dashed line indicates a reference TTP of approximately 60 min, based on the observed NTC amplification behaviour. Individual data points represent replicate reactions (n = 3), and error bars indicate SD for reactions with measurable TTP values. N/A indicates no detectable amplification within the experimental period. 79

3-29 Analytical performance of the two-step and one-pot HPV16 detection assays. (a) Linear regression of time-to-positive (TTP) against the logarithm of HPV16 target concentration (5.8×10^4–5.8×10^8 copies/reaction) for the two-step assay. (b) Real-time fluorescence amplification curves at different HPV16 target concentrations (5.8×10^4–5.8×10^8 copies/reaction) using the one-pot assay. (c) Linear regression of TTP against the logarithm of HPV16 target concentration (5.8×10^5–5.8×10^8 copies/reaction) for the one-pot assay. Error bars in (a) and (c) represent standard deviation (SD, n = 3) . . . 80

3-30 : Analytical performance of the two-step HPV18 detection assay. (a) Real-time amplification curves at different HPV18 target concentrations, including the no-template control (NTC). (b) Linear relationship between time-to-positive (TTP) and the logarithm of target concentration. Error bars represent standard deviation (SD, n = 3). 81

3-31 Real-time amplification curves of the one-pot HPV18 detection assay at different target concentrations, including the no-template control (NTC). n=3. 81

3-32 Analytical performance of the two-step HPV52 detection assay. (a) Real-time amplification curves at different HPV52 target concentrations, including the no-template control (NTC). Individual fluorescence curve represent triplicate reactions (n = 3 per condition). (b) Linear regression of time-to-positive (TTP) against the logarithm of target concentration. Error bars represent standard deviation (SD, n = 3). 82

4-1 Schematic illustration of the self-transcribing RPA primer design. The T7 promoter sequence was incorporated into the 5′ end of LFw (orange). The crRNA sequence, consisting of the handle (blue and underlined) and spacer (red), was incorporated into LRv. The amplified products contained both elements, enabling transcription of crRNA from the RPA amplicons. 87

4-2 Schematic illustration of RPA-IVT-CRISPR detection for HPV16. RPA amplification with LFw and LRv generates a crRNA-encoding amplicon, and the T7 promoter sequence in LFw enables IVT to produce a functional crRNA. In the presence of target DNA, the crRNA activates Cas12a, resulting in cleavage of the reporter probes and fluorescence generation. The PAM sequence is located on the FQ probe, while the R1 probe functions as an ssDNA trans-cleavage reporter. 91

4-3 Agarose gel analysis of RPA products using different primer pairs. (a) RPA amplification using the short Fw/Rv primer pair, generating an expected 137 bp product without purification. (b) RPA amplification using the extended LFw/LRv primer pair, generating an expected 203 bp product after column purification. As illustrated in the schematics above the gels, LFw and LRv were designed by incorporating a 25 bp T7 promoter sequence and a 44 bp crRNA-encoding sequence, respectively, at the 5′ ends of the original primers. The input HPV16 concentration was $1x10^7$ copies/reaction; L, 100 bp DNA ladder; NTC, no-template control; PC, positive control. 92

4-4 Feasibility study of RPA-IVT-CRISPR. Real-time fluorescence of (a) three-step RPA-IVT-CRISPR assay and (b) two-in-one step RPA-(IVT-CRISPR) assay. P: purified RPA product; un: unpurified RPA product; T: HPV16 target (10^7 copies/reaction); NTC: non-template control. (c) Agarose gel of RPA products before and after purification and the corresponding IVT product. 93

4-5 (a–c)Predicted RNA secondary structures and corresponding primer sequences for Original LRv, New LRv1 and New LRv2 designs. Magenta and blue text indicate the spacer and handle regions, respectively. The circled regions show the predicted handle secondary structures. (d) Endpoint fluorescence intensity at 120 min. NTC, no-template control; T, target-containing reaction. Single measurement, n=1. 95

4-6 The RPA-IVT-CRISPR assay with extended detection time. (a) Agarose gel of RPA product. (b) Real-time fluorescence of (a) product. 1-5 are serial dilutions of HPV16 target from $1x10^9$ to $1x10^5$ copies/reaction. 6 is non-template control. Data represent the mean and range of two replicates. . . . 96

4-7 Investigation of the source of non-specific signals in the RPA–IVT–CRISPR assay. (a) Effect of the presence or absence of RPA primers and reagents. (b) different primer combinations and R1 probe addition in the absence of RPA reagents. IVT, CRISPR and the FQ probe were included in all reactions. Experimental conditions are summarised in the tables above the fluorescence curves. n=1. 97

4-8 Investigation of the source of non-specific signals in the RPA–IVT–CRISPR assay, IVT and CRISPR steps. (a) Effect of the presence or absence of the IVT step. (b) Effect of the presence or absence of the CRISPR ste. Experimental conditions are summarised in the tables above each fluorescence curve. n=1. 98

4-9 Proposed model for crRNA generation from the LRv primer. The 3′ end of LRv is proposed to fold back and hybridise with an internal complementary region, allowing T7 RNA polymerase to initiate RNA extension and form a DNA–RNA chimera. Continued extension may generate a full-length crRNA-like sequence without target DNA. Blue and black sequences represent the original LRv DNA primer, orange indicates the proposed newly synthesised RNA, and yellow highlights indicate complementary bases potentially involved in self-priming. 99

4-10 Evidence for transcription from the LRv primer. (a) Urea PAGE gel analysis of transcription products before and after DNase and RNase treatment. Lane L: 50 bp DNA ladder; lane 1: transcription products; lane 2: DNase-treated products; lane 3: DNase- and RNase-treated products; lane 4: RNase-treated products; lane 5: RNase- and DNase-treated products; lane 6: LRv ssDNA template. (b) Fluorescence kinetics of the IVT–CRISPR assay using different concentrations of the LRv primer as the transcription template. Data represent the mean and range of two replicates. 100

4-11 Strategy for reducing non-specific signals. (a) Comparison of fluorescence generated by the T7HPV16 dsDNA and the LRv primer using the R1 probe. n=1. (b) Reducing both primer concentrations from 480 nM and 50 nM using the R1 probe. (c) Reducing both primer concentrations from 480 nM and 50 nM using both R1 and FQ probes. HPV16 targets were at 1×10^8 and 1×10^6 copies/reaction; NTC, no-template control. Data represent the mean and range of two replicates. 101

4-12 Performance of the RPA–IVT–CRISPR assay in different formats. (a) Real-time fluorescence of the three-step assay. (b) Endpoint fluorescence at 90 min for the three-step assay. (c) Real-time fluorescence of the two-in-one RPA–(IVT–CRISPR) assay. (d) Endpoint fluorescence at 60 min for the two-in-one assay. HPV16 targets ranged from 1×10^3 to 1×10^9 copies per reaction. NTC, no-template control. FQ probe only. Data are shown as mean ± SD (n=3). Statistical significance was determined using an unpaired two-tailed Student's t-test. ns, not significant; ****P<0.0001. 103

4-13 Analytical sensitivity of the three-step and two-in-one RPA–IVT–CRISPR assays. (a) Real-time fluorescence signals generated by the three-step assay using HPV16 targets at 1, 10, 10^2, and 10^3 copies per reaction. (b) Endpoint fluorescence of the three-step assay at 60 min. (c) Real-time fluorescence signals generated by the two-in-one assay at the corresponding target concentrations. (d) Endpoint fluorescence of the two-in-one assay at 240 min. Data are presented as mean ± SD, n = 3. Statistical significance was determined using an unpaired two-tailed Student's t-test. ns, not significant; **P < 0.01. 104

4-14 Specificity of the three-step RPA–IVT–CRISPR assay.(a) Real-time fluorescence signals generated from HPV16, HPV18, HPV52, NTC and HPV16 with a non-targeting FQ probe (HPV16 mirFQ). (b) Endpoint fluorescence at 60 min. Data are shown as mean ± SD (n=3). Statistical significance was determined using one-way ANOVA followed by Dunnett's multiple comparisons test, comparing HPV16 with NTC, HPV18 and HPV52. Adjusted p-values were used to account for multiple comparisons. ****P < 0.0001. . 105

5-1 Overview of the STSR-CRISPR platform. (A) Schematic illustration of the self-transcription and self-recognition mechanism, where a single ssDNA template functions as both the transcription and Cas12a activation material. (B) miRNA sensing strategies based on direct TMSD activation (System 1) and target recycling-enhanced TMSD (System 2). 116

5-2 (a) Schematic illustration of self- transcription and self-recognition mechanism, where a single ssDNA template functions as both the transcription and Cas12a activation material. (b) Fluorescence signal under different reaction conditions. Signals were observed only in the presence of both T7 RNAP and Cas12a. ”+/-” indicates the presence or absence of polymerase. Mean ± SD (n = 3). (c) Real-time fluorescence signal at different template concentrations. Curves represent the mean of two replicate reactions (n=2). 117

5-3 Optimisation of the self-transcribing CRISPR assay. (a) Effect of FQ and R1 reporter concentrations on fluorescence generation. (b) Effect of Cas12a concentration on fluorescence kinetics. The input ssDNA template concentration was 10 nM. Data represent the range of two technical replicates. . . 118

5-4 miRNA-triggered activation of the STSR-CRISPR system. (a) Schematic of miR-21-triggered TMSD and free-template release. (b) Fluorescence kinetics of cr21-1 and cr21-2 with or without different cap sequences. Cr21 and cap were both used at 10 nM. (c) Endpoint fluorescence intensity after overnight incubation. (d) Evaluation of miR-21-triggered strand displacement. Probe 4 and miR-21 were used at 100 nM. FQ and R1 were 500 nM. Data represent the mean and range of two replicates. 119

5-5 Evaluation of probe candidates for miR-21 detection and universal crRNA. (a) Fluorescence intensity of probes 1 – 4 (10 nM) at 180 min with or without miR-21 target (10 nM). (b) Overnight fluorescence ratio between the target and no-target reactions (FT/FNTC). FQ and R1 were 500 nM. Data are presented as mean with range, n = 2. (c) Fluorescence kinetics of universal crRNA at 0.03, 0.3, 3, 30, and 300 nM over 180 min. The inset shows the fluorescence response from 0 to 120 min. (d) Endpoint fluorescence intensity at 130 min for crRNA from 0.03 to 30 nM and for 10 nM cr21-1 and cr21-2. The red line represents the linear regression fitted using the crRNA standards. The dashed line indicates the estimated fluorescence intensity of 10 nM crRNA calculated from the regression equation. FQ and R1 were 500 nM. n=1. 121

5-6 Design and evaluation of split crRNA system. (a) Schematic comparison of full-length crRNA generation and split crRNA assembly. For the split template design, spacer RNA is transcribed from spacer ssDNA and assembled with handle RNA generated from handle dsDNA to form functional split crRNA. (b) Fluorescence kinetics of handle dsDNA combined with different spacer templates. FQ and R1 reporter concentrations were both 500 nM. (c) Fluorescence kinetics using different handle dsDNA concentrations with 10 nM spacer template. FQ concentration was 500 nM. Data represent the mean and range of two replicates. 122

5-7 Comparison of split-template and ds-handle-mediated Cas12a activation. (a) Schematic of split crRNA assembly and ds-handle-mediated CRISPR activation. FQ serves as the cis-cleavage substrate, while R1 reports trans-cleavage activity. (b) Fluorescence validation of split template, ds-handle-only template, and full-length cr21-SE template at 10 nM with an FQ ratio of 1:1. (c) Effect of different FQ ratios on the fluorescence signal generated by the full-length cr21-SE template. Data represent the mean and range of two replicates. 123

5-8 Comparison of split and full-length cr21-CG-3bp templates. (a) Schematic of the new split template and full-length template systems. FQ serves as the cis-cleavage substrate, and R1 reports trans-cleavage activity. (b) Fluorescence validation of full-length cr21-CG-3bp, split Handle-CG-3bp/ds-spacer, and individual template components. (c) Effect of different FQ ratios with R1, and R1-only condition on the full-length cr21-CG-3bp system. Data represent the mean and range of two replicates. 125

5-9 Evaluation of cr21-CG-3bp activity and mir-FQ-assisted HPV target detection.(a) Sequence design of the full-length cr21-CG-3bp and Handle-CG-3bp templates. Red letters represent the spacer region, and blue letters represent the handle region. (b) Fluorescence kinetics of the two templates with FQ, R1, or mir-FQ reporters. FQ and R1 were used at 500 nM. Data are shown as the mean of two independent experiments. (c,d) Detection of HPV16 (c) and HPV18 (d) targets using the corresponding crRNAs, comparing R1 alone with R1 plus mir-FQ. The indicated concentrations, such as 5 nM, refer to target concentrations. FQ and R1 were used at 500 nM. NTC reactions served as negative controls. Data are shown as mean ± SD, n=3. 126

5-10 Validation of template-generated crRNA activity and target-specific reporter cleavage. (a) Fluorescence kinetics of different template–reporter combinations. (b) Endpoint fluorescence comparison of LRv, cr21-CG-3bp, and ss-spacer templates with FQ, mir-FQ, or R1 reporters. FQ is the cognate F/Q-labelled target for all crRNAs, whereas mir-FQ is an unrelated F/Q-labelled target control. n=1. (c) FAM-channel gel image showing fluorescent reporter cleavage products. (d) Stained gel image showing total nucleic acid bands under the same conditions. Lanes 1–3: LRv with FQ, mir-FQ, or R1; lanes 4–6: cr21-CG-3bp with FQ, mir-FQ, or R1; lanes 7–9: ss-spacer with FQ, mir-FQ, or R1; lane 10: synthetic universal crRNA with FQ as a positive control; lane 11: FQ-only control. 128

5-11 Validation of target-dependent cis-cleavage and trans-cleavage using universal crRNA. (a) Fluorescence kinetics of different target–reporter combinations. n=1. (b) FAM-channel gel image showing fluorescent reporter and cleavage products. (c) Stained gel image showing total nucleic acid bands under the same conditions. Lanes 1–5 contain synthetic universal crRNA as the positive crRNA control: lane 1, FQ with FQ reporter; lane 2, FQ with FQ and mir-FQ reporters; lane 3, TS-NTS with mir-FQ reporter; lane 4, TS-NTS with R1 reporter; lane 5, TS with R1 reporter. Lanes 6–11 are no-crRNA controls containing FQ, mir-FQ, FQ/mir-FQ, TS-NTS, TS, or mir-F, respectively. FQ is the cognate F/Q-labelled target, mir-FQ is an unrelated F/Q-labelled target control, and R1 reports trans-cleavage activity. 130

5-12 Comparison of PAM-containing and PAM-deficient dsDNA reporters (a) FAM-channel gel image showing fluorescent reporter and cleavage products. (b) Stained gel image showing total nucleic acid bands under the same conditions. Lanes 1–6 contain synthetic universal crRNA: lanes 1–3, FQ target with FQ, FQ/mir-FQ, or FQ/mir-FQ-noPAM reporters; lanes 4–6, TS-NTS target with mir-FQ, mir-FQ-noPAM, or FQ-noPAM reporters. Lanes 7–11 are no-crRNA controls containing mir-FQ, mir-FQ-noPAM, FQ, FQ-noPAM, or TS-NTS, respectively. noPAM indicates the corresponding sequence lacking the PAM region. 131

5-13 Evaluation of DNase I inactivation methods after crRNA transcription from ssDNA templates. (a) Schematic of DNase I-assisted crRNA preparation. After T7 RNAP transcription, DNase I was used to digest the DNA template, leaving crRNA for the subsequent Cas12a cleavage reaction with FQ and R1 reporters. (b) Comparison of different DNase I inactivation methods before Cas12a detection. DNase I was inactivated either by heat treatment alone or by EDTA followed by heat treatment, and reactions with or without Cas12a were included to evaluate background fluorescence. n=1. 133

5-14 Evaluation of column purification after DNase I treatment. Fluorescence kinetics were measured under different DNase I, column purification, and Cas12a conditions.(a-c) Cas12a reactions using different reporter combinations after DNase I treatment and/or column purification.(d) No-Cas12a controls. Solid lines indicate the conditions highlighted in each panel legend, while dashed lines represent the other conditions from the same experiment for comparison. n=1. 134

5-15 Design of LRv-based cr21 templates with different predicted self-priming strengths. (a) Sequence display of the parental LRv template and designed cr21 variants. (b) Summary of cr21 variants designed to tune 3′ self-priming stem length and self-folding efficiency. 135

5-16 Validation of the screened cr21 template. (a) Fluorescence kinetics of different cr21 variants. cr21-CG-3bp showed the strongest signal and was selected for further validation. (b–d) Validation of the selected cr21-CG-3bp template by comparison with universal crRNA and LRv at 10 nM (b), 1 nM (c), and 0.1 nM (d). Fluorescence intensity was monitored over time to evaluate RNA-generation efficiency. Blank reactions were included as negative controls. Data represent the mean and range of two replicates. 136

5-17 Validation of miR-21-mediated cap displacement from cr21 templates. (a) Native PAGE gel analysis of cr21/cap complexes in the presence or absence of miR-21. Lanes 1-4 show cr21-1 or cr21-CG-3bp complexed with different caps in the presence of miR-21; lanes 5–8 show the corresponding cr21/cap complexes without miR-21; lane 9 contains miR-21 alone; lanes 10–11 contain free cr21-1 and cr21-CG-3bp templates. (b) Schematic of miR-21-triggered toehold-mediated strand displacement (TMSD). miR-21 displaces the cap from the cr21 template to release the free template for downstream self-transcription and CRISPR activation. 137

5-18 Probe screening and miR-21 detection using cr21-CG-3bp. (a) Sequence design of cr21-CG-3bp, universal crRNA, and cap1/cap3. (b) Schematic representation of the CC3 and CC3U probe designs. (c) Fluorescence intensities of CC1, CC3, CC1U, and CC3U probes using cr21-CG-3bp. PC represents reactions with 1 nM miR-21 target, and NC represents reactions without miR-21 target. (d) Fluorescence response of the CC3 probe to miR-21 at 6.6 nM and 66 pM, with NTC as the no-template control. Data are presented as mean ± SD (n = 3). Statistical significance was determined using an unpaired two-tailed Student's t-test between the indicated groups. *P < 0.05; ****P < 0.0001. 138

5-19 Target recycling-enhanced TMSD strategy and structural characterisation of DH probes. (a) Schematic illustration of miRNA-triggered target recycling of the STSR-CRISPR system. (b) Predicted secondary structure of the DH probe generated by NUPACK. 139

5-20 Evaluation of dragon hairpin designs for miR-21-responsive template release.(a) Native PAGE gel analysis of different dragon hairpin constructs in the presence of miR-21. DH_12, DH_14, DH_15, and DH_16 indicate different dragon hairpin designs, and miR-21-only controls are included. (b) Fluorescence comparison of DH_12, DH_14, DH_15, and DH_16 at 10 nM and 1 nM target concentrations. NTC reactions were included as negative controls. Data are shown as mean ± SD, n=3. 140

5-21 Sensitivity evaluation of the dragon hairpin-based miR-21 detection system. (a) Fluorescence kinetics of miR-21 detection from 1 nM to 1 pM. (b) Endpoint fluorescence comparison of the corresponding miR-21 concentrations in (a). (c) Fluorescence kinetics of low-concentration miR-21 detection from 1 pM to 1 fM. (d) Endpoint fluorescence comparison of the corresponding miR-21 concentrations in (c). NTC reactions served as negative controls. R1 probe was used at 500 nM. Each condition contains nine data points, with three same-colour points representing technical replicates from the same transcription product. 142

5-22 Characterisation of RNA products generated by promoter-independent transcription and their CRISPR activity. Bioanalyzer electropherograms of RNA products generated from (a) LRv, (b) cr21-2, and (c) cr21-CG-3bp templates. The LRv, cr21-2, and cr21-CG-3bp DNA templates were 71, 59, and 63 nt long, respectively. (d) CRISPR fluorescence generated by the corresponding transcription products using FQ as the reporter. FQ in water was included as the negative control. n=1. 144

5-23 Top 10 most abundant RNA products generated from the LRv template. Identical sequencing reads aligned to the LRv template were grouped and ranked by read count. Sequences are shown in the reference-aligned orientation. The complete crRNA region (positions 1–43) consists of the spacer region (positions 1–22) and handle region (positions 23–43). Products were classified according to the presence of the complete crRNA region (A), complete handle region only (B), or neither complete region (N). Percentages indicate the proportion of each product among total sequencing reads. 146

5-24 Top 10 most abundant RNA products generated from the cr21-2 template. . 147

5-25 Top 10 most abundant RNA products generated from the cr21-CG-3bp template. 147

5-26 Comparison of the three ssDNA template sequences and their predicted priming sites for promoter-independent RNA extension. The shared crRNA region (positions 1–43) is shown for LRv, cr21-2, and cr21-CG-3bp. Potential priming sites (a–c) were predicted based on complementarity between the 3′-terminal sequence and internal regions of each template. The predicted sites were used to compare potential priming positions with the RNA product patterns observed by sequencing; however, these sites were not directly confirmed by the current sequencing analysis. 148

5-27 AgniAlign sequence analysis of cr21-CG-3bp IVT products. P1, P9 and P10 were aligned to the original 63 nt cr21-CG-3bp template for visualisation. P9 and P10 were 71 and 76 nt long, and therefore extended beyond the expected sequence length. In both products, the sequence following the expected template boundary corresponded to the 5′ region of the cr21-CG-3bp template, forming an apparent end-to-start junction. Blue rectangles represent the input DNA template in the reference orientation, while red rectangles represent the corresponding antisense-oriented sequence used by AgniAlign for alignment. Red circles indicate RNA product nucleotides. 149

5-28 Spacer retention in RNA products containing a complete crRNA handle. RNA products containing the full handle region (positions 23–43) were grouped according to how many spacer nucleotides were retained immediately before the handle. The groups were 0, 1–5, 6–10, 11–15, 16–21, and 22 nt, where 22 nt represents a complete crRNA. Percentages were calculated from the total trimmed reads for each sample. The value above each bar shows the total percentage of reads containing a complete handle. 152

List of Tables

1-1 Comparison of commonly used isothermal nucleic acid amplification methods. 3

2-1 Primers used for ABM amplification. 24

2-2 Effect of primer mismatch on heterodimer and target binding affinity . . . 35

2-3 Design of alternative primer binding positions to minimise heterodimer formation. 37

3-1 PCR primers used for target DNA template synthesis. 46

3-2 Primer sequences used for loop amplification. 46

3-3 crRNA sequences used for CRISPR/Cas 12a. 48

3-4 Predicted self-dimer and heterodimer formation of candidate primers for HPV16, HPV18 and HPV52. 52

4-1 Primers and oligonucleotides used in the RPA–IVT–CRISPR assay. 87

5-1 The oligonucleotides used in this study. 111

5-1 The oligonucleotides used in this study (continued). 112

5-1 The oligonucleotides used in this study (continued). 113

5-2 Summary of sequencing results for the three RNA products. 150

Abbreviations

ABM	Abstract model-based isothermal amplification
APS	Ammonium persulfate
ASLAMP	Asymmetric stem-loop-mediated isothermal amplification
BHQ1	Black Hole Quencher 1
BIP	Backward inner primer
bp	Base pair
Cas	CRISPR-associated protein
CPA	Cross-priming amplification
CRISPR	Clustered regularly interspaced short palindromic repeats
CRISPR-Dx	CRISPR-based diagnostics
crRNA	CRISPR RNA
DH	Dragon hairpin
DMF	N,N-dimethylformamide
DNase	Deoxyribonuclease
dNTPs	Deoxyribonucleoside triphosphates
dsDNA	Double-stranded DNA
EDTA	Ethylenediaminetetraacetic acid
FA	Formamide
FAM	6-Carboxyfluorescein
FIP	Forward inner primer
FP	Folding primer
FQ	Fluorophore–quencher probe
FRET	Förster resonance energy transfer
Fw	Forward primer
GuCl	Guanidine chloride
HDA	Helicase-dependent amplification

HPV	Human papillomavirus
HR-HPV	High-risk human papillomavirus
IDT	Integrated DNA Technologies
IVT	In vitro transcription
LAMP	Loop-mediated isothermal amplification
LbCas12a	Lachnospiraceae bacterium Cas12a
LFw	Long forward primer
LOD	Limit of detection
LP	Loop primer
LRv	Long reverse primer
miRNA	MicroRNA
NASBA	Nucleic acid sequence-based amplification
NC	Negative control
NCBI	National Center for Biotechnology Information
NTC	No-template control
NTS	Non-target strand
nt	Nucleotide
PAGE	Polyacrylamide gel electrophoresis
PAM	Protospacer adjacent motif
PC	Positive control
PCR	Polymerase chain reaction
POCT	Point-of-care testing
PS	Phosphorothioate
PS-LAMP	Phosphorothioate-modified loop-mediated isothermal amplification
RCA	Rolling circle amplification
RFU	Relative fluorescence units
Rn	Normalised Reporter Signal (in qPCR)
ΔRn	Change in Normalised Reporter Signal (in qPCR)
RNAP	RNA polymerase
RNA-seq	RNA sequencing
RNase	Ribonuclease
rNTPs	Ribonucleoside triphosphates
RNP	Ribonucleoprotein

RPA	Recombinase polymerase amplification
RT-qPCR	Reverse transcription quantitative polymerase chain reaction
Rv	Reverse primer
SDA	Strand displacement amplification
SSB	Single-stranded DNA-binding protein
ssDNA	Single-stranded DNA
STSR-CRISPR	Self-Transcribing Self-Recognition CRISPR
T7 RNAP	T7 RNA polymerase
TBE	Tris–borate–EDTA
TEMED	N,N,N′,N′-Tetramethylethylenediamine
Tm	Melting temperature
TMAC	Tetramethylammonium chloride
TMSD	Toehold-mediated strand displacement
TP	Turn-back primer
TS	Target strand
TSP	Template-specific primer
TTP	Time to positive

Chapter 1

Introduction

1.1 Nucleic Acid Isothermal Amplification in Diagnostics

Currently, with the increasing prevalence of infectious diseases and other pathogenic threats, the development of rapid, low-cost, and accurate nucleic acid detection methods is of great importance for bioanalysis, disease diagnosis, and therapeutic applications[16,17]. Nucleic acids, such as DNA and RNA, are important biomarkers for early diagnosis and biological analysis[18]. However, their concentrations in biological samples are often too low for direct detection[19]. Therefore, Polymerase Chain Reaction (PCR) has developed as a gold-standard nucleic acid amplification technique[20,21]. Despite the advantages, PCR usually requires high-cost thermal cyclers, which limit its applications in point-of-care testing (POCT). Isothermal nucleic acid amplification methods provide an attractive alternative, as they are not restricted by thermal cycling and can be performed at a constant temperature[19]. For diagnostic applications, it is also desirable to extend these methods from single-target detection to multiplex detection. The simultaneous detection of multiple targets can improve diagnostic efficiency and is particularly useful when different pathogens or genotypes need to be distinguished in a single sample[22–24].

1.1.1 Overview of isothermal amplification methods

Isothermal nucleic acid amplification methods have been increasingly adopted across a wide range of applications[25,26]. Research interest in these methods has also increased substantially (Figure 1-1)[1]. In particular, loop-mediated isothermal amplification (LAMP) has remained one of the most widely studied isothermal amplification methods, while the number of publications related to Recombinase Polymerase Amplification (RPA) has also increased rapidly. Rolling Circle Amplification (RCA) and Nucleic Acid Sequence-Based Amplification (NASBA) have maintained relatively stable research activity, whereas fewer studies

have focused on Strand Displacement Amplification (SDA) and Helicase-dependent Amplification (HDA). A bibliometric analysis of 5,388 publications also reported a steady increase in research on isothermal amplification between 2013 and 2022, with LAMP being the most frequently used keyword[27]. The popularity of LAMP among isothermal nucleic acid amplification techniques (INAATs) can be partly attributed to its well-established assay-development ecosystem, including dedicated primer design software - PrimerExplorer, as well as its compatibility with multiple readout methods suitable for point-of-care testing[28]. For example, amplification can be observed directly through a colour change using colorimetric indicators, monitored through the turbidity caused by magnesium pyrophosphate formation, or detected using lateral flow strips for a simple visual readout[29–31].

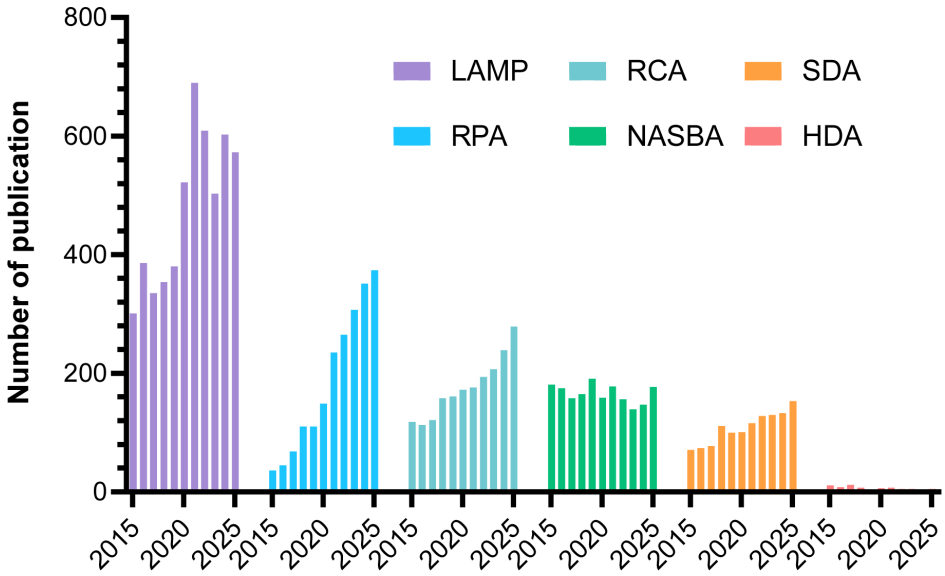


Figure 1-1: Publication trends for selected nucleic acid isothermal amplification methods from 2015 to 2025. Figure adapted from reference[1].

Although these methods can all operate under isothermal conditions, they use different mechanisms to support amplification (Table 1-1). LAMP uses a strand-displacing DNA polymerase together with four core primers that recognise six regions of the target sequence[32]. Recombinase polymerase amplification (RPA) avoids extensive thermal denaturation by using recombinase–primer complexes to search templates and promote strand invasion. This mechanism allows RPA to operate at relatively low temperatures and generally requires only two amplification primers[33]. Rolling circle amplification (RCA) uses a circular nucleic acid as the amplification template. Continuous polymerase extension around the circular template produces long repeated amplicon sequences[34]. However, diagnostic RCA always requires the formation of a circular template, often using a padlock probe followed by ligation, which introduces an additional reaction step[35]. Nucleic acid sequence-based amplification (NASBA) combines reverse transcription, RNase H-mediated degradation, and T7 RNA polymerase-driven transcription in a continuous reaction, allowing RNA sequences to be amplified at

approximately 41°C[36]. However, the use of multiple enzymes often requires further optimisation. In addition, amplification at low temperature can increase non-specific primer interactions, and poorly designed primers may resulting in false-positive signals[37,38]. Strand displacement amplification (SDA) instead uses repeated nicking and strand-displacement synthesis[39]. However, the requirement for both polymerase and nicking/restriction enzyme increases the complexity of the reaction. Besides, classical SDA can require long amplification time of approximately 2 h, which may limit its use for rapid diagnostics.[25] Cross-priming amplification (CPA) avoids the requirement for a nicking enzyme by using cross primers and a strand-displacing polymerase[4]; however, its use of multiple interacting primers makes primer design relatively complex.

Table 1-1: Comparison of commonly used isothermal nucleic acid amplification methods.

Method	**Key mechanism**	**Typical temperature**	**Main enzymes**	**Number of primers**	**Main limitations**
LAMP	Strand displacement; loop formation	60–65 °C	Bst polymerase	4–6	Complex primer design; non-specific amplification
RPA	Recombinase-mediated primer invasion	37–42 °C	Recombinase, SSB, Bsu DNA polymerase	2	Primer-dependent non-specific amplification; limited primer-design predictability
RCA	Rolling-circle synthesis	30–37 °C	Phi29 polymerase	1–2	Requires a circular template
NASBA	RNA transcription-based amplification	41 °C	RT, RNase H, T7 RNAP	2	Requires multiple enzymes
SDA	Nicking; strand displacement	37–55 °C	DNA polymerase; nicking enzyme	4	Multiple enzymes; relatively long reaction time
CPA	Cross-priming; strand displacement	60–65 °C	Bst polymerase	5–6	Complex primer design

Overall, these methods demonstrate that isothermal amplification can be achieved through several distinct mechanisms, including loop formation, recombinase-mediated strand invasion, rolling-circle synthesis, transcription-based amplification, enzyme-mediated nicking and cross-primer strand displacement. Their different requirements for enzymes, primers and reaction temperatures also result in different levels of assay complexity. These differences are particularly important when considering the development of simplified and multiplex

nucleic acid amplification systems[40].

1.1.2 Structure-driven isothermal amplification

Among these mechanisms, the formation of functional nucleic acid secondary structures provides a particularly useful strategy for processing isothermal amplification. In these systems, primers are designed not only to recognise the target sequence but also to introduce complementary regions into newly synthesised products. These regions can subsequently fold into hairpin or loop structures, creating new sites for primer binding or self-priming. Loop-mediated isothermal amplification (LAMP) is a representative example of this principle. LAMP was first proposed by Notomi et al. in 2000[32]. This amplification system consists of four primers (FIP, BIP, F3, B3) that target six specific regions in the target sequence. (Figure 1-2) To eliminate the need for a separate denaturation step, the reaction is typically performed at around 65 °C using Bst polymerase, which has strong strand-displacement activity and can promote primer extension while displacing the downstream strand. Taking the BIP side as an example, the inner primer BIP (B1c-B2) first hybridises with the B2c region and initiates extension, while extension from the outer primer B3 subsequently displaces the BIP-extended strand. The inner primers FIP and BIP were designed with special 5' regions (F1c, B1c) that can hybridise with the complementary sites (F1, B1) in the newly synthesised strand to form loop structures. The formation of the loop or dumbbell structure is the key step in establishing the cycling amplification. During amplification, newly synthesised strands containing multiple primer-binding sites continuously serve as templates for further amplification. Repeated self-priming and strand-displacement extension eventually generate a mixture of stem-loop and cauliflower-like products containing multiple loops.

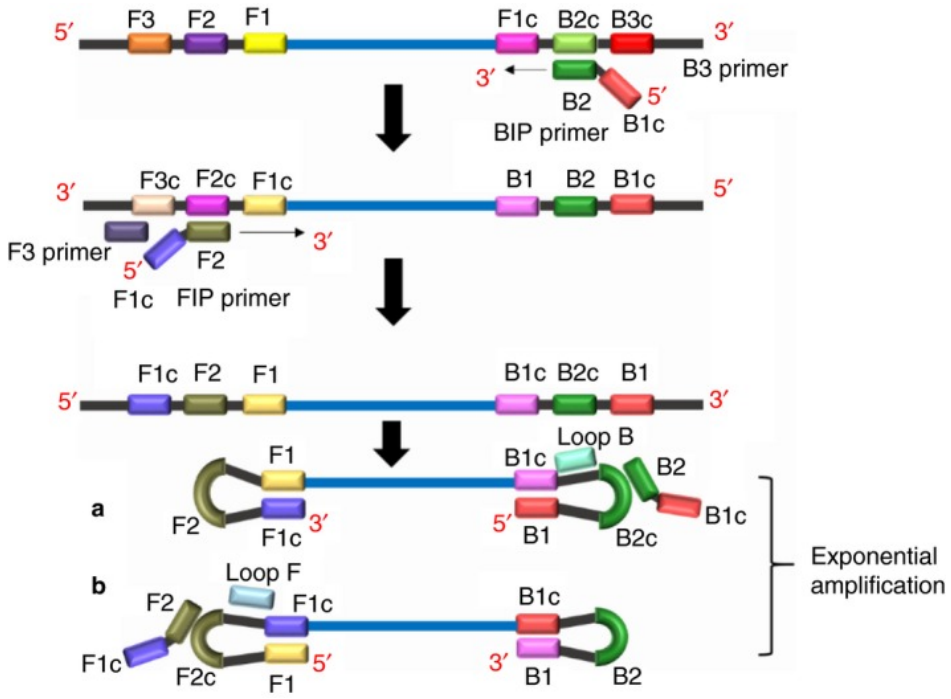


Figure 1-2: Primer organisation and formation of the stem–loop intermediates that initiate loop-mediated isothermal amplification. Adapted from Ref.[2]

LAMP, as the most typical structure-derived isothermal amplification method, with high efficiency to generate 10^9 copies of target within 60 min, has been widely used for pathogen and virus detection, as well as point-of-care diagnosis[2]. The structural features of LAMP products have subsequently been further exploited to improve amplification efficiency. Nagamine et al. introduced additional loop primers to accelerate the reaction[41]. Gandelman et al. further demonstrated that the stem regions of LAMP intermediates could also be targeted by additional primers[42]. These stem primers provided alternative priming sites and accelerated amplification, showing that both the loop and stem regions of LAMP products can be used as functional components of the amplification reaction. Swarm primers introduce additional amplification initiation routes into conventional LAMP and were shown to increase amplification speed[43]. These developments demonstrate that the amplification behaviour of LAMP can be adjusted by changing the number, position and accessibility of functional priming sites within its stem-loop intermediates.

Beyond introducing additional priming sites, the stability of these loop-stem structures can also be deliberately modified. Cai et al. developed phosphorothioate-modified LAMP (PS-LAMP), in which phosphorothioate modifications were introduced into the primers to reduce local duplex stability of the hairpin and promote terminal hairpin formation and extension. This enabled efficient LAMP at rather low temperature[44]. More recently, turn-back loop primer-accelerated LAMP (TLAMP) further modified the architecture of conventional loop primers. The resulting turn-back loop primers provide additional amplification pathways and achieve rapid detection within 20 min[45]. A particularly relevant development is asymmet-

ric stem-loop-mediated isothermal amplification (ASLAMP), which simplifies the structural principle of LAMP by using two specially designed primers adopted from conventional PCR primers.[3] (Figure 1-3) The system contains a turn-back primer (TP) and a folding primer (FP). TP contains the forward primer F at its 3' end together with an additional R sequence at the 5′ end, whereas FP contains the reverse primer sequence R at its 3′ end and can additionally include a self-complementary sequence (D-Dc) at the 5′ end. After TP binds to the target and is extended, FP hybridises to the newly synthesised strand and initiates strand-displacement synthesis. The released single-stranded product contains complementary sequence regions that allow it to fold into an asymmetric dumbbell-like structure. In this structure, the 3′ end can hybridise intramolecularly with an internal complementary region and initiate self-primed extension. Repeated self-folding, self-priming and primer-assisted extension then sustain the amplification cycle. Importantly, this design retains the stem-loop-mediated amplification principle of LAMP while reducing the number and complexity of primers. The original study showed that the target region required for primer design could be as short as approximately 40 bp. A third "boost primer" could optionally be introduced to accelerate amplification.

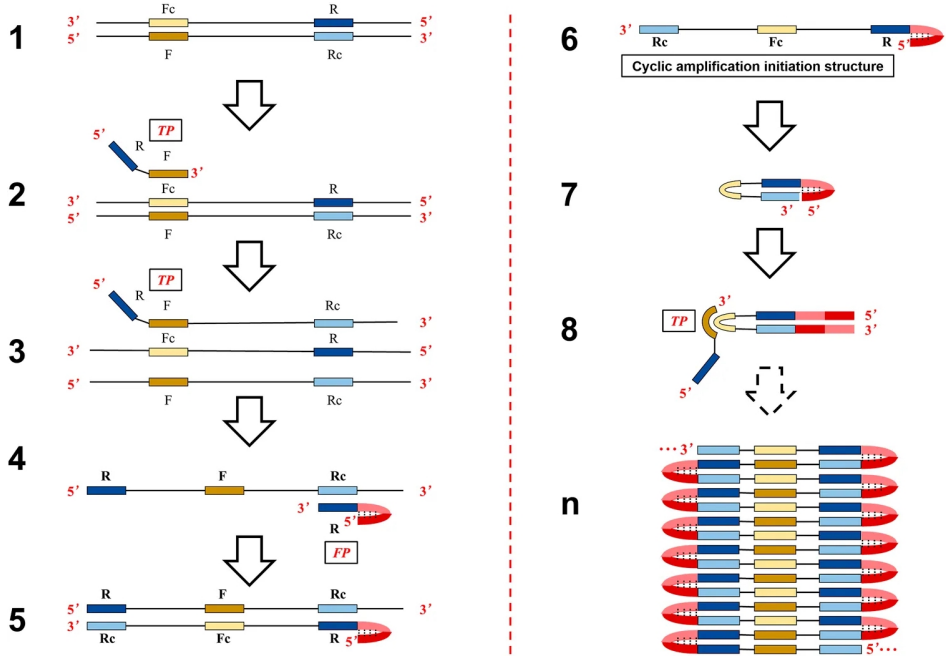


Figure 1-3: Schematic representation of asymmetric stem-loop-mediated isothermal amplification (ASLAMP). Adapted from Ref.[3]

Another typical hairpin structure-driven amplification is cross-priming amplification (CPA)[4,46]. CPA is driven by Bst DNA polymerase and specially designed cross primers. In single-crossing CPA (Figure 1-4), the cross primer contains a target-complementary 3′ region (1s) and a non-complementary 5' region corresponding to the 2a sequence. Following primer extension and displacement by the upstream primer 4s, the 2a sequence is introduced into the newly synthesised strand as an additional priming site. Subsequent extension by primers

2a, 3a and 5a generates single-stranded intermediates containing complementary terminal regions. These intermediates can fold into intramolecular hairpin-like structures, which provide accessible sites for further primer binding and extension. Repeated formation and extension of these structures produce the 1s/2a and 1s/3a amplification products and sustain the amplification cycle. Therefore, although LAMP and CPA use different primer arrangements, both rely on the deliberate introduction of sequence domains that allow amplification products to form functional secondary structures.

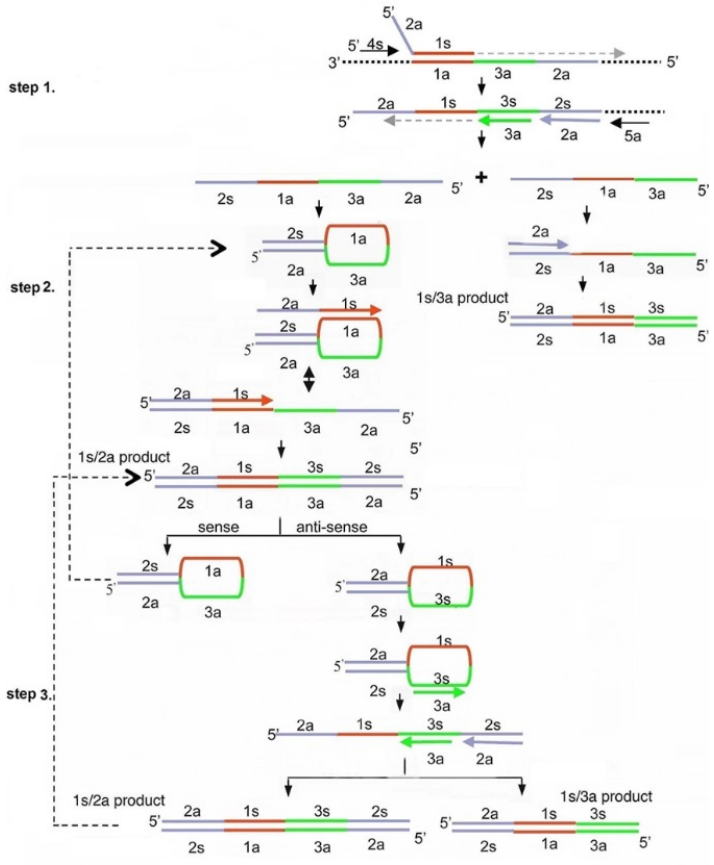


Figure 1-4: Schematic representation of single-crossing cross-priming amplification (CPA). Adapted from Ref.[4].

These studies show a gradual transition from using secondary structures as intermediates in a defined amplification method to using these structures as programmable functional elements. This concept was further generalised by Xu *et al*. within our research group using an abstraction-based model (ABM) for isothermal nucleic acid amplification[5]. In this model, LAMP and CPA can be described using a common set of basic structural and reaction elements. In CPA, a key single-stranded intermediate was represented as 3a–1s–2s–3s (Figure 1-5a), whereas the corresponding LAMP intermediate was represented as 2a–1s–2s–3s–4s–3a (Figure 1-5a). In this model, a functional intermediate can fold to generate an accessible priming region. Primer extension and strand displacement then produce new intermediates that re-enter the amplification cycle. The same universal sequence (us) was added to the 5′ ends

of two target-specific primers, generating a simplified us–1s–2s–ua intermediate after primer extension and strand displacement ((Figure 1-5c, d). The complementary us and ua regions allow this intermediate to fold back and enter the same type of amplification circuits. This design therefore separates the structure-forming sequence from the target-specific regions and provides a more flexible strategy for designing new isothermal amplification systems.

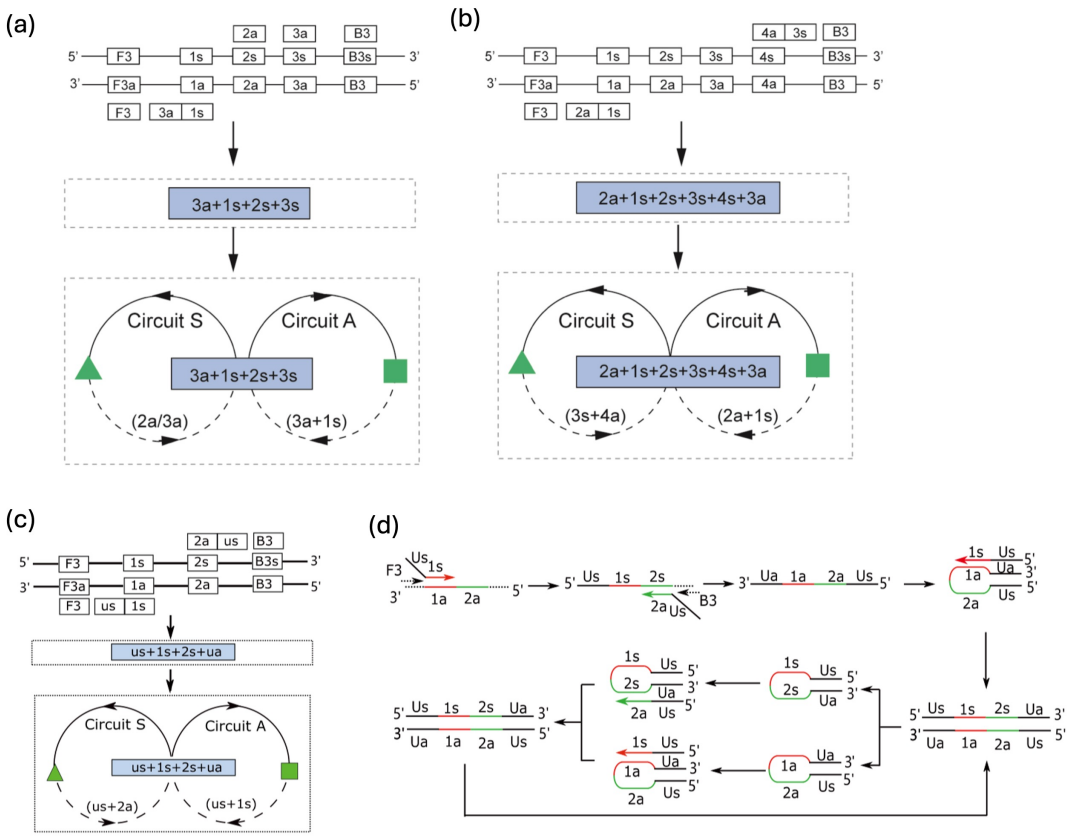


Figure 1-5: Abstraction-based representation and programmable design of structure-driven isothermal amplification. (a) Cross-priming amplification (CPA) and (b) loop-mediated isothermal amplification (LAMP) are represented using common reaction circuits based on functional single-stranded intermediates. (c) Introduction of a universal sequence (us) simplifies the amplification intermediate to us–1s–2s–ua while retaining the same basic amplification circuits. (d) Proposed amplification pathway of the simplified programmable system, in which complementary us/ua regions promote intramolecular folding, followed by primer extension and strand displacement to regenerate amplification intermediates. Adapted from Ref.[5].

Structure-driven amplification therefore offers a flexible way to control amplification pathways through programmed primer interactions and secondary-structure formation. However, the same complementary regions that enable the intended folding and self-priming can also participate in unintended intra- or intermolecular interactions[47]. These competing interactions may reduce primer availability, disrupt formation of the desired intermediates, or lead to non-specific amplification. The design of such systems therefore requires a balance between efficient formation of functional stem-loop structures and suppression of undesired

primer interactions. This consideration becomes particularly important in multiplex assays, where the presence of multiple primers and complementary domains further increases the number of possible interactions[48]. Simplifying primer architecture and controlling structural interactions are therefore important for developing robust multiplex isothermal amplification systems.

1.1.3 Recombinase polymerase amplification

Recombinase polymerase amplification (RPA) was first introduced by Piepenburg et al. in 2006[33]. It mainly involves primers, recombinase, single-stranded DNA-binding protein (SSB), and DNA polymerase. First, the recombinase binds to the primers with the assistance of a loading factor, forming nucleoprotein filaments that search for homologous sequences in double-stranded DNA. Once the complementary region is located, the primer invades the duplex and hybridises with the target strand, while the displaced strand is stabilised by SSB. The recombinase then dissociates, allowing the DNA polymerase to extend from the 3′ end of the primer and displace the opposite strand. Repeated extension from the forward and reverse primers generates new double-stranded templates, resulting in exponential amplification[6]. Conventional RPA can sometimes adopt PCR primers, which may simplify primer design. Its primer architecture is therefore simpler than that of LAMP, although this does not necessarily mean that primer optimisation is easier[49].

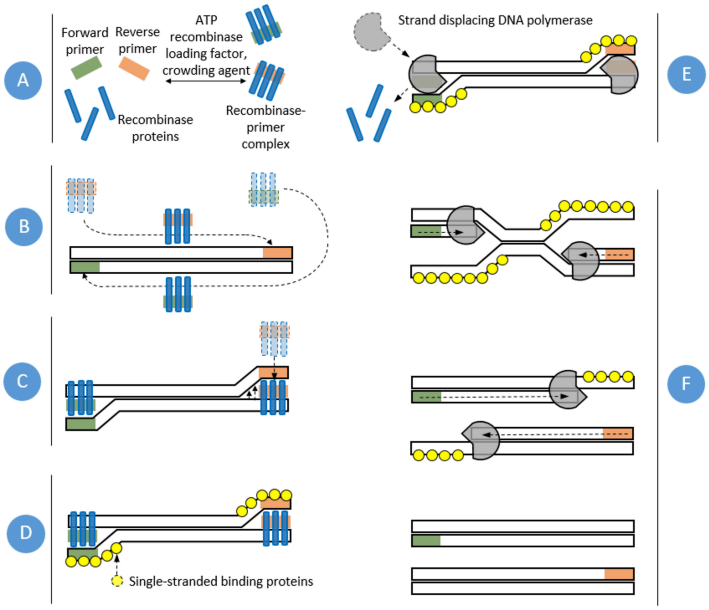


Figure 1-6: Schematic representation of recombinase polymerase amplification (RPA). Adapted from Ref.[6].

This mechanism allows RPA to operate at 37–42 °C and typically complete rapidly within 30 min. However, RPA also has several limitations. First, there is no dedicated software for

RPA primer design. RPA primers are relatively long (30-35 nt); although PCR primers can sometimes be adopted, they often need to be screened experimentally[50]. Second, RPA can tolerate some sequence mismatches, which may lead to non-specific amplification[51]. It also complicates detection using intercalating dyes like SYBR Green, which cannot distinguish target amplicons from primer dimers[6]. Third, RPA products may require purification before gel electrophoresis because they remain associated with proteins and crowding agents.

1.1.4 Challenges of isothermal amplification in multiplexing diagnostics

Although isothermal amplification is attractive for rapid diagnostics, multiplexing is more difficult than single-plex. Several primer sets must work in the same reaction conditions. This increases the possibility of interactions between primers and makes it more difficult to maintain similar amplification efficiency for different targets, and can reduce the overall sensitivity of the assay. Primer design, primer concentration and target-specific readout are therefore important factors in multiplex isothermal amplification[7,48]. Multiplex assays can generally be divided into one-pot amplification, where several targets are amplified in the same reaction, and parallelised amplification, where targets are separated into different reaction regions or chambers[52]. Parallelisation can reduce interaction between primer sets, but requires additional device design and is not a true homogeneous multiplex reaction.

Primer-derived interactions can be a concern in multiplex LAMP because each target typically requires multiple primers. Meagher et al. showed that LAMP primers can form primer dimers and self-amplifying hairpins. The long inner primers were especially prone to these structures if they have 3' end self-complementary[47,53]. Combining several primer sets increases the number of potential primer interactions, although primer binding to its intended target may reduce the availability of free primers for competing interactions. The recent review by Crego-Vicente et al. therefore highlighted primer design as a major challenge in multiplex LAMP and noted that no standardised design method has yet been established. Another major challenge is distinguishing different LAMP targets. Intercalating dyes and turbidity can report DNA amplification but cannot identify which target has been amplified. Several target-specific readout strategies have therefore been developed (Figure 1-7). DARQ-LAMP[54], QUASR[55] and molecular beacon[56] use fluorescent probes to distinguish different targets. Melting curve analysis can separate products with sufficiently different melting temperatures[57,58], while gel electrophoresis can differentiate amplification products according to their sizes or banding patterns[59], However, this can be challenging for LAMP because its amplification products often produce complex ladder-like banding patterns. Lateral-flow detection provides a simpler visual readout by introducing target-specific labels that are captured at different test lines[60]. These approaches improve multiplex detection but usually

introduce additional probes, processing steps or instrumentation.

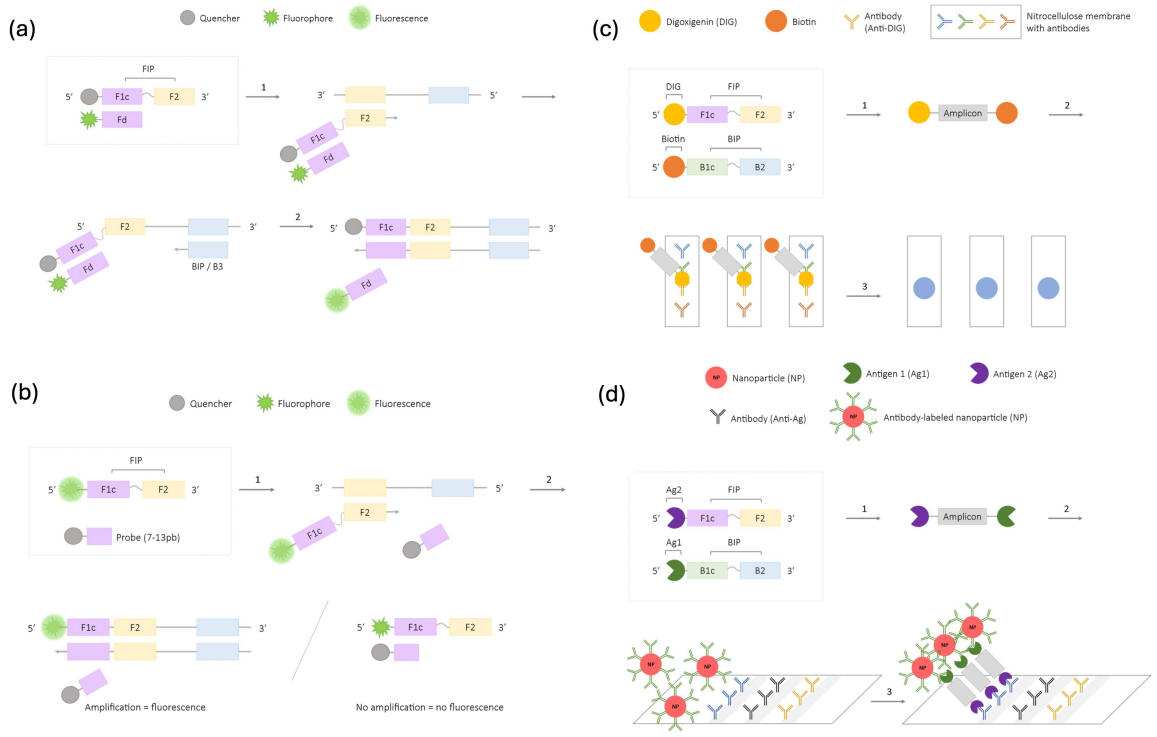


Figure 1-7: Representative strategies for target-specific readout in multiplex LAMP. (a) DARQ-LAMP, in which amplification-driven strand displacement separates the fluorophore-labelled oligonucleotide from its quencher, generating a target-specific fluorescence signal. (b) QUASR-LAMP, where a fluorophore-labelled primer is incorporated into the amplification product, while unincorporated primers are quenched by a complementary quencher oligonucleotide after amplification. (c) Lateral-flow detection using DIG- and biotin-labelled primers to generate dual-labelled amplicons that are captured on antibody-functionalised test lines. (d) Multiplex lateral-flow detection using different antigen labels and corresponding antibodies to distinguish amplification products from different targets. Different fluorophores or capture labels can be assigned to individual targets to enable multiplex discrimination. Adapted from Ref.[7].

RPA requires only two amplification primers per target and has a simpler primer architecture for one-pot multiplexing, but different primer sets may compete or amplify at different rates. Primer concentration and primer ratio are therefore important optimisation parameters in multiplex RPA. RAMP method combined multiplex RPA with subsequent LAMP reactions and enabled detection of more than 16 targets[61]. However, it requires additional reaction stages or specialised devices.

In summary, multiplexing involves more than simply adding additional primer sets. Multiplex LAMP requires careful primer design to manage potential primer-derived amplification and suitable readouts to distinguish amplification products[62,63], whereas RPA has a simpler primer architecture but requires careful balancing of competing amplification reactions. Current solutions include sequence-specific fluorescent reporters, melting analysis,

post-amplification detection and spatial separation. However, these approaches often increase assay complexity. Simplifying the amplification architecture while maintaining reliable target discrimination therefore remains important for practical multiplex isothermal diagnostics.

1.2 CRISPR/Cas12a for nucleic acid detection

Clustered regularly interspaced short palindromic repeats (CRISPR) and CRISPR-associated (Cas) proteins, initially developed as genome-editing tools, have subsequently been adapted for nucleic acid detection[64–66]. CRISPR-based diagnostics (CRISPR-Dx) platforms have emerged as powerful tools and have revolutionised molecular diagnostics to some extent[17,67]. Up to now, several promising CRISPR-Dx systems have been established as next-generation diagnostic tools, such as DETECTR (RPA and LbCas 12a)[9], HOLMES (LAMP and LbCas 12a)[68], and SHERLOCK (RPA and LwCas 13a)[69]. Among these Cas effectors, Cas12a has been widely investigated for DNA detection because target recognition activates its collateral cleavage activity against ssDNA reporters. This property allows Cas12a to be readily coupled with isothermal nucleic acid amplification and has also enabled the development of amplification-free detection strategies[68,70].

1.2.1 Cas12a target recognition and cleavage

Cas12a, formerly known as Cpf1, is a Class 2 type V RNA-guided endonuclease that uses a guide RNA (crRNA) to recognise complementary target sequences[66]. Target recognition generally starts from a protospacer adjacent motif (PAM), typically 5′-TTTV-3′. After PAM recognition, the DNA duplex is locally unwound, allowing the spacer region of the crRNA to hybridise with the complementary target strand (TS). This forms an R-loop and displaces the non-target strand (NTS), which activates the nuclease activity of Cas12a. During this process, the REC1 domain supports the initial crRNA–DNA pairing, whereas REC2 undergoes conformational rearrangement as the R-loop extends and helps prepare the DNA for cleavage[8,71].

As illustrated in Figure 1-8, R-loop formation activates the RuvC nuclease domain of Cas12a. The displaced NTS is first directed into the RuvC active site and cleaved. The TS then goes to the same catalytic site and is subsequently cleaved. This sequence-specific cleavage of the recognised target DNA is referred to as cis-cleavage. Following cleavage of both DNA strands, Cas12a remains in an activated state. The activated complex can bind surrounding single-stranded nucleic acids and cleave them without sequence specificity, a process known as trans-cleavage or collateral cleavage[8].

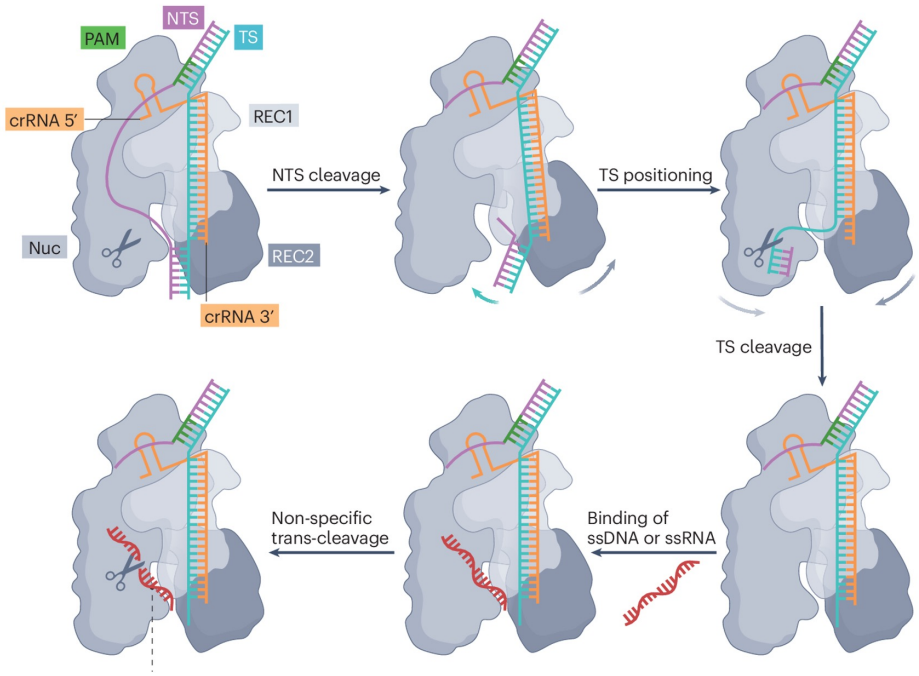


Figure 1-8: Schematic illustration of CRISPR-Cas12a target recognition and cleavage mechanism. Figure adapted from Ref.[8].

The specificity of Cas12a target recognition is highly dependent on the binding between crRNA and target DNA, but mismatch discrimination varies across the target sequence[72]. Mismatches within the PAM-proximal seed region can strongly reduce the target binding and R-loop formation. In contrast, PAM-distal mismatches are more tolerated[73]. Kinetic studies showed that PAM-proximal mismatches reduced the target-binding rate by approximately 150 to 600-fold, compared with reductions of up to 65-fold for PAM-distal mismatches[74]. Such off-target activation is particularly important to be considerate in molecular diagnostics.

Although ssDNA is generally considered the preferred substrate for Cas12a trans-cleavage, several studies have shown that activated Cas12a can also cleave or nick non-target dsDNA under certain conditions. Short dsDNA reporters have been shown to undergo trans-cleavage, with their susceptibility influenced by duplex stability and ionic conditions such as salt and Mg^{2+} concentration.[75–77]. In contrast, more stable blunt-ended dsDNA is relatively resistant to trans-cleavage. The presence of exposed ssDNA regions can substantially increase dsDNA cleavage; for example, a 3′ overhang of approximately 8 nt or longer can promote degradation of an otherwise resistant dsDNA substrate, with 3′ overhangs being more susceptible than equivalent 5′ overhangs[78]. Cas12a can also nick supercoiled dsDNA, including partially mismatched targets, indicating that dsDNA nicking is influenced by target complementarity and DNA topology[79].

Overall, these studies show that Cas12a specificity should be considered at two different levels. Off-target cleavage arises from imperfect recognition of target sequence, whereas

trans-cleavage occurs after Cas12a has been activated and can act on additional nucleic acid substrates. Although trans-cleavage is strongest towards ssDNA, certain dsDNA structures can also be susceptible. Therefore, Cas12a activity is determined not only by target recognition but also by the structural properties of the surrounding nucleic acid substrates. These properties should therefore be considered when designing Cas12a-based detection systems, particularly when complex DNA substrates or amplification products are present.

1.2.2 Integration of Cas12a and isothermal amplification

The programmable target recognition and trans-cleavage activity of Cas12a provide a useful platform for nucleic acid detection. However, the sensitivity of amplification-free Cas12a detection is often insufficient for low-copy targets. Cas12a has therefore been widely combined with isothermal amplification method[80,81]. A representative example is DETECTR, which combined RPA with Cas12a for HPV16 and HPV18 detection[9] (Figure 1-9a). Although this format allows the two reactions to be optimised independently, additional handling increases assay complexity and the risk of amplicon contamination. Consequently, later studies increasingly integrated the two steps into closed-tube or one-pot systems. RPA is particularly suitable for this approach because its relatively low reaction temperature is compatible with Cas12a. For example, AIOD-CRISPR integrates RPA and Cas12a in a single reaction[10] (Figure 1-9b). During RPA, strand displacement exposes single-stranded target regions that can be recognised by the crRNA, allowing Cas12a activation without PAM-dependent recognition of intact dsDNA. LAMP–Cas12a systems have also been widely developed, although differences in their optimal reaction temperatures often require temporal or physical separation of the two reactions even when they are performed within the same tube.[82]

Most existing systems use Cas12a as a downstream detector following amplification. More recently, Cas12a cleavage has also been used to initiate or regulate subsequent isothermal amplification, for example by generating active primers[83]. A similar recognition-first strategy was recently demonstrated in CASTSA, where Cas12a first recognises and cis-cleaves the target to generate a 5′ terminus. (Figure 1-9c) A terminal-specific primer (TSP) then recognises the cleavage product and initiates subsequent amplification, whereas uncleaved sequences cannot be amplified.[11]. These approaches shift Cas12a from a downstream detection element to an upstream molecular trigger, allowing target recognition to directly control the initiation of amplification.

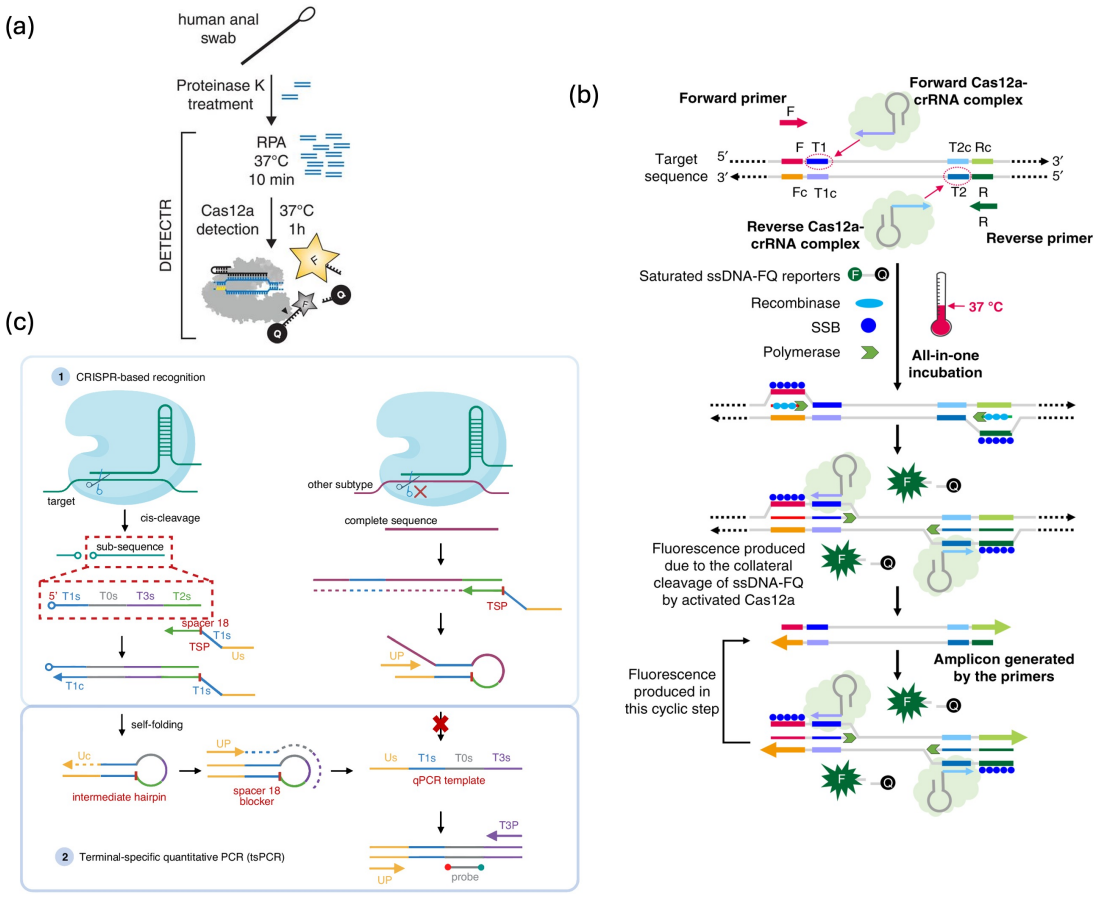


Figure 1-9: Representative strategies for integrating CRISPR/Cas12a with nucleic acid amplification. (a) DETECTR; (b) AIOD-CRISPR; (c) CASTSA. Adapted from Ref.[9–11]

However, integration also introduces additional constraints. Amplification enzymes and Cas12a must function under compatible temperature, buffer and Mg^{2+} conditions, while primer, crRNA and Cas12a concentrations must be balanced to avoid competition or inhibition[84]. Sequence design also becomes more restricted because amplification regions must accommodate both primer-binding sites and suitable Cas12a recognition sites, including the PAM requirement. Alternative PAM engineering and non-canonical Cas12a activation strategies have therefore been investigated to broaden target selection[85].

These challenges become more pronounced in multiplex detection. Although different crRNAs can specifically recognise multiple targets, the trans-cleavage signal itself is generally not target-specific. This means different Cas12a-crRNA complexes typically generate indistinguishable signals in the same reaction[67,86,87]. Current approaches include using Cas effectors with orthogonal collateral-cleavage preferences[88], spatially separating individual CRISPR reactions[24], or introducing different reporter[89]. However, these strategies generally increase assay or device complexity. When CRISPR detection is further combined with multiplex isothermal amplification, primer competition and unequal amplification introduce an additional layer of complexity. Thus, multiplex CRISPR-Dx requires both efficient multiplex

amplification and, importantly, a method to generate distinguishable target-specific outputs.

1.2.3 Multiplex HPV Detection

Cervical cancer is the fourth most common cancer in women worldwide, and persistent human papillomavirus (HPV) infection is the leading cause of cervical cancer, especially in those infected with high-risk HPV genotypes (HR-HPV), HPV 16, 18, 31, 33, 35, 39, 45, 51, 52, 56, 58, 59, 66, 68[63]. Among these, HPV 16 and 18 are reported to be the most virulent, causing approximately 70% of invasive cervical cancers. High-risk HPV tests are crucial for early cervical cancer diagnosis and prompt clinical treatment[90,91]. Many commercial tests like Cobas and BD Onclarity allow simultaneous detection of a panel of high-risk HPV types using PCR-based methods, while only selected genotypes are identified individually[92]. Isothermal amplification has also been investigated as a simpler alternative for multiplex HPV detection. One strategy is to increase target coverage within a single amplification assay. Seely et al. developed an RPA-based assay to detect 14 high-risk HPV types within 30 min, demonstrating that broad HPV coverage can be achieved using universal primers[93]. However, broad detection alone does not necessarily identify which genotype is present. In contrast, Barra et al., developed a multiplex LAMP assay for HPV16, 18, and 45 together with a human cellular control in a single tube[94]. This provided type-specific detection, but the number of individual HPV targets remained limited.

CRISPR-based detection has therefore been combined with isothermal amplification to provide an additional sequence-specific recognition step[95]. Zheng et al. coupled RAA with Cas12a and Cas13a to distinguish HPV16 and HPV18 using two orthogonal detection channels, while Ghouneimy et al. used three thermostable Cas enzymes for one-pot detection of HPV16, HPV18 and an internal control[96,97]. Liu et al. further combined multiplex RPA with type-specific Cas12a recognition for six high-risk HPV genotypes, including HPV16, 18, 31, 33, 35 and 45. Although six HPV types were amplified simultaneously in one RPA reaction, it still required separate Cas12a reactions[98]. These studies demonstrate that CRISPR can improve specific readout after multiplex amplification. However, increasing the number of HPV types may require additional specific crRNAs, Cas proteins, orthogonal reporters or separate detection channels. Overall, current multiplex HPV methods show a trade-off between target coverage, specificity and complexity. Developing amplification strategies that retain target-specific information while simplifying the reaction design therefore remains important for rapid multiplex HPV detection.

1.3 Transcription-assisted CRISPR detection

1.3.1 T7 RNA polymerase and in vitro transcription

T7 RNA polymerase (T7 RNAP) is a DNA-dependent RNA polymerase widely used for in vitro transcription (IVT). Conventional transcription is initiated through recognition of a specific double-stranded T7 promoter[99,100]. Once initiated, the same DNA template can be repeatedly transcribed to generate multiple RNA molecules. Therefore, IVT can provide transcriptional signal amplification in biosensing systems[101].

This property has been widely exploited in CRISPR-based nucleic acid detection, particularly with RNA-targeting Cas13. In SHERLOCK, RPA or RT-RPA introduces a T7 promoter into the amplification product, which is subsequently transcribed into RNA to activate Cas13 collateral cleavage[12,69]. (Figure 1-10a) The compatibility of RPA, T7 transcription and Cas13 has subsequently enabled more integrated formats. For example, Li et al. combined these reactions in a microfluidic RPA-T7-Cas13a platform, while later single-step assays incorporated RPA, transcription and Cas13 detection in the same reaction[102].

The role of transcription in CRISPR diagnostics is not limited to the conventional RPA–T7–Cas13 pathway. Zhang et al. showed that full-length RNA targets can directly activate the trans-cleavage activity of Cas12a and developed the UNIVERSE assay, in which T7 transcription converts DNA targets into RNA and thereby removes the PAM requirement of Cas12a[13]. (Figure 1-10b) More recently, a minimal transcription-template strategy was used to couple DNA recognition directly to T7 transcription and Cas13a detection without amplification step[103]. These studies demonstrate that transcription can function as both a target-conversion and signal-generation module in CRISPR diagnostics.

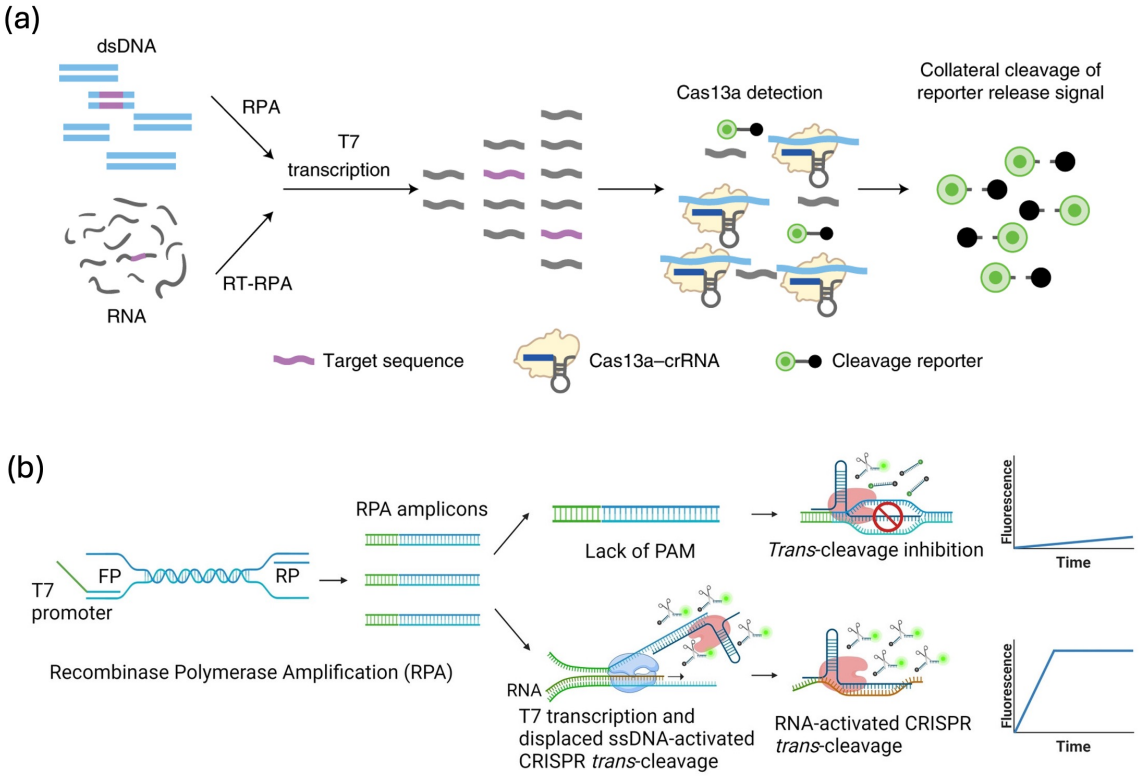


Figure 1-10: Representative strategies coupling isothermal amplification, transcription and CRISPR-based detection. (a) Schematic of SHERLOCK. (b) UNIVERSE assay. Adapted from Ref.[12,13].

Although T7 RNAP conventionally initiates transcription from a specific promoter, several non-canonical activities have also been reported. Promoter-independent transcription can initiate from the termini of double-stranded DNA, and its efficiency is influenced by the sequence and structure of the DNA end[104,105]. T7 RNAP can also extend nucleic-acid 3′ ends without promoter and perform RNA-templated RNA synthesis, including self-primed extension and the generation of replicating RNA products[106–108]. Greenwald et al. systematically characterised this activity and termed the resulting covalently linked DNA-RNA products DragonRNA[14]. Their results support a model in which the DNA 3′ end first base-pairs with a complementary region either intra- or intermolecularly and acts as a primer (Figure 1-11a). The RNA polymerase then adds the first ribonucleotide directly to the DNA 3′ end, followed by template-directed RNA extension. Using Rpo41, the authors further showed that DragonRNA extension can proceed into a double-stranded DNA region. During extension, the polymerase displaced the non-template DNA strand, indicating that strand-displacement activity can accompany DNA-primed RNA synthesis when either a nick or a short gap is present at the primer–template junction.(Figure 1-11b). Together, these observations show that RNA synthesis is not strictly restricted to the promoter-dependent transcription and provide a basis for alternative transcription-coupled sensing strategies.

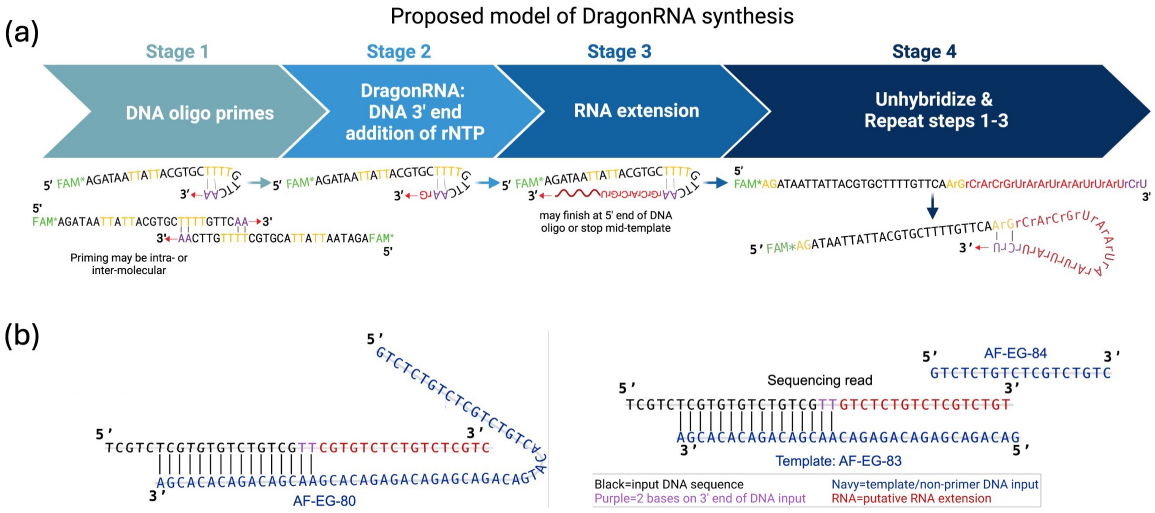


Figure 1-11: Proposed mechanism and strand-displacement activity associated with DragonRNA synthesis. (a) Proposed model of DragonRNA formation. (b) DragonRNA extension on double-stranded DNA substrates by Rpo41. Adapted from Ref.[14].

1.3.2 In situ generation of crRNA

Conventional CRISPR diagnostics generally require pre-synthesised crRNA to form an active Cas–crRNA complex. An alternative strategy is to generate crRNA in situ by transcription, allowing crRNA production itself to be controlled by the target recognition. An early example was reported by Wang et al., who used microRNA-triggered rolling circle transcription to produce a long RNA containing repeated crRNA units[109]. Similar self-supply strategies were subsequently developed using proximity extension,95 target-dependent primer extension[110], or regulated transcription templates[111] to generate multiple crRNA for Cas12a activation. T7-transcribed crRNA has also been coupled with proximity ligation for viral DNA detection[112] and with controlled-release sensing systems for microRNA detection[113]. A further development was to encode the crRNA sequence directly within the product of nucleic acid amplification. Karlikow et al. developed Functionalized Amplification CRISPR Tracing (FACT), in which amplification primers introduce a T7 promoter and crRNA-coding sequence into HDA or RT-HDA products[114]. More recently, this concept has been integrated with RPA. In OL-CRISPR, crRNA is synthesised during the reaction, delaying formation of the Cas12a–crRNA complex and allowing RPA to proceed before strong CRISPR activity[115]. TOP-CRISPR similarly uses target-dependent RPA amplicons to generate crRNA, while a primer-derived tag subsequently activates Cas12a, reducing the requirement for an additional crRNA and a PAM within the original target[116].

CREST uses isothermal amplification to trigger the synthesis and reassembly of a split crRNA[117]. Wakaba et al. demonstrated that tailed primers enable PCR or LAMP products to serve as templates for crRNA transcription before Cas12a detection[118]. However, such integration means that assay performance depends on the correct formation and transcrip-

tion of the intended DNA template. Potential non-specific amplification or unintended transcription therefore represents an additional source of background that should be considered when designing self-transcribing CRISPR systems, particularly in one-pot amplification–transcription–CRISPR reactions.

1.3.3 microRNA detection

MicroRNAs (miRNAs) are small non-coding RNAs of approximately 22 nucleotides that regulate gene expression[119]. Dysregulated miRNA expression has been associated with many diseases, making miRNAs attractive candidates for diagnostic biomarkers.[120] However, their short length, low abundance and high sequence similarity among related family members make sensitive and sequence-specific detection challenging[120,121]. A range of methods, including Northern blotting, microarrays, RT-qPCR and sequencing, have been used for miRNA analysis[120]. Because miRNAs are too short for conventional amplification, additional target-conversion strategies are often required. For example, stem-loop primers are widely used for reverse transcription before qPCR[122], while ligation, primer extension and circularisation also provide another opportunity to convert the miRNA into longer DNA products for amplification[123,124]. Similar strategies have been combined with isothermal amplification and CRISPR detection. CAL-LAMP uses miRNA-dependent ligation before LAMP and Cas12a detection[125], whereas Yan et al. developed a one-pot RCA–Cas12a assay in which miRNA-dependent padlock ligation initiates RCA and Cas12a further enhances signal amplification[126]. Although these assays provide high sensitivity and specificity, they show that miRNA detection often requires additional probes, enzymes and molecular conversion steps. CRISPR provides programmable sequence recognition and has also been applied to miRNA sensing. Cas13 can directly recognise RNA targets[127].

Transcription provides another way for converting miRNA signal into an amplified output. Rather than directly amplifying the miRNA, target recognition usually used to control the transcription template. Target-responsive hairpin systems have been used to activate T7 transcription and generate multiple RNA outputs following miRNA binding[128,129]. These studies suggest that transcription can provide an alternative interface between short-RNA recognition and downstream signal generation, without requiring direct amplification of the miRNA itself.

1.4 Aim and Objectives

The overall aim of this thesis was to develop and investigate programmable nucleic acid detection strategies by integrating structure-driven isothermal amplification, in situ crRNA generation and CRISPR/Cas12a technologies. Attention was placed on reducing assay com-

plexity and improving compatibility with multiplex nucleic acid detection, using HPV DNA as the primary model target, while further exploring the applicability of these principles to miRNA detection. To achieve this aim, the following objectives were established:

1. **To evaluate a programmable, structure-driven isothermal amplification strategy for HPV detection.** To investigate whether an abstract model-based (ABM) amplification strategy could be applied to HPV16 detection; to assess the feasibility of the proposed hairpin-mediated amplification mechanism; to optimise primer design and reaction conditions.

2. **To develop a simplified CRISPR/Cas12a-integrated loop amplification strategy for multiplex HPV detection.** To investigate whether Cas12a target recognition and cleavage could be used to facilitate the initiation of loop amplification; to design and evaluate different primer combinations and amplification pathways; to investigate the compatibility between CRISPR and loop amplification; to characterise the analytical performance of the individual assays; and to explore the feasibility of duplex and triplex HPV detection.

3. **To develop a self-transcribing RPA–CRISPR/Cas12a detection strategy.** To design extended RPA primers that enable the amplification products to encode and generate crRNA through in vitro transcription; to investigate the feasibility of integrating RPA, transcription and Cas12a detection within the same workflow; to identify and reduce sources of non-specific signal; and to evaluate the analytical sensitivity and specificity of the assay using HPV16 as a model target.

4. **To investigate promoter-independent self-transcription as a basis for simplified CRISPR/Cas12a sensing.** To investigate whether promoter-independent transcription from designed ssDNA templates could generate RNA products capable of activating Cas12a; to examine the effects of template structure, transcription conditions and CRISPR components on system activation; to investigate the underlying mechanism of the self-transcribing CRISPR reaction; and to explore the feasibility of adapting the platform for miR-21 detection using direct target-mediated strand displacement and target-recycling strategies.

Chapter 2

Abstract model-based isothermal amplification assay for nucleic acid detection

2.1 Introduction

The concept of using target-specific DNA secondary structure as amplification motif has been widely used in assay design, such as loop-mediated DNA amplification (LAMP)[32] and cross-priming amplification (CPA)[4]. Among the isothermal approaches developed to date, an abstract model-based (ABM) programmable design strategy for isothermal nucleic acid detection has been proposed by our group[5]. It exploited the self-assembly, disassembly, and primer extension reactions of functional hairpins to develop an automatic primer design system. This hairpin and amplicon-mediated nucleic acid isothermal amplification system only requires that users input the target DNA sequence into the software, and then the primers for amplification can be quickly obtained. Theoretically, only four primers and one enzyme are needed, and this scheme can achieve rapid amplification of the target sequence which has the advantages of high efficiency, simple processing, and increased user-friendliness. In the previous study, the generic tail strategy enabled miRNA detection down to 2 fM and was demonstrated for hepatitis B virus detection using clinical samples and multiplex HIV detection.[5] These findings support the potential of ABM as a programmable approach for nucleic acid detection with simplified assay design. Building on this work, this chapter aims to evaluate whether the ABM programmable primer design strategy developed by our group could be applied to HPV16 DNA detection, and to assess whether the predicted hairpin-mediated amplification mechanism could produce target-specific and reproducible amplification.

2.2 Material and Methods

2.2.1 Primer design

The DNA sequence encoding the HPV16 E6 protein (GenBank no. MH370216.1) was acquired from the database of the National Centre for Biotechnology Information (NCBI) (https://www.ncbi.nlm.nih.gov/). LAMP was included as a reference isothermal amplification method for comparison with the ABM assay. The two assays shared the same outer primers (F3 and B3). The LAMP primer set, including the outer primers (F3 and B3) and inner primers (FIP, BIP), was designed using PrimerExplorer V5 software (http://primerexplorer.jp/lampv5e/). The ABM inner primers (us-1s and us-2a) were designed according to the sequence located between the selected F3 and B3 primer regions using Primer Designer software developed by Xu et al[5]. (Figure 2-1).

The target sequence was first analysed for GC content and sequence complementarity using the Primer Designer software. Candidate primer sequences containing consecutive complementary or symmetric regions were excluded. The default primer length of 22–24 bp was used, and sequences with continuous self- or hetero-complementarity exceeding 5 bp or with a high potential for primer-dimer formation were excluded. Using these criteria, 697 candidate primer sets were generated by the software. (Figure 2-1) The specificity of the designed primers and the amplified fragments was further evaluated using Primer-BLAST to ensure accurate targeting of the HPV16 E6 gene. Table 2-1.

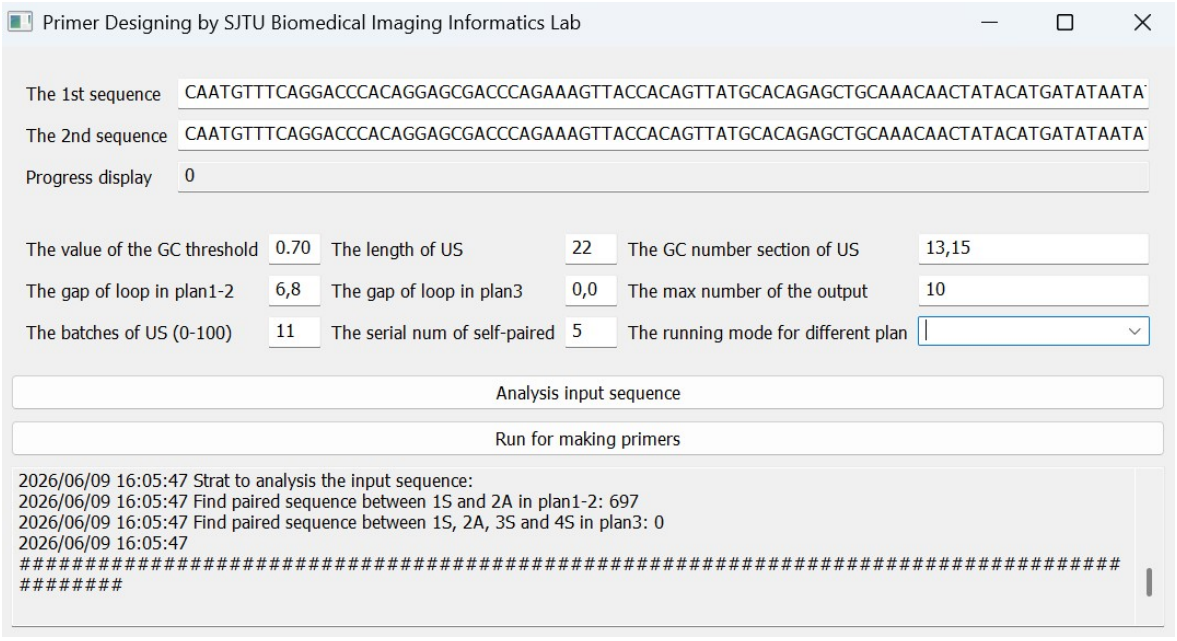


Figure 2-1: Interface of the Primer Designer software.[15]

Table 2-1: Primers used for ABM amplification.

Primer	Sequence (5'-3')
16-F3	ATGCACCAAAAGAGAACTG
16-B3	AGCATATGGATTCCCATCTC
us-1s	CAGTACCTCTCATGTCGGCAGCCAATGTTTCAGGACCCACAG GA
us-2aa	CAGTACCTCTCATGTCGGCAGCTGTGCATAACTGTGGTAACTT TCTG
us-2ab	CAGTACCTCTCATGTCGGCAGCTCTGTGCATAACTGTGGTAAC TTT
us-2ac	CAGTACCTCTCATGTCGGCAGCAGCTCTGTGCATAACTGTGGT AA
16-FIP	GCAGCTCTGTGCATAACTGTCAATGTTTCAGGACCCACA
16-BIP	TTAGAATGTGTGTACTGCAAGCATCCCGAAAAGCAAAGTCAT
1-3C	CAGTACCTCTCATGTCGGCAGCCAATGTTTCAGGACCCCCAG GA
1-5C	CAGTACCTCTCATGTCGGCAGCCAATGTTTCAGGACCCACCG GA
2-4G	CAGTACCTCTCATGTCGGCAGCAGCTCTGTGCATAACTGGGG TAA
us-1s short	CAGTACCTCTCATGTCGGCAGCCAATGTTTCAGGACC
us-2ad	CAGTACCTCTCATGTCGGCAGCGGTAACTTTCTGGGTCGC
us-2ae	CAGTACCTCTCATGTCGGCAGCGGTAACTTTCTGGGTCGCTCC
us-2af	CAGTACCTCTCATGTCGGCAGCATAACTGTGGTAACTTTCTG
us-2ag	CAGTACCTCTCATGTCGGCAGCTCTGTGCATAACTGTGGTAA

2.2.2 Reaction conditions

For the ABM amplification, the reaction contained 1 µM of each inner primer (us-1s, us-2a), 0.1 µM of each outer primer (F3, B3), 0.8 mM dNTPs, 1 M betaine, 1 × isothermal amplification buffer (20 mM Tris–HCl, pH 8.8, 10 mM $(NH_4)_2SO_4$, 10 mM KCl, 2 mM $MgSO_4$, 0.1 % Triton X-100), 1 × EvaGreen dye (Biotium, CA) , 8 U Bst 2.0 WarmStart DNA polymerase (New England Biolabs, MA), and varying amounts of template DNA in a total volume of 20 µL. Fluorescence signal measurements were performed using a QuantStudio™ 5 Real-Time PCR System at 63 °C. The results were analysed by the provided QuantStudio™ Design & Analysis Software (Applied Biosystems). All the oligonucleotides and double-stranded DNA template were synthesized from Eurofins Scientific (Ebersberg, Germany).

For the LAMP amplification, the reaction contains 1.6 µM inner primer (FIP, BIP), 0.2 µM outer primer (F3, B3), 0.8 mM dNTPs, 1 M betaine, 1 × isothermal amplification buffer, 6 mM $MgSO_4$, 1 × EvaGreen dye, 8 U Bst 2.0 WarmStart DNA polymerase, and varying amounts of template DNA in a total volume of 20 µL. The QuantStudio™ 5 Real-Time PCR system was used to monitor the reaction at 63 °C. Template concentrations are reported as

final concentrations in the complete 20 µL reaction volume.

2.2.3 Gel extraction and sequencing

A 2 % agarose gel was prepared by dissolving 1 g of UltraPure™ Agarose (Invitrogen, Thermo Fisher Scientific, USA) in 50 mL of 1 × TAE buffer (Invitrogen, Thermo Fisher Scientific, USA). The mixture was heated in a microwave oven until completely dissolved and boiled twice. After cooling to a temperature safe to handle, 5 µL of SYBR™ Safe DNA Gel Stain (Invitrogen, Thermo Fisher Scientific, USA) was added and mixed thoroughly. The solution was then poured into a gel casting tray, and a comb was inserted to form wells. The gel was allowed to solidify at room temperature for approximately 20 min. Subsequently, 10 µL of the amplification product was mixed with 2 µL of 6× DNA loading dye, and 10 µL of the mixture was loaded into each well. Electrophoresis was performed at 100 V for 90 min. After electrophoresis, the gel was visualised using a PXi imaging system (Syngene, MD, USA).

DNA was extracted using the QIAquick Gel Extraction Kit (Qiagen, Hilden, Germany) according to the manufacturer's instructions. Briefly, the target DNA band was excised carefully from the agarose gel under blue-light illumination using a sterile blade. The gel slice was weighed, and 300 µL of Buffer QG was added per 100 mg of gel. The mixture was incubated at 50 °C for approximately 10 min until the gel was completely dissolved. Subsequently, 100 µL of isopropanol was added, and the solution was mixed thoroughly. The mixture was then transferred to a spin column and centrifuged at 13,000 rpm for 1 min. The flow-through was discarded. The column was washed with 500 µL of Buffer QG and centrifuged, followed by the addition of 750 µL of Buffer PE and another centrifugation step. Finally, nuclease-free water was added directly to the centre of the membrane, incubated briefly, and centrifuged to elute the DNA. The elution step was repeated to maximise the yield of DNA. The purified DNA fragments were subsequently submitted to Eurofins Genomics (Ebersberg, Germany) for Sanger sequencing analysis.

2.2.4 Data analysis

Time-to-positive (TTP) values were automatically calculated by the instrument software from the real-time fluorescence amplification curves. Unless otherwise stated, experiments were performed in triplicate, and individual data points are presented. Target concentrations are reported as copies/µL, with the corresponding copy number per reaction calculated based on the addition of 2 µL of template to each 20 µL reaction. Throughout this thesis, single measurements (n = 1) are presented without error bars. For n = 2, data are presented as individual replicates or mean values, with error bars indicating the range where applicable.

For $n \geq 3$, error bars represent standard deviation (SD), unless otherwise stated.

2.3 Results and discussion

The abstract model-based isothermal amplification (ABM) is based on the hairpin-mediated nucleic acid isothermal amplification mechanism, enabling fast amplification by introducing a universal sequence (us) at each end of the inner primer. The amplification system contains two inner primer, us-1s and us-2a; two outer primers, F3 and B3. The letters ”s” and ”a” in this chapter represent the sense and antisense strands in the primer name, respectively.

As illustrated in Figure 2-2, the hairpin structure intermediate (us+1s+2s+ua) acts as functional building block for amplification. In the presence of the target ”F3-1s-2s-B3s”, the primer us-2a will first hybridise with the target strand and be extended by DNA polymerase. Subsequently, primer B3 hybridises to the target and displaces the newly synthesised us-2a strand. A similar strand-displacement process occurs following the binding and extension of primers us-1a and F3. After that, the newly synthesised strand ”us-1s-2s-ua” is able to self-fold into a hairpin structure. In this case, the newly exposed domain 2a in the loop will serve as an initial site for primer us-2a hybridisation and extension, resulting in the formation of a double-stranded DNA (dsDNA) structure. The newly synthesised duplex, us+1s+2s+ua, contains complementary domains that allow each strand to fold into a hairpin. This intramolecular self-folding is proposed to promote disassembly of the duplex, generating two hairpin products with exposed primer-binding sites. The exposed primer site on the loop of the hairpin will then recruit more primers for further extension. Therefore, amplification is achieved through repeated cycles of self-folding, primer binding, and DNA polymerase-mediated strand extension.

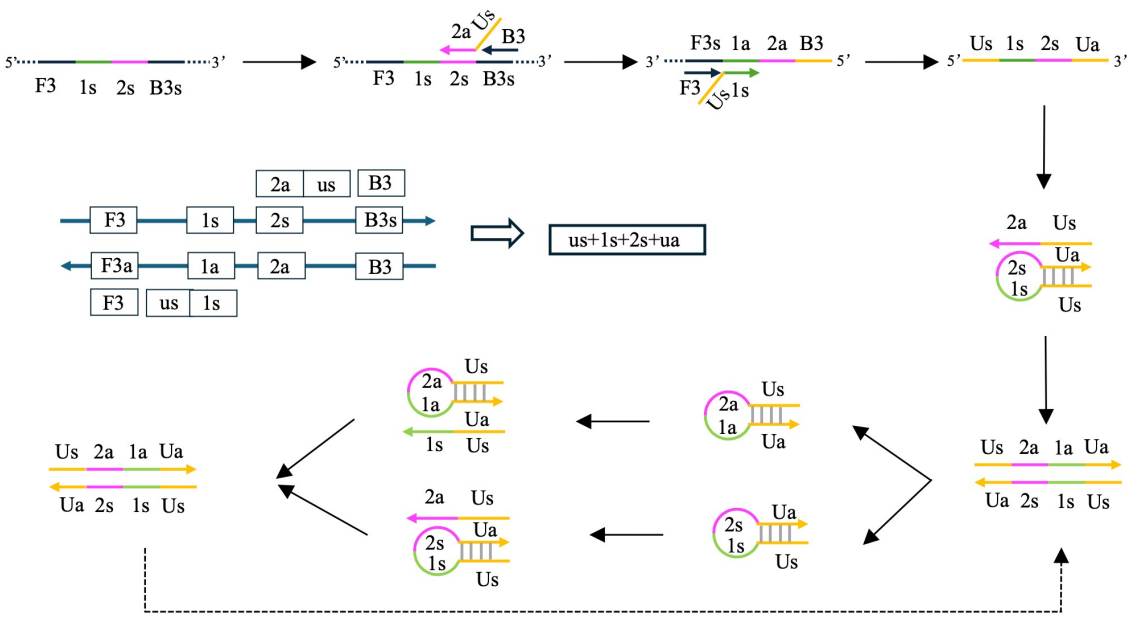


Figure 2-2: Schematic of ABM isothermal amplification. Initially, primer us-2a hybridises to the 2s region of the target, followed by B3 binding to B3s and strand displacement. Subsequently, primers us-1s and F3 bind to the complementary strand, respectively, generating a single-stranded DNA product that can fold into a hairpin structure. The exposed loop regions (2s or 1a) provide binding sites for us-2a or us-1s, respectively, enabling further primer extension and duplex formation. The resulting duplex is proposed to regenerate hairpin structures, allowing repeated amplification cycles.

2.3.1 Primer design and selection

The primers were generated by the Primer design software. As depicted in Figure 2-1, the software has found 697 candidate primer sequences for the 1s and 1a regions. Among the first 11 batch primer sets, the us-1s primer remained unchanged, whereas the us-2a primers differed by only a few nucleotides. Three us-2a primers with the greatest sequence differences were selected: us-2aa, us-2ab, us-2ac, together with us-1s for the experimental test. This allowed an initial evaluation of whether small changes in the us-2a binding region could influence amplification efficiency.

To further verify the functionality of the outer primers F3 and B3, a conventional LAMP assay targeting the same sequence was designed and tested. In Figure 2-3, all three ABM primer sets were capable of generating amplification signal. However, the non-template control (NTC) in Figures 2-3a, b exhibited clear amplification, indicating that the signals generated by us+2aa and us+2ab were not target-specific. In contrast, the primer set containing us+2ac amplified in the presence of target DNA, while no amplification was observed in the NTC during the experimental period. Under these initial screening conditions, us–2ac therefore showed a clearer separation between the target-containing reactions and the NTC than us+2aa and us+2ab. The LAMP assay shown in Figure 2-3d also amplified in the pres-

ence of target DNA, supporting the functionality of the selected outer primers F3 and B3 in a conventional LAMP system. However, this result does not directly establish their functionality within the proposed ABM amplification mechanism. LAMP was included as a reference control at 10^6 copies/µL and was therefore not tested across the same concentration range during this initial screening experiment. Although us+2ac showed the best initial separation between target and NTC, this single screening experiment was not sufficient to establish assay reliability. Also, the Therefore, the selected primer set was further evaluated across a wider concentration range and in repeated experiments. Initial screening and optimisation experiments were performed in duplicate to enable efficient comparison of a large number of reaction conditions, while key experimental conditions were subsequently validated with additional replicates. Overall, the initial screening results were considered preliminary, and no conclusive evidence of reliable target-specific amplification was established from these experiments.

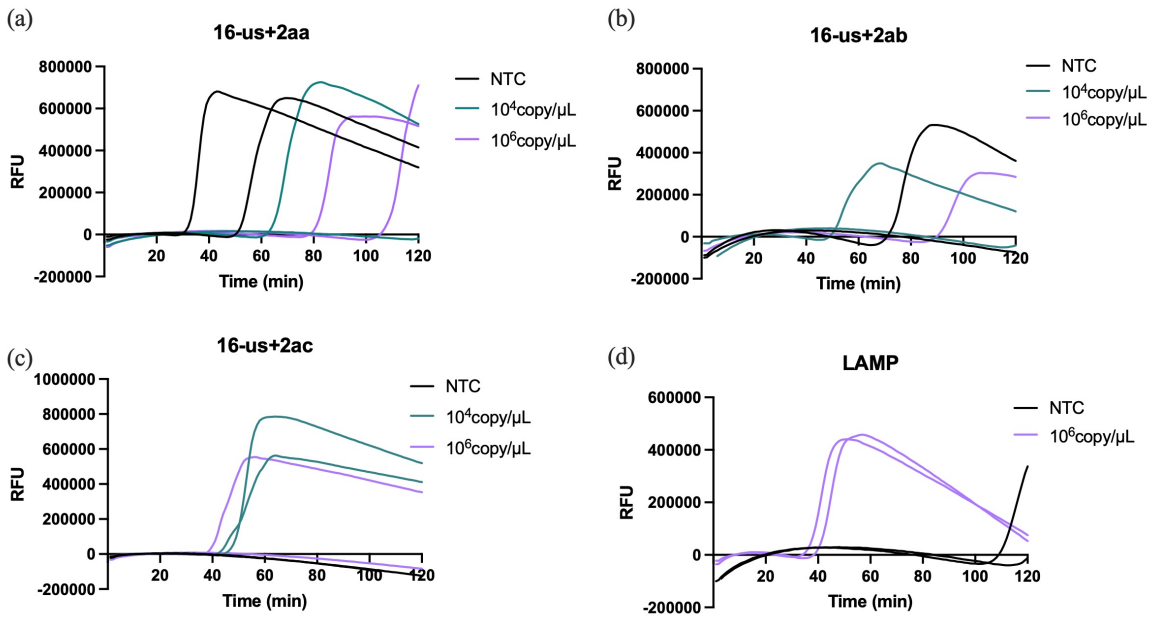


Figure 2-3: Screening of candidate primers for the ABM system. (a–c) Real-time amplification curves using three candidate primers (us-2aa, us-2ab, and us-2ac) together with F3, B3, and us-1s. (d) Conventional LAMP amplification using F3, B3, FIP, and BIP as a positive control for validating F3 and B3. NTC: non-template control. RFU: relative fluorescence unit. n=2.

The amplification behaviour was then evaluated using the selected primer set us-1s and us-2ac (Figure 2-4). The time to positive (TTP) was automatically calculated by the instrument software. A TTP cutoff of 120 min was empirically selected based on the onset of amplification observed in the no-template controls (NTCs). Nevertheless, this cutoff was not statistically established and therefore could not reliably distinguish target-specific amplification from non-specific amplification. Amplification was observed across a wide range of target concentrations, but the absence of a concentration-dependent response and the occurrence of

NTC amplification prevented these signals from establishing target-specific analytical sensitivity. However, results at such a low copy number should be interpreted with caution, as stochastic sampling and pipetting variation can affect the actual number of target molecules present in each reaction[130].

Furthermore, several reactions at higher target concentrations, such as 10^3 and 10^4 copies/µL (2×10^4 and 2×10^5 copies/reaction, respectively), showed amplification after 120 min, whereas some reactions at lower concentrations showed shorter TTP values than those at 10^6 copies/µL (2×10^7 copies/reaction). Overall, TTP did not show a clear correlation with target concentration, although higher target concentrations would generally be expected to result in shorter TTP. Therefore, the analytical sensitivity of the assay could not be established under the tested conditions. Further validation with a larger number of NTC replicates would therefore allow a more robust cutoff to be established. Subsequent experiments focused on a narrower concentration range of 10^3–10^5 copies/µL (2×10^4–2×10^6 copies/reaction).

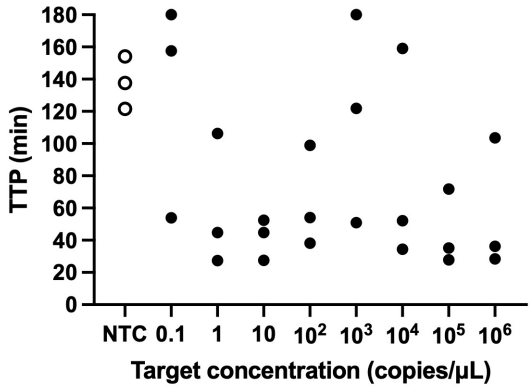


Figure 2-4: Evaluation of the analytical performance of the ABM system using the us-2ac primer set. Time-to-positive (TTP) values obtained from reactions containing HPV16 DNA concentrations from 0.1 to 10^6 copies/µL and no-template controls (NTC). n=3.

To further investigate the amplification product, three concentrations from 10^5 to 10^3 copies/µL were used (Figure 2-5). The 10^5 concentration amplified consistently in both replicates. In contrast, the 10^3 concentration showed large variation, with one replicate amplifying at a similar time to the 10^5, while the other amplified close to the NTC. Unexpectedly, no amplification was observed for the 10^4 concentration, which was considered a technical failure or assay variability and should be repeated before exclusion. Melting curve analysis showed that all amplified samples had similar melting temperatures (Figure 2-5b), suggesting that the amplified products were likely to have similar composition. A low-temperature melting peak was observed for the 10^4 sample at a similar temperature to the NTC. As no clear amplification product was observed for this sample, this peak was considered more likely to arise from background or non-specific products rather than the expected ABM product. However, the melting curves alone cannot confirm whether the products were the expected ABM amplification intermediates. To further analyse the amplification products, agarose gel

electrophoresis was performed (Figure 2-5c). Based on the proposed ABM mechanism, the functional hairpin intermediate "Us–1s–2s–Ua" was expected to have a size of approximately 102 bp. A distinct band near 100 bp was observed in all amplified samples. In addition, several higher-molecular-weight bands were observed above the expected 100 bp product. These larger products may form from further extension and assembly of the hairpin intermediates by polymerase during amplification[5].

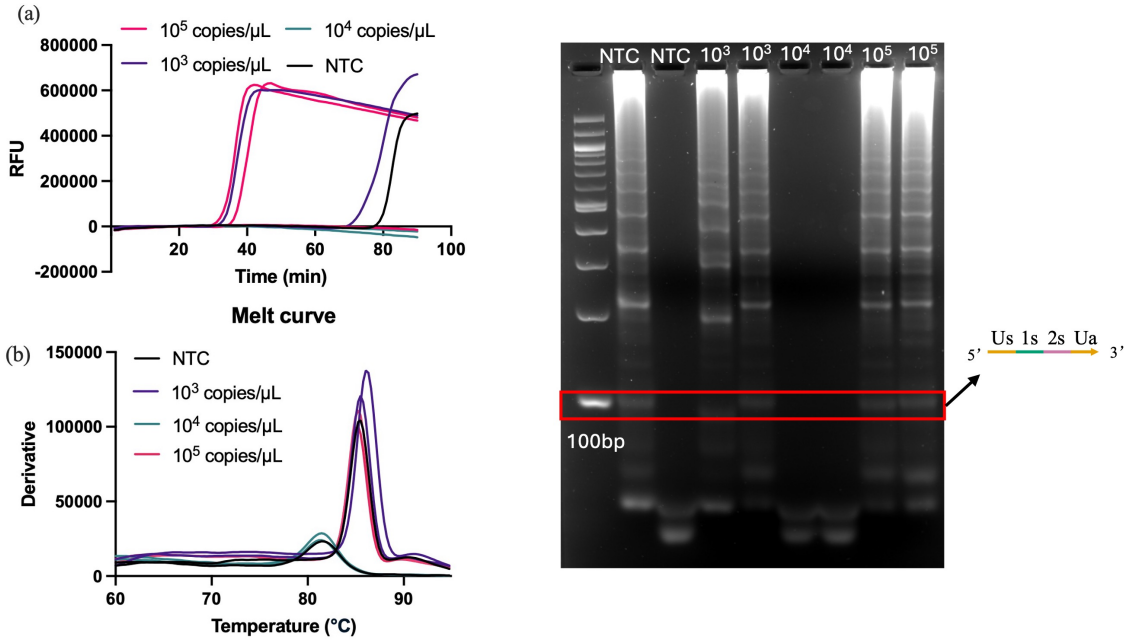


Figure 2-5: Verification of the ABM amplification products. (a) Real-time amplification curve of different concentrations of target. (b) Melting curve of (a). n=2. (c) Agarose gel electrophoresis. The band shown at approximately 100 bp (red box) indicates a band migrating near the predicted size of the "us–1s–2s–ua" intermediate product.

Subsequently, the 10^3 concentration was chosen to test the reproducibility of the ABM system. Four independent experiments were performed, including replicates conducted on the same day and on different days, using the same reaction conditions (Figure 2-6). However, the variation was significant. Amplification was detected in 6 out of 12 target groups, while amplification was also observed in 4 out of 12 NTC groups. The results indicate that amplification at 10^3 concentration was unstable; although amplification can be detected, the large variation between experiments and the occasional amplification of NTC made it difficult to reliably distinguish true positive signal from non-specific signal. This suggests that 10^3 concentration may be close to the edge of differentiating NTC and target signal.

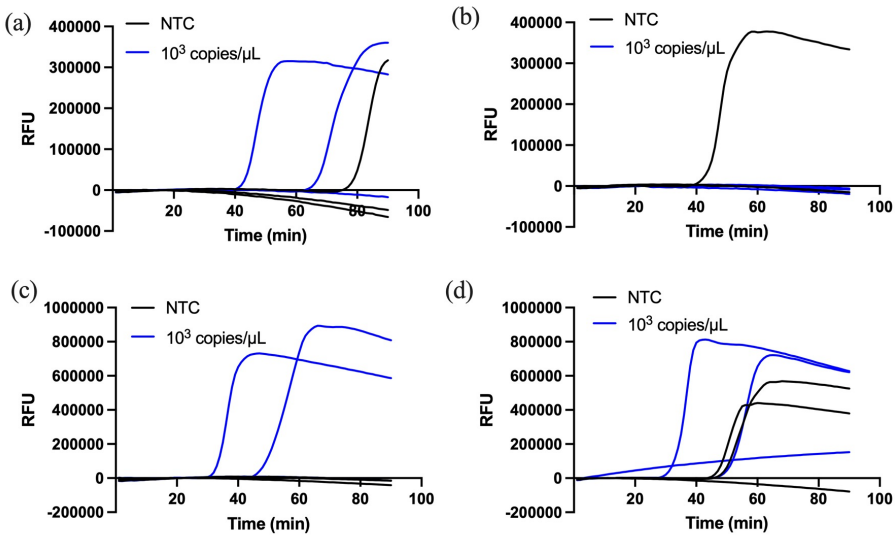


Figure 2-6: Reproducibility test of ABM system. (a–d) Amplification curves obtained from four independent experiments using HPV16 DNA (10^3copies/µL) and no-template controls (NTC). n=3.

2.3.2 Optimisation of ABM amplification

Because the selected primer set showed poor reproducibility and occasional NTC amplification, optimisation was performed to determine whether these issues could be improved. Reaction conditions, primer concentration, reaction additives, polymerase choice, and primer sequence design were evaluated, as these factors may affect primer binding, strand-displacement amplification, and the formation of non-specific primer dimers.

Reaction temperature was first investigated because it can influence primer hybridisation and polymerase extension, thereby affecting both amplification efficiency and specificity. In strand-displacement isothermal amplification, the optimal temperature generally reflects a balance between efficient primer binding and polymerase extension, while lower temperatures may also favour non-specific *Bst*-mediated amplification[131]. However, hairpin stability does not necessarily correlate directly with amplification efficiency, as primer hybridisation and polymerase activity are also temperature-dependent. LAMP can be relatively tolerant to changes in reaction temperature. François et al. reported that LAMP maintained high specificity and similar performance over a relatively broad temperature range of 57–67 °C[132]. Although ABM has a different amplification pathway from LAMP, it similarly relies on the formation of functional structures and *Bst*-mediated strand-displacement extension[5]. In Figure 2-7a, both NTC reactions amplified earlier than the target reactions at 60 °C, indicating substantial target-independent amplification under this condition. This behaviour is consistent with previous observations that non-specific *Bst*-mediated DNA synthesis can be favoured at lower reaction temperatures[131]. At 63 °C, both target reactions amplified, while

no NTC amplification was observed within the experimental period. However, NTC amplification was still observed inconsistently at 65 °C and 68 °C. Thus, increasing the reaction temperature did not progressively improve assay specificity. Although 63 °C provided the clearest separation between target and NTC reactions among the conditions tested, the absence of a consistent temperature-dependent trend suggests that multiple factors may contribute to the observed amplification behaviour. Further investigation would be required to determine whether hairpin formation contributes to the NTC amplification.

Primer concentration was subsequently investigated because it can directly influence amplification kinetics and the likelihood of non-specific primer interactions. In hairpin-based isothermal amplification, increasing primer concentration can accelerate amplification while excessive primer concentrations may also promote primer cross-talk and non-specific amplification[133]. Primer concentration was tested subsequently (Figure 2-7b). Increasing the concentration of both primers from 1x to 1.5x and 2x resulted in earlier amplification of both target and NTC. This suggests that increasing primer concentration enhances overall amplification but does not improve specificity. To further test the contribution of individual primer, the us-1s and us-2a concentrations were reduced to 0.5x accordingly. When the concentration of us-1s was reduced, no target amplification was observed, whereas amplification remained detectable in the NTC. This suggests that the amplification behaviour was sensitive to the concentration of us-1s, although its specific contribution to the proposed ABM amplification pathway could not be established. In contrast, decreasing us-2a slightly delayed amplification but without specific improvement. This result suggested that reducing the primer concentration alone could not eliminate NTC amplification. The NTC signal was still observed when the concentration of us-1s was reduced, suggesting that non-specific amplification may be generated from partial primer extension products or asymmetric primer reactions rather than the expected ABM pathway.

Chemical additives show promise to improve amplification efficiency, especially in eliminating non-specific amplification[62]. Tetramethylammonium chloride (TMAC)[134] and formamide (FA)/N,N-dimethylformamide (DMF)[135] have been reported to suppress non-specific amplification, whereas pullulan[136] and guanidine chloride (GnCl)[137] are commonly used to enhance amplification efficiency. Therefore, TMAC, FA/DMF and pullulan were expected to improve the separation between target and NTC reactions by suppressing background amplification, whereas guanidine hydrochloride was expected to accelerate amplification. However, none of the additives produced the expected improvement in the ABM system (Figure 2-7c). For both TMAC and FA/DMF, the NTC group amplified earlier than the target group, indicating that the reported suppression of non-specific amplification did not translate to the ABM system under the conditions tested. Pullulan and GnCl appeared to reduce variation between replicates, although amplification was still observed in the NTC. Among the additives tested, GnCl showed the greatest effect on reaction kinetics, resulting in shorter

TTP for both target and NTC. This result is consistent with its reported acceleration effect in LAMP, but indicates that the enhancement in ABM was not selective for target-dependent amplification[137]. Therefore, while some additives influenced amplification behaviour, none substantially improved assay specificity.

Previous comparisons of Bst polymerase variants have shown differences in amplification speed and activity between Bst LF and Bst 2.0[138]. Bst 2.0 and Bst LF were therefore compared to determine whether polymerase choice could improve the separation between specific and non-specific ABM amplification. (Figure 2-7d). Bst LF showed a modestly shorter target TTP and a slightly greater separation between target and NTC reactions, although the overall difference between the two polymerases was limited. The limited difference between the two enzymes suggests that polymerase choice was not a major determinant of the observed NTC amplification. Bst LF was nevertheless selected for subsequent experiments because it provided a slightly greater separation between target and NTC reactions.

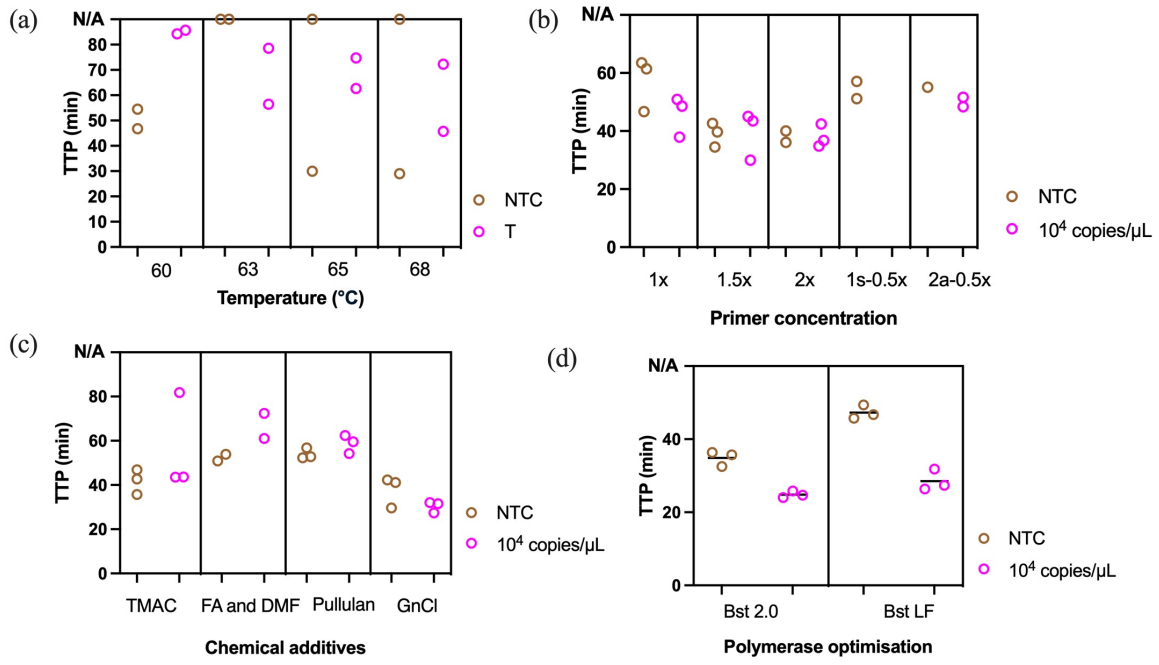


Figure 2-7: Optimisation of the ABM system.
(a) Temperature optimisation. n=2. (b) Primer concentration optimisation. n=3. (c) Effect of chemical additives. n=3. (d) Effect of polymerase. n=3.

The ratio between us-1s and us-2a was further investigated because both primers contribute to the formation and subsequent amplification of the functional hairpin products in the ABM pathway. The original ABM study also identified primer concentration as an important optimisation parameter[5]. Therefore, altering the relative concentrations of main primers us-1s and us-2a was expected to change the balance between target specific amplification and non-specific amplification, potentially improving the separation of TTP between target and NTC reactions. Several primer ratios were initially screened (Figure 2-8). NTC can still be

observed under all the tested conditions. Although some primer ratios show slightly better separation between target and NTC, no clear trend can be determined. Based on the Figure 2-8a results, the ratios 1.2:0.4, 1:0.5 were selected for multiple independent tests (Figure 2-8b). However, the TTP from the target and NTC still largely overlapped, and the improvement shown in the initial screening cannot be reproduced. This lack of reproducibility made it difficult to determine whether the observed differences were caused by the primers themselves or by normal experimental variation between runs. Overall, the persistence of NTC amplification across all tested conditions indicates that non-specific amplification is likely associated with the amplification mechanism itself rather than primer concentration balance alone.

The non-specific amplification observed in the NTCs may share similarities with leakage reactions reported in DNA logic circuits, particularly those involving hairpin-mediated strand displacement[139]. In these systems, unintended interactions between DNA strands or spontaneous opening of hairpin structures can initiate reactions in the absence of the intended trigger, resulting in background signals[140]. A similar mechanism may contribute to the NTC amplification observed in this study. Unintended hairpin structures formed by primers or primer-derived extension products could potentially provide sites for further primer binding and Bst-mediated strand-displacement synthesis, leading to non-specific amplification. This hypothesis is consistent with the observed NTC amplification and the presence of primer-related sequences in the sequencing results.

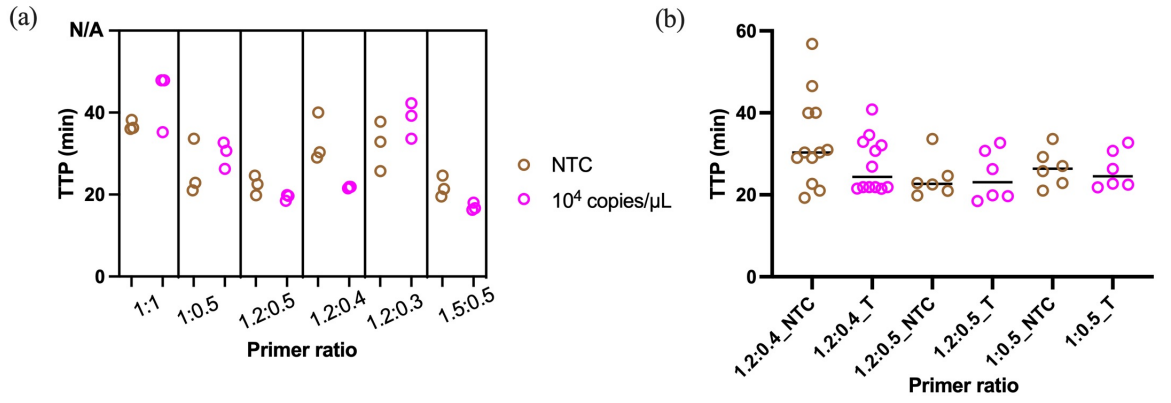


Figure 2-8: Optimisation of primer ratios in the ABM system. (a) Initial screening of different primer ratios using HPV16 DNA (10^4copies/µL) and NTCs. (b) Reproducibility assessment of selected primer ratios based on multiple independent experiments. Each point represents one experimental replicate.

As optimisation of reaction temperature, primer concentration, chemical additives, polymerase and primer ratio did not consistently suppress NTC signal or improve the separation between target and NTC reactions, the primer sequences were subsequently examined to determine whether intrinsic primer–primer interactions contributed to the background ampli-

fication. This analysis was intended not only to improve the current assay, but also to identify sequence-dependent factors that may inform future ABM primer design. After analysis of the selected primer pair, it reveals that us-1s and us-2a primers contained a 6 bp complementary region with a predicted heterodimer free energy ΔG of -9.92 kcal/mol (Figure 2-9), suggesting a relatively high risk of primer crosstalk as a result of non-specific amplification.

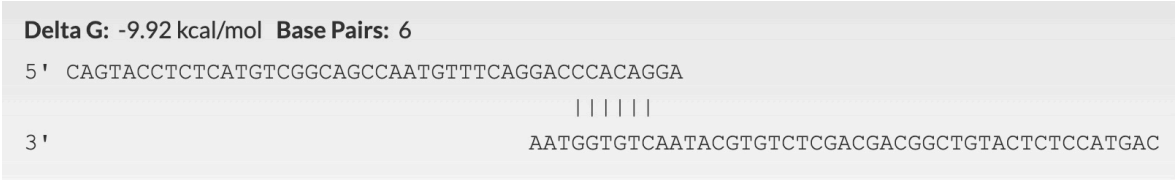


Figure 2-9: Heterodimer analysis of us-1s and us-2ac by Oligo Analyzer.

Single-base mismatches are known to alter the thermodynamic stability of DNA duplexes, although the magnitude of destabilisation depends on the mismatch type and surrounding sequence[141]. Intentional mismatches have also been incorporated into LAMP and allele-specific amplification primers to modulate duplex stability and suppress undesired primer extension, demonstrating that controlled mismatch introduction can be used as a strategy to enhance amplification specificity[142]. Therefore, a single mismatch was introduced within the complementary region to reduce the predicted stability of the primer heterodimer while also maintaining efficient primer binding to the target. As shown in Table 2-2, the three mismatch designs reduced primer–primer complementarity from 6 bp to 3–4 bp and increased the predicted heterodimer ΔG from -9.92 kcal mol^{-1} to between -6.21 and -8.09 kcal mol^{-1}. In contrast, the predicted target-binding free energy was only moderately changed, from -45.43 kcal mol^{-1} to between -43.29 and -44.23 kcal mol^{-1}. These predictions therefore suggested that the mismatch designs preferentially weakened primer–primer interaction while largely maintaining target binding. However, this predicted improvement was not reflected consistently in the experimental results. As shown in Figure 2-10, NTC remained detectable for the mismatch-modified primer sets, and the TTP of the target and NTC reactions were not consistently separated. Therefore, reducing the predicted stability of the us-1s/us-2a heterodimer alone was insufficient to eliminate background amplification.

Table 2-2: Effect of primer mismatch on heterodimer and target binding affinity

Primer name	1s	1a	Base Pairs	ΔG of Heterodimers (kcal mol^{-1})	ΔG of target+1s+2a (kcal mol^{-1})
Original	us-1s	us-2a	6	-9.92	-45.43
1-3C	3A to 3C	us-2a	3	-6.21	-44.23
1-5C	5A to 5C	us-2a	3	-6.68	-43.29
2-4G	us-1s	4T to 4G	4	-8.09	-44.23

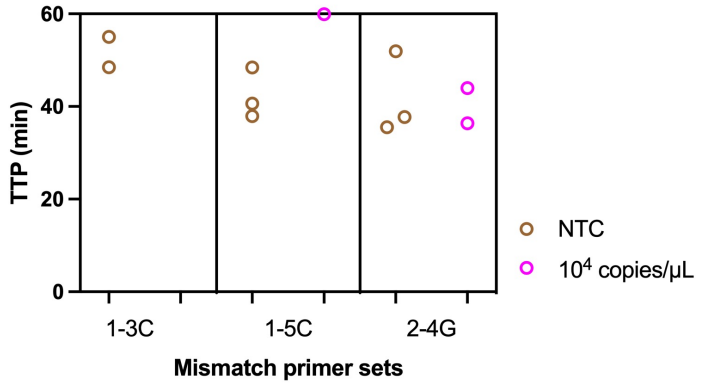


Figure 2-10: Evaluation of mismatch-modified primer sets, TTP values using different primer sets with intentional single-base mismatches designed to reduce primer-dimer formation. n=3.

As the mismatch of primers did not improve assay specificity, the primer design was re-examined. Analysis of the target sequence shows several repeating sequence regions (Figure 2-11). The original primer set (1s and 2ac) partially overlapped with these regions, which typically increase the non-specific amplification. This is because us-1s and us-2ac bind opposite strands, primers designed against similar sequence motifs can contain complementary sequences after reverse-complement conversion. Such primer–primer complementarity, particularly when thermodynamically stable, can promote heterodimer formation and subsequent non-specific amplification[143]. Therefore, alternative primer-binding positions were selected outside these repeated regions. To avoid these repeated regions, a shortened version of us-1s (1s-short) was designed and combined with four alternative us-2a primers (2d, 2e, 2f, 2g) selected from the primer candidates (Table 2-3). These primer sets were chosen because they avoided the repeated sequence regions and had fewer complementary base pairs and lower predicted heterodimer stability than the original primer set.

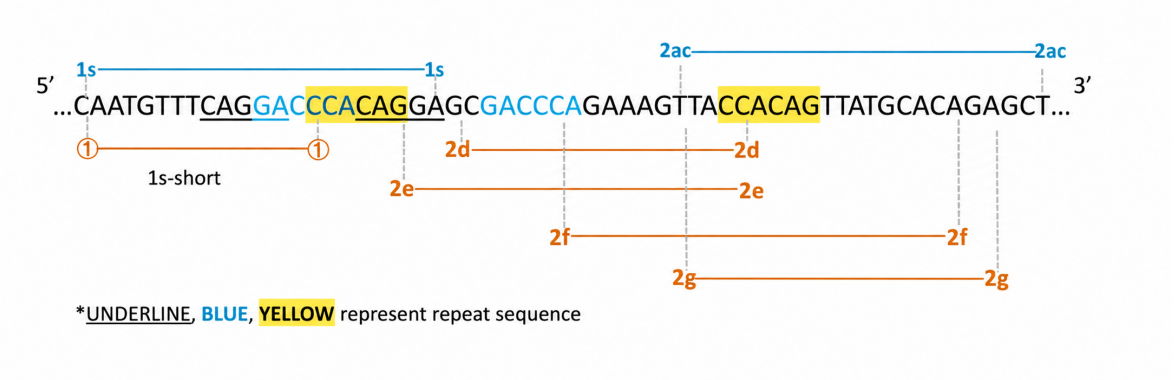


Figure 2-11: Primer sequence optimisation. The positions of primer regions 1s and 2ac, together with the alternative designs (1s-short and 2d–2g), are indicated by horizontal lines along the target DNA sequence (5′–3′). Vertical dashed lines mark the boundaries of the primer-binding regions. Underlined, blue-coloured and yellow-highlighted sequences indicate repeated sequence motifs.

Table 2-3: Design of alternative primer binding positions to minimise heterodimer formation.

Primer set	Position	Base Pairs	ΔG of Heterodimers (kcal mol^{-1})
us-1s, us-2ac	1-20; 36-58	6	-9.92
us-1s-short, us-2ad	1-16; 23-40	3	-6.21
us-1s-short, us-2ae	1-16; 20-40	3	-6.21
us-1s-short, us-2af	1-16; 29-53	3	-6.35
us-1s-short, us-2ag	1-16; 36-55	3	-6.21

These new primer sets were first evaluated (Figure 2-12). The newly designed primer sets generally produced longer TTP than the original. This suggests that avoiding the repeated regions and reducing heterodimer formation may have in some extent slowed the overall amplification. Among these, the us-1s-short + us-2ad and us-1s-short + us-2af primer sets performed better than the original primer set (us-1s, us-2ac). The us-2af primer set showed a larger difference in TTP between the target and NTC, while no NTC amplification was observed for us-2ad during the initial screening. In contrast, the other primer sets still showed similar TTP for target and NTC. Based on these results, the us-2ad and us-2af primer sets were selected for further testing (Figure 2-12b). However, the target and NTC still showed a large degree of overlap. Although some target samples amplified earlier than the NTC, the overall variation between repeats was still quite high. Since repeated primer redesign and optimisation failed to consistently improve specificity, sequencing analysis was performed to investigate the sequence component of the amplification products.

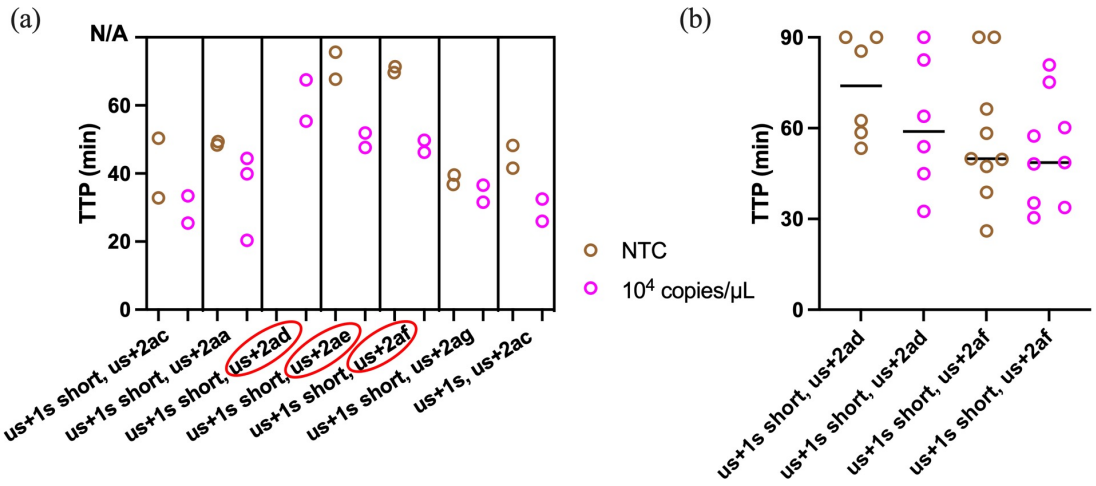


Figure 2-12: Alternative primer combination test. (a) Screening of different primer combinations using shortened Us+1s (Us+1s short) and alternative Us+2 primers, with full-length Us+1s combinations included for comparison. n = 2. (b) Repeat testing of the selected primer combinations (Us+1s short/Us+2ad and Us+1s short/Us+2af) across multiple independent experiments. Each point represents one experimental replicate and the horizontal line indicates the median TTP value.

2.3.3 Sequencing analysis

Despite multiple rounds of optimisation, non-specific amplification was still observed in the ABM amplification. Sequencing was considered to identify the products. To obtain preliminary sequence information on the ABM amplification products, Sanger sequencing was selected as an accessible and relatively simple method requiring minimal additional library preparation. Two sample preparation approaches were evaluated. First, purified whole-reaction products were sequenced directly. Second, the major DNA bands were excised from the agarose gel and purified before sequencing.[144] Gel purification was included to reduce interference from residual primers, short fragments, and amplification products of different sizes, and to determine whether selection of a defined product-size range could improve sequence quality.

us-1s was used as the sequencing primer (Figure 2-13). Based on the design, the ideal amplicons should contain specific region - highlighted in green. However, in the given results, only around 80 bp could be read reliably. This may reflect the heterogeneous and repetitive nature of the amplification products, although mixed templates, product secondary structures and sample purity may also have contributed to the reduced sequencing quality. Such repetitive amplicons are known to be challenging for Sanger sequencing and often result in limited read lengths and poor sequence resolution.[145]

As us-1s was used as the sequencing primer, the expected sequence immediately downstream of the primer was the 13-nt target-specific region, followed by the 2s-1a region, as shown in the ideal amplicon in Figure 2-13. However, the confidently readable sequences obtained from both the 10^4-copy target reaction and the NTC aligned mainly with the 2s-1a region, while the target-specific region could not be identified. There are two possible explanations for this result. First, the target-specific region was located immediately downstream of the sequencing primer. Sanger sequencing commonly produces low-quality sequence within the first 15–40 bases of a read, and therefore this short region (13 nt) may not have been reliably resolved.[146] Second, the sequenced products may have been primer-derived products that lacked the target-specific region, resulting in the recovery of only the 2s-1a sequence. The detection of a similar 2s-1a sequence in the NTC is consistent with the latter possibility. However, because of the poor sequence quality close to the primer-binding site, these Sanger sequencing results could not distinguish conclusively between the two explanations or confirm the presence of the complete expected amplicon.

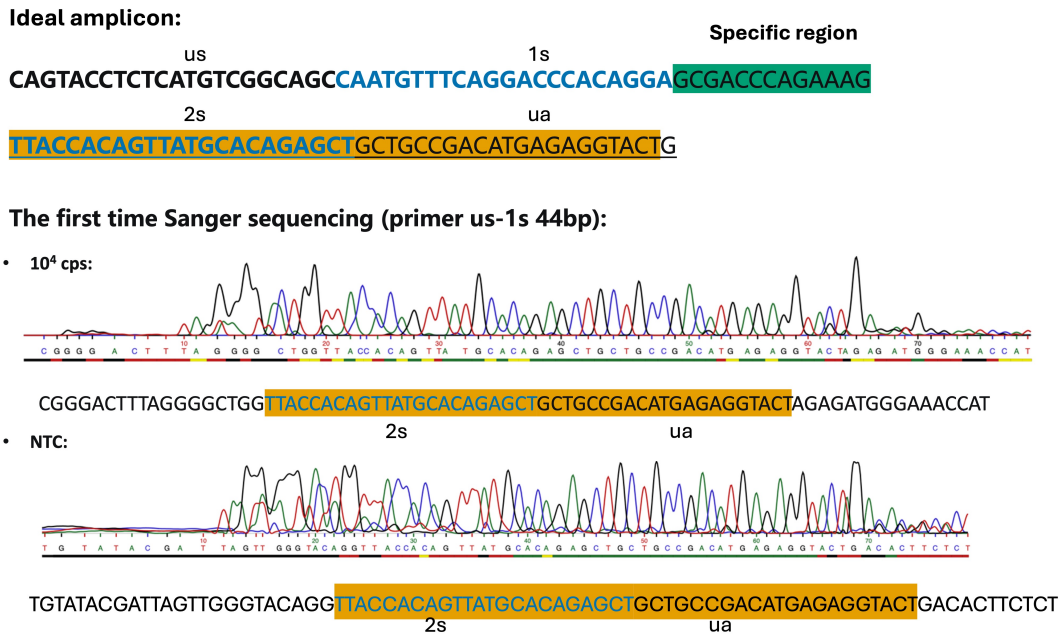


Figure 2-13: The first Sanger sequencing results. The upper panel shows the expected ABM amplicon sequence, with the primer-derived regions (us, 1s, 2s and ua) and the target-specific region indicated. The lower panels show Sanger sequencing chromatograms and corresponding sequences of amplification products obtained using the 44 bp us-1s primer. Orange highlighting indicates sequences matching the expected 2s and ua regions. Both products contained these regions, whereas the expected target-specific sequence was not confirmed.

To obtain cleaner and less complicated products for sequencing, certain bands were cut from the agarose gel, extracted, purified, and sent for the second round of sequencing. Three distinct bands from the target group were cut independently for Sanger sequencing (Figure 2-14). The shorter us primer was used to move the sequencing start site further upstream and potentially improve recovery of the target-specific region. Despite differences in the molecular weights, all the bands generated highly similar sequencing results. As no substantial differences were observed among the three target bands, only the lowest molecular weight band is presented as a representative example (Figure 2-15) with the NTC band. Because the predicted ideal amplicon structure, sequencing with the us primer could theoretically generate reads in either direction, corresponding to 1s–target-specific region–2s–ua or 2a–complementary target-specific region–1a–ua. However, the readable sequence from the target band aligned mainly with 1a followed directly by ua, whereas the NTC read contained a 1a-related sequence without a confidently identifiable downstream ua region.

Neither result matched a complete expected sequencing path. The recovery of primer-derived regions without a clear target-specific sequence was consistent with the presence of incomplete, rearranged, or mixed amplification products. Direct Sanger sequencing produces a combined signal from all templates in the sample and therefore cannot reliably resolve the structures of individual products in a mixed population[147]. In addition, gel purification sep-

arates DNA mainly by size and does not ensure that all molecules within one band have the same sequence. Therefore, similarly sized products may still have been present in the excised bands and may have caused the partial or mixed sequencing results.

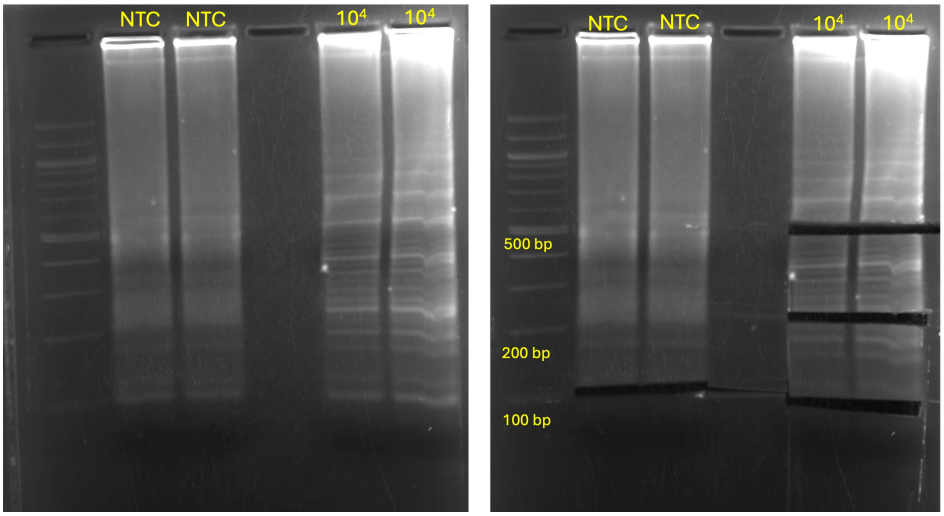


Figure 2-14: Agarose gel of the amplification product. The left panel shows the original gel, while the right panel indicates the fragments cut for Sanger sequencing.

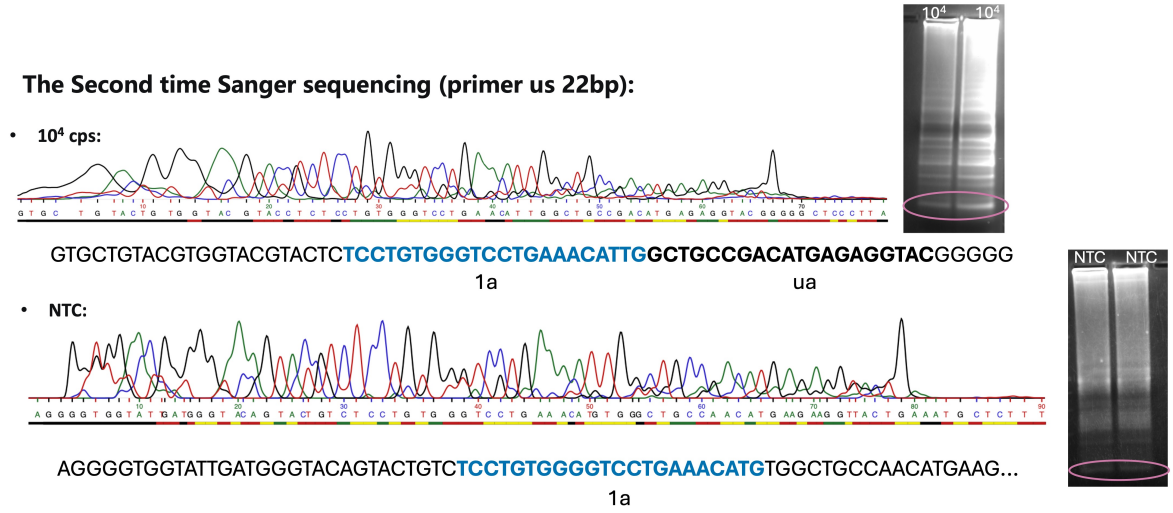


Figure 2-15: The second Sanger sequencing of the cut band. Sanger sequencing analysis of gel-excised amplification products. Sanger sequencing chromatograms and corresponding sequences of products generated using the 22 bp us primer.

Overall, the sequencing results suggested the possible presence of primer-derived amplification products rather than the expected target-specific amplicons. However, the repetitive nature of the sequences and the limited resolution of the Sanger sequencing data prevented definitive identification of the amplification products. This may explain why non-specific amplification persisted throughout the optimisation process and why it remained difficult to distinguish the target group from the NTC group. Although the sequencing experiments were

intended to determine whether the amplification products corresponded to the expected sequences, the results remained inconclusive due to the repetitive sequences and insufficient resolution. Therefore, the complete structures and origins of the amplification products could not be reliably established. In future work, cloning of individual products or high-throughput sequencing could be used to further identify the structures and relative abundance of the different amplification products, providing a clearer understanding of the non-specific amplification pathways in the ABM system. Cloning would isolate individual products and reduce the mixed signals observed during direct Sanger sequencing. Previous studies have used restriction digestion, gel purification or cloning to obtain more uniform fragments before Sanger sequencing[148]. High-throughput sequencing would provide sequence information from a much larger number of individual molecules and could therefore distinguish target-derived products from different primer-derived or non-specific products and estimate their relative frequencies.[149 150]

2.4 Conclusion

This chapter systematically investigated the applicability of the previously reported ABM strategy to HPV16 detection. A series of primer designs and reaction conditions were evaluated to investigate their effects on amplification performance and target specificity. Although amplification signals were observed under several conditions, the lack of clear discrimination between target and non-target control indicated that target-specific amplification was not established. The optimisation experiments further highlighted the persistence and variability of non-specific amplification, suggesting that changes in reaction conditions alone were insufficient to reliably suppress background amplification. In addition, sequencing analysis was performed to investigate the identity of the amplification products, although the repetitive nature of the sequences limited their interpretation. Overall, this study provides an experimental evaluation of the ABM strategy for HPV16 detection and suggests that the tested primer designs and reaction conditions were not sufficient to achieve reliable target-specific amplification. However, these findings do not exclude the possibility that alternative primer designs and target selection could enable successful HPV16 detection using the ABM strategy.

Several practical design considerations for ABM assays can therefore be developed from this study. First, amplification products should be verified at the sequence level early during assay development, as the presence of a strong amplification signal does not necessarily confirm formation of the intended target-specific product. Second, optimisation should focus on the separation between target and NTC reactions rather than amplification speed alone, since several conditions accelerated both specific and non-specific amplification. Third, predicted primer heterodimer stability should not be used as the only criterion for primer selection, as

reducing primer complementarity did not consistently eliminate NTC amplification. Finally, target sequence, primer and reaction conditions should be considered together, since modification of individual reaction parameters alone was insufficient to achieve reliable specificity.

Overall, the ABM system was capable of generating amplification products and showed some features consistent with the proposed self-folding amplification mechanism. However, persistent target-independent amplification limited its reliability for diagnostic detection in its current designed form. The previously reported ABM system achieved miRNA detection down to 2 fM and demonstrated applications to viral nucleic acid detection. In contrast, the present HPV16 did not establish target-specific amplification, highlighting the challenges of transferring this strategy to a different target rather than indicating a general limitation of ABM. A key learning from this chapter is that amplification efficiency should not be evaluated independently of amplification fidelity. For self-folding isothermal amplification systems, product identity should be confirmed alongside reaction optimisation to ensure that the observed signal originates from the intended amplification pathway. It should be noted that a positive control reproducing the previously reported ABM system was not included in this study. Therefore, no definitive conclusion can be drawn as to whether the lack of target-specific amplification resulted from limitations in the selected target and primer design or from differences in the experimental conditions compared with the original study. Future work should include replication of the previously validated ABM system as a positive control to distinguish between these possibilities.

Chapter 3

Development of a CRISPR/Cas12a-integrated Loop Amplification Assay for multiplex HPV detection

3.1 Introduction

Accurate multiplex HPV detection can improve diagnostic efficiency by enabling detection of multiple HPV genotypes in a single reaction. This reduces the need for multiple individual tests and consequently decreases the overall cost and sample consumption, as separate singleplex assays require the clinical sample to be divided among several reactions. These advantages are particularly important for population screening in resource-limited areas, where reducing reagent use, testing cost, and sample requirements is highly desirable.[52]

However, existing multiplex LAMP assays often require a large number of primers, with 4 to 6 primers typically needed for each target. Therefore, a triplex LAMP assay may require approximately 12 to 18 primers in a single reaction, increasing the number of possible primer interactions and the need for careful optimisation.[151] Nevertheless, successful multiplex LAMP has been reported, including triplex LAMP assays and five-target detection using digital LAMP with amplification curve analysis.[152,153] These studies demonstrate that a large number of primers does not inherently prevent multiplex detection. Therefore, exploring amplification strategies that require fewer primers may provide an alternative approach to simplifying assay design, while their effects on specificity and multiplexing performance require experimental evaluation.

CRISPR-based detection platforms provide specificity, they heavily rely on indiscriminate

trans-cleavage for signal output.[9] For example, SHERLOCKv2 achieved four-target multiplex detection using orthogonal CRISPR enzymes and fluorescent reporters[88,97], while DETECTR demonstrated attomolar sensitivity and HPV16/18 detection in clinical samples[9]. However, multiplex CRISPR detection may require additional Cas effectors, reporters, or separate detection reactions, depending on the assay design. Furthermore, some multiplex approaches use devices such as microfluidics to spatially separate reaction reagents, which can increase device fabrication and operational complexity despite providing effective target separation[24]. Therefore, exploring alternative amplification strategies with simplified primer architectures and compatibility with CRISPR-based detection remains valuable, particularly for reducing assay design complexity while retaining target discrimination.

CRISPR technologies are typically used after amplification to improve detection specificity.[67] Recently, our team dveloped CRISPR-based terminal-specific amplification (CASTSA), in which Cas12a-mediated target recognition and cleavage generate DNA fragments with defined 5′ termini for subsequent terminal-specific PCR amplification. This approach demonstrated the feasibility of using CRISPR cleavage as an upstream recognition step rather than solely as a downstream detection mechanism.[11] Inspired by this concept, we investigated whether CRISPR cleavage products could be directly utilised to initiate an isothermal amplification. Compared with PCR, isothermal amplification methods are more suitable for point-of-care applications as they do not require thermal cycling.[154] In particular, several simplified loop amplification strategies have recently been reported that reduce the number of primers required for amplification[3,155].

Based on these studies, a CRISPR/Cas12a-integrated loop amplification assay was developed and is reported in this chapter. Cas12a cleavage generates staggered double-stranded DNA breaks with 5′ overhangs. These cleavage products expose the PAM-distal region and may facilitate primer binding through local ”breath effect” that destabilises the DNA duplex. A template-specific primer (TSP) containing a stem–loop structure was adapted[3] and designed to exploit this feature. Together with a second amplification primer, loop amplification could be achieved using only two core primers. By reducing the number of primers required for amplification, the proposed strategy may simplify primer architecture, although improved multiplex performance has not been established through direct comparison with conventional LAMP.

In this chapter, the feasibility of a CRISPR/Cas12a-integrated loop amplification assay is demonstrated using HPV16, HPV18 and HPV52 as model targets. Primer design, amplification mechanism and reaction conditions were systematically evaluated. The performance of the assay was assessed in singleplex, duplex and triplex formats, and its analytical performance was characterised. The study therefore extends our previously reported CRISPR-assisted amplification concept towards an isothermal platform while evaluating the potential and limitations of a two-core-primer design for multiplex nucleic acid detection.

3.2 Material and Methods

3.2.1 Primer design

The target DNA sequence for HPV16 (GenBank no. AF393502.1) and HPV18 (GenBank no. MH057749.1) was synthesised by PCR amplification using primer pairs PF-T and PR-T (Table 3-1). Synthetic HPV52 DNA gBlocks (GenBank: MK387726.1) and HPV18 were purchased from Eurofins Scientific (Eurofins Scientific, Luxembourg). All the DNA and RNA oligonucleotide sequences were synthesised by Eurofins Scientific or Integrated DNA Technologies (IDT). The primers were designed and analysed by the Oligo Analyzer (https://eu.idtdna.com/calc/analyzer). All the sequences used in this assay are listed in Table 3-2 and 3-3.

Unlike conventional LAMP assays that require four to six primers, the amplification strategy developed in this work was designed to use only two core primers (Figure 3-1). To achieve efficient loop-mediated amplification with this simplified primer set, several design criteria were considered during primer design. First, the target-binding region of the TSP primer was designed to be 18 – 25 nucleotides in length with a GC content between 40% and 60% to ensure sufficient binding affinity to the target sequence. Second, potential primer heterodimers and self-dimers were evaluated using Gibbs free energy (ΔG) values. The ΔG values at both the 5′ and 3′ primer ends were maintained above -9 kcal mol^{-1}, and primer designs containing more than two consecutive base pairs at the 3′ end were avoided. This helps minimise non-specific amplification caused by primer interactions while maintaining efficient target binding. Third, a ”e-f-e*” stem–loop structure was introduced at the 5′ end of the TSP primer to support exponential amplification. This design was inspired by the loop-mediated amplification mechanism of LAMP. Unlike conventional LAMP, the stem–loop structure was incorporated directly into the TSP primer, allowing LAMP-like amplification to be achieved using only two primers. Three TSP designs were investigated. TSP1 was designed as a minimal stem–loop structure and contained a 8 bp stem and a 2 nt loop. In contrast, TSP2 and TSP3 were designed with larger stem–loop structures to investigate whether additional primer-binding sites could improve amplification efficiency. TSP2 contained a 13 bp stem and a 20 nt loop, while TSP3 contained a 12 bp stem and an 18 nt loop. The larger loop regions were designed to provide extra binding sites for additional loop primers, mimicking the function of loop primers in LAMP and potentially enhancing the amplification rate. In addition to the core TSP–P primer system, several alternative primer combinations were designed and evaluated during assay development. The optimal primer set was selected based on amplification performance and specificity.

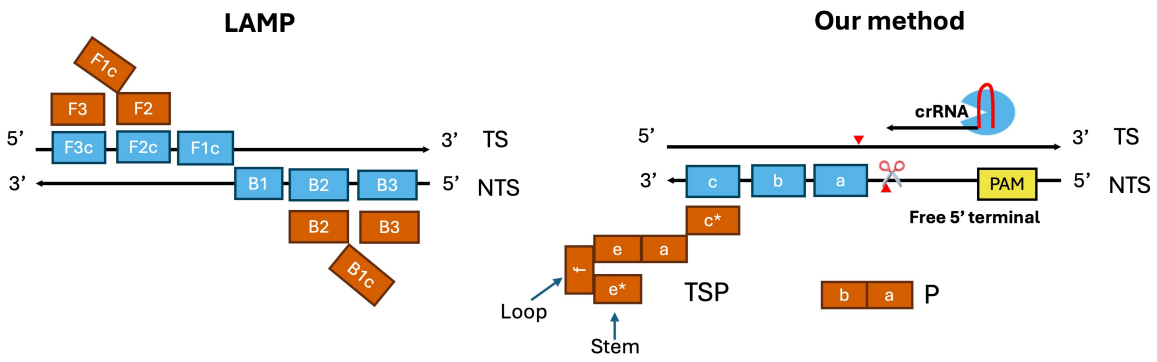


Figure 3-1: Comparison of primer design and target recognition between conventional LAMP (left) and the proposed CRISPR/Cas12a-integrated loop amplification assay (right)

Table 3-1: PCR primers used for target DNA template synthesis.

Primer	Sequence (5'-3')	Target
HPV16PF-T	ACCTGCATTTGCTGCATAAGCACTAGCATTTT CTGTGTCATCCAATTTATTTAATAAAGGATGG CCACTA	HPV16
HPV16PR-T	GCCTGTGTAGGTGTTGAGGTAGGTCGTGGTCA GCCATTAGGTGTGGGCATTAGTGGCCATCCTT TATTAA	HPV16
HPV18PF-T	GACACAGTTATGTATTTTGGGCTGTGCCCCTG CTATTGGGGAACACTGGGCTAAAGGCACTGC TTGTAAA	HPV18
HPV18PR-T	GTGTTTTTAAGTTCTAAAGGGGGGCAATCGCC CTGTGATAAAGGACGCGATTTACAAGCAGTG CCTTTAG	HPV18

Table 3-2: Primer sequences used for loop amplification.

Primer	Sequence (5'-3')	Target
16-TSP1	CAACAAGGTATCCTTGTTGTTTCTGTGTCATCCAA TGAGGTAGGTCGTGGTCAGCC	HPV16
16-TSP2	GCGAGAGTGAGCCGGTCGGCTTCGTCGTATCGTG GCTCACTCTCGCTTTCTGTGTCATCCAATGAGGTA GGTCGTGGTCAGCC	HPV16
16-P1	TTTCTGTGTCATCCAATTTATTTAATAAAGGATGG CCACTAATGCCC	HPV16
16-P2	TTTCTGTGTCATCCAATCCACTAATGCCCACACCT AAT	HPV16

Continued on next page

Table 3-2: Primer sequences used for loop amplification (continued).

Primer	Sequence (5'-3')	Target
16-ssDNA (a-b1-b2-c)	TTTCTGTGTCATCCAATTTATTTAATAAAGGATGGCCACTAATGCCCACACCTAATGGCTGACCACGACCTACCTC	HPV16
18-TSP1	CAACAAGGTATCCTTGTTGGGGGAACACTGGGCTAACTAAAGGGGGGCAATCGCC	HPV18
18-PS-TSP1	C*A*A*C*A*A*G*G*T*A*T*C*C*T*T*G*T*T*G*GGGGAACACTGGGCTAACTAAAGGGGGGCAATCGCC	HPV18
18-TSP1.1	CATCTAGGTATCCTAGATGGGGGAACACTGGGCTAACTAAAGGGGGGCAATCGCC	HPV18
18-TSP3	CGGAGAGTGAGCCGGTCGGCTTCGTCGTATCGTGGCTCACTCTCCGGGGGAACACTGGGCTAACTAAAGGGGGGCAATCGCC	HPV18
18-P1	GGGGAACACTGGGCTAAAGGCACTGCTTGTAAATCGC	HPV18
18-P2	GGGGAACACTGGGCTAAGTAAATCGCGTCCTTTATCACAG	HPV18
18-b1	AGGCACTGCTTGTAAATCGC	HPV18
18-b3	CTGCTTGTAAATCGCGTCCT	HPV18
18-f	GTCGCTTCGTCGTATCGT	HPV18
18-a*f	TTAGCCCAGTGTTCCCCGTCGCTTCGTCGTATCGT	HPV18
18-cutPF	GTTATGTATTTTGGGCTGTG	HPV18
18-cutPR	AGTTCTAAAGGGGGGCAATC	HPV18
18-d-outer	CAGTATCTACCATATCACCATCT	HPV18
CUT1S	GGGGAACACTGGGCTAAAGGCACTGCTTGTAAATCGCGTCCTTTATCACAGGGCGATTGCCCCCCTTTAGAACTTAAAAACAC	HPV18
CUT1A	GTGTTTTTAAGTTCTAAAGGGGGGCAATCGCCCTGTGATAAAGGACGCGATTTACAAGCAGTGCCTTTAGCCCAGTGT	HPV18
18-ssDNA	GGGGAACACTGGGCTAAAGGCACTGCTTGTAAATCGCGTCCTTTATCACAGGGCGATTGCCCCCCTTTAG	HPV18
52-TSP1	CAACAAGGTATCCTTGTTGCCTTACCCCACCACCGGCAGTAGAAGTTACAAATCTGTATGT	HPV52

Continued on next page

Table 3-2: Primer sequences used for loop amplification (continued).

Primer	Sequence (5'-3')	Target
52-P1	CCTTACCCCACCACCGTCTGCATCTTTGGAGGAC	HPV52
52-TSP2	CAACAAGGTATCCTTGTTGGGGGCCGATGATGCA GGGTTACAGGCAGGGCTACAGG	HPV52
52-P2	GGGGCCGATGATGCAGGGCGTTTTAGTTTGG	HPV52

* in the sequence indicates the phosphorothioate-modified DNA backbone.

Table 3-3: crRNA sequences used for CRISPR/Cas 12a.

Primer	Sequence (5'-3')	Target
16-crRNA	UAAUUUCUACUAAGUGUAGAUCUGCAUAAG CACUAGCAUUU	HPV16
18-crRNA	UAAUUUCUACUAAGUGUAGAUGGCUGUGCC CCUGCUAUUGG	HPV18
52-crRNA1	UAAUUUCUACUAAGUGUAGAGAGGACUGGC AAUUUGGCCU	HPV52
52-crRNA2	UAAUUUCUACUAAGUGUAGAUUCUUUGUGG AGGUACGUGG	HPV52

3.2.2 Template synthesis

The 120 bp HPV16 and HPV18 double-stranded DNA (dsDNA) template were generated by PCR amplification using primers PF-T and PR-T. A total volume of 20 µL of PCR system included 1× PCR buffer, 0.25 mM dNTPs, 0.2 µM PF-T and PR-T, 1× EvaGreen, 1 U *Taq* DNA polymerase (New England Biolabs, MA). PCR amplification condition: 95 °C for 10 s, 55 °C for 30 s, 10 cycles. Subsequently, the PCR products were purified by QIAquick PCR purification kits (Qiagen, Hilden, Germany) according to the manufacturer's instructions. The purified DNA was quantified using a NanoDrop 2000 spectrophotometer (Thermo Fisher Scientific, MA).

3.2.3 Loop amplification assay

For loop amplification, single-stranded DNA templates (16-ssDNA and 18-ssDNA) were initially used as a proof of concept. Each reaction contained 1 µM of each core primer (TSP and P), 1.4 mM dNTPs, 6 mM $MgSO_4$, 1× isothermal amplification buffer (20 mM Tris–HCl, pH 8.8, 10 mM $(NH_4)_2SO_4$, 10 mM KCl, 2 mM $MgSO_4$, and 0.1 % Triton X-100), 1× EvaGreen dye (Biotium, CA, USA), 8 U of Bst 2.0 WarmStart DNA polymerase (New England

Biolabs, MA), and varying amounts of template DNA in a total reaction volume of 20 µL. Fluorescence measurements were performed using a QuantStudio™ 5 Real-Time PCR System at 63 °C. Amplification data were analysed using QuantStudio™ Design & Analysis Software (Applied Biosystems, USA). Time to positive (TTP) was determined automatically by the software. For the phosphorothioate (PS)-modified primer assay, the core primer pair (TSP and P) was replaced with a single PS-modified TSP primer (PS-TSP), while all other reaction components and conditions remained the same.

3.2.4 CRISPR/Cas12a cis- cleavage and verification

For the *cis*-cleavage assay, the LbCas12a ribonucleoprotein (RNP) complex was first assembled by mixing the crRNA (300 nM) and LbCas12a (1 µM) in the 1 x r2.1 buffer at room temperature for 10 min. 50 nM target dsDNA was added to the pre-assembled RNP complex (30 nM Cas12a-crRNA) and incubated at 37 °C for cleavage. After cleavage, the enzyme was inactivated either by heating at 65 °C for 10 min or by treatment with Proteinase K (Thermo Fisher Scientific, MA) for 10 min.

For native polyacrylamide gel electrophoresis verification, a 15% native PAGE gel stock solution was prepared by mixing Acrylamide: Bis-acrylamide 29:1 (40% solution, Thermo Fisher Scientific) with 1× UltraPure TBE buffer (Invitrogen, USA), stored in the fridge until use. To prepare the gel, 12 mL gel stock solution was mixed with 120 µL Ammonium Persulfate (APS, Bio-Rad Laboratories Ltd), 12 µL N,N,N', N'-tetramethylethylenediamine (TEMED, Bio-Rad Laboratories Ltd); the solution was immediately poured between the assembled glass plates (1.5 mm thickness). A comb was inserted, and the gel was allowed to polymerise at room temperature for 20 min. Once the gel was solidified, 10 µL of the CRISPR cleavage product was loaded into the well and run in 1× TBE buffer at 100 V for 90 min on ice. After electrophoresis, the gel was stained with 1× SYBR Gold (Invitrogen, ThermoFisher Scientific) for 10 min and visualised using a PXi imaging system (Syngene, MD, USA).

For PCR verification, 2 µL of the cleavage product was added to a PCR mixture containing 0.2 µM cutFP and cutRP primers, 0.2 µM probe, 1× PCR reaction buffer, 0.25 mM dNTPs, and 1 U Taq DNA polymerase. PCR amplification conditions: 95 °C for 10 s, 60 °C for 90 s and 65 °C for 20 s, 40 cycles.

3.2.5 CRISPR/Cas12a-integrated loop amplification assay

For the two-step assay, 300 nM crRNA and 1 µM LbCas12a were mixed in the 1× r2.1 buffer (containing 6 mM $MgSO_4$) with different concentrations of target DNA in a total volume of 30 µL, followed by incubation at 37 °C for 10 min to allow CRISPR cleavage. Subsequently,

3 µL CRISPR product was added to the loop amplification mixture containing 1 µM of each core primer (TSP and P), 1.4 mM dNTPs, 6 mM $MgSO_4$, 1× isothermal amplification buffer, 1× EvaGreen dye, and 8 U of Bst 2.0 WarmStart DNA polymerase, giving a total reaction volume of 20 µL. The reaction was performed in the QuantStudio 5 Real-Time PCR machine at 63 °C.

For one-pot assay, 45 nM crRNA, 50 nM LbCas12a, 0.8× r2.1 buffer, 1 µM of TSP and P primer, 1.4 mM dNTPs, 1× Evagreen dye, and 8 U Bst 2.0 polymerase were mixed together with the target DNA. The reaction were performed in the QuantaStudio 5 Real-Time PCR machine at 37 °C 10 min for CRISPR cleavage, and 63 °C 60 min for amplification.

For multiplex detection, duplex assay were performed under the same conditions as the above singleplex assay with two sets of crRNA and core primers. Triplex assays were performed using similar reaction conditions, except that the concentration of each primer set was reduced from 1 µM to 700 nM.

3.3 Results and discussion

In this work, we established a CRISPR/Cas12a-integrated loop amplification assay for HPV detection. Two core primers, namely the template-specific primer (TSP) and primer P (P1/P2), were designed based on the PAM-distal region of the target sequence. The 3' end of the TSP was designed to hybridise to the "c" region of the NTS; the middle region "a" was designed to provide loop back opportunity for the new extended TSP strand; an extra loop structure (e-f-e*) was incorporated at the 5' end of the TSP as an extra loop for enhanced amplification (Figure 3-2). In brief, after recognition of the target DNA by the Cas12a/crRNA ribonucleoprotein (RNP) complex, the activated Cas12a generates staggered double-stranded DNA breaks with free 5′ overhangs. The TSP primer "e-f-e*-a-c" was designed to bind the "c*" region upstream of the cleavage site and initiate strand extension. Extension is expected to stop at the 5′ terminal "a", allowing the stem–loop structure of the TSP to fold back to itself and serve as a template for subsequent extension; therefore, a stem-loop structure (e*-f-e-a-c*-b2-b1-a*-e*-f*-e) was formed. A second primer (P1/P2) was designed to hybridise to the stem–loop structure (b1/b2) generated by TSP extension. Binding of P1/P2 was expected to open the stem–loop structure and extend further rounds of amplification. When the stem-loop structure was opened, the 3' end "e" is expected to self loop back with "e*", resulting in the formation of a secondary stem-loop structure. The process may displace the new P1/P2 strand and start another round of extension.

By combining Cas12a-generated 5' overhangs with the engineered stem-loop structure, this design enables LAMP-like amplification using two core primers and provides a simplified framework for multiplex HPV detection.

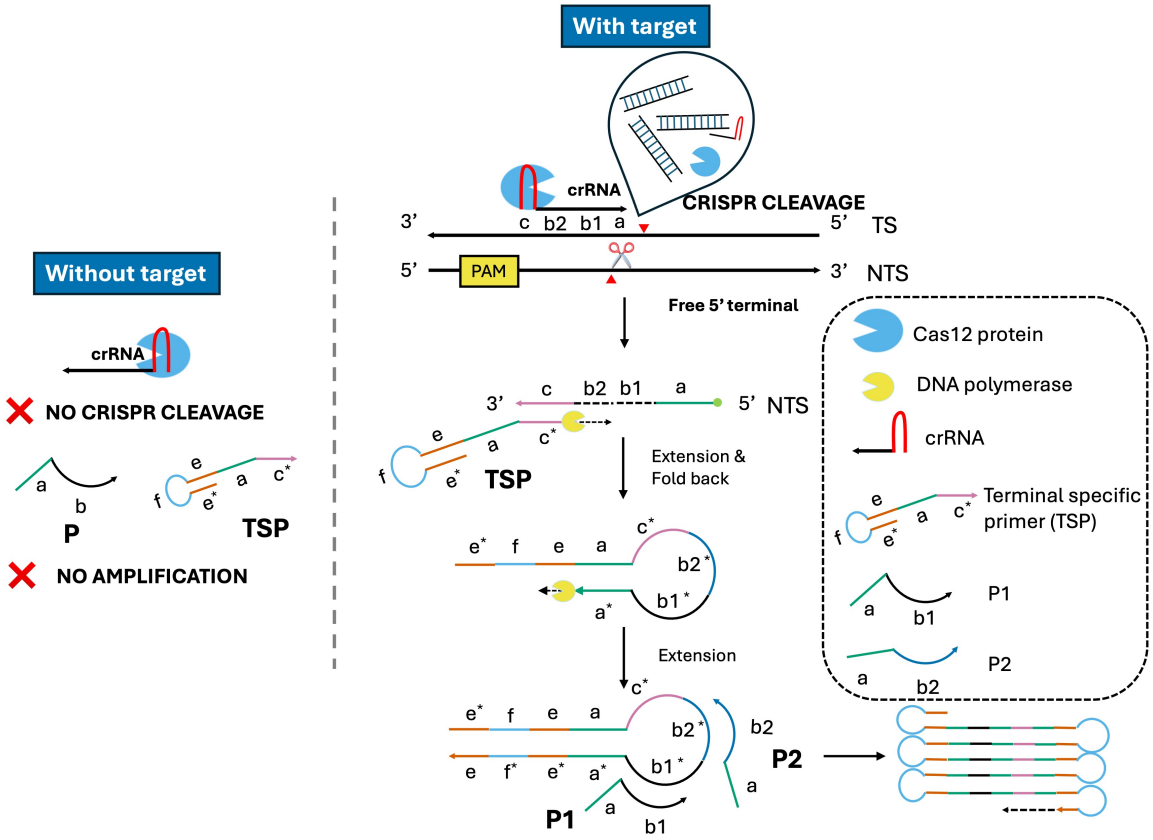


Figure 3-2: Schematic of CRISPR/Cas12a integrated loop amplification assay and primer target region. In the presence of target DNA, Cas12a cleavage generates a free 5′ terminal on the non-target strand (NTS), enabling TSP binding and extension. Subsequent hairpin formation and primer extension by P1 or P2 support further amplification. In the absence of target DNA, the CRISPR and amplification pathway is not initiated. Different colours represent sequence domains, and asterisks indicate complementary sequences.

3.3.1 Primer design and selection

Core primer selection

Conventional LAMP primer design software could not be used for the proposed amplification system because the available primer-binding region was constrained by the Cas12a PAM sequence (TTTV), and no suitable alternative software was available. Therefore, we determined the optimal crRNA region first and then screened primer sites around the PAM-distal region. The free energy ΔG and primer dimer were calculated and predicted by the IDT OligoAnalyzer Tool to get specific amplification and avoid non-specific primer crosstalk.

According to the manufacturer's recommendation, primer pairs with ΔG values more negative than -9 kcal mol^{-1} have stronger binding affinity and are more likely to form non-specific dimers, thus should be avoided. However, this rule could not be directly applied to the TSP primers because the stem–loop structure intentionally contains self-complementary

sequences. Therefore, predicted dimer formation was classified as low risk ($\Delta G > -7$ kcal mol^{-1}), moderate risk ($-15 < \Delta G \leq -7$ kcal mol^{-1}), and high risk ($\Delta G \leq -15$ kcal mol^{-1}) (Table 3-4).

Table 3-4: Predicted self-dimer and heterodimer formation of candidate primers for HPV16, HPV18 and HPV52.

Primer / Primer Pair	Type	ΔG (kcal mol^{-1})	Base Pairs	Risk
16-TSP1	Self-dimer	-13.81	8	Moderate
16-TSP2	Self-dimer	-25.78	13	High
16-P1	Self-dimer	-13.19	6	Moderate
16-P2	Self-dimer	-5.25	4	Low
16-TSP1 + 16-P1	Heterodimer	-9.66	6	Moderate
16-TSP1 + 16-P2	Heterodimer	-6.97	5	Low
16-TSP2 + 16-P1	Heterodimer	-9.5	5	Moderate
16-TSP2 + 16-P2	Heterodimer	-6.97	5	Low
18-TSP1	Self-dimer	-13.81	8	Moderate
18-TSP1.1	Self-dimer	-12.23	8	Moderate
18-TSP3	Self-dimer	-25.71	13	High
18-P1	Self-dimer	-5.09	3	Low
18-P2	Self-dimer	-10.36	4	Moderate
18-TSP1 + 18-P1	Heterodimer	-6.84	5	Low
18-TSP1 + 18-P2	Heterodimer	-6.84	5	Low
18-TSP1.1 + 18-P1	Heterodimer	-6.21	3	Low
18-TSP1.1 + 18-P2	Heterodimer	-9.52	6	Moderate
18-TSP3 + 18-P1	Heterodimer	-7.81	4	Moderate
18-TSP3 + 18-P2	Heterodimer	-9.52	6	Moderate
52-TSP1	Self-dimer	-13.81	8	Moderate
52-TSP2	Self-dimer	-13.81	8	Moderate
52-P1	Self-dimer	-7.05	4	Low
52-P2	Self-dimer	-9.28	4	Moderate
52-TSP1 + 52-P1	Heterodimer	-6.69	4	Low
52-TSP2 + 52-P2	Heterodimer	-9.28	4	Moderate

Risk classification was based on predicted Gibbs free energy (ΔG): Low risk, $\Delta G > -7$ kcal mol^{-1}; Moderate risk, $-15 < \Delta G \leq -7$ kcal mol^{-1}; High risk, $\Delta G \leq -15$ kcal mol^{-1}.

For HPV16, 16-TSP1 + 16-P1 primer set was first tested using different primer concentration ratios (Figure 3-3). As this was a preliminary exploratory experiment, most of the assay was performed in duplicate. As shown in Figure 3-3a, the shortest time-to-positive (TTP) was achieved when the TSP1:P1 ratio was 1:1 (red curve). When the concentration of P1 was increased, amplification was observed in the no-template control (NTC), indicating non-specific amplification. Therefore, a 1:1 ratio was selected for further experiments. However, background amplification was still observed in repeated experiments under the same conditions (Figure 3-3c). Melting curve analysis showed different melting temperatures between

the target and NTC, confirming that the NTC signals were caused by non-specific amplification. According to Table 3-4, P1 showed a moderate predicted risk, which was consistent with the observed background amplification. Therefore, P2 was selected as an alternative primer to reduce non-specific amplification.

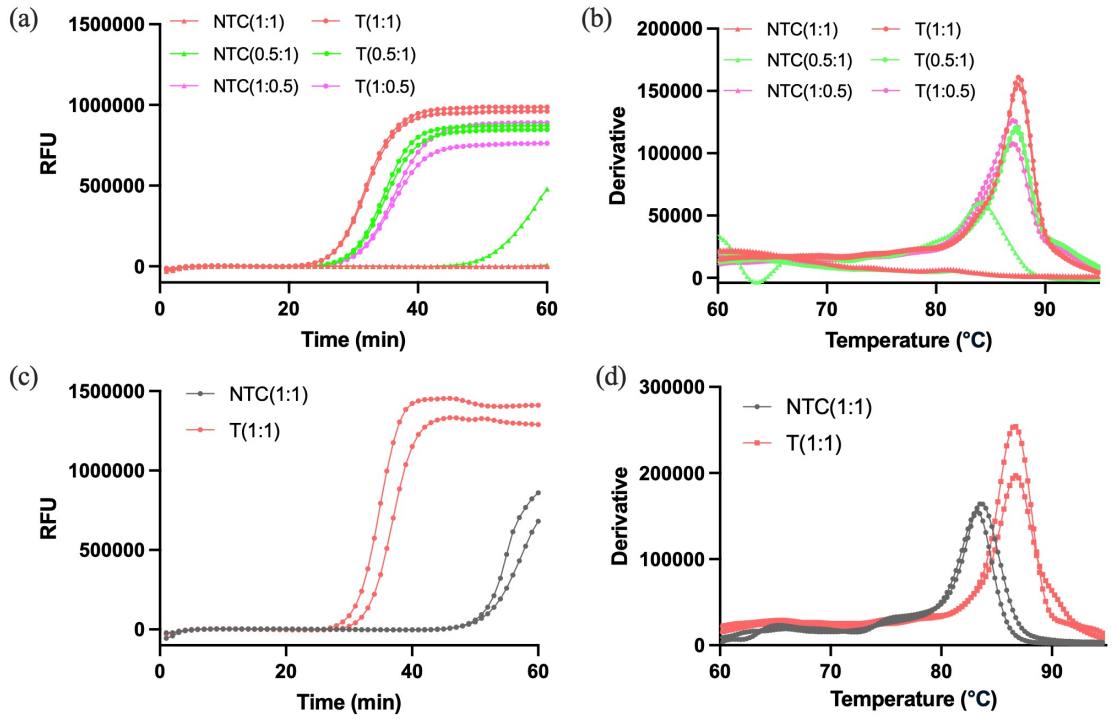


Figure 3-3: Comparison of different concentration ratios of core primers TSP1 and P1. (a) Real-time fluorescence amplification curves obtained using different TSP1:P1 concentration ratios (1:1, 0.5:1, and 1:0.5). (b) Melting curve analysis corresponding to the amplification products shown in (a). (c) Real-time fluorescence amplification curves obtained using the optimised TSP1:P1 ratio of 1:1. (d) Melting curve analysis of (c). T: with template; NTC: non-template control. RFU: relative fluorescence unit. n=2.

For HPV18 (Figure 3-4), all designed primer sets successfully amplified the target DNA. TSP1.1 was designed with reduced complementarity compared with TSP1 and was predicted to have a lower risk of non-specific amplification, but both primers showed similar TTP and no obvious background amplification within 60 min. TSP3 contained a longer stem and larger loop region than TSP1, resulting in a more negative predicted ΔG value and a higher risk of non-specific amplification. However, a larger loop structure provides an opportunity to introduce additional loop primers in future designs, which may improve amplification efficiency. Therefore, there is a trade-off between amplification performance and the risk of non-specific amplification when using TSP3. Interestingly, the results showed promising comparable amplification efficiency in Figure 3-4a, c. Among all primer combinations tested, non-specific amplification was consistently observed in primer sets containing P2, which was consistent with the high dimerisation risk predicted for P2 in Table 3-4. Therefore, P2 was

not selected for further experiments. The apparent decrease in fluorescence after the peak should be consider caused by the instrument's baseline correction rather than an actual loss of fluorescence, as the raw fluorescence remained stable during this period.

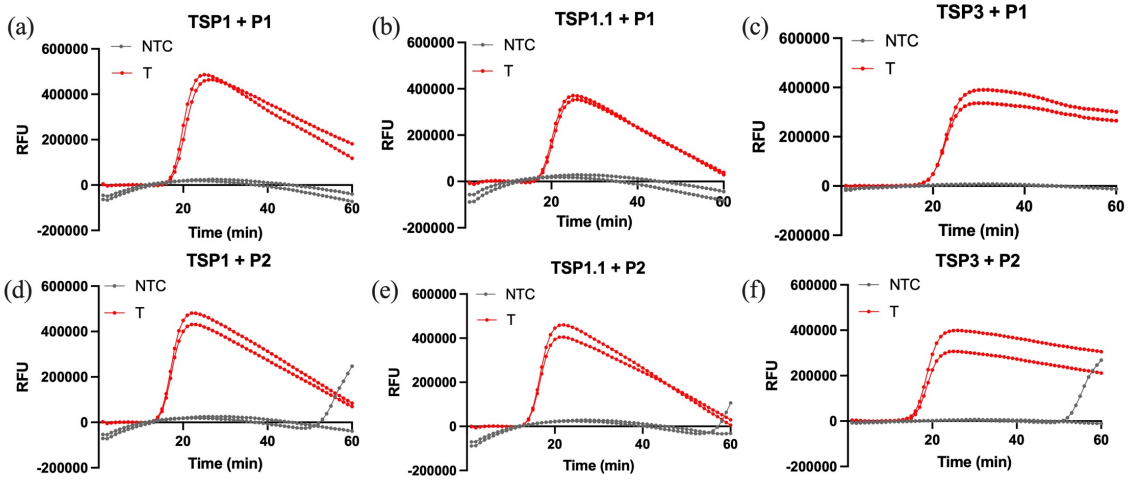


Figure 3-4: Comparison of different HPV18 core primer sets. (a) TSP1+P1. (b) TSP1.1+P1. (c) TSP3+P1. (d) TSP1+P2. (e) TSP1.1+P2. (f) TSP3+P2. T: with template; NTC: non-template control. n=2.

For HPV52 (Figure 3-5), both TSP1+P1 and TSP2+P2 amplified the target DNA successfully. However, the TSP2+P2 primer set also produced strong amplification in the NTC, while TSP1+P1 showed no background curve. Therefore, TSP1+P1 was selected for further studies.

Overall, the experimental results were generally consistent with the predicted dimerisation risk. Primer sets with lower predicted risk showed less background amplification while maintaining efficient target amplification.

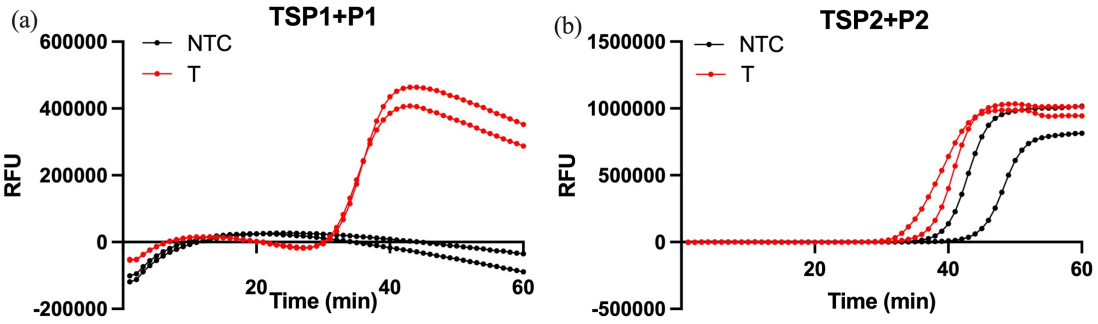


Figure 3-5: Comparison of different HPV 52 primer sets. (a) TSP1+P1. (b) TSP2+P2. n=2.

Evaluation of addition loop primers

After the screening of the core primer set, we studied whether amplification efficiency can be further enhanced by adding additional loop primers, as is the case in conventional LAMP. Therefore, we designed and evaluated several alternative primers for the HPV18 target (Figure 3-6). The original system consisted of TSP1 and P1, while the extra primers b1, b3, f, and a*-f were used to explore different amplification strategies. After the introduction of the big loop TSP3, simplified P primers (b1/b3) were designed to hybridise to different regions of the amplification intermediate. In addition, primers f and a*-f were designed to act as loop primers to accelerate amplification after formation of the e-f-e* stem-loop structure. The primer a*-f was designed to mimic the first loop-back structure, providing more loop binding sites for efficient amplification.

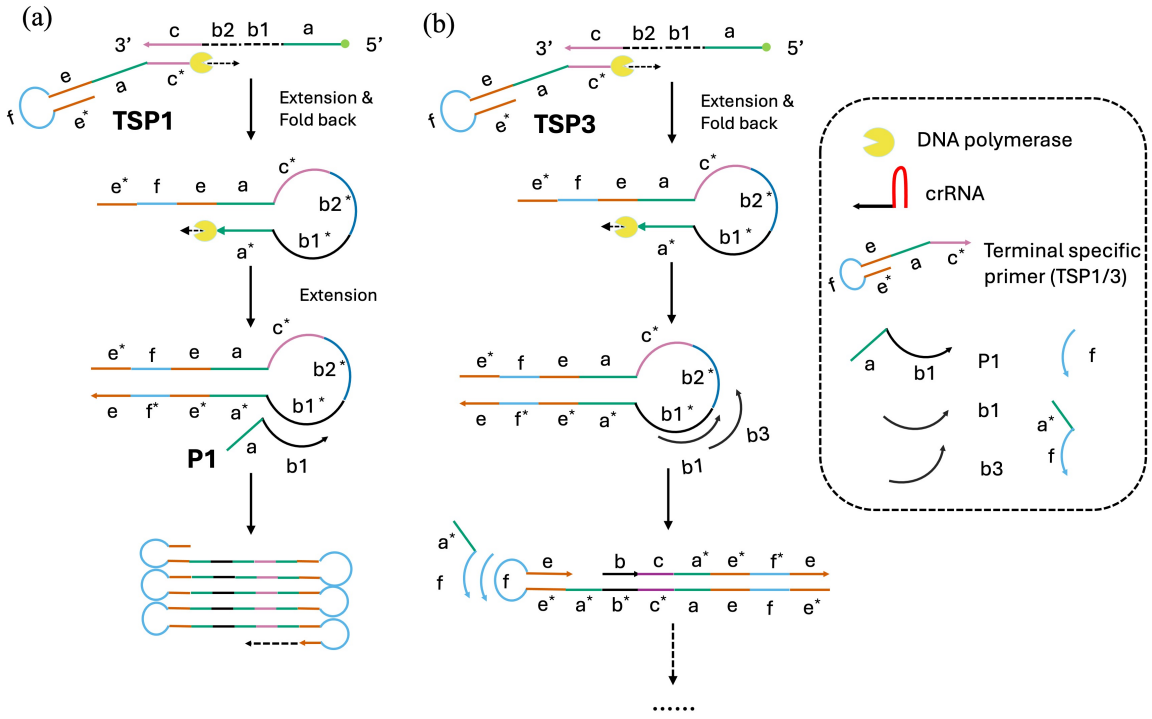


Figure 3-6: Schematic of amplification using the core primers (TSP1 and P1) (a) and the modified primers with extended TSP and additional loop primers (TSP3, b1, b3, f, a*-f) (b).

To evaluate these primer designs, we used 78 bp dsDNA (CUT1S1A) as template to mimic the product after CRISPR cleavage of 120 bp full-length dsDNA template (CRISPR-treated). As shown in Figure 3-7a, the TSP3-based systems generally have longer TTP than the TSP1-based system. This result was inconsistent with the previous results (Figure 3-4) and may be related to the lower target concentration (10^7 copies) used in this experiment compared with the primer screening studies (10^9 copies). Therefore, the larger stem-loop structure of TSP3 may require longer time to reach the TTP. We also noticed that the simplified P primers (b1 and b3) produced shorter TTP than P1, with b3 showing slightly shorter TTP values than b1.

Additional loop primers (f and a*-f) were subsequently evaluated using the TSP3 system. Figure 3-7b. For the b1 primer set, the addition of primer f showed a tendency to reduce the TTP, suggesting moderately faster amplification. In contrast, only minor changes in TTP were observed for the b3 primer set after the addition of the loop primers. These results suggest that the kinetic benefit of the additional loop primers may be dependent on the primer combination. However, given the limited number of replicates (n = 2), these observations should be interpreted as preliminary, and no statistical significance could be established.

Although several alternative primer sets showed promising results, the improvement in amplification speed was relatively small compared with the increased complexity of the primer system. Therefore, the additional loop primers were not selected for further experiments, while the TSP3+b1 primer combination was selected for further evaluation using CRISPR-treated templates.

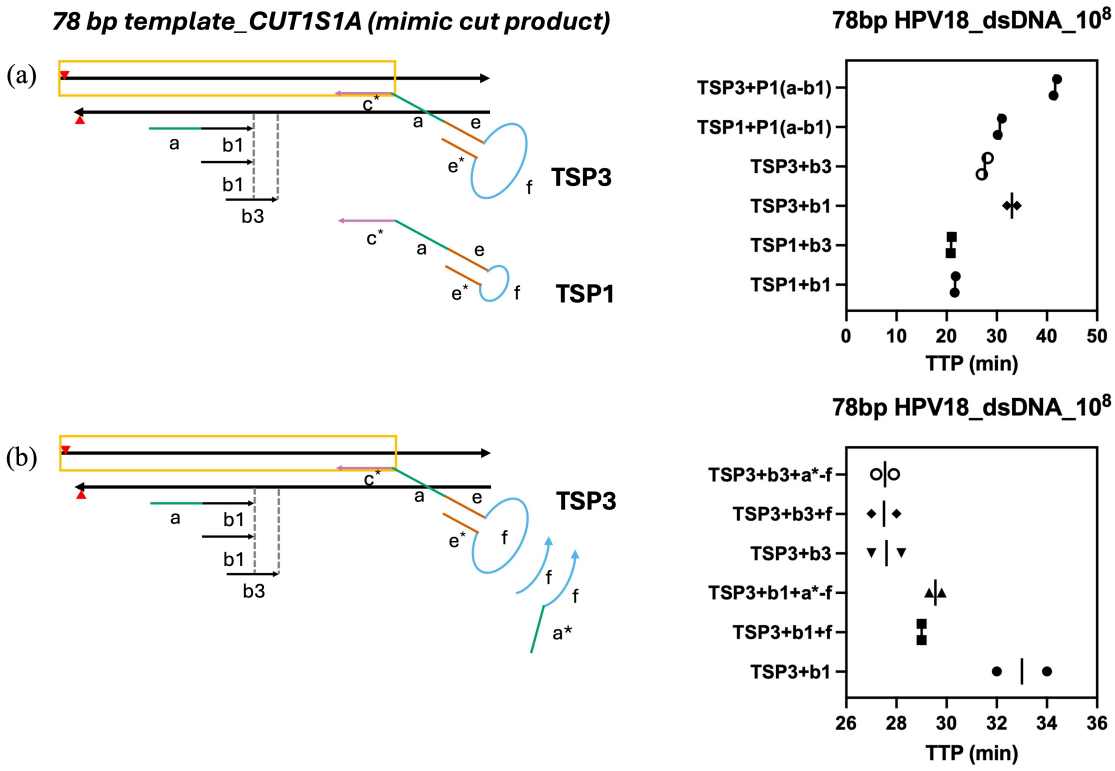


Figure 3-7: Evaluation of different primer combinations using the 78 bp mimic CRISPR cut product as template. (a) Screening of TSP1- and TSP3-based primer combinations and their corresponding amplification TTP. (b) Evaluation of additional primer designs based on the TSP3 primer set. Amplification efficiency was compared by time-to-positive (TTP) values using 10^7 copies of HPV18 dsDNA, the right panel. n=2. Statistical comparisons were not performed due to the limited number of replicates.

Another commonly used design in the LAMP assay is the introduction of outer primers, which helps the TSP strand separate from the template[156]. Therefore, an outer primer ”d” was designed in Figure 3-8. Interestingly, b1 performed better than P1 when tested using

the short mimic 78bp template, whereas it was the opposite in the CRISPR-treated template. One possible explanation is that b1 and b3 are shorter primers and may bind more efficiently to the short mimic template. In contrast, P1 was designed to target the amplification intermediate generated after TSP extension and may therefore be better suited for repeated amplification cycles in the real assay. The addition of outer primer "d" further reduced the TTP time, indicating the "d" primer can enhance amplification. However, considering the slight improvement and increased complexity, primer d was not used in the final assay.

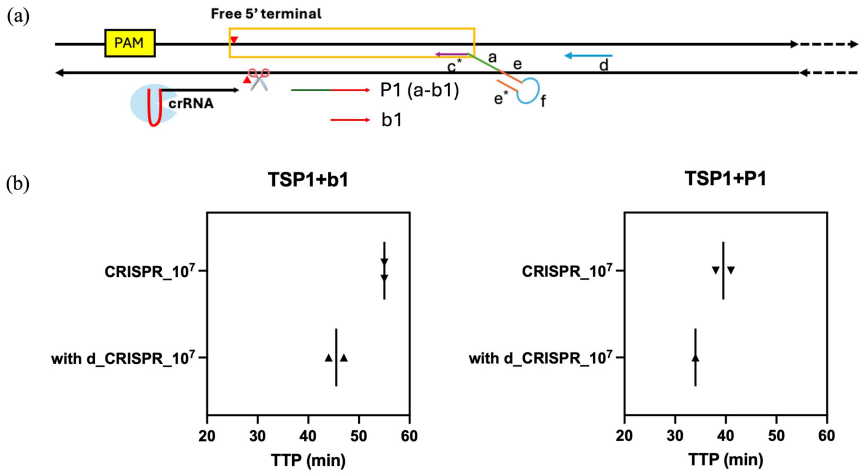


Figure 3-8: Effect of outer primer d. (a) schematic of primer target region. (b) TTP values of using TSP1+b1 and TSP1+P1 primer sets respectively. n=2. Statistical comparisons were not performed due to the limited number of replicates.

Phosphorothioate (PS)-modified primer

In a multiplex detection system, minimising the number of primers may reduce the number of possible primer–primer interactions, although improved assay specificity must be demonstrated experimentally. However, in our design, without the assistance of the P primer, the amplification efficiency would be substantially reduced, or amplification would not occur at all if it solely relied on the continuous spontaneous self-folding of TSP loop (e-f-e*). In order to achieve amplification using a single primer, phosphorothioate (PS) was introduced into the backbone of the e-f-e* sequence. It has been reported that the PS-modified DNA can destabilise the base stacking interaction within the double-helical structure and consequently reduce the melting temperature.[157,158] Although no mature software is currently available to accurately predict the change in melting temperature caused by PS modification, individual phosphorothioate linkages have been reported to destabilise DNA duplexes by approximately (0.12 kcal/mol) on average[159]. Li et al. reported that a phosphorothioated hairpin could achieve exponential isothermal amplification through repeated self-priming and DNA polymerase extension.[158] Based on this principle, the stem–loop structure formed after TSP primer extension and folding was expected to exhibit reduced duplex stability between its

complementary 3′- and 5′-terminal regions. This destabilisation may facilitate dissociation of the terminal stem, allowing the e-f*-e* sequence at the 3′ end to self-fold more readily and initiate the next amplification cycle. Therefore, the PS-modified TSP primer alone was hypothesised to support target amplification without the assistance of additional primers, as illustrated in Figure 3-9.

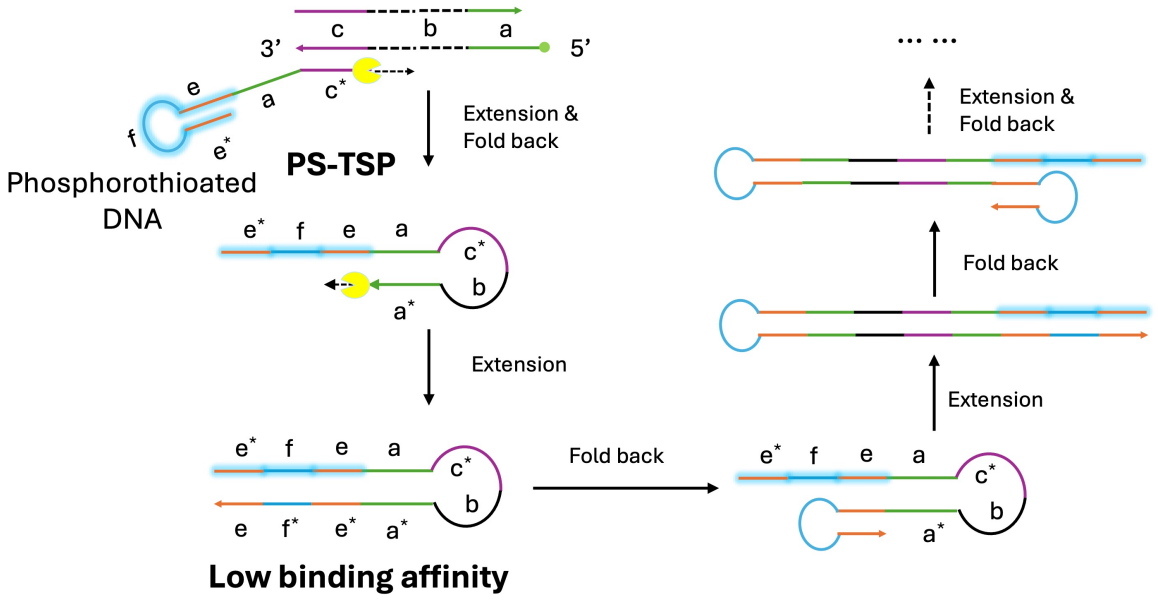


Figure 3-9: Schematic illustration of the proposed self-priming amplification mechanism using a phosphorothioate-modified primer (PS-TSP). Following primer binding and extension, the resulting DNA folds back to form a hairpin structure, enabling further extension and repeated self-priming. Cyan highlighting (e-f-e*) indicates phosphorothioate-modified DNA regions, and asterisks represent complementary sequence domains.

Figure 3-10 compares the amplification profiles of PS-TSP1 and unmodified TSP1 primers using a single-stranded DNA template at different temperatures. Both instrument-generated ΔRn and manually baseline-corrected fluorescence data ΔF were presented for comparison. Amplification was observed for PS-TSP1 at all temperatures, with the strongest ΔRn signal at 72 °C. In contrast, although fluorescence increases were also observed for the unmodified TSP1 reactions in the manually corrected data (Figures 3-10d, h and l), these increases may reflect time-dependent background fluorescence rather than DNA amplification. The negative-going ΔRn traces may be associated with the instrument's automatic baseline subtraction, which can introduce artefacts when applied to isothermal amplification data.

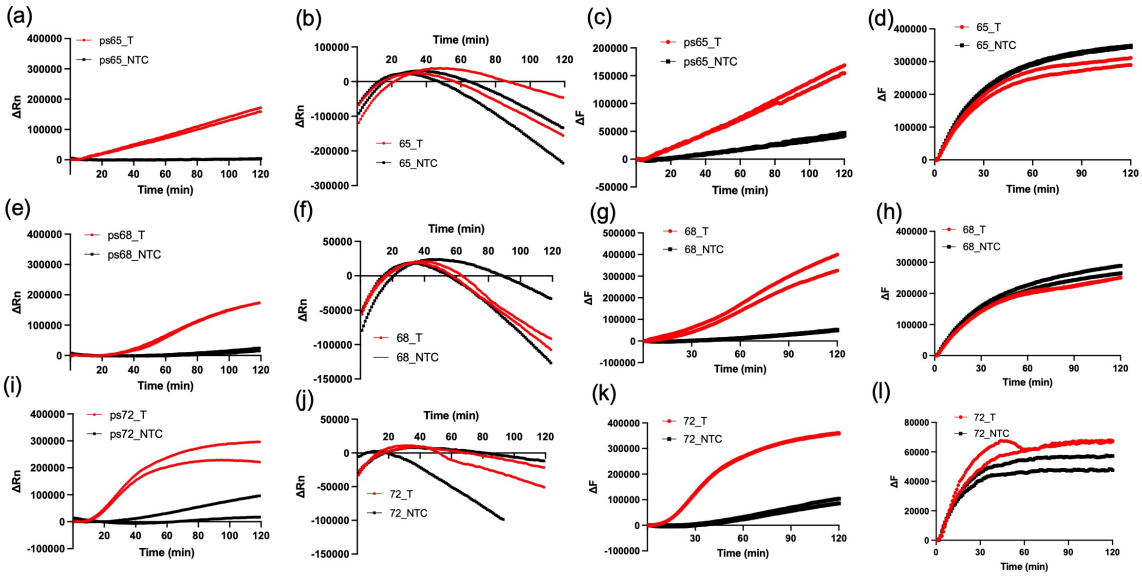


Figure 3-10: Comparison of PS-modified and unmodified TSP1 at different reaction temperatures using instrument-generated ΔRn and manually baseline-corrected fluorescence (ΔF). Panels (a, e, i) and (b, f, j) show the instrument-generated ΔRn curves for PS-TSP1 and unmodified TSP1 at 65, 68, and 72 °C, respectively. Panels (c, g, k) and (d, h, l) show the corresponding manually baseline-corrected fluorescence (ΔF) curves. Manual baseline correction was performed by subtracting the fluorescence of the first measurements from each individual Rn. Red and black lines represent reactions with target DNA (T) and no-template controls (NTC), respectively. Individual replicates are shown (n = 2). The negative-going ΔRn curves may result from the instrument's automatic baseline subtraction, whereas the manually corrected ΔF curves retain time-dependent background fluorescence changes.

To confirm whether the amplified product was long, concatenated double-stranded DNA as we expected, agarose gel electrophoresis was performed in Figure 3-11. Lanes 1, 3, and 5 represent the PS-TSP-1 amplification products obtained at reaction temperatures of 65 °C, 68 °C, and 72 °C, respectively, while lanes 2, 4, and 6 correspond to the NTC for each. Brighter DNA bands were observed at higher temperatures, suggesting greater accumulation of amplification products, although the gel results alone could not confirm their proposed concatenated structures.. No obvious products were observed for the unmodified primer lane (lanes 7 and 8), further supporting the important role of the PS modification, despite the fluorescence increase observed in Figure 3-11l. This suggests that the fluorescence increase was not necessarily associated with detectable DNA amplification, although the origin of the background signal remains unclear. These results support the role of PS modification in facilitating detectable amplification using TSP1 without an additional primer under the tested conditions.

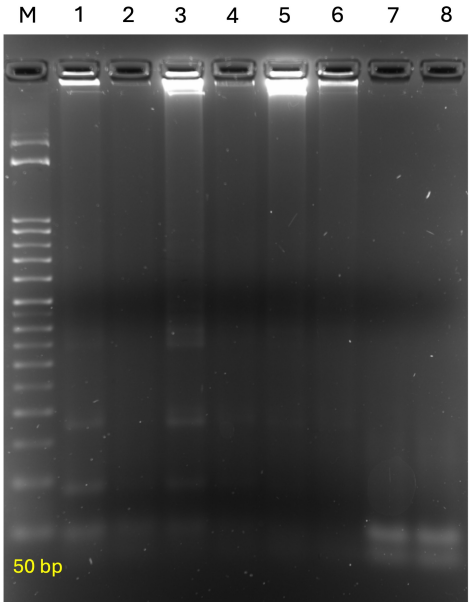


Figure 3-11: Agarose gel electrophoresis of PS-TSP1 and TSP1 with or without target DNA at different temperatures. Lanes 1–6 represent PS-TSP1 incubated at 65, 68, and 72 °C in the presence (odd-numbered lanes) or absence (even-numbered lanes) of target DNA. Lanes 7 and 8 represent non-modified TSP1 incubated at 72 °C in the presence and absence of target DNA, respectively.

After confirming that PS-TSP1 alone could support amplification using an ssDNA template, the single-primer system was further tested using CRISPR-treated DNA templates. In this experiment, dsDNA targets were first cleaved by the Cas12a–crRNA complex, and the resulting cleavage products were used as amplification templates to better mimic the template generated in the complete assay. Higher target concentrations produced larger fluorescence increases during the 90-min reaction (Figure 3-12). Unlike the typical sigmoidal curves observed in the two-primer system, the PS-TSP1 reactions showed a gradual increase in fluorescence without a clear exponential phase. Therefore, TTP was not suitable for analysing this reaction, and the final fluorescence change was used instead[160]. This different kinetic pattern may be related to the repeated opening, refolding and self-priming steps required in the single-primer system. Although 10^7 copies produced a higher final fluorescence than the NTC, the difference was small and only became clear near the end of the reaction. Lower target concentrations were not tested, so the limit of detection could not be determined. However, the small difference at 10^7 copies suggests that lower concentrations may be difficult to detect under the tested conditions. Therefore, although the single-primer system was feasible, it did not show a clear advantage over the two-primer system and was not investigated further.

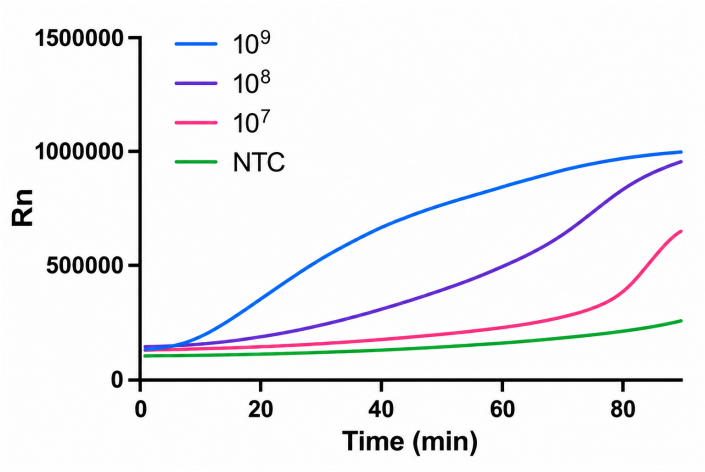


Figure 3-12: Real-time fluorescence curve for different target DNA concentrations using a PS-modified primer at 68 °C. Curves represent the mean of two replicate reactions per condition (n = 2). Target DNA concentrations are expressed as copies per reaction.

Optimizations of amplification condition

Following primer screening, the HPV16 (16-TSP1+16-P2) primer set was selected as a model system for loop amplification reaction conditions optimisation. Several key factors were chosen for optimisation, including primer concentrations, P2 primer capture lengths, reaction temperatures and Mg^{2+} concentrations.

Different concentrations of TSP and P2 were first evaluated to optimise the primer ratio (Figure 3-13 a, b). When the TSP concentration was maintained at 2 μM, decreasing P2 from 2 to 1 μM increased the target TTP from approximately 30.5 to 39 min, indicating that a higher P2 concentration improved amplification efficiency. In comparison, decreasing TSP2 from 2 to 1 μM, while maintaining P2 at 2 μM, only slightly increased the TTP to approximately 32 min and prevented detectable amplification in the NTCs during the reaction period. (Figure 3-13a) Further comparison showed that the 1:2 μM TSP:P2 condition produced the fastest target amplification, with a TTP of approximately 26–27 min, whereas NTC amplification occurred much later, at approximately 50–56 min. (Figure 3-13b) Therefore, considering both the rapid target amplification and the approximately 23–30 min separation between the target and NTC signals, a TSP:P2 concentration ratio of 1:2 was selected for subsequent experiments.

TSP2 was designed with an extended loop region to allow loop primer (LP) binding. As shown in Figure 3-13c, adding LP reduced the target TTP from approximately 31–34 min to 18–19 min with the P1 primer set, confirming that the loop primer accelerated amplification. However, LP also caused earlier NTC amplification with P1, reducing the separation between the target and NTC signals. In comparison, the P2 primer set showed faster target amplification and better separation from the NTC, and was therefore selected for further optimisation.

Different P2 capture lengths within the TSP loop region were then tested (Figure 3-13d). All designs produced similar target TTP values of approximately 20 min. However, the 18, 19, and 22 nt designs showed NTC amplification within the reaction period, whereas no NTC amplification was detected with the 21 nt design within 90 min. Therefore, the 21 nt capture length was selected for subsequent experiments.

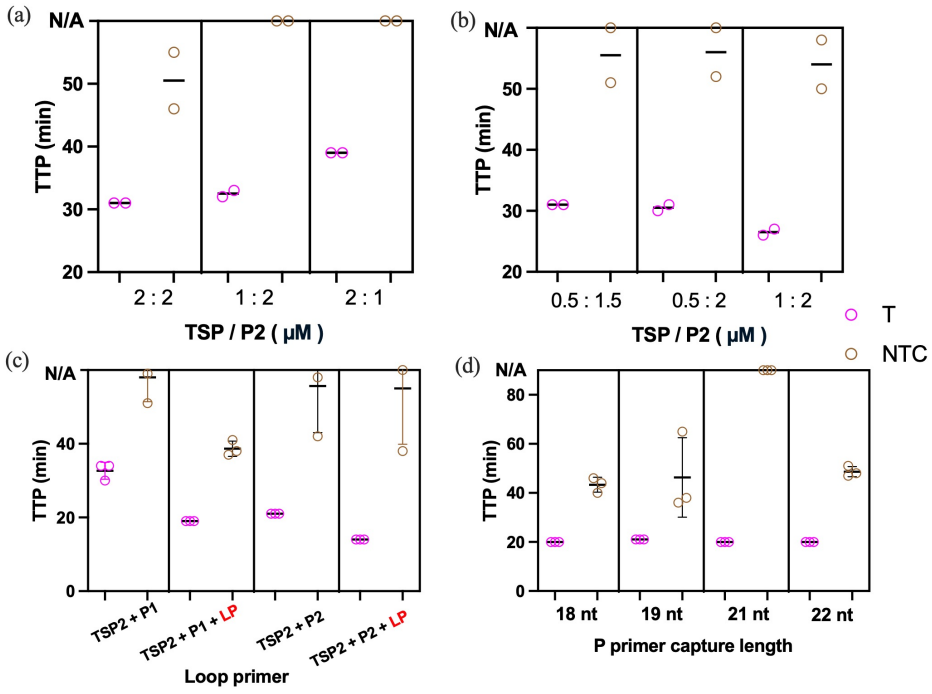


Figure 3-13: Optimisation of primer conditions. (a)-(b) the ratio of primer TSP and P2; n=2. (c) Effect of the second loop primer (LP) addition on Time-to-positive time (TTP); n=3. (d) Effect of loop primer capture length on TTP. n=3. T: with template, NTC: non-template control. N/A indicates no amplification detected during the experiment period. Due to the limited replicate numbers and the presence of reactions without measurable TTP values, the results were interpreted descriptively without statistical significance testing.

The reaction temperature was then optimised between 60 °C and 69 °C (Figure 3-14a). This range was selected because it covers the recommended operating temperature of Bst 2.0 polymerase.[161] Although reaction temperature is known to influence amplification efficiency and specificity in isothermal amplification[162], consistent amplification performance was observed across this window. Specifically, comparable time-to-positive (TTP) values of approximately 26–29 min were recorded between 63 °C and 67 °C. At 60 °C, the mean TTP increased to 35.5 min (8.5 min slower than at 65 °C), This slower amplification may be attributed to reduced template breathing at the lower temperature, which could limit primer accessibility and delay primer-mediated amplification initiation.[47]. Although 65 °C yielded the absolute fastest TTP (26 min), 63 °C was selected because it maintained rapid target amplification while providing better separation from the NTC.

The Mg^{2+} concentration was then evaluated from 4 to 10 mM, as Mg^{2+} affects polymerase

activity and non-specific amplification[163]. Increasing Mg^{2+} from 4 mM to 6 mM markedly decreased target TTP from 58 min to 27 min. However, concentrations above 6 mM triggered noticeable background amplification in non-template controls (NTC TTP dropped from >80 min to 42 min at 10 mM). This is consistent with previous studies showing that Mg^{2+} concentration must be carefully optimised because, although Mg^{2+} supports Bst polymerase DNA synthesis, excessive Mg^{2+} can promote non-target amplification, including primer dimer products[164]. Consequently, 6 mM Mg^{2+} was selected to achieve optimal amplification speed while maintaining strict specificity.

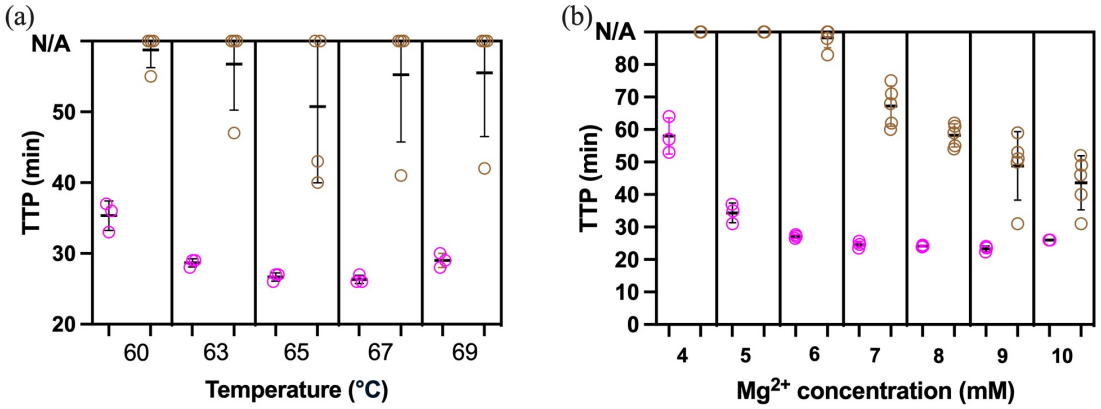


Figure 3-14: Optimization of amplification temperature (a) and magnesium ion concentration. Magenta circles represent reactions containing target DNA (n=3), while brown circles represent non-template controls (NTC, n=5). Individual data points are shown. N/A indicates reactions in which no amplification was detected within the experimental period. Horizontal bars and error bars represent the mean ± SD of reactions with measurable TTP values, where applicable.

.

The effect of betaine and OptiGene mastermix was also evaluated during reaction optimisation.(Figure 3-15) Betaine was tested because it is commonly used in LAMP to destabilise DNA duplexes and reduce GC-dependent secondary structures, which can improve strand displacement and amplification efficiency[165]. However, in the present assay, betaine delayed target amplification rather than improving it (Figure 3-15a). A similar inhibitory effect of betaine has previously been reported in other isothermal amplification reactions[166]. This may be due to the mechanism of this assay depending on the formation of stem-loop structures, whereas betaine is known to reduce DNA secondary structure. Therefore, the addition of betaine may interfere with the formation of functional intermediates and delay the reaction. Therefore, betaine was not included in the final reaction. The OptiGene Mastermix was then tested to determine whether a commercial isothermal amplification mastermix could improve reaction performance (Figure 3-15b). However, amplification signals were observed in all primer groups even in the absence of target DNA, including reactions containing TSP1, P2, or TSP1+P2 alone. This indicates that the OptiGene mastermix generated strong non-specific

amplification under these conditions. Therefore, it was not used in subsequent experiments.

Based on these results, the final amplification conditions consisted of a TSP1:P2 ratio of 1:2, a 21 nt P2 capture length, a reaction temperature of 63 °C, and 6 mM Mg^{2+}. These conditions were used in all subsequent experiments unless otherwise stated.

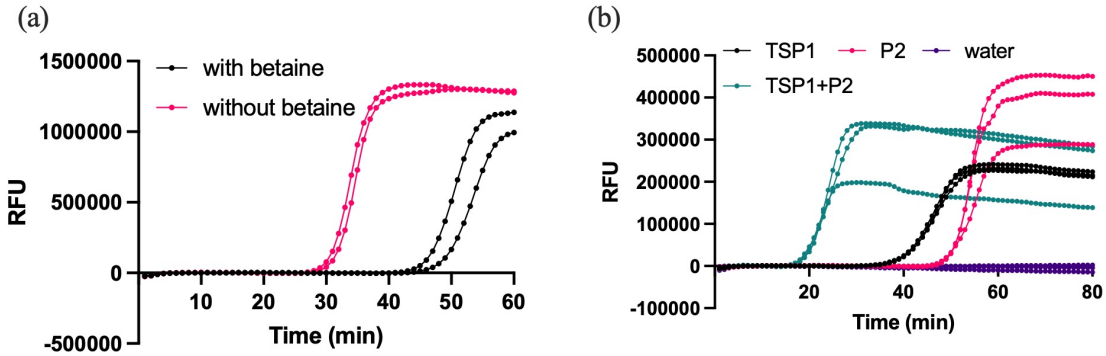


Figure 3-15: Effect of betaine addition and evaluation of the OptiGene Mastermix. (a) Real-time fluorescence amplification curves obtained in the presence and absence of betaine. n=2. (b) Amplification performance using the OptiGene master mix with different primers in the absence of target DNA. Water was used as the negative control. n=3.

3.3.2 CRISPR/Cas12a cleavage verification

One notable function of the CRISPR/12a system *cis*- cleavage is its ability to recognise target sequences under the guidance of crRNA, and the Cas12a-crRNA complex could cleave the double strands and generate staggered DNA ends. To evaluate the *cis*- cleavage activity of the Cas12a, we designed a pair of PCR primers targeting the template region across the cleavage site (Figure 3-16a). After CRISPR treatment, the template was cut into two separate parts, thereby preventing successful amplification by PCR primers. In contrast, untreated templates remain intact and can be amplified more efficiently. Therefore, the cleavage activity of CRISPR can be assessed by comparing the amplification performance at the same template concentration. Additionally, the cleaved products can be directly visualised using gel electrophoresis.

As shown in (Figure 3-16b), a clear band of HPV18 template was observed at 120 bp size. In the presence of both Cas12a and crRNA, the band of the 120 bp band almost disappeared, indicating successful cleavage of the target DNA. In contrast, no obvious reduced band intensity was observed when either Cas12a or crRNA was omitted, confirming that both components are required for sequence-specific target cleavage. The band near the sample loading well may be the r2.1 buffer.

To further investigate the effect of CRISPR cleavage, treated and untreated templates were analysed by real-time PCR (Figure 3-16c). For all template concentrations tested, the CRISPR-

treated samples showed delayed amplification compared with the untreated controls. This result suggests that Cas12a cleavage reduced the amount of intact template available for PCR amplification[11]. The difference between the treated and untreated samples became smaller at lower template concentrations, indicating that the qPCR-based cleavage assay had a reduced ability to distinguish cleaved from uncleaved templates at low copy numbers.

It is surprising to see the 120 bp template band was almost invisible in the last lane. Cas12a only cut the template into two fragments of 78 bp and 42 bp. One possibility is that the template was very short. Once the cis-cleavage was triggered, the remaining fragments may become partially separated into single-stranded DNA, and Cas12a can further cleave the ssDNA via its *trans*- cleavage activity. As a result, the cleavage products may have been degraded and not visible on the gel.

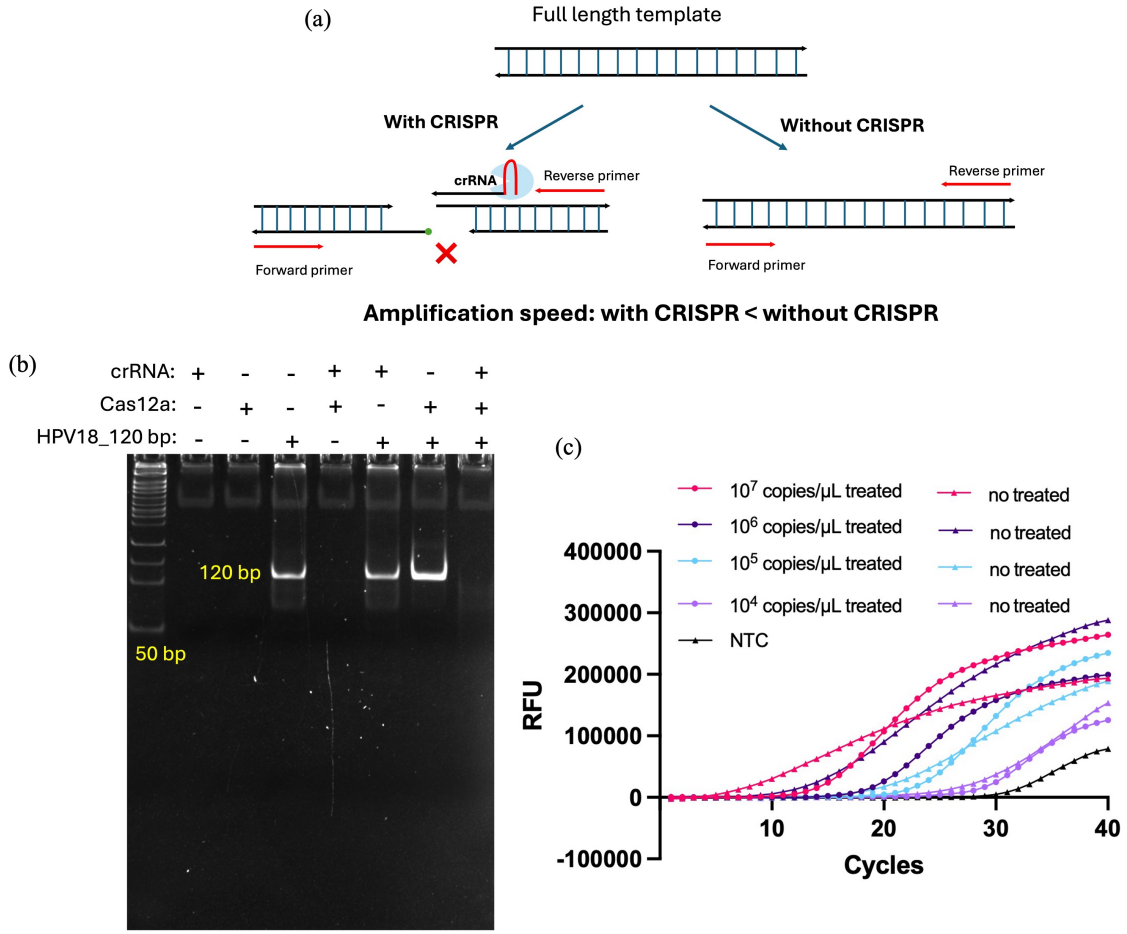


Figure 3-16: Verification of CRISPR/Cas12a cleavage efficiency by PCR amplification. (a). Two primers were designed to amplify the sequence adjacent to the CRISPR target region. (b). Denaturing PAGE gel electrophoresis of 120 bp template for identification of cis-cleavage. (c). Real-time fluorescence curves of PCR amplification for CRISPR-treated and untreated templates. Curves represent the mean of two replicate reactions per condition (n = 2).

To verify our hypothesis, the target template was extended from 120 bp to 307 bp. After

cleavage of the 307 bp template, a longer DNA fragment was expected to show up and be visible on the gel. As shown in Figure 3-17a, the intensity of the target strand was gradually decreased, while a new band showed up just below the target strand, which is the cleavage product. The second 42 bp cleavage product was too small and not expected to be seen on the gel. Interestingly, even after 30 min incubation, the first band still did not disappear. We assumed it was because the amount of input DNA was too high. According to the manufacturer's recommendation, the optimal ratio of Cas12a: crRNA: target DNA is 10:10:1. As the cis-cleavage owns single turnover rate, excessive template may not be digested completely. Therefore, we tried to reduce the input DNA from 26 ng to 13 ng and 5.2 ng. Meanwhile, we tested different inactivation methods, including heat and Proteinase K treatment. In Figure 3-17b, when the input template amount was reduced to 13 ng, the upper band disappeared (lane 5), indicating that the input target was fully cleaved by Cas12a. In addition, we find that the band near the loading well disappears after Proteinase K treatment (lane 6), suggesting that this band is from the r2.1 buffer, which contains recombinant albumin that can also be digested by Proteinase K.

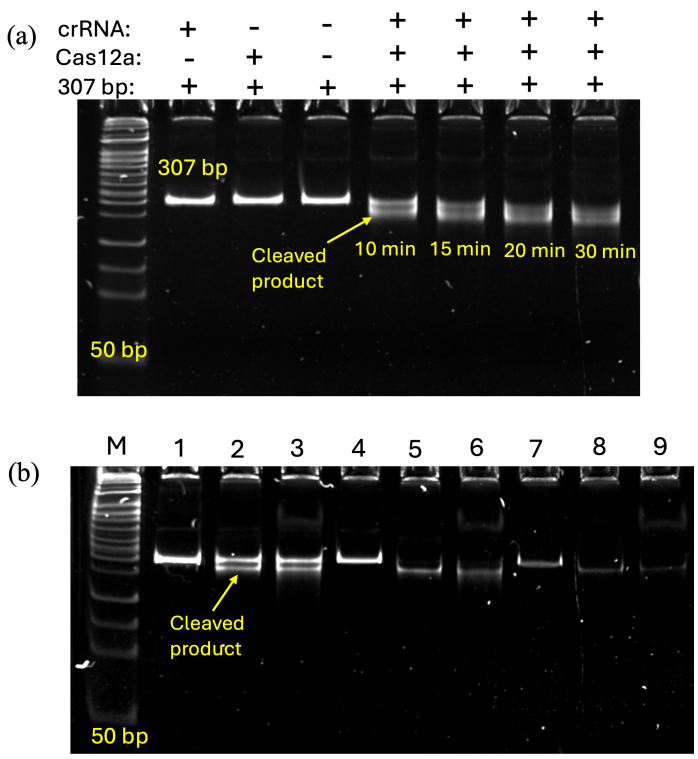


Figure 3-17: Denaturing PAGE gel electrophoresis of 307 bp template after CRISPR treatment. (a) Cis-cleavage of the 307 bp template at different digestion times (10, 15, 20, and 30 min). (b) Cleavage analysis of different amounts of template after 10 min and Cas12a inactivation methods. Lanes 1–3, 4–6, and 7–9 contained 26 ng, 13 ng, and 5.2 ng template, respectively. Lanes 2, 5, and 8 were treated with Proteinase K, whereas lanes 3, 6, and 9 were heat-treated.

3.3.3 Development of CRISPR/Cas12a-integrated loop amplification assay

Analytical evaluation of loop amplification assay

The analytical performance of loop amplification using core primers was first evaluated. To evaluate the detection performance of the loop amplification assay independently, a synthetic single-stranded DNA template (a-b1-b2-c) was employed. 16-TSP1 (c*-a-e-f-e*) and 16-P2 (a-b) were used as primers for amplification. As demonstrated in Figure 3-18a, the HPV16 target signal could be clearly distinguished from the NTC, demonstrating the feasibility of the amplification system. Serial dilutions of template were tested to investigate the lowest detectable input under the tested conditions (Figure 3-18b). The TTP increased progressively as the template concentration decreased from 10^9 to 10^5 copies/reaction, showing an approximately linear relationship between the logarithm of template concentration and TTP. Within a 60 min reaction, 10^5 copies/reaction was consistently detected, while no amplification was observed in the NTC. When the reaction time was extended, 10^4 copies/reaction was also detected, with a TTP of approximately 70 min (Figure 3-18c). Therefore, the lowest detected concentration within the 60 min assay period was 10^5 copies/reaction, although detection of 10^4 copies/reaction was possible with a longer reaction time. This sensitivity is sufficient for evaluating the amplification mechanism and for subsequent integration with CRISPR-based signal detection. However, further improvement would be required for applications involving low target concentrations, particularly clinical samples without prior target enrichment.

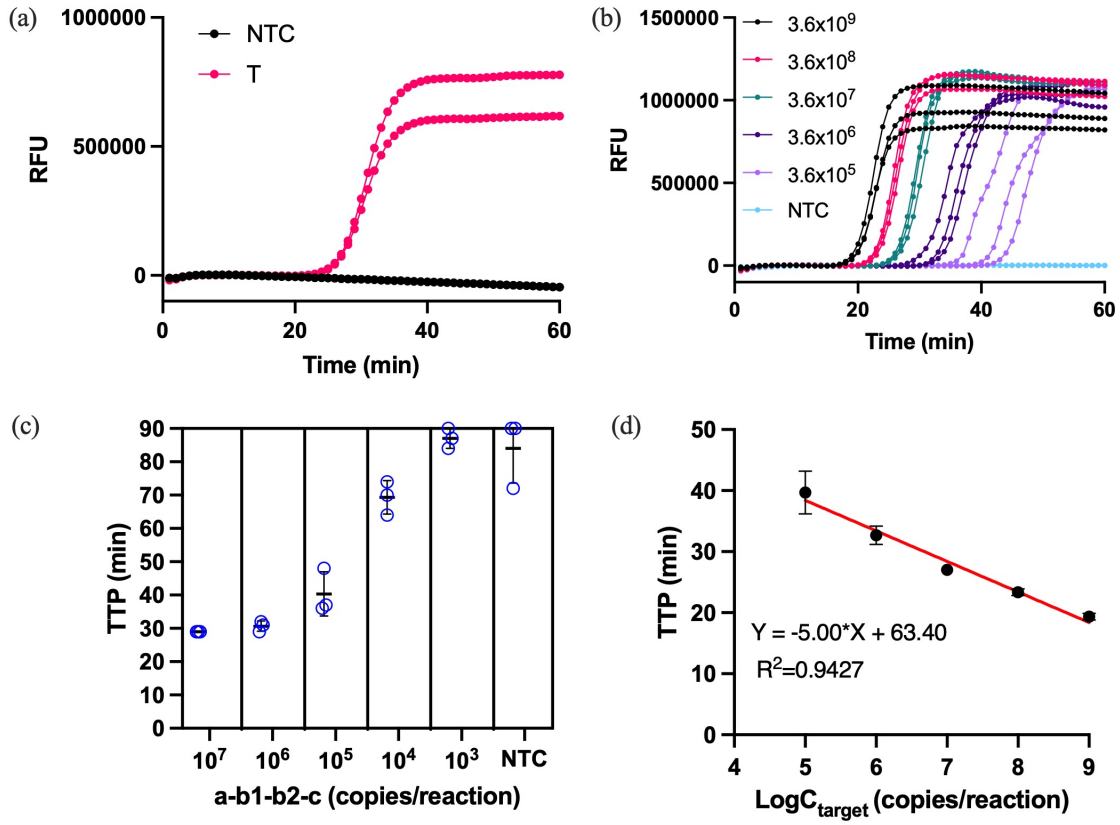


Figure 3-18: Evaluation of the feasibility and concentration-dependent amplification behaviour of the loop amplification system. (a) Real-time fluorescence amplification curves using the HPV16 "a-b1-b2-c" ssDNA template. (b) Real-time fluorescence curves at different target DNA concentrations (3.6×10^5–3.6×10^9 copies/reaction). (c) Time-to-positive (TTP) values for target concentrations ranging from 10^3 to 10^7 copies/reaction over a 90 min reaction period. (d) Linear regression of TTP against the logarithm of target concentration over the range of 10^5–10^9 copies/reaction during a 60 min reaction period. Individual measurements are shown in (c), and error bars represent mean ± SD (n = 3) in (c) and (d).

The analytical performance of the HPV18 assay was evaluated in the same manner using serial dilutions of HPV18 ssDNA (Figure 3-19). The TTP value increased as the template concentration decreased. Amplification in both replicates was observed down to 10^5 copies/reaction, while lower concentrations showed larger variation and overlapped with the NTC group, indicating reduced reproducibility at lower inputs. In particular, no amplification was observed at 10^4 copies/reaction, whereas only one of the two 10^3 copies/reaction replicates amplified at approximately 56 min. This isolated positive result was not considered reliable detection, as it may have resulted from stochastic amplification at low template concentration or non-specific amplification. Therefore, 10^5 copies/reaction was considered the lowest tested input at which amplification was observed in both replicates of the HPV18 assay under these conditions.

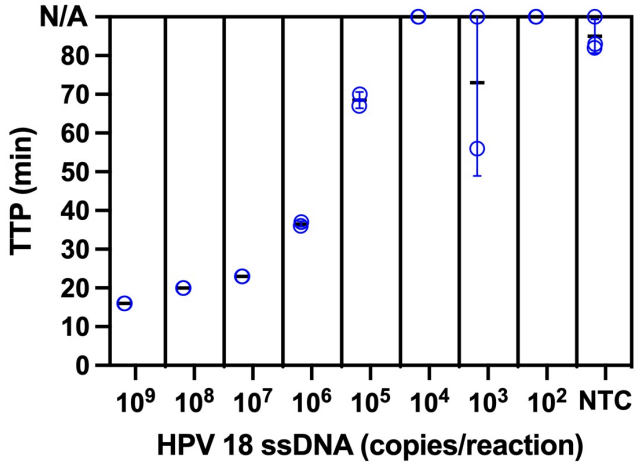


Figure 3-19: Time-to-positive (TTP) values for HPV18 ssDNA amplification at different target concentrations (10^2–10^9 copies/reaction). Individual data points are shown, with horizontal bars representing the mean and error bars indicating the range (n = 2). N/A indicates reactions in which no amplification was detected within the 90 min experimental period.

The analytical performance of the HPV52 assay was also evaluated using both TSP1+P1 primer set and the TSP1+P1+d-outer primer set. The TSP1+P1 primer set can detect 10^5 copies/reaction (Figure 3-20a). After adding the d-outer primer, amplification was observed at 10^3 copies/reaction, representing a 100-fold lower detected input than the 10^5 copies/reaction observed without the outer primer (Figure 3-20b). Although one replicate at 10^2 copies/reaction produced amplification, the result was not reproducible and was therefore not considered reliable detection. These results indicate that the outer primer enhanced amplification from low-copy-number templates, likely by providing an additional strand-displacement initiation site. These results demonstrate that the addition of an outer primer can serve as an effective strategy for improving the sensitivity of the loop amplification assay.

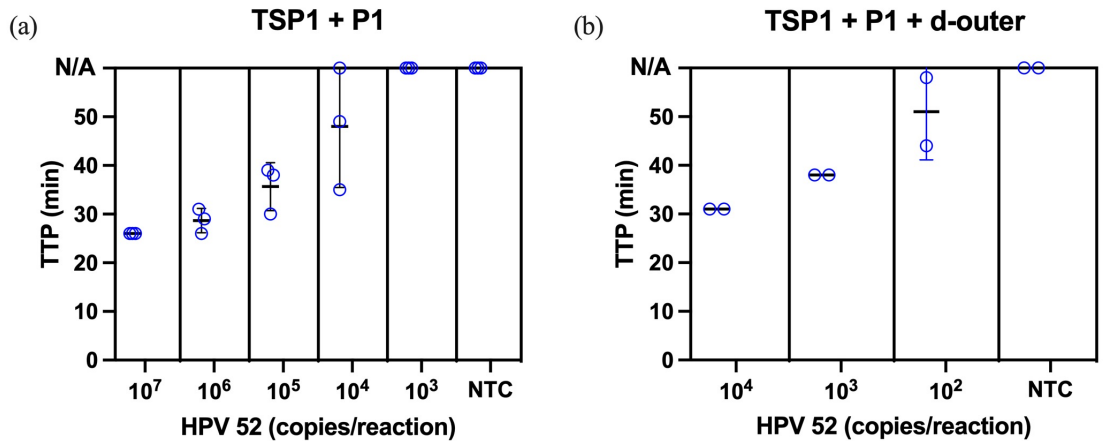


Figure 3-20: Time-to-positive (TTP) for HPV52 amplification at different target DNA concentrations with (b) and without (a) the d-outer primer. Individual data points represent replicate reactions (n = 3 for panel a and n = 2 for panel b). N/A indicates reactions in which no amplification was detected within the experimental period.

Compatibility between amplification and CRISPR/Cas12a reactions

The TTP time of intact 120 bp template (UNCUT), CRISPR-treated 120 bp template (CRISPR), and 78 bp mimic cut product (CUT1S1A) was compared using the TSP3+b1 primer set. As shown in Figure 3-21, the mimic cut product showed the shortest TTP time (21 min), followed by the intact template (23 min). In contrast, the CRISPR-treated template showed a longer TTP (32 min). This observation is consistent with the previous cleavage experiments, which showed that 120 bp template was digested by Cas12a after cleavage. Template loss may have contributed to the delayed TTP. However, amplification of the intact template shows that a Cas12a-generated end was not essential for amplification under these conditions, leaving the proposed initiation pathway incompletely established. Based on these results, a longer HPV 52 template (500 bp) was selected for further investigation.

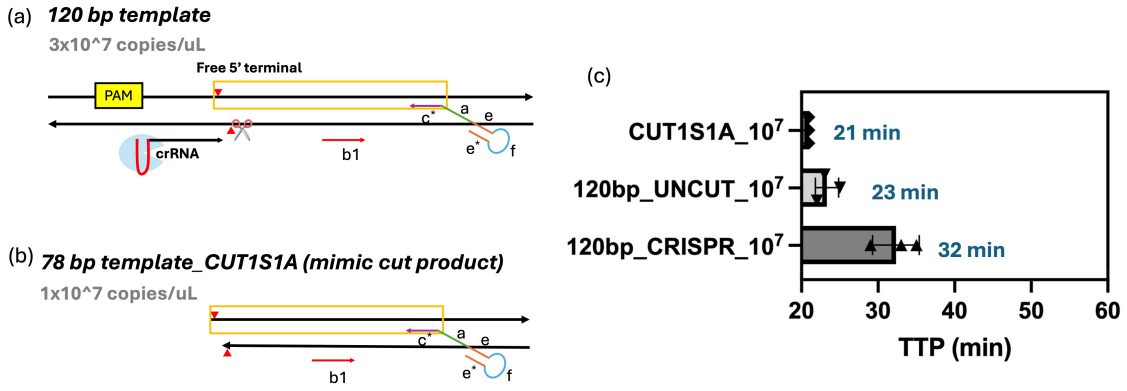


Figure 3-21: Comparison of amplification using intact (UNCUT), CRISPR-cleaved (CRISPR), and mimic cut-product templates (CUT1S1A). (a) Schematic of the 120 bp template showing the CRISPR/Cas12a cleavage site and primer-binding regions. (b) Schematic of the 78 bp mimic cut-product template and primer-binding regions. (c) TTP comparison using the TSP3+b1 primer set. Individual data points represent replicate reactions (n = 3), and bars and error bars represent mean ± SD.

The delayed amplification observed after CRISPR treatment may be caused by several factors. One possibility is that the 120 bp template was too short and was degraded after CRISPR cleavage, leaving less template available for amplification. Another possibility is that some components in the CRISPR reaction were not compatible with the loop amplification system and therefore inhibited amplification efficiency. To investigate these possibilities, a longer HPV52 template (500 bp) was selected for further studies. In addition, the effects of different CRISPR reaction components on loop amplification were systematically evaluated. Interestingly, amplification was also observed with the intact template, suggesting that Cas12a cleavage was not strictly required for amplification initiation under the tested conditions. One possible explanation is that the primer-binding region may become transiently accessible through local DNA strand opening, allowing primer hybridisation and subsequent extension even without cleavage. Therefore, rather than serving as an essential initiation step, Cas12a cleavage may facilitate amplification by generating a more accessible DNA end for primer binding. However, this potential advantage was not clearly demonstrated in the present experiment, as the CRISPR-treated template showed delayed amplification, possibly due to excessive cleavage of the short template or inhibition by CRISPR reaction components. Further investigation would be required to establish the contribution of Cas12a cleavage to primer accessibility and amplification efficiency.

As shown in Figure 3-22a, the amplification-only reaction showed the shortest TTP value. In contrast, the mock-CRISPR, CRISPR-treated and spike-in CRISPR groups all showed delayed amplification. Since the mock-CRISPR group did not contain active target cleavage, and spike-in CRISPR did not perform CRISPR reaction process, this result suggests that the slower amplification was not only caused by template digestion, and the components of the CRISPR reaction may also inhibit amplification. To identify where the inhibitor comes from,

the input CRISPR volume and r2.1 buffer volume were reduced separately (Figure 3-22b). The original CRISPR still had the slowest amplification. When the CRISPR reaction volume was reduced from 3 µL to 1.5 µL (green curve to orange curve), the amplification advanced. A further improvement was observed in the reduced r2.1 buffer group (purple curve). In contrast, adding extra r2.1 buffer to the amplification only delayed amplification (red curve). These results suggest that r2.1 buffer was responsible for the delay.

However, as the r2.1 buffer is essential for the CRISPR environment, we further tested which component affected the amplification most. In Figure 3-22c, Tris-HCl, BSA and NaCl showed only minor effects on the amplification, while $MgCl_2$ caused a delay, suggesting that the high Mg^{2+} concentration is one of the main factors affecting the reaction. Based on these findings, a homemade 2.1 buffer was prepared and compared with the original NEB r2.1 buffer (Figure 3-22d). The homemade buffer improved amplification performance, and the reduction of Mg^{2+} led to additional improvement.

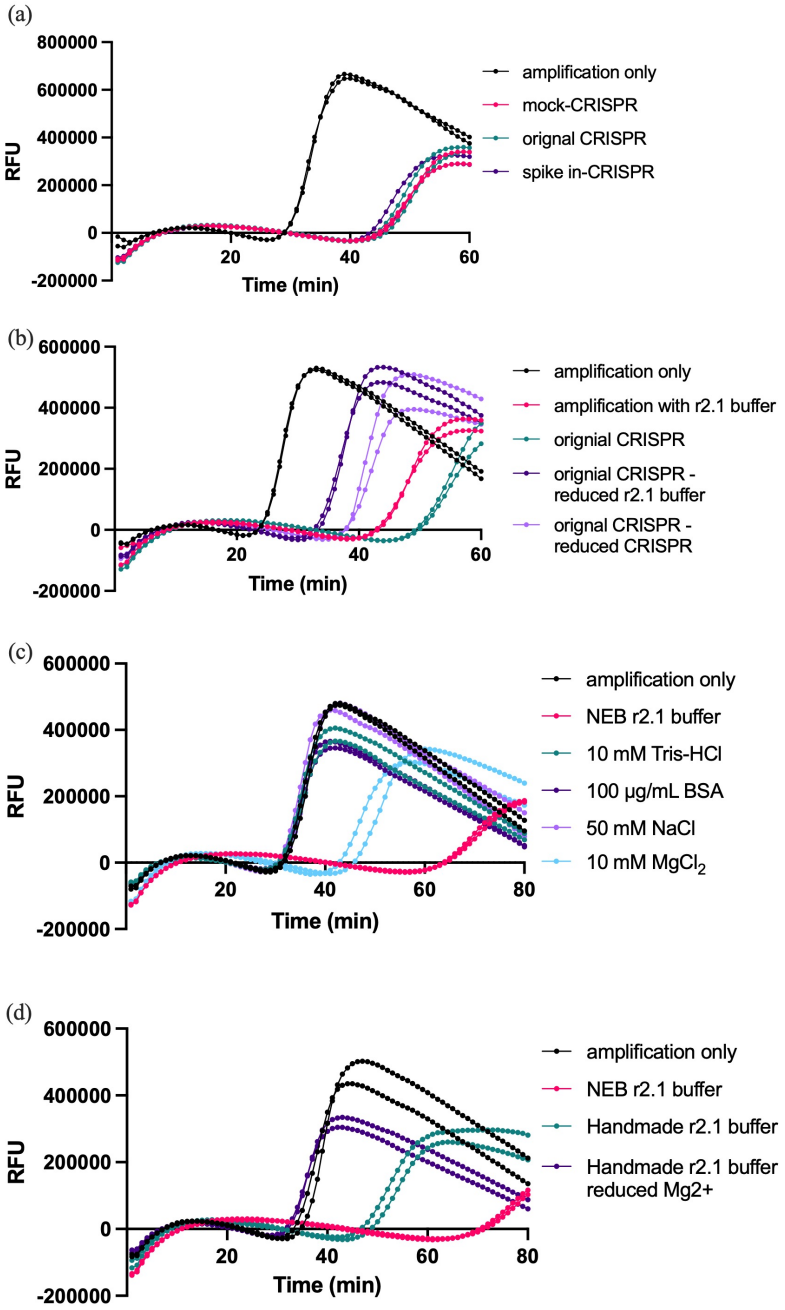


Figure 3-22: Investigation of the delayed amplification observed following the addition of CRISPR/Cas12a reaction components. (a) Comparison of amplification-only, mock-CRISPR, original CRISPR, and spike-in CRISPR reactions. Amplification-only refers to reactions without CRISPR components. Mock-CRISPR refers to reactions using non-targeting HPV16/18 crRNA instead of HPV52 crRNA, while original CRISPR contains the target-specific HPV52 crRNA and Cas12a. In spike-in CRISPR reactions, the CRISPR mixture was pre-incubated without target DNA before the template was added. (b) Effect of reducing buffer and CRISPR/Cas12a components. Reduced r2.1 buffer refers to a lower contribution of Mg^{2+} from the CRISPR buffer, while reduced CRISPR refers to a reduced volume of the CRISPR reaction mixture added to the amplification system. (c) Effect of individual buffer components on amplification, including Tris-HCl, BSA, NaCl, and $MgCl_2$. (d) Comparison of commercial and handmade r2.1 buffer formulations, including a formulation with reduced Mg^{2+} concentration. Individual fluorescence traces represent duplicate reactions for each condition (n = 2).

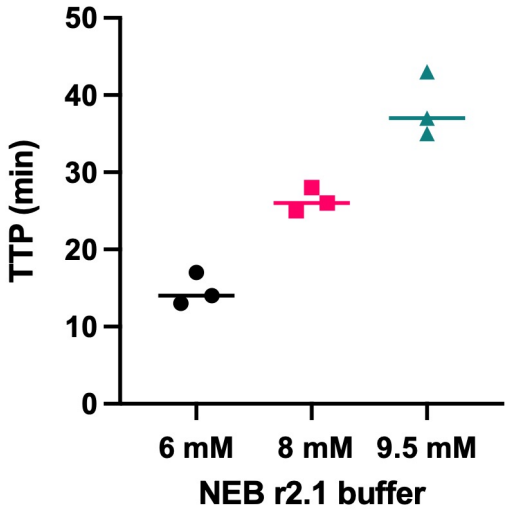


Figure 3-23: Optimisation of total Mg^{2+} concentration in the CRISPR/Cas12a-integrated loop amplification assay. Time-to-positive (TTP) values were compared at total Mg^{2+} concentrations of 6, 8, and 9.5 mM. Individual data points represent replicate reactions (n = 3), and horizontal bars indicate the mean TTP.

The total Mg^{2+} concentration was further optimised for the integrated loop amplification–CRISPR/Cas12a assay (Figure 3-23). Increasing the Mg^{2+} concentration from 6 to 9.5 mM progressively delayed amplification, with the mean TTP increasing from approximately 14 min at 6 mM to 37 min at 9.5 mM. Mg^{2+} is required for Cas12a-mediated DNA cleavage and has been shown to stabilise PAM-distal DNA unwinding, thereby promoting target-strand binding and cleavage required for complete dsDNA cleavage.[167] However, Mg^{2+} also affects primer hybridisation, DNA secondary structure, and polymerase activity, and excessive Mg^{2+} may affect the efficiency of isothermal amplification. In the amplification-only optimisation, increasing the Mg^{2+} concentration accelerated both target and non-specific amplification. In contrast, in the integrated CRISPR–amplification system, increasing the Mg^{2+} concentration from 6 to 9.5 mM progressively delayed the TTP. This difference suggests that the optimal Mg^{2+} concentration was altered by the inclusion of the CRISPR components, rather than indicating a general inhibitory effect of high Mg^{2+} on loop amplification. The delay may therefore reflect changes in the balance between Cas12a cleavage and subsequent amplification, or interactions among Mg^{2+}, CRISPR components and amplification intermediates. Since 6 mM Mg^{2+} produced the shortest TTP under the integrated reaction conditions, it was selected for subsequent experiments.

Comparison of loop amplification only, two-step, and one pot detection

After optimisation, the amplification-only, two-step, and one-pot formats were compared using different concentrations of HPV18 template (Figure 3-24). The one-pot assay produced the shortest TTP values across the tested template concentrations, followed by the two-step

assay, whereas the amplification-only format showed the longest TTP values. The difference became more pronounced at lower template concentrations. One possible explanation is that Cas12a cleavage alters the structure of the target dsDNA and increases the accessibility of the primer-binding regions. In the one-pot format, cleavage and amplification occur simultaneously, allowing the cleavage-treated template to enter the amplification process immediately. In contrast, the two-step format requires transfer of the CRISPR-treated product into a separate amplification reaction, which introduces an additional handling step and dilutes the template. However, the exact mechanism responsible for the shorter TTP in the one-pot assay was not directly investigated. Overall, the one-pot format provided the fastest amplification under the tested conditions.

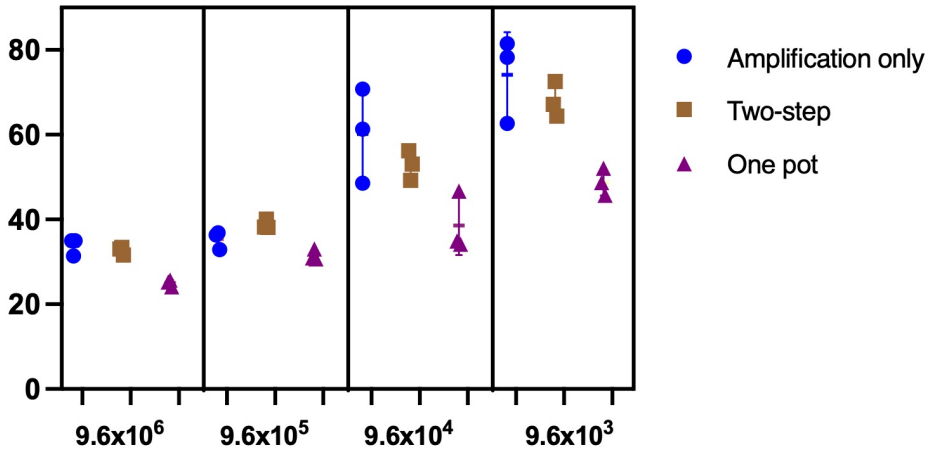


Figure 3-24: Comparison of the TTP values obtained by amplification-only, two-step, and one-pot detection formats at different target DNA concentrations (9.6×10^3–9.6×10^6 copies/reaction). Individual data points represent replicate reactions (n = 3 per condition), and horizontal bars indicate the mean TTP.

3.3.4 Development of multiplex detection assay

We also demonstrated the multiplexing capability of the developed CRISPR-integrated loop amplification assay through the detection of high-risk HPV16 and HPV18, and HPV 52 genomic DNA.

The feasibility of duplex detection of HPV16 and 18 was initially validated using synthetic ssDNA (a-b1-b2-c) as a model template. As shown in Figure 3-25, amplification curves indicated successful detection of individual and dual targets without observable cross-interference. Moreover, melting curve analysis in Figure 3-25b showed distinct melting temperatures for the HPV16 and HPV18 single-target products and a distinct melting profile for the mixed sample. These results support discrimination of the single-target products. The mixed HPV16/18 sample exhibited a single intermediate melting peak rather than two clearly resolved peaks corresponding to the individual targets. This observation may be consistent with the presence

of mixed amplification products with overlapping melting profiles. However, the identity of the products could not be determined from melting curve analysis alone. This highlights a limitation of the melt-based readout for distinguishing multiple targets within the same reaction. Future work could employ gel electrophoresis or high-resolution melting analysis to further characterise the amplification products and evaluate the reliability of duplex discrimination.

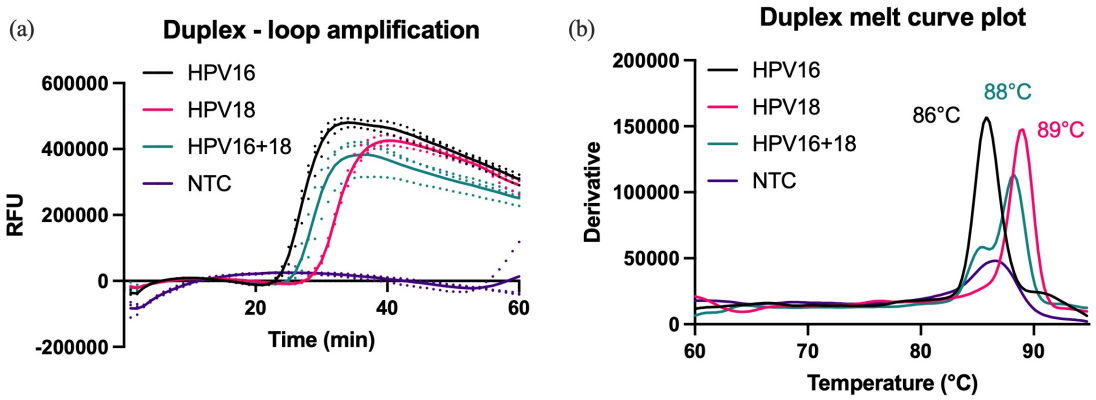


Figure 3-25: Duplex HPV16/18 amplification using the loop amplification system. (a) Real-time fluorescence curves for individual HPV16 and HPV18 targets, their mixture (HPV16+18), and the no-template control (NTC). (b) Melting curve analysis of the amplification products, showing melting peaks at approximately 86 °C for HPV16, 89 °C for HPV18, and an intermediate peak at 88 °C for the mixed sample. Each target was tested at 10^7 copies/reaction. Three replicate reactions were performed per condition (n = 3).

The duplex assay was then combined with the CRISPR/Cas12a system in both two-step and one-pot formats (Figure 3-26). In the two-step assay, HPV16 and HPV18 could both be detected individually (Figure 3-26a). Similar results were obtained with the one-pot assay (Figure 3-26c). In both formats, HPV16 reached the amplification threshold earlier than HPV18. In the two-step assay, the TTP values were approximately 30 min for HPV16 and 50 min for HPV18. In the one-pot assay, HPV16 reached the threshold at approximately 42 min, around 6–8 min earlier than HPV18, confirming that HPV16 amplified faster under both conditions. Melting curve analysis also showed distinct melting peaks for individually tested HPV16 and HPV18 targets and an intermediate melting profile for the mixed samples (Figure 3-26b, d). HPV16 and HPV18 produced different melting peaks when tested separately. In the mixed samples, a broader peak appeared between the HPV16 and HPV18 peaks. This intermediate melting profile is consistent with the possible presence of mixed amplification products, although the identity and relative abundance of the individual products cannot be determined from melting curve analysis alone.Similar melting patterns were observed for both the two-step and one-pot assays.

Multiplex HPV detection has also been demonstrated using conventional LAMP-based approaches. For example, Barra et al. developed a single-tube multiplex LAMP assay for

HPV16, HPV18 and HPV45, together with a human cellular control, demonstrating the feasibility of multiplex detection despite the use of multiple primer sets[94]. In comparison, the present study explored a simplified two-core-primer amplification architecture integrated with CRISPR/Cas12a. Although the duplex assay produced distinguishable melting peaks for individual HPV16 and HPV18 targets, the mixed sample exhibited a broad intermediate peak rather than two clearly resolved peaks. This indicates that reliable genotype discrimination in mixed samples remains to be established.

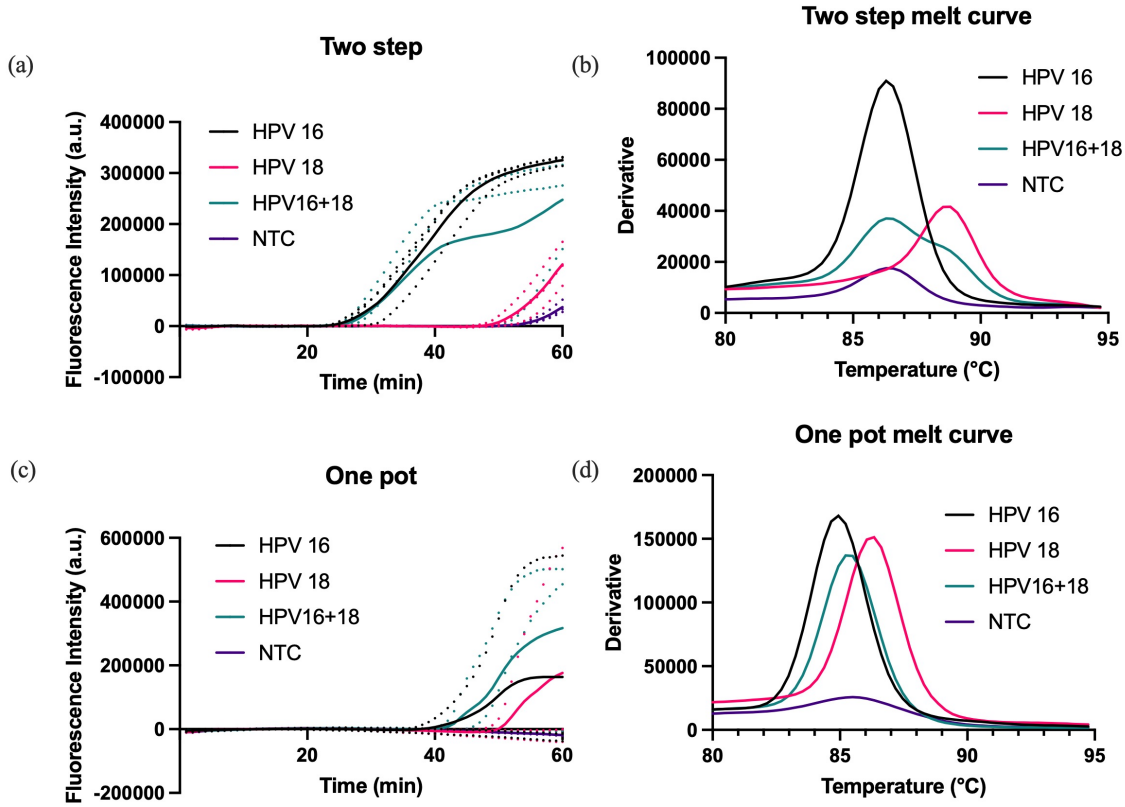


Figure 3-26: Multiplex HPV16 and 18 detection using CRISPR-integrated loop amplification. (a) Real-time fluorescence amplification curves and (b) melting curve for the two-step assay. (c) Real-time fluorescence amplification curves and (d) melting curve analysis for the one-pot assay. Each target was tested at 10^5 copies/reaction. HPV16+18 represents reactions containing both HPV16 and HPV18 targets, while NTC represents the no-template control. Three replicate reactions were performed per condition (n = 3). The mixed HPV16/18 samples exhibited overlapping or intermediate melting peaks rather than two clearly resolved peaks, indicating a limitation of melt-based discrimination.

Triplex detection of HPV16, HPV18 and HPV52 was further evaluated (Figure 3-27). In the CRISPR-integrated loop amplification assay, HPV16 showed the shortest TTP value, followed by HPV18 and HPV52 (Figure 3-27a), indicating different amplification efficiencies among the three targets. Melting curve analysis showed distinct melting temperatures for the three HPV subtypes, with HPV16, HPV52 and HPV18 producing peaks at approximately 86, 87 and 88 °C, respectively (Figure 3-27b). The three HPV subtypes produced distinct

melting peaks, showing that their individual amplification products could be distinguished by melting curve analysis under the triplex assay conditions. The triplex primer mixture was also evaluated in a one-pot format (Figure 3-27c). HPV16 and HPV18 maintained efficient amplification, whereas HPV52 showed a longer TTP value, potentially due to competition among the multiple primer sets and CRISPR components. Nevertheless, each of the three HPV targets could be detected when tested individually in the presence of all three primer sets. These results support the feasibility of the CRISPR-integrated loop amplification system for amplification of individually tested HPV targets under triplex primer conditions.

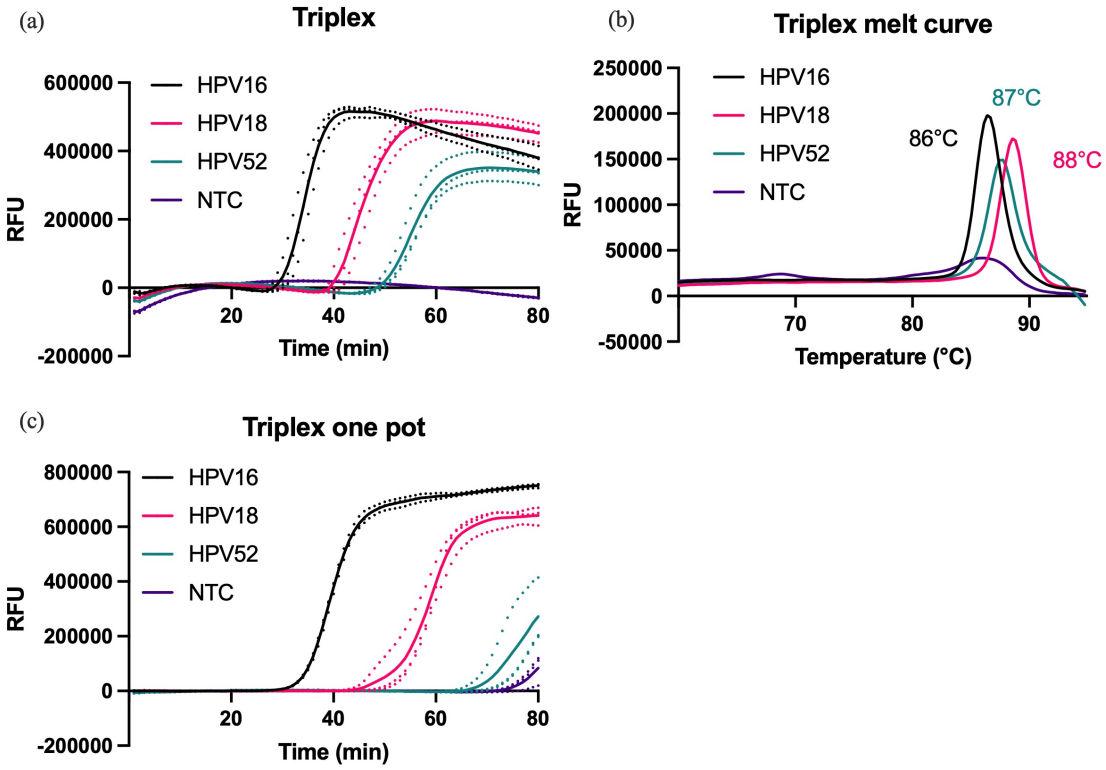


Figure 3-27: Detection of HPV16, HPV18 and HPV52 using a triplex CRISPR-integrated loop amplification assay. (a) Real-time fluorescence amplification curves and (b) melting curve analysis for the two-step assay. (c) Real-time fluorescence amplification curves for the one-pot assay. The colored numbers in (b) indicate the melting temperatures (Tm) of the corresponding amplicons. Each target was tested at 10^7 copies/reaction. n=3. Melting curve analysis was performed for the two-step assay, while the one-pot assay was evaluated using real-time fluorescence measurements only.

In order to reduce non-specific amplification signal in the triplex assay, different primer concentrations were evaluated (Figure 3-28a). At the original primer concentration of 1 µM, amplification was observed in the NTC group within 30 min. In contrast, reducing the primer concentration to 750, 700, 650 or 600 nM substantially delayed background amplification, with NTC signals appearing after 100 min. Therefore, 700 nM was selected for subsequent triplex experiments. Using the optimised primer concentration, triplex detection of HPV16,

HPV18 and HPV52 was evaluated with different concentrations (Figure 3-28a, b). Both HPV16 and HPV18 could be detected at 10^5 copies, with TTP values below the 60 min threshold. HPV52 showed longer TTP values and greater variation, indicating lower amplification efficiency. Nevertheless, all three HPV targets could be distinguished from the NTC group, demonstrating the feasibility of triplex detection using the optimised primer concentration.

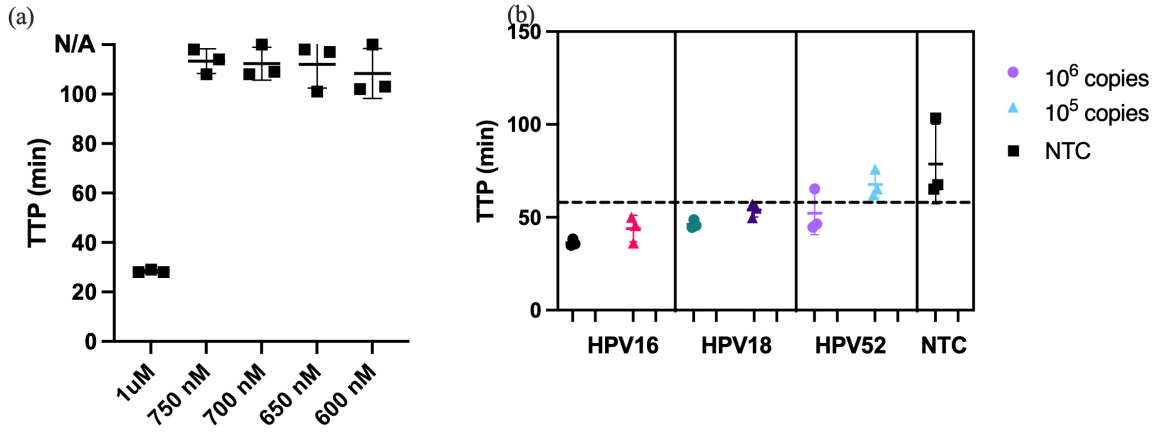


Figure 3-28: Evaluation of primer concentration for triplex loop amplification. (a) TTP values of no-template controls (NTCs) at different primer concentrations. (b) TTP values for HPV16, HPV18 and HPV52 at 10^6 and 10^5 copies/reaction, using a primer concentration of 700 nM. The dashed line indicates a reference TTP of approximately 60 min, based on the observed NTC amplification behaviour. Individual data points represent replicate reactions (n = 3), and error bars indicate SD for reactions with measurable TTP values. N/A indicates no detectable amplification within the experimental period.

Previous studies have demonstrated that multiplex LAMP can achieve detection of multiple targets in one reaction. For instance, Malpartida-Cardenas et al.[152] demonstrated five-target digital LAMP using single-channel amplification curve analysis. In comparison, the present study investigated a simplified amplification strategy requiring two core primers per target and explored its compatibility with CRISPR/Cas12a in two-step and one-pot formats. Under the triplex primer conditions, HPV16, HPV18 and HPV52 generated distinguishable amplification responses when tested individually, while the two-step assay produced different melting temperatures for the three targets. Although reducing primer concentration delayed non-specific amplification in the NTC, the present study did not establish that using fewer primers inherently reduces non-specific amplification compared with conventional LAMP. Future studies should directly compare the proposed two-core-primer amplification system with conventional LAMP to determine whether reducing the number of primers can simplify assay optimisation, reduce non-specific amplification, and improve multiplexing performance.

3.3.5 Analytical performance of CRISPR/Cas12a integrated loop amplification

The analytical performance of the CRISPR/Cas12a-integrated loop amplification assay was evaluated using serial dilutions of HPV16, HPV18, and HPV52 genomic templates. For HPV16, both the two-step and one-pot assays showed an inverse relationship between target concentration and TTP (Figure 3-29). As the target concentration decreased, the TTP increased because fewer initial template molecules required more amplification cycles to reach the fluorescence threshold. An approximately linear relationship was observed between the logarithm of target concentration and TTP, with R^2 values of 0.9154 for the two-step assay and 0.9423 for the one-pot assay. This trend is expected for exponential nucleic acid amplification, in which a ten-fold decrease in starting template concentration produces a progressive delay in threshold detection. Both assay formats detected HPV16 down to 10^4 copies per reaction.

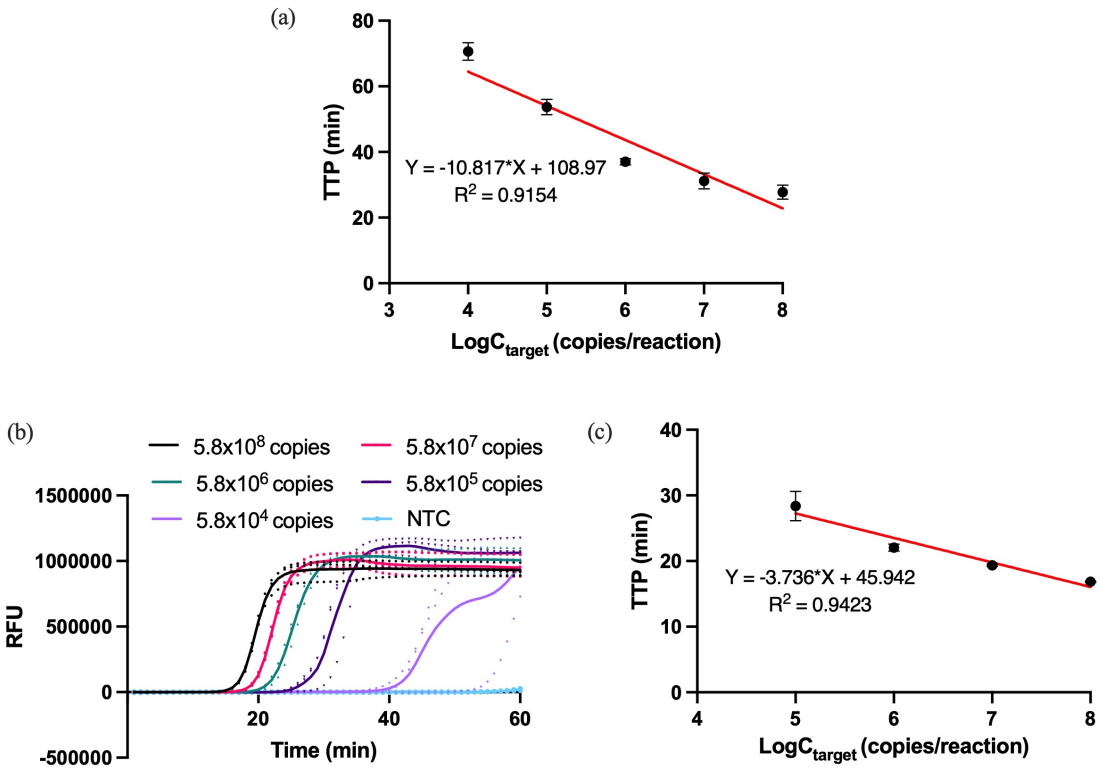


Figure 3-29: Analytical performance of the two-step and one-pot HPV16 detection assays. (a) Linear regression of time-to-positive (TTP) against the logarithm of HPV16 target concentration (5.8×10^4–5.8×10^8 copies/reaction) for the two-step assay. (b) Real-time fluorescence amplification curves at different HPV16 target concentrations (5.8×10^4–5.8×10^8 copies/reaction) using the one-pot assay. (c) Linear regression of TTP against the logarithm of HPV16 target concentration (5.8×10^5–5.8×10^8 copies/reaction) for the one-pot assay. Error bars in (a) and (c) represent standard deviation (SD, n = 3)

A similar trend was observed for HPV18 (Figures 3-30, 3-31). The TTP value increased with decreasing target concentration. The two-step assay showed good linearity ($R^2 = 0.9695$) and detected approximately 10^4 copies per reaction. In the one-pot format, amplification could still be observed at lower template concentrations 10^2 copies, indicating improved sensitivity.

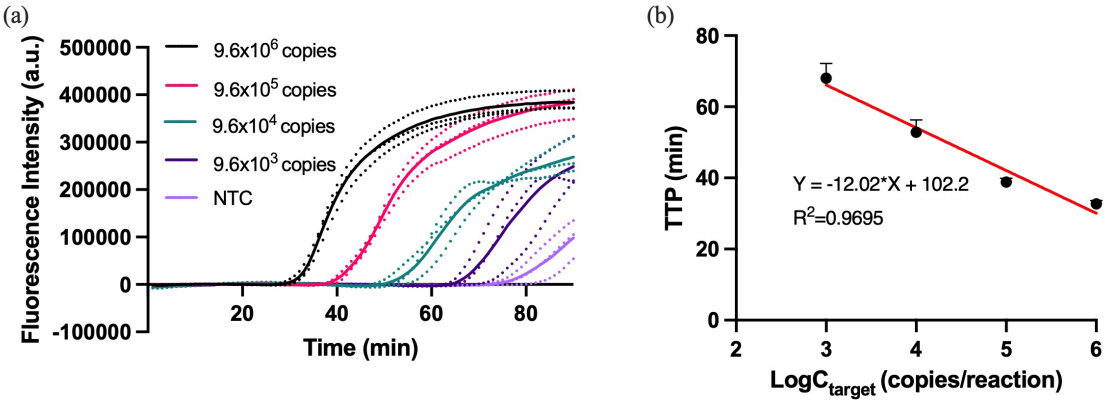


Figure 3-30: : Analytical performance of the two-step HPV18 detection assay. (a) Real-time amplification curves at different HPV18 target concentrations, including the no-template control (NTC). (b) Linear relationship between time-to-positive (TTP) and the logarithm of target concentration. Error bars represent standard deviation (SD, n = 3).

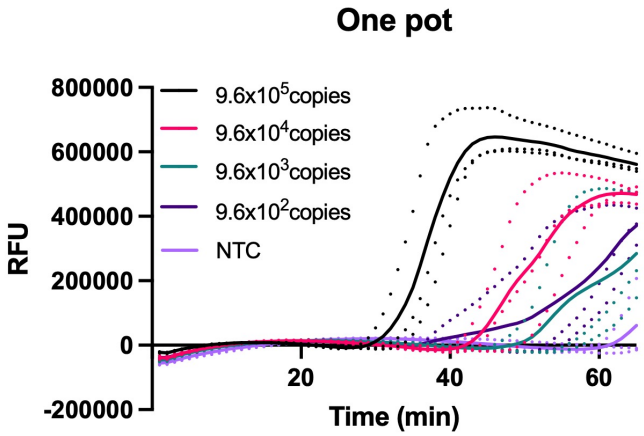


Figure 3-31: Real-time amplification curves of the one-pot HPV18 detection assay at different target concentrations, including the no-template control (NTC). n=3.

The analytical performance of the HPV52 two-step assay was also evaluated (Figure 3-32). A linear relationship between target concentration and TTP was obtained ($R^2 = 0.9077$), and amplification was detected down to approximately 10^3 copies per reaction. n=3.

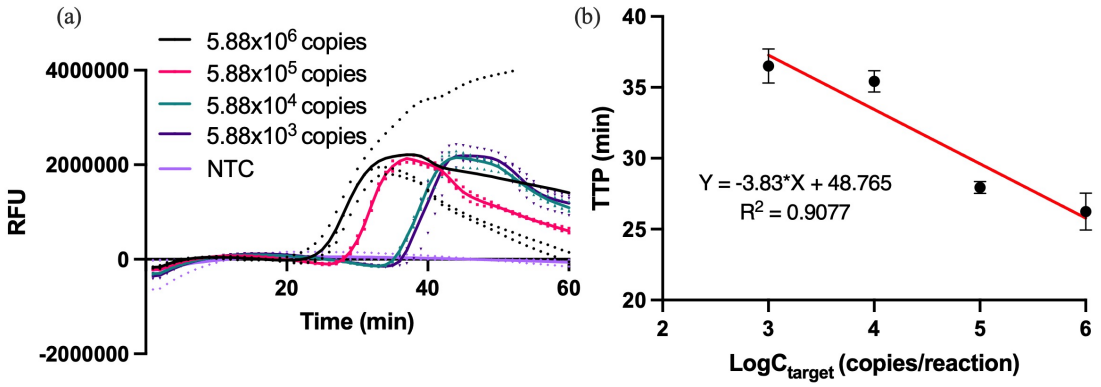


Figure 3-32: Analytical performance of the two-step HPV52 detection assay. (a) Real-time amplification curves at different HPV52 target concentrations, including the no-template control (NTC). Individual fluorescence curve represent triplicate reactions (n = 3 per condition). (b) Linear regression of time-to-positive (TTP) against the logarithm of target concentration. Error bars represent standard deviation (SD, n = 3).

Overall, the analytical performance evaluation showed that the developed assay was capable of detecting HPV16, HPV18 and HPV52 over a broad concentration range. For all targets, the TTP value increased as the template concentration decreased, and a good correlation between target concentration and TTP was observed. Both the two-step and one-pot formats demonstrated reliable amplification performance, with the one-pot format generally showing shorter TTP values. These results showed a concentration-dependent TTP relationship over the tested range, suggesting potential for semi-quantitative analysis after further validation.

3.4 Conclusion

In this chapter, a simplified CRISPR/Cas12a-integrated loop amplification assay was developed and evaluated for HPV16, HPV18 and HPV52 detection, including preliminary duplex and triplex formats.. The main contributions, key findings, and future directions are summarised below:

- Assay Principle and Simplified Design. Unlike conventional LAMP assays that rely on complex, multi-primer sets (typically 4–6 primers), this study extended previously reported CRISPR-triggered amplification and stem–loop amplification strategies towards a simplified isothermal amplification system. After target recognition, Cas12a cleavage generates DNA fragments with 5′ overhangs, potentially improving primer access to the PAM-distal region. In the proposed amplification mechanism, the cleaved DNA end was designed to act as a termination point for primer extension, thereby facilitating target self-foldback and subsequent loop amplification using only two core primers. However, amplification was also observed using intact templates, suggesting

that the Cas12a-generated 5′ end was not essential for amplification initiation under the tested conditions. Instead, Cas12a cleavage may facilitate amplification by increasing primer accessibility. The precise contribution of cleavage to the amplification mechanism remains to be established.

- Rational Primer Engineering and Optimisation. A systematic primer screening workflow was developed by integrating Gibbs free energy (ΔG) predictions with experimental validation, categorising candidates into risk groups to identify optimal primer sets for HPV16, 18, and 52. Advanced modifications (including extended loop structures, loop-targeting primers, outer primers, and phosphorothioate bonds) were comprehensively evaluated; while some enhanced reaction speed, they introduced unwanted non-specific amplification or assay complexity and were therefore not included in the final design. These results provided useful insights into the influence of primer design on amplification behaviour.

- Mechanistic Insights and System Compatibility. Optimisation revealed critical conditions for system integration: a TSP ratio of 1:2, a 21-nt P primer capture region, a 63 °C reaction temperature, and 6 mM Mg^{2+}. The compatibility between loop amplification and the CRISPR/Cas12a was also investigated. Mg^{2+} concentration was found to play a significant role in the overall assay performance. Importantly, the optimisation studies identified several factors affecting system compatibility. Betaine and certain commercial master mixes were not suitable for the assay under the tested conditions. Short DNA templates also showed delayed amplification following CRISPR treatment, which may have resulted from further degradation of the cleavage products together with inhibitory effects from components of the CRISPR reaction.

- Analytical Performance and Multiplexing Capability. The platform demonstrated an inverse relationship between target concentration and time-to-positive (TTP) values across several orders of magnitude. Under the tested conditions, the lowest detected concentrations ranged from 10^2 to 10^4 copies per reaction, depending on the HPV subtype and assay format. Both two-step and one-pot duplex assays produced amplification responses from mixed HPV16/18 samples, with an intermediate melting peak observed rather than two clearly resolved peaks. Under triplex primer conditions, HPV16, HPV18 and HPV52 were successfully amplified when tested individually in both assay formats. The two-step triplex assay produced distinguishable melting peaks for these individually tested targets, whereas melt-based discrimination was not evaluated in the one-pot triplex assay. Reliable genotype discrimination in mixed samples remains to be established.

- Future work and next steps. Although this study established the feasibility of CRISPR/Cas12a

loop amplification, its sensitivity remained lower than that of some established isothermal amplification assays[168]. The lowest observed detected input also varied among HPV targets, indicating that amplification efficiency was still dependent on the target sequence and primer set. In addition, the triplex assay was mainly demonstrated using relatively high target concentrations and synthetic DNA templates. Future work should focus on improving amplification efficiency at low target concentrations, further reducing non-specific amplification and establishing more general primer-design criteria. Direct comparisons with conventional LAMP under matched experimental conditions would help determine whether reducing the number of primers simplifies assay optimisation, decreases non-specific amplification, or improves multiplexing performance. Further evaluation of mixed-target samples using gel electrophoresis or high-resolution melting analysis would also help establish the reliability of genotype discrimination. The one-pot reaction should also be optimised by balancing Cas12a, crRNA, Mg^{2+} and primer concentrations. Finally, the assay should be evaluated using extracted clinical HPV samples and samples containing mixed HPV genotypes to determine its performance in more realistic diagnostic conditions.

Chapter 4

An RPA-Based Self-Transcribing CRISPR/Cas12a Assay for HPV16 Detection

4.1 Introduction

Recombinase polymerase amplification (RPA) is emerging as a promising tool for the rapid amplification of nucleic acids under isothermal conditions[50]. The reaction only requires two primers and can achieve highly sensitive detection (single target copy) within relatively short time (5-20 min)[33,49]. Because of its high amplification efficiency and less complex primer setting, RPA has been widely incorporated with CRISPR/Cas system for nucleic acid detection[169]. CRISPR-based diagnostic platforms, such as DETECTR[9] and SHERLOCK[12], have shown high sensitivity and specificity for molecular detection. In DETECTR, RPA is coupled with Cas12a-mediated detection, whereas conventional SHERLOCK combines RPA with T7 transcription and Cas13a-mediated RNA detection. Both strategies rely on target recognition to activate collateral cleavage of fluorescent reporter probes. Although these systems are powerful, the requirement for externally synthesised crRNA can increase the risk of degradation and complexity of the assay.

Recent studies have attempted to generate crRNA during the detection process. For example, FACT combined helicase-dependent amplification (HDA) with CRISPR/Cas12a and used the amplification product to generate crRNA through transcription[114]. The RePAIR module showed a sensitivity of 20 pM for synthetic DNAcrRNA without upstream amplification, whereas the fully integrated FACTOR system achieved detection of DNA targets at 50 aM. Another study used a split-crRNA design, in which the amplification product generated part of the crRNA handle sequence, while an additional double-stranded DNA template was required to provide for spacer RNA generation[117]. This split-crRNA-based assay achieved

attomolar-level detection of DNA and RNA targets within 15–20 min. Although these studies demonstrated that in situ crRNA generation is possible, additional components were still required and the assay design remained relatively complex. Therefore, a sensitive and simpler template design strategy in which the amplification product itself encodes a complete crRNA would be advantageous.

In this study, a self-transcribing RPA-IVT-CRISPR assay was developed for HPV16 detection. By incorporating a T7 promoter and a crRNA-encoding sequence into the RPA primers, the amplified product can serve as template for in vitro transcription (IVT), enabling in situ crRNA generation before CRISPR/Cas12a detection. This design also reduced the dependence of primer design on the PAM position. A PAM-containing FQ probe was designed to activate Cas12a. In this system, the FQ probe functions as both activator and fluorescence reporter. This is different from conventional Cas12a assay, which usually rely on the trans-cleavage of universal reporter probe. As the FQ probe is sequence-specific, this design may also provide a possibility for future multiplex detection. Therefore, the aim of this chapter was to develop and evaluate a self-transcribing RPA-IVT-CRISPR assay for HPV16 detection. The feasibility of the extended primer design was first tested, followed by investigation of non-specific background signals, assay optimisation, sensitivity and specificity evaluation.

4.2 Material and Methods

4.2.1 Primer design

The RPA primers, Fw and Rv, were designed to target the L1 gene of HPV16 (GenBank no. MG849741.1)[9]. To enable the amplicons to self-transcribe into crRNA, T7 promoter sequence was added to the forward primer (LFw), and the full crRNA sequence containing both handle and spacer regions was added to the reverse primer (LRv). (Figure 4-1). The primer was evaluated using the Multiple Primer Analyser (Thermo Fisher Scientific) for primer dimer detection. After amplification, the RPA products can serve as templates for in vitro transcription (IVT) to produce crRNA. For the FQ probe, the F and Q strands were labelled with a fluorophore (FAM) and a quencher (BHQ1), respectively. Upon annealing, the fluorescence was quenched due to the close proximity of the fluorophore and quencher through Förster resonance energy transfer (FRET). The spacer sequence encoded in LRv was designed to be complementary to the target region of the FQ probe. In addition, the FQ probe contained a ”TTTC” PAM sequence, allowing it to serve both as the activator and reporter of the CRISPR/Cas12a reaction. Following transcription of the crRNA, the FQ probe could be recognised and cleaved through target recognition-dependent cis-cleavage, resulting in fluorescence release. To further enhance signal output, an additional reporter probe (R1) was introduced. R1 was a short ssDNA reporter (5 nt) labelled with FAM and BHQ1 at opposite

ends. Once Cas12a was activated by cleavage of the FQ probe, the trans-cleavage activity of Cas12a could further cleave the R1 reporter, generating additional fluorescence and amplifying the detection signal. All the used sequences are listed in Table 4-1.

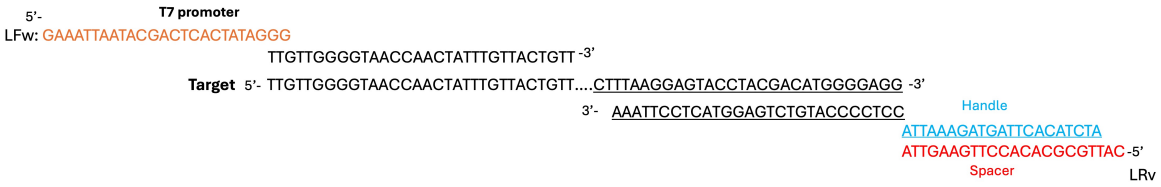


Figure 4-1: Schematic illustration of the self-transcribing RPA primer design. The T7 promoter sequence was incorporated into the 5′ end of LFw (orange). The crRNA sequence, consisting of the handle (blue and underlined) and spacer (red), was incorporated into LRv. The amplified products contained both elements, enabling transcription of crRNA from the RPA amplicons.

Table 4-1: Primers and oligonucleotides used in the RPA–IVT–CRISPR assay.

Primer	Sequence (5'-3')	Length (nt)
Fw	TTGTTGGGGTAACCAACTATTTGTTACTGTT	31
Rv	CCTCCCCATGTCTGAGGTACTCCTTAAA	28
LFw	GAAATTAATACGACTCACTATAGGGTTGTTGGGG TAACCAACTATTTGTTACTGTT	56
LRv	CATTGCGCACACCTTGAAGTTAATCTACACTTAGT AGAAATTACCTCCCCATGTCTGAGGTACTCCTTAA A	71
F	FAM-CATTGCGCACACCTTGAAGTTAGAAA	26
Q	TTTCTAACTTCAAGGTGTGCGCAATG-BHQ1	26
R1	FAM-TTATT-BHQ1	5
New LRv1	CATTGCAGGTTTGACTTACTATCTACACTTAGTAG AAATTACCTCCCCATGTCTGAGGTACTCCTTAAA	69
New LRv2	CATTGCATCCTTTGACCATTTTCGTTCTACACTTA GTAGAAATTAGTTCCTCCCCATGTCGTAGGTACTC CTTAAA	76
TS1	TTCAGACATTGCAGGTTTGACTTACTGAAA	30
NTS1	TTTCAGTAAGTCAAACCTGCAATGTCTGAA	30
TS2	ATCATTGCAGCCTTTGACCATTTTCGGAAA	30
NTS2	TTTCCGAAAATGGTCAAAGGCTGCAATGAT	30

4.2.2 RPA assay

The reaction mixture consisted of 10 µL 2× reaction buffer, 3.6 µL 10 mM dNTPs, 2 µL 10× Basic E-Mix, 1 µL each of 1 µM forward and reverse primers, and 1 µL 20× Core Reaction Mix. The components were mixed thoroughly. An aliquot of 18.6 µL of the reaction mixture was transferred to a new reaction tube. Subsequently, 0.6 µL of 280 mM MgOAc and 0.8 µL

of target DNA were added separately to the tube lid without contacting each other. The tube was closed and inverted 10 times to initiate the reaction, followed by brief centrifugation. The reaction was incubated at 37 °C for 30 min. The RPA amplicons were stored at −20 °C for further use. The final RPA reaction volume was 20 µL, containing 0.8 µL of target DNA. The initial target input was calculated by multiplying the DNA concentration (copies/µL) by the template volume (0.8 µL). Throughout this chapter, DNA concentrations are expressed as copies/reaction for the initial target input in RPA assays.

For the purification, RPA products were purified using the QIAquick PCR Purification Kit (Qiagen, Hilden, Germany) according to the manufacturer's instructions. The purified DNA was eluted in 50 µL of nuclease-free water and stored at −20 °C until further use.

4.2.3 Denaturing Urea polyacrylamide gel electrophoresis

A 15% 7 M Urea PAGE gel solution was prepared by adding 42.42 g Urea (Sigma), 10 mL 10X TBE buffer, 37.5 mL 40% 29:1 Bis/Acrylamide and distilled water to a final volume of 100 mL. The solution was stirred using magnetic stirrer until completely dissolved. To prepare the gel, 12 mL gel stock solution was mixed with 120 µL APS (Ammonium Persulfate, Bio-Rad Laboratories Ltd), 12 µL TEMED (N,N,N',N'-tetramethylethylenediamine, Bio-Rad Laboratories Ltd). Before sample loading, the gel was pre-run at 200 V for 30 min. Meanwhile, samples were prepared by mixing with an equal volume of 2x RNA loading dye (Thermo Fisher Scientific, MA), heating at 70 °C for 10 min, chilling on ice for 3 min and briefly centrifuging before loading onto the gel. The sample was loaded quickly and electrophoresed at 180 V for 30 min. After electrophoresis, the gel was stained with 1× SYBR gold (Invitrogen, ThermoFisher Scientific) for 10 min and visualised using a PXi imaging system (Syngene, MD, USA) equipped with UltraSlim Blue filter.

4.2.4 Three-step RPA–IVT–CRISPR assay

The RPA step was performed as described in Section 4.2.2. Briefly, 1 µL RPA product was added to the transcription mixture containing 1× RNAPol reaction buffer, 0.5 mM ribonucleotide solution mix (rNTPs), 1 U/µL RNase inhibitor, and 5 U/µL T7 RNA polymerase (New England Biolabs, MA). The reaction was incubated at 37 °C for 2 h for in vitro transcription (IVT). Subsequently, 2 µL of IVT product was added to the CRISPR mixture containing 1× r2.1 reaction buffer and 33 nM Cas12a, incubated at room temperature for 20 min. Afterwards, the FQ probe was added to a final concentration of 500 nM. Where indicated, the R1 reporter was also included at a final concentration of 500 nM. A total volume of 27 µL reaction mix was then loaded into a black 384-well round bottom plate (Corning Life Sciences), and sealed with MicroAmp™ Optical Adhesive Film (Applied Biosystems,

ThermoFisher Scientific). The fluorescence was measured by the Synergy HT Microplate Reader (BioTek Instruments, Inc., Agilent, CA) with excitation wavelength 480/20 nm and emission wavelength 528/20 nm, gain 50, and incubation temperature of 37 °C.

4.2.5 Two-in-one RPA–(IVT–CRISPR) assay

The RPA step was performed as described in Section 4.2.2 without purification. Briefly, 1 µL of RPA product was added to a reaction mixture containing 1× RNAPol reaction buffer, 0.5 mM rNTPs, T7 RNA polymerase, 1× r2.1 reaction buffer, 33 nM Cas12a, and 500 nM FQ probe. For experiments using R1, the reporter was also included at a final concentration of 500 nM. The final reaction volume was 30 µL. Subsequently, 27 µL of the reaction mixture was transferred to a black 384-well round-bottom microplate (Corning Life Sciences) for fluorescence monitoring.

4.2.6 Data analysis

Fluorescence data were exported from the plate reader and analysed. Real-time fluorescence curves were plotted as relative fluorescence units (RFU) against reaction time. Data were presented as the mean ± standard deviation (SD) for three or more replicate measurements, or as the range for duplicate measurements. Statistical analysis was performed using an unpaired two-tailed Student's t-test for comparisons between two independent groups. One-way ANOVA followed by Dunnett's multiple comparisons test was used to compare HPV16 with NTC, HPV18 and HPV52 in the specificity analysis (Figure 4-14). Adjusted p-values were used to account for multiple comparisons. A p-value below 0.05 was considered statistically significant. For exploratory detection experiments, fluorescence responses were assessed relative to the corresponding no-template controls (NTCs). Where statistical comparisons were performed, significant differences between target-containing reactions and NTCs were used to support the interpretation of target-dependent signal generation. For experiments without statistical testing, responses were interpreted descriptively based on the observed fluorescence separation from the NTC. These assessments were not based on a predefined, independently validated positivity threshold and therefore did not establish a statistically validated limit of detection.

4.3 Results and discussion

4.3.1 Design principle of the self-transcribing RPA-CRISPR assay

In this work, we designed a self-transcribing RPA-based CRISPR/Cas12a assay for HPV16 detection. The assay integrates recombinase polymerase amplification (RPA), in vitro transcription (IVT), and CRISPR/Cas12a detection into a sequential workflow. As shown in Figure 4-2, the RPA employed a long forward primer (LFw) containing a T7 promoter sequence and a long reverse primer (LRv) containing a crRNA-encoding sequence. In this design, the RPA products would contain a complete transcription cassette, with the T7 promoter positioned upstream of the crRNA-encoding sequence. Therefore, only target-dependent amplification products should efficiently generate full-length crRNA after IVT. In the presence of the target HPV16, RPA amplification produces multiple copies of double-stranded DNA (dsDNA) amplicons incorporating both functional elements. These amplicons subsequently serve as templates for transcribing full-length crRNA. The transcribed crRNAs will then associate with Cas12a to form an active ribonucleoprotein (RNP) complex. The FQ probe in this system serves both as a PAM-containing activator and as a fluorescence reporter. Upon recognition of the PAM-activator sequence, the activated Cas12a exhibits collateral nuclease activity, resulting in cleavage of the FQ probe and releases fluorescence signal. An additional reporter probe, R1, can be added to further increase the fluorescence signal through Cas12a-mediated trans-cleavage.

Compared with conventional CRISPR assays that require pre-synthesised crRNA, this strategy generates crRNA, eliminating the need for external RNA reagents and potentially reducing the impact of RNA degradation during storage and handling. Furthermore, this design reduces the dependence on PAM sequences in the target DNA, making primer and target design more flexible. The sequence-specific dsDNA probe also improves assay specificity and has the potential to support multiplex detection in the future.

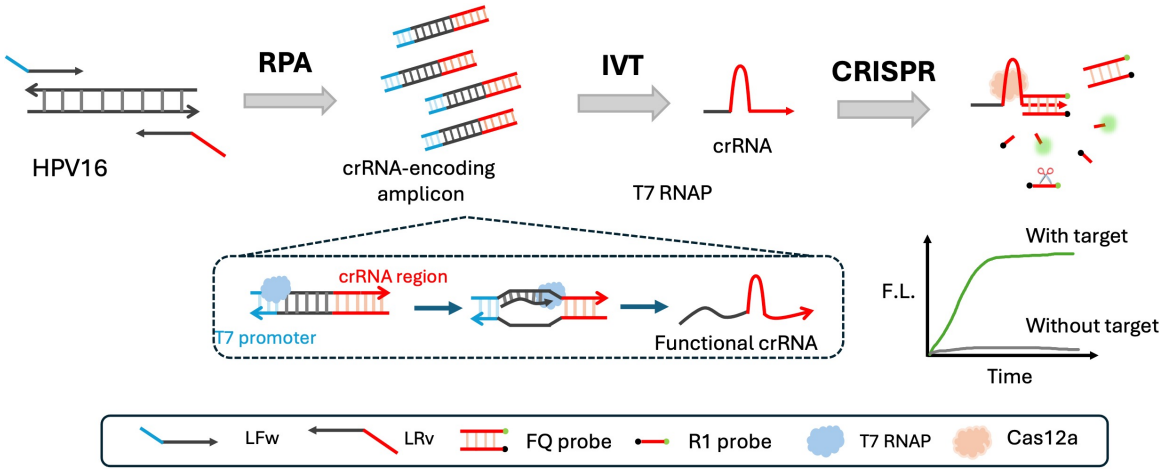


Figure 4-2: Schematic illustration of RPA-IVT-CRISPR detection for HPV16. RPA amplification with LFw and LRv generates a crRNA-encoding amplicon, and the T7 promoter sequence in LFw enables IVT to produce a functional crRNA. In the presence of target DNA, the crRNA activates Cas12a, resulting in cleavage of the reporter probes and fluorescence generation. The PAM sequence is located on the FQ probe, while the R1 probe functions as an ssDNA trans-cleavage reporter.

4.3.2 Validation of extended RPA primers

As both LFw and LRv contain long non-target extension parts, it was necessary to verify that these modified primers could still support efficient RPA amplification. Therefore, RPA reactions were performed using both the original primer pair (Fw/Rv) and the modified primer pair (LFw/LRv), and the amplification products were analysed by agarose gel electrophoresis. As shown in Figure 4-3, the Fw/Rv primer pair generated the expected amplicon size (137 bp), while the extended LFw/LRv primer pair generated a larger amplicon (203 bp) due to the additional sequences added to the primers. The products shown in Figure 4-3a were loaded directly without purification. Consequently, the bands appeared relatively diffuse, and bright bands were observed near the wells, likely from the residual reaction components. The positive control (PC) provided with the RPA kit produced the expected amplification product. For the LFw/LRv primer pair, a clear band corresponding to the expected 203 bp product was observed (Figure 4-3b), confirming successful amplification with the extended primers. Multiple faint bands were observed in the NTC lane, which were likely generated from non-specific amplification products or primer dimers. These results showed that the modified primers were still able to amplify the target DNA. However, the faint bands observed in the NTC indicated that some non-specific products were also generated, which could contribute to background signal in the downstream IVT–CRISPR assay.

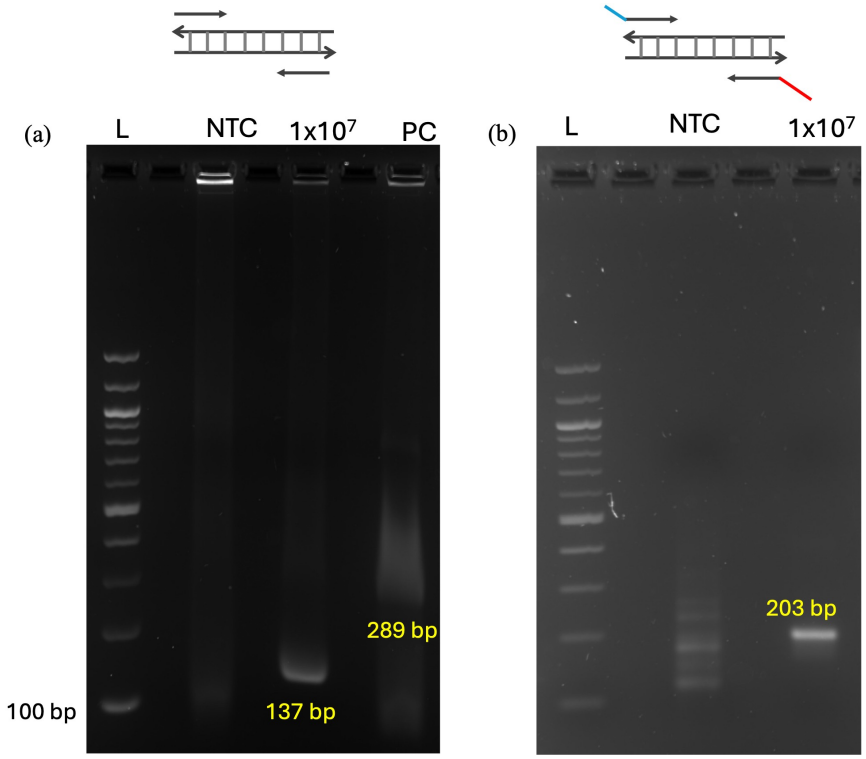


Figure 4-3: Agarose gel analysis of RPA products using different primer pairs. (a) RPA amplification using the short Fw/Rv primer pair, generating an expected 137 bp product without purification. (b) RPA amplification using the extended LFw/LRv primer pair, generating an expected 203 bp product after column purification. As illustrated in the schematics above the gels, LFw and LRv were designed by incorporating a 25 bp T7 promoter sequence and a 44 bp crRNA-encoding sequence, respectively, at the 5′ ends of the original primers. The input HPV16 concentration was $1x10^7$ copies/reaction; L, 100 bp DNA ladder; NTC, no-template control; PC, positive control.

4.3.3 Feasibility of the integrated RPA-IVT-CRISPR assay

After confirming successful RPA amplification, the assay was further integrated with IVT and CRISPR/Cas12a. Two reaction formats were evaluated: a three-step assay consisting of separate RPA, IVT and CRISPR reactions, and a two-step assay in which IVT and CRISPR were combined in a single reaction. The effect of RPA product purification on the downstream performance was also investigated. As shown in Figure 4-4a, the purified RPA product generally produces a higher fluorescence signal than the unpurified in the three-step format. This suggests the RPA reaction component is likely to inhibit the downstream IVT and CRISPR. However, the purified non-template control (NTC) generated even stronger fluorescence signal than the target (T), whereas the opposite trend was observed in the unpurified group. This might be due to the purification removing most of the inhibitory substance and enhancing both specific and non-specific products. As a result, background signal from the non-specific amplification may have become more prominent after purification. A similar trend was observed in the two-step assay (Figure 4-4b); purified products had higher fluores-

cence than the unpurified products. The purified NTC still generated higher signal, whereas only small difference between target and NTC was observed in the unpurified groups.

The products were then verified by agarose gel electrophoresis. In Figure 4-4c, very slightly difference can be seen between the unpurified RPA (lanes 1 and 3) product and purified products (lanes 2 and 4). Both target groups showed expected amplicons, indicating the purification process did not change the integrity of the RPA product. The IVT products were also analysed to further investigate the fluorescence source observed in the Figure 4-4a and 4b. For the target IVT group (lane 8), a bright band that was smaller than the original RPA product was shown. This is consistent with the expected transcription product, as the reaction initiates after the T7 promoter sequence (25 bp) and therefore the size will be reduced consequently. In contrast, the IVT product (lane 7) from the NTC showed a smeared band with multiple sizes, suggesting the non-specific products from RPA were also transcribed by the T7 RNA polymerase. This observed IVT product with multiple bands may explain the high background fluorescence in the purified NTC group. Together with the fluorescence results, these findings indicate that non-specific amplification products in the RPA can activate the CRISPR/Cas12a in some way.

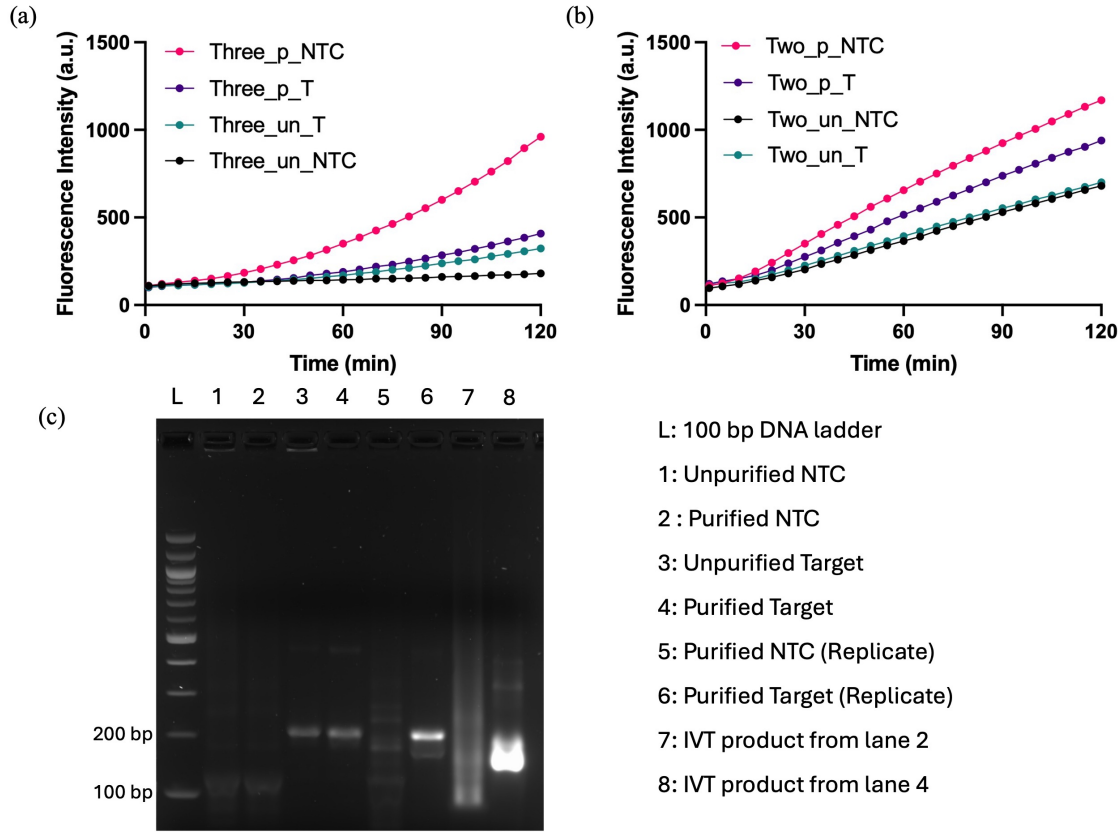


Figure 4-4: Feasibility study of RPA-IVT-CRISPR. Real-time fluorescence of (a) three-step RPA-IVT-CRISPR assay and (b) two-in-one step RPA-(IVT-CRISPR) assay. P: purified RPA product; un: unpurified RPA product; T: HPV16 target (10^7 copies/reaction); NTC: non-template control. (c) Agarose gel of RPA products before and after purification and the corresponding IVT product.

Effect of transcribed crRNA secondary structure on Cas12a activation

The higher fluorescence observed in the NTC could not be simply explained by non-specific amplification, as the agarose gel showed the target (T) group generally produced brighter and more concentrated IVT product band. Therefore, it is unlikely that the NTC generated more functional transcripts than the target group. Another possibility is that the transcribed crRNA was not fully functional, leading to the indiscriminate signal. In a conventional CRISPR/Cas12a system, the crRNA is usually around 40 nt. In this assay, however, the transcribed crRNA was around 180 nt. Longer RNAs are more likely to form secondary structure, which might affect the crRNA function. By analysing the previous studies that use similar strategies[117,170], the spacer region was generally designed to remain open and free from strong secondary structures. This may make the spacer more accessible for target recognition and Cas12a activation.

To investigate this possibility, the hairpin structure of the RNA transcribed from the original LRv primer was predicted. As shown in Figure 4-5a, a long hairpin structure was predicted within the crRNA-encoding region. (Red circle). This structure may interfere with the interaction between the crRNA spacer and the activator, potentially reducing the efficiency of Cas12a activation. Therefore, two new LRv primers were designed to reduce complementarity within the spacer and handle region to minimise secondary structure formation (Figure 4-5b, c). In addition, new LRv2 contained a mutation (A to T) in the crRNA handle sequence to test whether Cas12a activity was affected by the changes in the handle. The results are shown in Figure 4-5d, it is surprising to see that the reduced predicted secondary structure did not improve the assay performance. Instead, the difference between NTC and T gets even larger. These results suggest that the predicted secondary structure was not the dominant factor limiting assay performance under the tested conditions. One possible reason is that free LRv primers in the NTC could undergo unintended transcription, generating RNA products capable of activating Cas12a. In contrast, target-dependent RPA amplification may reduce the availability of free LRv primers or alter the composition of the transcription products, resulting in lower fluorescence. The reduced fluorescence observed with the handle-mutated LRv2 further supports that the signal was dependent on Cas12a-compatible crRNA formation. However, given the single measurement (n = 1) and the sequence differences between primer designs, further experiments would be required to determine the specific contribution of the handle mutation to Cas12a activation.

Interestingly, the higher NTC fluorescence also suggests the possibility of using a target-dependent decrease in fluorescence as an alternative detection mechanism. In this approach, target presence would be indicated by signal suppression rather than fluorescence enhancement. However, at low target concentrations, the difference between target-containing samples and the NTC may become smaller, reducing analytical sensitivity and making target discrimination more difficult. Nevertheless, this inverse fluorescence response could be con-

sidered as an alternative approach for target detection.

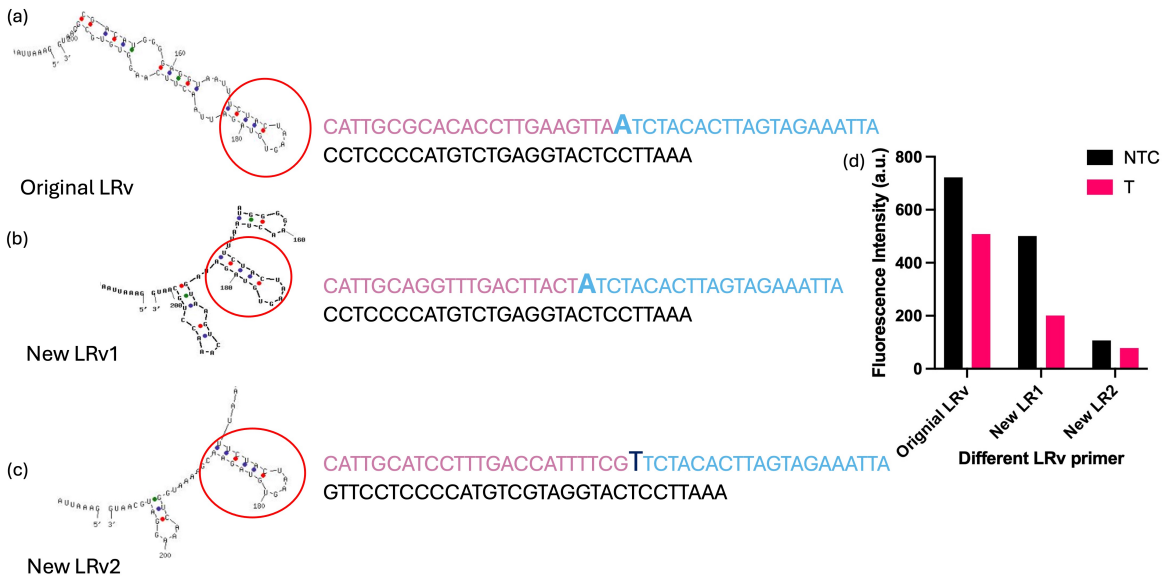


Figure 4-5: (a–c)Predicted RNA secondary structures and corresponding primer sequences for Original LRv, New LRv1 and New LRv2 designs. Magenta and blue text indicate the spacer and handle regions, respectively. The circled regions show the predicted handle secondary structures. (d) Endpoint fluorescence intensity at 120 min. NTC, no-template control; T, target-containing reaction. Single measurement, n=1.

To further investigate whether the non-specific signal could eventually be overcome by target-specific products, the RPA-IVT-CRISPR assay was monitored for an extended reaction time. As shown in Figure 4-6a, all target-containing samples produced the expected RPA amplicon. The band intensity was similar across the dilution series. The corresponding fluorescence results are shown in Figure 4-6b. All target-containing samples generated strong fluorescence signals after prolonged incubation. However, the NTC also produced a strong fluorescence signal and reached the plateau earlier than others. This result suggests that the target and NTC signals could not be separated simply by extending the reaction time, despite the target reaction showing a more intense band than the NTC. The NTC signal increased rapidly and eventually reached a level similar to or even higher than the target signal.

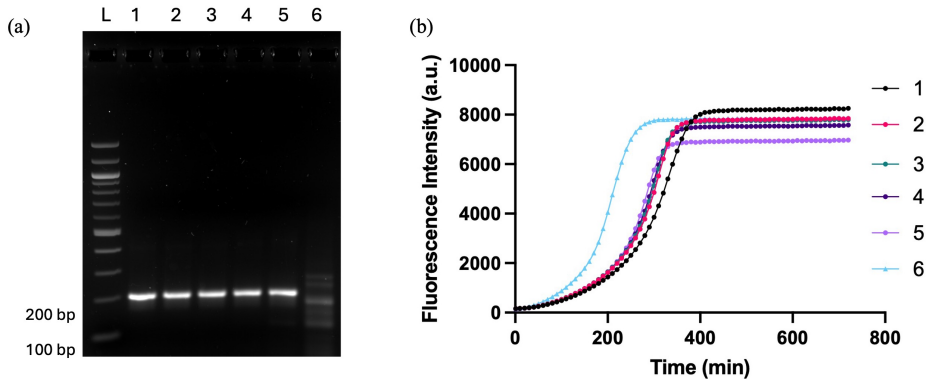


Figure 4-6: The RPA-IVT-CRISPR assay with extended detection time. (a) Agarose gel of RPA product. (b) Real-time fluorescence of (a) product. 1-5 are serial dilutions of HPV16 target from $1x10^9$ to $1x10^5$ copies/reaction. 6 is non-template control. Data represent the mean and range of two replicates.

Investigation of non-specific signal

To identify the origin of the target-independent fluorescence, the assay was deconstructed into the RPA, IVT and CRISPR components. All the following experiments were performed in the absence of the target DNA.

We first determined whether the background signal originated from non-specific RPA amplification products or from the primers themselves. As shown in Figure 4-7a, reaction 1, which contained primers and RPA reagents, generated moderate fluorescence signal. However, reaction 3, which contained both primers but no RPA reagents, produced much higher fluorescence. Reactions 2 and 4 were background. These results indicated that the non-specific signal was not solely caused by RPA-generated primer dimers. Instead, transcription products generated from the primers, particularly LRv, may have contributed directly to Cas12a activation and the resulting fluorescence signal. To further determine which primer was responsible for this effect, LFw and LRv were tested individually and together in the absence of RPA reagents (Figure 4-7b). For each primer condition, both the FQ and R1 probes were included to evaluate their contribution to the signal. The highest fluorescence was shown with both primers and probes (reaction 1). However, reaction containing the LRv primer alone also generated strong fluorescence (reactions 3 and 4), whereas the LFw primer produced no signal (reactions 5 and 6). This result indicates that LRv is the primary source of the non-specific signal. In addition, the absence of the R1 probe results in decreased signal also suggesting that Cas12a trans-cleavage activity was happening. Since the R1 probe can only generate fluorescence after CRISPR activation, this result further confirms that the observed signal originated from CRISPR activity rather than inappropriate opening of the annealed FQ probe.

Together, these experimental results give strong evidence that the primer LRv is the ma-

jor source of the non-specific signal. This is mainly because the LRv contains the crRNA-encoded sequence that has potential for self-transcription. One thing that also surprised is that all reactions were purified before IVT. In principle, this purification should remove most of the primers, salts and other components. However, non-specific signals were still observed after purification. One possibility is that the purification kit only guarantees to remove DNA fragments smaller than 40 bp or larger than 100 bp (QIAquick PCR purification kit, no. 28104). However, our two primer sizes are between that intermediate range and thus might escape from the purification. Nevertheless, it is still unclear whether the fluorescence signal is from correctly transcribed crRNA or from other non-specific products.

(a)

	1	2	3	4
Primers (LRv + LFw)	+	-	+	-
RPA reagents	+	+	-	-
IVT	+			
CRISPR				
FQ probe				
R1 probe				

(b)

	1	2	3	4	5	6
Primers	LRv+LFw	LRv+LFw	LRv	LRv	LFw	LFw
RPA reagents	-					
IVT	+					
CRISPR						
FQ probe	+	+	+	+	+	+
R1 probe	+	-	+	-	+	-

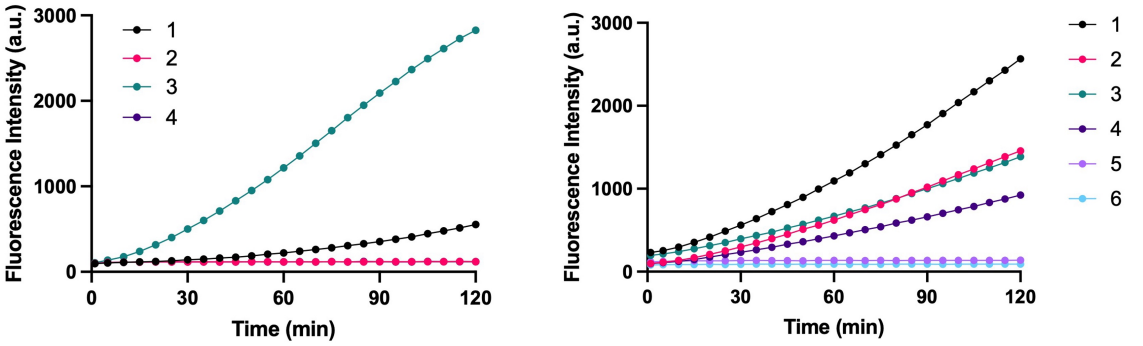


Figure 4-7: Investigation of the source of non-specific signals in the RPA–IVT–CRISPR assay. (a) Effect of the presence or absence of RPA primers and reagents. (b) different primer combinations and R1 probe addition in the absence of RPA reagents. IVT, CRISPR and the FQ probe were included in all reactions. Experimental conditions are summarised in the tables above the fluorescence curves. n=1.

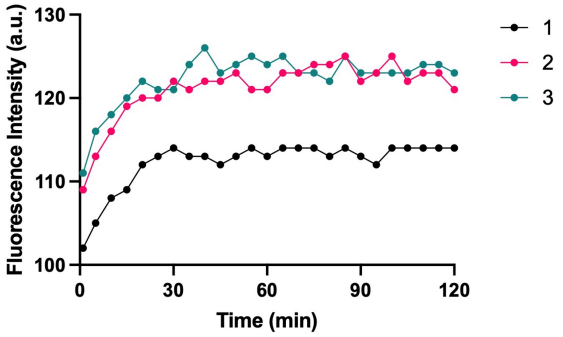
Next, we tried to find answers in the IVT and CRISPR steps. As the Figure 4-8a, the T7 polymerase was removed from the IVT step, no fluorescence signal was observed in each group. This indicates that transcription is essential for signal generation. In Figure 4-8b, Cas12a was removed from the CRISPR step. In contrast to reaction 1, which contained the complete IVT–CRISPR system, reaction 2 remained at the baseline. This shows that Cas12a activation is responsible for fluorescence generation. Taken together, these results confirmed that the observed fluorescence signal depends on both IVT transcribing and CRISPR activation. LRv alone produced a stronger fluorescence signal than the two-primer reaction, suggesting that the non-specific signal mainly originates from LRv itself rather than from primer-dimer formation.

(a)

	1	2	3
Primers	LRv+LFw	LRv	LFw
RPA reagents	-		
IVT	-		
CRISPR	+		
FQ probe			
R1 probe			

(b)

	1	2	3	4
Primers	LRv+LFw	LRv+LFw	LRv	LFw
RPA reagents	-			
IVT	+			
CRISPR	+	-	+	+
FQ probe	+			
R1 probe				



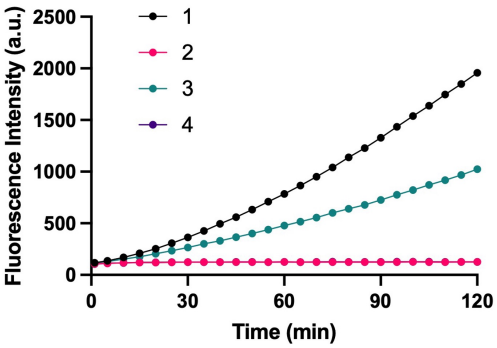


Figure 4-8: Investigation of the source of non-specific signals in the RPA–IVT–CRISPR assay, IVT and CRISPR steps. (a) Effect of the presence or absence of the IVT step. (b) Effect of the presence or absence of the CRISPR ste. Experimental conditions are summarised in the tables above each fluorescence curve. n=1.

A recent study by Greenwald et al. (2025)[14] reported that a single DNA primer can act as both template and substrate for self-transcription, even when only two complementary bases at the 3' ends. This finding supports our observation that LRv alone is capable of self-transcribing and generating strong fluorescence signals in the absence of target DNA. Based on this report and our experimental results, a possible mechanism is proposed in Figure 4-9. The LRv primer contains several complementary bases near its 3′ end. These bases may allow the primer to fold back on itself and form a short hairpin structure. This folded structure may provide a starting point for T7 RNA polymerase and allow transcription to occur without a normal double-stranded DNA template. After transcription starts, part of the folded primer may be extended, generating a DNA-RNA hybrid molecule. This intermediate could then serve as a template for further transcription. Through repeated rounds of extension and transcription, full-length crRNA molecules may eventually be produced. Once enough crRNA is generated, the CRISPR/Cas12a system can be activated, resulting in fluorescence signal generation.

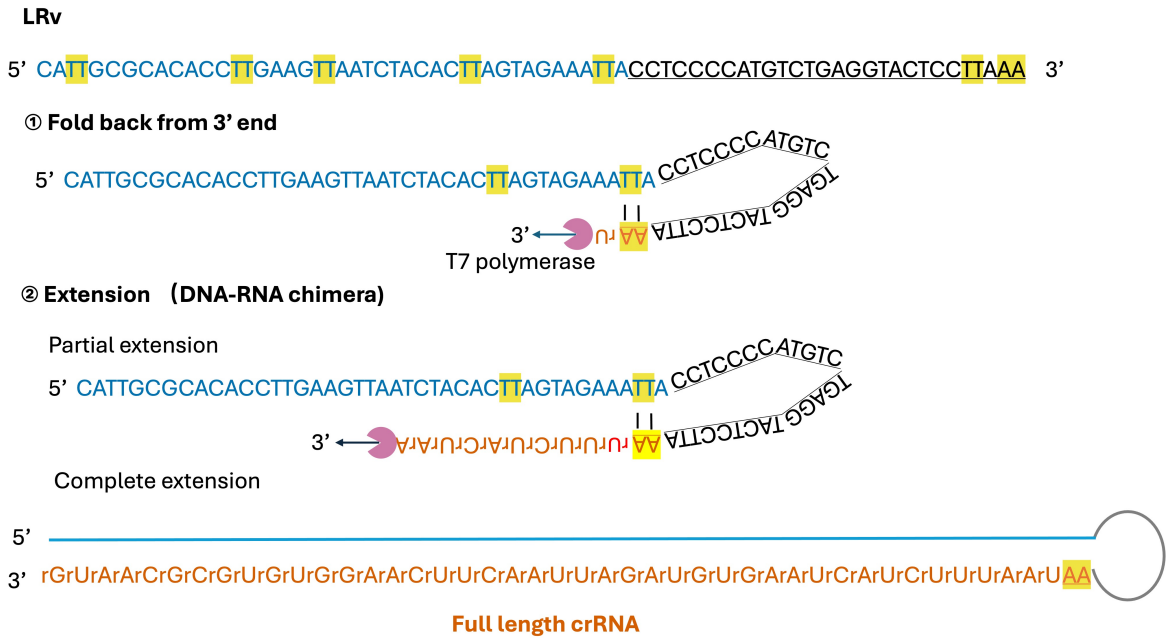


Figure 4-9: Proposed model for crRNA generation from the LRv primer. The 3′ end of LRv is proposed to fold back and hybridise with an internal complementary region, allowing T7 RNA polymerase to initiate RNA extension and form a DNA–RNA chimera. Continued extension may generate a full-length crRNA-like sequence without target DNA. Blue and black sequences represent the original LRv DNA primer, orange indicates the proposed newly synthesised RNA, and yellow highlights indicate complementary bases potentially involved in self-priming.

To further investigate whether LRv could generate RNA transcripts, the IVT products were analysed using 15% denaturing urea PAGE, which provides better separation of short RNA molecules. As shown in Figure 4-10a, multiple bands were observed after the transcription reaction (lane 1). After DNase treatment (lane 2), several bands were still visible, indicating that the remaining bands are RNA. In contrast, most bands disappeared after RNase treatment (lane 4). When both DNase and RNase were added (lane 3 and lane 5), almost no bands remained. These results suggest that RNA was successfully generated from the LRv template. Interestingly, multiple bands with different sizes were shown in the IVT products, indicating that different lengths were generated during the reaction. Combined with the proposed mechanism in Figure 4-9, it is possible that transcription was terminated at different positions during RNA synthesis, resulting in RNA products in various lengths. Different concentrations of LRv were tested in the IVT-CRISPR step. As shown in Figure 4-10b, fluorescence increased with the LRv concentration.

As the transcription product is concentration-related, it is reasonable to think that adjusting the primer concentration may solve the background problem. From an experimental perspective, the lower the amount of primer/transcript introduced into the final CRISPR reaction, the lower the background signal is expected to be. In the previous experiments, 5 µL of RPA product was added to the transcription reaction, and 6 µL of transcription product

was subsequently added to the CRISPR reaction. This not only introduced more LRv for unintended transcription, but also transferred additional reaction components that could affect the CRISPR reaction environment. Therefore, in the subsequent experiments, the volume of RPA product added to the transcription reaction was reduced from 5 µL to 1 µL, and the volume of transcription product added to the CRISPR reaction was reduced from 6 µL to 2 µL.

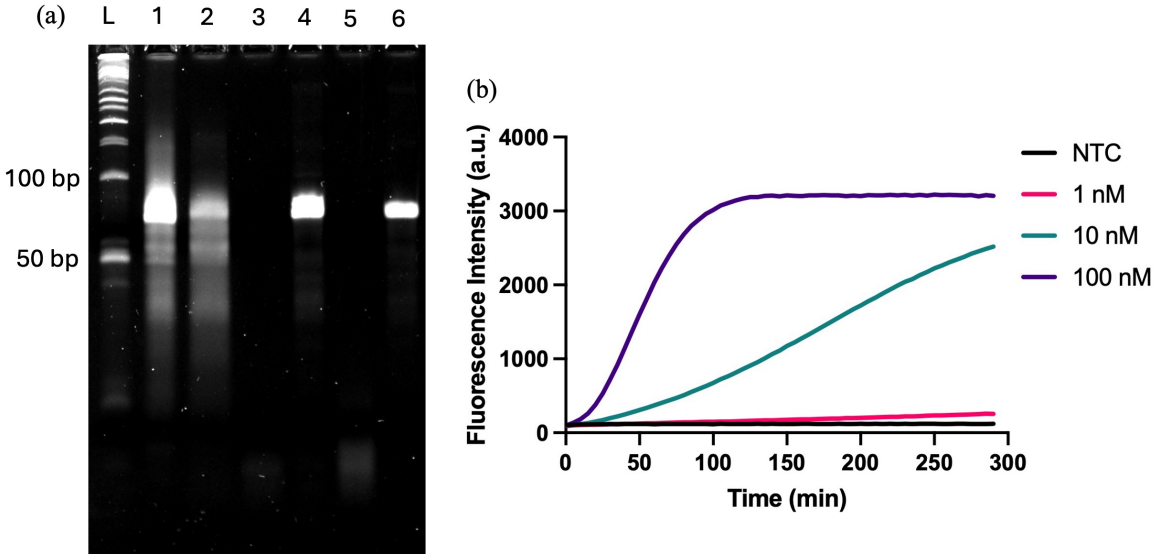


Figure 4-10: Evidence for transcription from the LRv primer. (a) Urea PAGE gel analysis of transcription products before and after DNase and RNase treatment. Lane L: 50 bp DNA ladder; lane 1: transcription products; lane 2: DNase-treated products; lane 3: DNase- and RNase-treated products; lane 4: RNase-treated products; lane 5: RNase- and DNase-treated products; lane 6: LRv ssDNA template. (b) Fluorescence kinetics of the IVT–CRISPR assay using different concentrations of the LRv primer as the transcription template. Data represent the mean and range of two replicates.

The assay contains two potential transcription templates: the real RPA amplicon and the LRv primer. Although the LRv primer alone was able to generate transcripts and activate the CRISPR system, the real RPA amplicon was expected to produce more functional crRNA. As reported previously, T7 polymerase prefers to transcribe dsDNA that contains T7 promoter, even in the presence of other ssDNA[14]. Therefore, a synthetic amplicon, T7HPV16, was designed to mimic the expected RPA product and compare its performance with the ssDNA LRv primer. As shown in Figure 4-11a, both groups with the same concentration generated fluorescence signals. However, the T7HPV16 increased rapidly after 150 min and eventually exceeded the LRv. This suggested that, if efficient target amplification could be maintained at a lower primer concentration, the background signal might become negligible. Therefore, the concentration of both primer was reduced from 480 nM to 50 nM. The results using only R1 probe are shown in Figure 4-11b. The amplification with target apparently shows higher fluorescence than the NTC, which proves that reducing the primer concentration can suppress

the background from the LRv while still allowing efficient target amplification through RPA.

It is interesting to notice that even though there is no PAM-contained activator FQ, fluorescence is still generated from the R1 probe in Figure 4-11a and 11b. This may be due to the DNA amplicon that was used for transcription also containing the complementary part of the crRNA spacer. The spacer of crRNA is unique part that can specifically recognise targets. Therefore, once the crRNA was generated, it can use the amplicon itself as the target and activate the trans-cleavage of R1 probe. However, as the amplicon does not contain a PAM sequence, the activation efficiency won't be very high. In Figure 4-11c, both activator FQ and R1 probe were added to the reaction. The addition of FQ provides a sequence-specific PAM-containing activator, while R1 provides an additional substrate for collateral cleavage. The fluorescence therefore increased 20-fold and reached the plateau after around 150 min. In contrast, the NTC remained at a low level of fluorescence. This finding suggests that reducing the primer concentration successfully suppressed the background signal and improved the contribution of target-derived products.

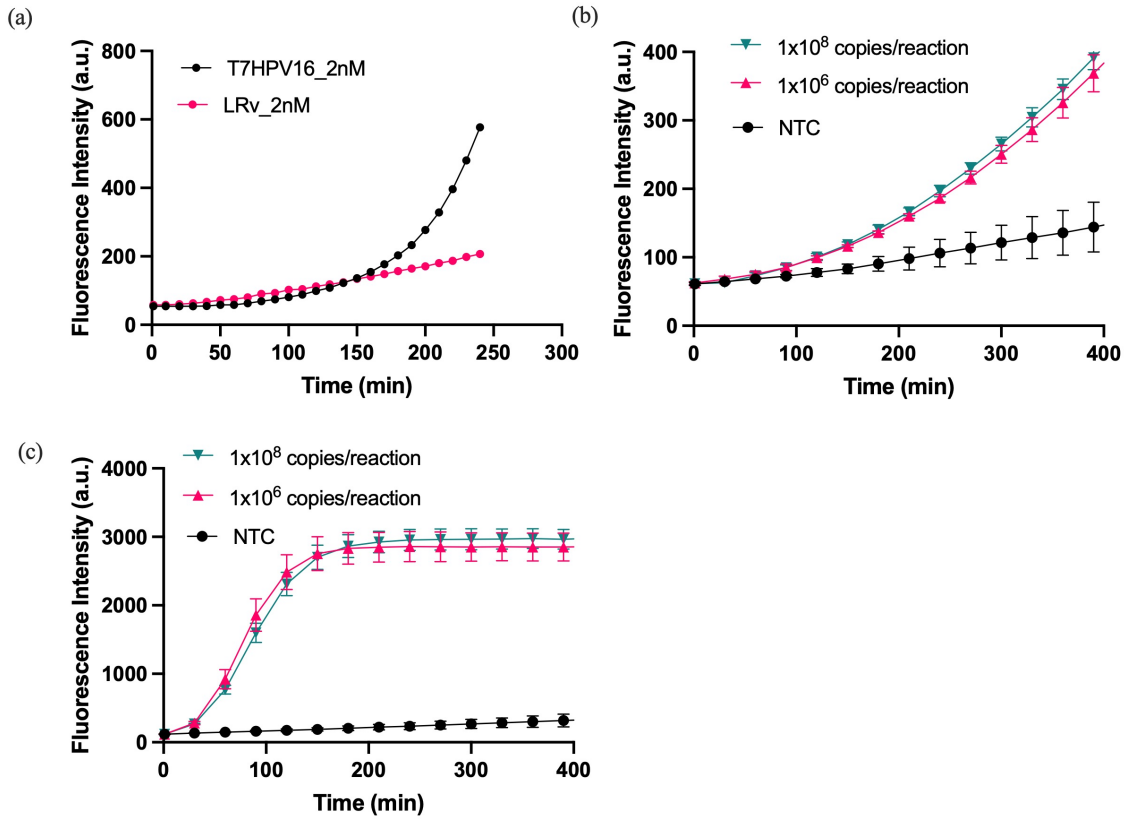


Figure 4-11: Strategy for reducing non-specific signals. (a) Comparison of fluorescence generated by the T7HPV16 dsDNA and the LRv primer using the R1 probe. n=1. (b) Reducing both primer concentrations from 480 nM and 50 nM using the R1 probe. (c) Reducing both primer concentrations from 480 nM and 50 nM using both R1 and FQ probes. HPV16 targets were at 1×10^8 and 1×10^6 copies/reaction; NTC, no-template control. Data represent the mean and range of two replicates.

4.3.4 Analytical performance of the RPA-IVT-CRISPR assay

Following the feasibility of the RPA-IVT-CRISPR assay, we tested the assay in different formats. The RPA was conducted first to ensure the correct dsDNA products generation for the subsequent reaction. In the three-step format, each reaction is performed separately, while in the two-in-one assay, the IVT and CRISPR were combined in a single reaction. As shown in Figure 4-12a and c, both formats successfully detected HPV16 from $1x10^9$ to $1x10^3$ copies per reaction. In both formats, $1x10^3$ copies per reaction could be clearly distinguished from the NTC, requiring 90 min in the three-step format and 60 min in the two-in-one format. Interestingly, a second increase in fluorescence was observed after the initial plateau in the two-in-one assay (Figure 4-12c). The mechanism behind this behaviour remains unclear. One possible explanation is that additional RNA products were generated during prolonged incubation, leading to a second phase of Cas12a-mediated reporter cleavage. Alternatively, changes in the fluorescence properties of the reporter during the reaction may have contributed to this observation. However, the accumulation of non-specific probe cleavage products alone may not fully explain the renewed fluorescence increase. This could be investigated by analysing the RNA products and FQ probe cleavage at different time points before and after the second fluorescence increase.

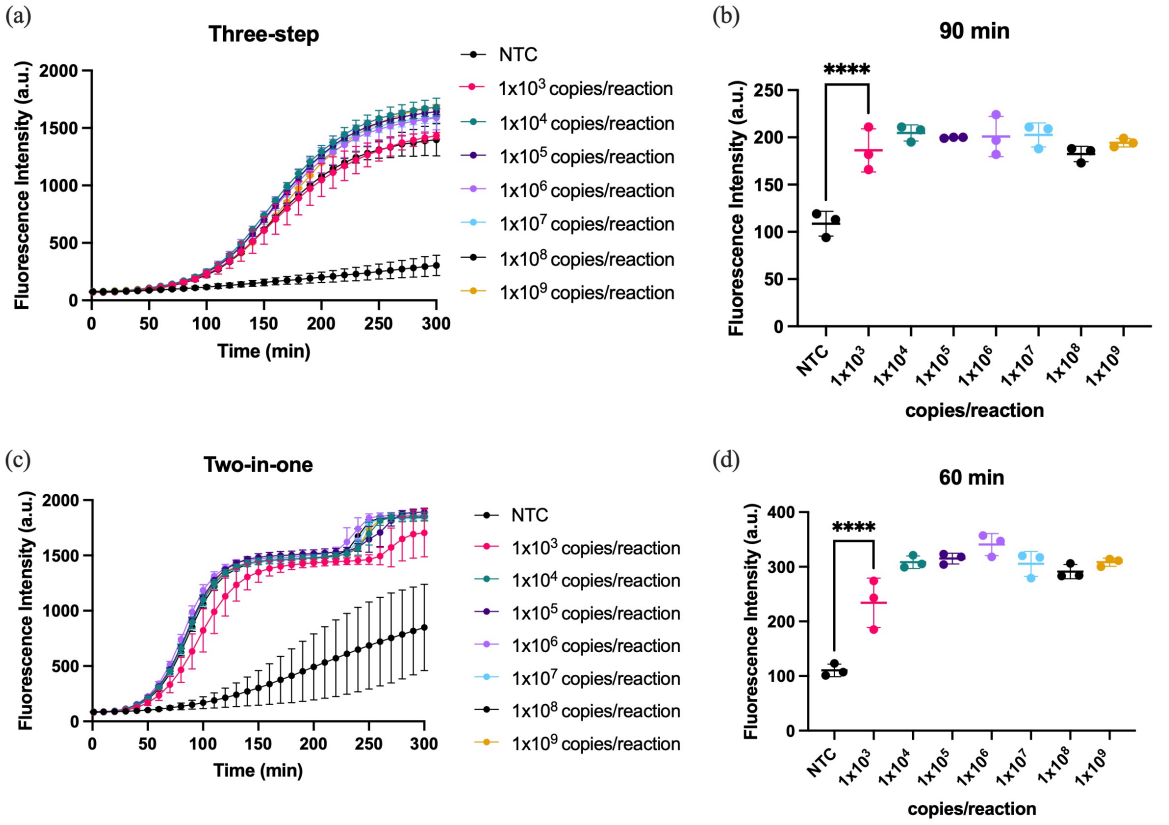


Figure 4-12: Performance of the RPA–IVT–CRISPR assay in different formats. (a) Real-time fluorescence of the three-step assay. (b) Endpoint fluorescence at 90 min for the three-step assay. (c) Real-time fluorescence of the two-in-one RPA–(IVT–CRISPR) assay. (d) Endpoint fluorescence at 60 min for the two-in-one assay. HPV16 targets ranged from 1×10^3 to 1×10^9 copies per reaction. NTC, no-template control. FQ probe only. Data are shown as mean ± SD (n=3). Statistical significance was determined using an unpaired two-tailed Student's t-test. ns, not significant; ****P<0.0001.

To further determine the detection limit of the assay, lower target concentrations ranging from $1x10^3$ to 1 copy per reaction were tested (Figure 4-13). In the three-step format, 10 copies per reaction generated a higher fluorescence than the NTC after 60 min, whereas 1 copy per reaction could not be distinguished from the NTC (Figure 4-13b). In the two-in-one format, 1×10^2 and 1×10^3 copies per reaction produced fluorescence signals above the NTC, whereas considerable variation was observed at 10 copies per reaction. (Figure 4-13d) Therefore, 100 copies per reaction was considered the lowest concentration reliably detected under the tested conditions. Different endpoint times were selected for the initial format comparison and low-copy-number sensitivity experiments because low-copy-number reactions required longer monitoring, particularly in the two-in-one format.

The three-step format provided better control over each reaction stage and showed higher apparent sensitivity, but it required more handling steps and longer workflow. In contrast, the two-in-one format reduced operation complexity by combining IVT and CRISPR detection, although this simplification may reduce sensitivity because the transcription and Cas12a

cleavage reactions must occur under the same buffer environment. Therefore, the three-step format is more suitable for mechanistic validation, whereas the two-in-one format is more suitable for future simplified diagnostic applications.

One thing needs to be noticed, although the FQ probe is cleaved by a sequence-specific cis-cleavage reaction, the final fluorescence signal did not show a linear relationship with the target concentration. This is mainly because RPA and IVT both act as amplification steps. After amplification, different starting copy numbers can produce similar amounts of crRNA and activate similar levels of Cas12a. In addition, the limited amount of Cas12a and FQ probe causes the reaction to reach a plateau. Therefore, the assay is more suitable for qualitative detection than accurate quantification.

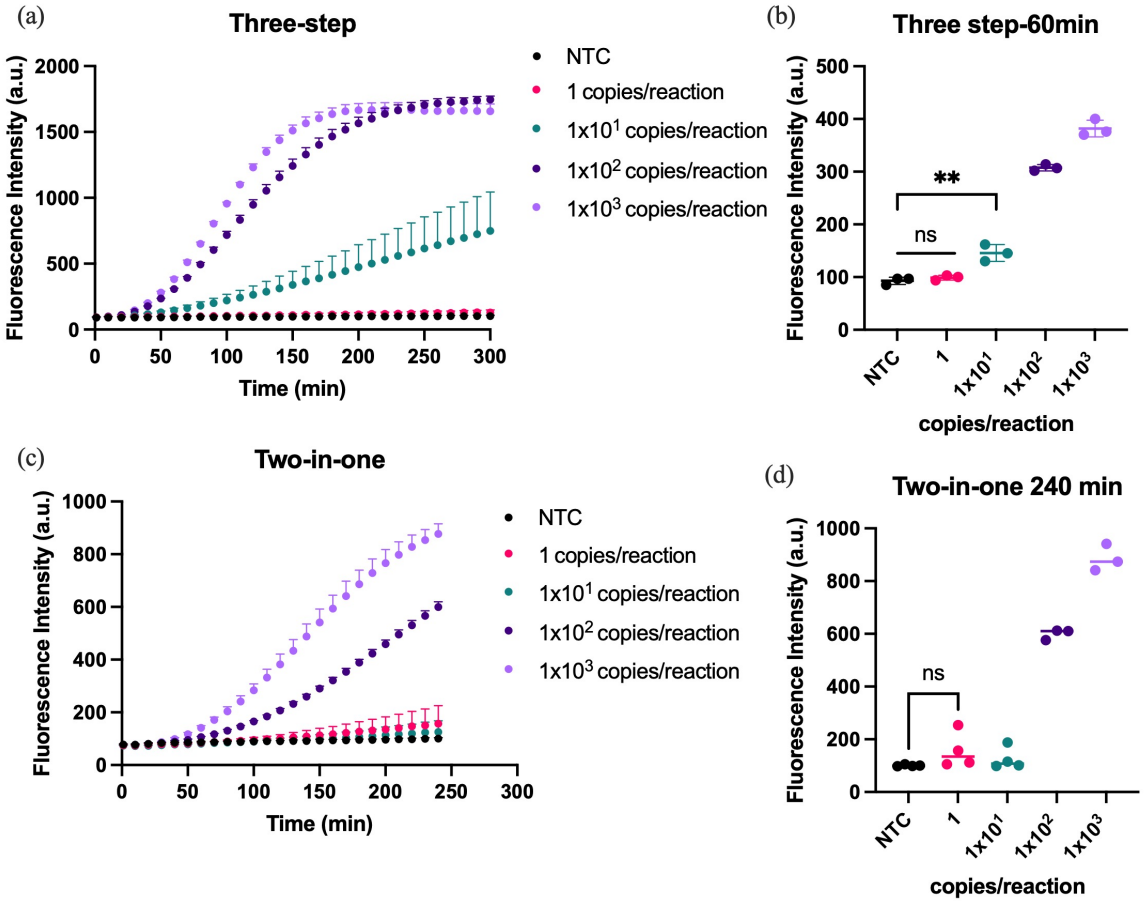


Figure 4-13: Analytical sensitivity of the three-step and two-in-one RPA–IVT–CRISPR assays. (a) Real-time fluorescence signals generated by the three-step assay using HPV16 targets at 1, 10, 10^2, and 10^3 copies per reaction. (b) Endpoint fluorescence of the three-step assay at 60 min. (c) Real-time fluorescence signals generated by the two-in-one assay at the corresponding target concentrations. (d) Endpoint fluorescence of the two-in-one assay at 240 min. Data are presented as mean ± SD, n = 3. Statistical significance was determined using an unpaired two-tailed Student's t-test. ns, not significant; **P < 0.01.

The specificity of the three-step RPA-IVT-CRISPR assay was evaluated using HPV16, HPV18

and HPV52 DNA targets. As shown in Figure 4-14a, only HPV16 generated a significantly increased fluorescence signal, while HPV18, HPV52 and the NTC remained at background levels throughout the reaction. In addition, when the HPV16 target was tested using a non-targeting PAM probe (HPV16 mirFQ), no fluorescence increase was observed, further confirming that signal generation was dependent on the correct target-probe recognition. The endpoint fluorescence values at 60 min are shown in Figure 4-14b. HPV16 produced significantly higher fluorescence than HPV18, HPV52 and the NTC ($P < 0.0001$), whereas HPV18, HPV52 and the NTC showed low fluorescence under the tested conditions. These results demonstrate that the assay can specifically distinguish HPV16 from closely related HPV genotypes and that both the crRNA-target interaction and the sequence-specific FQ probe are required for fluorescence generation.

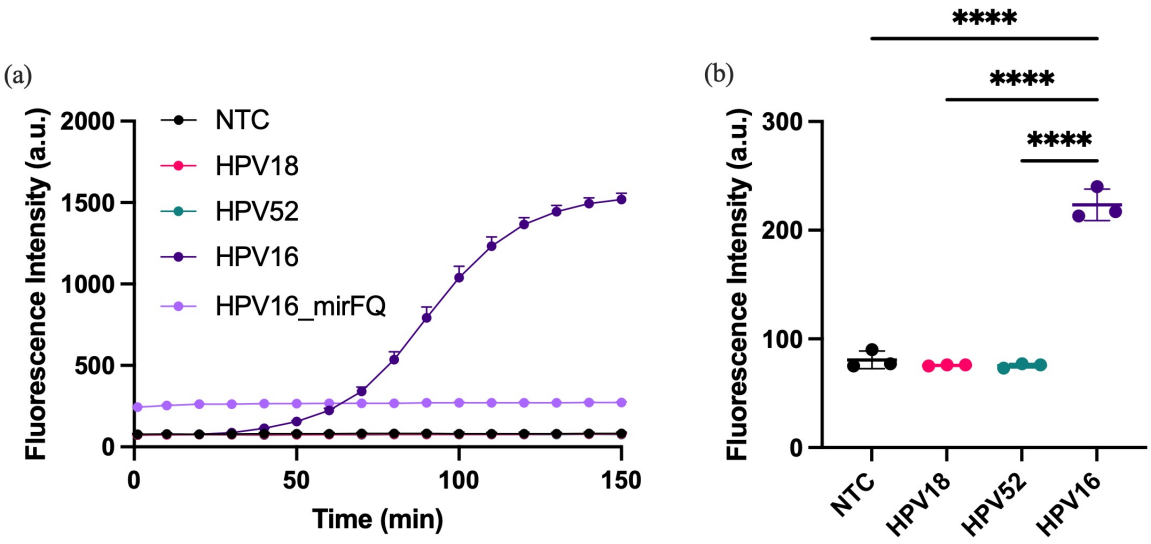


Figure 4-14: Specificity of the three-step RPA–IVT–CRISPR assay.(a) Real-time fluorescence signals generated from HPV16, HPV18, HPV52, NTC and HPV16 with a non-targeting FQ probe (HPV16 mirFQ). (b) Endpoint fluorescence at 60 min. Data are shown as mean ± SD (n=3). Statistical significance was determined using one-way ANOVA followed by Dunnett's multiple comparisons test, comparing HPV16 with NTC, HPV18 and HPV52. Adjusted p-values were used to account for multiple comparisons. ****$P < 0.0001$.

4.4 Conclusion

In this chapter, a self-transcribing RPA-IVT-CRISPR assay was developed for HPV16 detection. By incorporating a T7 promoter and a crRNA-encoding sequence into the both RPA primers, the amplified DNA products could serve as templates for in vitro transcription, enabling crRNA generation and subsequent Cas12a activation. In summary,

- The extended RPA primer design successfully generated the expected sequence-encoded

amplicons, demonstrating the feasibility of integrating RPA, IVT and CRISPR into a single detection workflow.

- Initial experiments revealed unexpectedly high background signals, particularly after purification of the RPA products. Analysis of the transcribed RNA secondary structure indicated that crRNA folding was unlikely to be the major cause of the non-specific signal.
- Mechanistic studies demonstrated that the background signal relied on both IVT and CRISPR activities. Transcription products generated from the LRv primer contributed substantially to background activation.
- Reducing the primer concentration from 480 nM to 50 nM effectively suppressed background signals while maintaining RPA amplification efficiency.
- Using the optimised conditions, both the three-step and two-in-one assay formats successfully detected HPV16 over a wide concentration range. The three-step format detected as few as 10 copies per reaction, while the simplified two-in-one format achieved detection down to 100 copies per reaction.
- Specificity testing demonstrated that the assay could clearly distinguish HPV16 from HPV18 and HPV52, with no detectable cross-reactivity under the conditions tested.
- The FQ probe used in this study functions as both the activator and reporter of the CRISPR reaction. Replacing the HPV16 FQ probe with a non-targeting probe (mirFQ) completely abolished signal generation, indicating that the assay requires the correct FQ sequence for activation. This feature may be useful for future multiplex detection, as different targets could be detected using different sequence-specific FQ probes.

Overall, this work demonstrates the feasibility of a self-transcribing RPA-IVT-CRISPR strategy for HPV16 detection. Established amplification-assisted CRISPR diagnostic platforms, such as DETECTR and SHERLOCK, have demonstrated attomolar-level sensitivity[9,12]. In the present study, the three-step and two-in-one formats produced detectable responses at 10 and 100 HPV16 copies per reaction, respectively, although these values represent the lowest detected inputs under the tested conditions rather than statistically validated limits of detection. Similar to previously reported in situ crRNA generation approaches, including FACTOR and split-crRNA-based methods[114,117], the present strategy aims to reduce reliance on externally synthesised crRNA, with a particular focus on generating complete crRNA from engineered RPA amplicons and controlling background signals. The study also highlights the importance of controlling primer-derived transcription products in self-transcribing CRISPR systems. The optimised assay provides proof-of-concept platform for HPV16 detectionand offers useful insights for the future development of integrated transcription-based CRISPR

diagnostics. This approach reduces dependence on conventional universal reporters and may facilitate the development of multiplex CRISPR diagnostic platforms in future studies.

Chapter 5

STSR-CRISPR: an amplification-free self-transcribing, self-recognition CRISPR-Cas12a for miRNA detection

5.1 Introduction

T7 RNA polymerase conventionally initiates transcription from promoter sequences in DNA templates[99]. However, T7 RNAP has also been reported to perform several non-canonical activities, including promoterless DNA-directed transcription, RNA-templated RNA synthesis and the extension of nucleic acid 3′ ends with ribonucleotides.[104,106] Moreover, Greenwald et al. showed that short internal complementarity may allow the 3′ end of the ssDNA to fold back and act as a primer, while the same DNA molecule serves as the template. This process generates a DNA-RNA chimeric product, termed "DragonRNA", in which the RNA extension is complementary to the upstream DNA sequence. This RNA-extension activity occurs with several RNA polymerases, including T7 RNAP[14,108]. Over the years, such promoter-independent products have generally been regarded as unintended by-products of conventional in vitro transcription and may complicate the interpretation of transcription reactions[171,172]. In Chapter 4, we also find out that the long reverse primer LRv unexpectedly generated fluorescence in the presence of T7 RNAP and Cas12a. Although this background signal interfered with target-specific detection, it also suggested that LRv might undergo DNA self-primed RNA extension and generate crRNA-like products capable of supporting Cas12a activation. Li et al. also developed a cell-free amplification circuit based on promoterless transcription[173]. These observations provided the starting point for the self-transcribing, self-recognition (STSR) CRISPR platform. A specifically designed ssDNA molecule is used as the central component. The ssDNA encodes a sequence capable of producing a crRNA-like product. At the same time, the original ssDNA or a corresponding

reporter sequence provides the recognition target for the generated Cas12a–RNA complex. Therefore, the same programmable sequence connects RNA generation, Cas12a recognition and fluorescence output. The approach avoids conventional target pre-amplification and external crRNA preparation.

MicroRNAs (miRNAs) are valuable biomarkers for early disease diagnosis and prognosis.[174] Abnormal miRNA expression is associated with disease development and progression.[175 176] Therefore, sensitive and accessible miRNA detection could support molecular diagnosis and point-of-care testing.[177] CRISPR/Cas systems have shown potential in miRNA detection[178 179 180]. However, existing nucleic acid detection methods often rely on multiple probes or external crRNA synthesis, leading to limited sensitivity and specificity as well as challenges in deploying these assays in low-resource environments or at the point-of-care.[181] Some transcription-triggered CRISPR assays require amplification primers, promoter sequences and multiple reaction components[114 128 129]. These requirements increase workflow complexity and may limit point-of-care implementation.

Previous studies have demonstrated simplified transcription-based strategies for miRNA detection. For example, Long et al. developed a hairpin-switch assay incorporating target recognition and a transcription template into a single ssDNA structure[128], while Dong et al. demonstrated in situ crRNA generation through amplification-assisted T7 transcription[113]. Although these studies simplified different aspects of miRNA detection, they still relied on conventional T7 promoter-dependent transcription. In contrast, this study explored whether promoter-independent RNA generation from designed ssDNA templates could be coupled with Cas12a activation without target pre-amplification or externally synthesised crRNA.

Therefore, this chapter aimed to develop and investigate an amplification-free self-transcribing and self-recognition CRISPR/Cas12a platform for miRNA detection. The ability of ssDNA templates to generate Cas12a-activating RNA products was first evaluated, followed by optimisation of template design, transcription conditions and CRISPR reaction components. The mechanism of Cas12a activation was further investigated using split-crRNA designs, DNase I treatment, PAM-containing and PAM-free probes, Bioanalyzer analysis and RNA sequencing. Finally, two miR-21 sensing strategies were evaluated: direct TMSD activation and dragon hairpin-mediated target recycling.

5.2 Material and Methods

5.2.1 Oligonucleotide design

The oligonucleotides used in the chapter (Table 5-1) were designed based on the unexpected signal observed from the RPA long reverse primer, LRv, in Chapter 4. In that chapter, LRv

generated a fluorescence signal in the presence of the T7 polymerase and Cas12a, suggesting that the single-stranded DNA oligo could facilitate a self-transcription-like process and produce crRNA-like products capable of activating Cas12a. The observation is consistent with the DragonRNA mechanism reported by Greenwald et al[14]. where RNA polymerase can extend the 3' end of DNA oligonucleotides with ribonucleotides, producing DNA-to-RNA chimeric product.

Based on this observation, new cr21 templates were designed to mimic key features of LRv while replacing the 3' end region with miR-21-related sequences. The handle and spacer regions remained the same. Different 3' end designs were introduced to investigate how the predicted self-priming ability affected CRISPR activation. cr21-1 was designed as the minimal miR-21-related template without additional sequence. cr21-2 contained an additional soft 3' end "AA" extension. cr21-SE was designed to mimic the soft 3' end "TTAAA" of LRv, while cr21-SE-5bp contained the same soft end but with a 5-bp predicated based pairing between the 3' end and the inter site. To test whether strong local 3' base pairing could improve self-priming, cr21-CG-3bp and cr21-CG-7bp were designed with 3-bp and 7-bp complementary regions from the 3' ends.

To make sure the cr21 template can respond to miR-21, cap strands were designed to block the 3' end of the ssDNA template. This design was adapted from the capture DNA strategy reported by Gholamalipour et al.,[107] where a short capture DNA complementary to the 3' end of the template inhibits self-primed extension driven by T7 polymerase. In their system, the capture DNA contained a 3'-amino modification that prevented nucleotide addition from the capture DNA itself. In our study, the same principle was adapted to block the 3' end of the cr21 template and the cap strands were designed to suppress template self-priming in the absence of miR-21. An 8 nt toehold was left for miR-21 binding, so that miR-21 could remove the cap through toehold-mediated strand displacement (TMSD). After cap displacement, the 3' end of the cr21 was expected to become available for self-priming and RNA generation. The 3' end of each cap strand was modified with an amino group to prevent the cap itself from priming.

Split crRNA designs were introduced to increase the chance of generating complete functional crRNA fragments. Based on the DragonRNA model, RNA polymerase can extend the 3' end of a DNA oligo, but the products may vary in length. Some products may stop before reaching the 5' ends, and thus produce incomplete crRNA fragments[14]. Therefore, the full-length crRNA DNA template was divided into short handle and spacer parts[117], so that each template only needed to generate a shorter functional RNA.

In the first split design, the spacer was produced from ssDNA spacer, while the handle sequence was produced from a T7 promoter-containing dsDNA (ds-handle) by conventional transcription. In the second split design, the position was opposite. Handle-CG-3bp was used as a self-transcribing handle template, while the dsDNA ds-spacer was used to generate

the spacer. This design was to test whether shortening the self-transcribing template could produce more functional crRNA-like molecules than the full-length crRNA template.

Dragon hairpin templates were designed to introduce target recycling into the miR-21 sensing system. Here, the 5' spacer was designed to be complementary to the 3' miR-21 specific region. DH_12, DH_14, DH_15 and DH_16 were designed with different stem lengths to compare the effect of hairpin stability on background signal and miR-21-triggered signal.

A synthetic universal crRNA was used as a positive control for Cas12a activation. The F and Q strands were annealed to form the FQ reporter, which served as the target for the universal crRNA and cr21 self-transcribed crRNA cis- cleavage. R1 was an ssDNA reporter to monitor the trans-cleavage. The mir-FQ reporter was related to the dragon hairpin-derived crRNA product and was later also used to evaluate the non-specific reporter opening. NoPAM reporter was designed by removing the PAM region from the corresponding reporter sequence and was used to evaluate PAM-dependent target recognition and reporter cleavage.

Table 5-1: The oligonucleotides used in this study.

Primer	Sequence (5'-3')	Function
LRv	CATTGCGCACACCTTGAAGTTAATCTACACT TAGTAGAAATTACCTCCCCATGTCTGAGGTA CTCCTTAAA	Model template
cr21-1	CATTGCGCACACCTTGAAGTTAATCTACACT TAGTAGAAATTATAGCTTATCAGACT	Minimal cr21 template
cr21-2	CATTGCGCACACCTTGAAGTTAATCTACACT TAGTAGAAATTATAGCTTATCAGACTAA	Soft-end cr21
cr21-CG-3bp	CATTGCGCACACCTTGAAGTTAATCTACACT TAGTAGAAATTACCGTAGCTTATCAGACTCG G	Optimised cr21
cr21-CG-7bp	CATTGCGCACACCTTGAAGTTAATCTACACT TAGTAGAAATTACCAGTCTTAGCTTATCAGA CTGG	Extended GC
cr21-SE	CATTGCGCACACCTTGAAGTTAATCTACACT TAGTAGAAATTATAGCTTATCAGACTTAAA	Soft-end cr21
cr21-SE-5bp	CATTGCGCACACCTTGAAGTTAATCTACACT TAGTAGAAATTAAGTAGCTTATCAGACTTAA	Extended stem
cap1	TCAACATCAGTCTGATAAGCTA-NH2	Blocking strand
cap2	TCAACATCAGTCTGATAAGCTATAA-NH2	Extended blocking strand

Continued on next page

Table 5-1: The oligonucleotides used in this study (continued).

Primer	Sequence (5'-3')	Function
cap3	TCAACATCAGTCTGATAAGCTACGG-NH2	CG-3bp blocking strand
ss-spacer1	CATTGCGCACACCTTGAAGTTATAGCTTATCAGACTTAAA	Split crRNA spacer
ss-spacer2	CATTGCGCACACCTTGAAGTTAGGATAGCTTATCAGACTCC	Alternative spacer
ds-handle-sense	TAATACGACTCACTATAGGGTAATTTCTACTAAGTGTAGAT	Split crRNA handle with T7 promoter
ds-handle-antisense	ATCTACACTTAGTAGAAATTACCCTATAGTGAGTCGTATTA	Split crRNA handle with T7 promoter
Handle-CG-3bp	ATCTACACTTAGTAGAAATTACCGTAGCTTATCAGACTCGG	Split crRNA handle
ds-spacer-sense	TAATACGACTCACTATAGGGTAACTTCAAGGTGTGCGCAATG	Split crRNA spacer with T7 promoter
ds-spacer-antisense	CATTGCGCACACCTTGAAGTTACCCTATAGTGAGTCGTATTA	Split crRNA spacer with T7 promoter
DH_12	TCAACATCAGTCTGATAAGCTAATCTACACTTAGTAGAAATTACCGTAGCTTATCAGACGG	Dragon hairpin
DH_14	TCAACATCAGTCTGATAAGCTAATCTACACTTAGTAGAAATTACCGTAGCTTATCAGACTCGG	Dragon hairpin
DH_15	TCAACATCAGTCTGATAAGCTACATCTACACTTAGTAGAAATTACCGTAGCTTATCAGACTCGG	Dragon hairpin
DH_16	TCAACATCAGTCTGATAAGCTACGATCTACACTTAGTAGAAATTACCGTAGCTTATCAGACTCGG	Dragon hairpin
Universal crRNA	UAAUUUCUACUAAGUGUAGAUUAACUUCAAGGUGUGCGCAAUG	Synthetic crRNA
F	FAM-CATTGCGCACACCTTGAAGTTAGAAA	For CRISPR
Q	TTTCTAACTTCAAGGTGTGCGCAATG-BHQ1	For CRISPR
R1	FAM-TTATT-BHQ1	For CRISPR
mir-F	FAM-TCAACATCAGTCTGATAAGCTACGGGAAA	For CRISPR

Continued on next page

Table 5-1: The oligonucleotides used in this study (continued).

Primer	Sequence (5'-3')	Function
mir-Q	TTTCCCGTAGCTTATCAGACTGATGTTGA-BHQ1	For CRISPR
noPamF	FAM-CATTGCGCACACCTTGAAGTT	For CRISPR
noPamQ	TAACTTCAAGGTGTGCGCAATG-BHQ1	For CRISPR
noPam-mirF	FAM-TCAACATCAGTCTGATAAGCTACGG	For CRISPR
noPam-mirQ	CCGTAGCTTATCAGACTGATGTTGA-BHQ1	For CRISPR

5.2.2 Oligonucleotide hybridisation

The cr21-cap duplex, dragon hairpin (DH) templates and all other double stranded DNA were annealed in TE buffer contains 12.5 mM Mg^{2+}, heated to 95 °C for 5 min, ramped down 1 °C per minute to 25 °C to anneal, followed by 4 °C hold.

5.2.3 In vitro self-transcribing crRNA and CRISPR assay

The IVT reaction contains $1\times$ RNAPol reaction buffer, 0.5 mM ribonucleotide solution mix (rNTPs), 1 U/µL RNase inhibitor, 5 U/µL T7 RNA polymerase (New England Biolabs, MA). and 1 µL of ssDNA template in a final volume of 20µL. The reaction was incubated at 37 °C for 2 h in vitro transcription (IVT). Subsequently, 6 µL of IVT product was added to the CRISPR mixture containing $1\times$ r2.1 reaction buffer and 33 nM Cas12a, incubated at room temperature 20 min. Afterwards, the FQ probe was added to a final concentration of 500 nM. Where indicated, the R1 reporter was also included at a final concentration of 500 nM. A total volume of 27 µL reaction mix was then loaded into a black 384-well round bottom plate (Corning Life Sciences), and sealed with MicroAmp™ Optical Adhesive Film (Applied Biosystems, ThermoFisher Scientific). The fluorescence was measured by the Synergy HT Microplate Reader (BioTek Instruments, Inc,. Agilent, CA) with excitation wavelength 480/20 nm and emission wavelength 528/20 nm, gain 50, incubation temperature of 37 °C.

5.2.4 Self-transcribing split crRNA assay

The reaction conditions were similar to those described in Section 5.2.3, except that the corresponding ssDNA and dsDNA templates were added together to generate split crRNA fragments. In the first split design, the ss-spacer template and ds-handle template were included in the IVT reaction. In the second split design, the Handle-CG-3bp template and ds-spacer

template were included instead. The generated spacer and handle RNA fragments were expected to assemble into functional split crRNA and were then used for the subsequent Cas12a cleavage assay.

5.2.5 Synthetic crRNA-based Cas12a assay

For the synthetic crRNA, the LbCas12a ribonucleoprotein (RNP) complex was first assembled by mixing the universal crRNA (300 nM) and LbCas12a (1 µM) in the 1 x r2.1 buffer at room temperature for 10 min. 500 nM target dsDNA FQ and R1 was added to the pre-assembled RNP complex (30 nM Cas12a-crRNA) and incubated at 37 °C for cleavage and fluorescence was monitored over time.

5.2.6 DNase I digestion and template removal

DNase I was used to remove the ssDNA template in the DNA-RNA chimeric products. For the DNase I digestion, 5 µL IVT product was mixed with 2U DNase I (Thermo Fisher Scientific, Waltham, MA) and 1 x reaction buffer in a final volume of 20 µL. The reaction was incubated at 37 °C for 30 min for digestion.

After digestion, three DNase I inactivation or removal methods were tested: heat inactivation, EDTA-assisted heat inactivation, and column purification. For heat inactivation, the product was heated at 65 °C for 10 min. For EDTA-assisted heat inactivation, 1 µL of 50 mM EDTA (Thermo Fisher Scientific, Waltham, MA) was added before heating at 65 °C for 10 min. For column purification, the product was purified using the Monarch® Spin RNA Cleanup Kit (New England Biolabs, Ipswich, MA) according to the manufacturer's instructions. No-DNase controls were processed using the same procedure, except that DNase I was omitted.

5.2.7 STSR-CRISPR assay for miR-21 detection

For the direct TMSD-gated STSR-CRISPR assay, miR-21, 50 nM cr21-cap duplex, and the IVT reaction components were mixed in a final volume of 20 µL. The reaction was incubated at 37 °C for 2 h to allow TMSD and self-transcription. After incubation, 6 µL of the IVT product was transferred to the Cas12a reaction. The final Cas12a reaction contained 33 nM Cas12a, 500 nM R1 reporter, and 1× r2.1 buffer in a total volume of 30 µL. Then, 27 µL of each reaction was loaded into a 384-well plate, and fluorescence was monitored at 37 °C.

For the dragon hairpin-mediated target recycling assay, 50 nM dragon hairpin probe was used instead of the cr21-cap duplex. The reaction was otherwise performed using the same procedure described above.

5.2.8 Native PAGE gel analysis

Native PAGE gel electrophoresis was performed as described in Section 3.2.4. Before nucleic acid staining, the gel was first imaged using the FAM channel to visualise FAM-labelled probes and cleavage products. The gel was then stained and imaged again to visualise total nucleic acids.

5.2.9 Bioanalyzer and smallRNA seq

Bioanalyzer analysis and RNA sequencing were performed by the MVLS Shared Research Facilities (SRF), University of Glasgow. Before submission, IVT products were purified using the Monarch® Spin RNA Cleanup Kit according to the manufacturer's instructions and stored at−80 °C until analysis. The small RNA libraries were sequenced on the Illumina NextSeq2000 platform. The reads were single and 100 bases long.

5.2.10 Bioinformatics

The resulting FASTQ files were processed using Cutadapt (version 4.9). The first three nucleotides of each read were removed, followed by trimming of the Clontech small RNA library adapter sequence (AAAAAAAAAA). Only reads containing the adapter sequence were retained. Reads were further quality-filtered using a score threshold of 20, and only trimmed reads with a final length of at least 17 nucleotides were retained for downstream analysis. The processed reads were aligned to the corresponding artificial reference sequences using Bowtie (version 1.2.3), generating alignment files in SAM format. The SAM files were subsequently converted to BAM format using SAMtools (version 1.11) for downstream analysis.

The FASTQ results were further analysed using DragonMostCommon, a tool developed by Greenwald et al.[182] to identify the 10 most abundant reads aligned to the artificial template. Additional analysis and visualisation code was generated with the assistance of ChatGPT and executed in Google Colab. The potential priming and base-pairing structure was modelled using AgniAlign (FireLabSoftware GitHub)[183].

5.3 Results and discussion

5.3.1 Establishing the self-transcribing CRISPR platform

In this system, a single-stranded DNA (ssDNA) template undergoes promoter-independent self-transcription to generate functional crRNA. In the presence of T7 RNA polymerase (T7

RNAP), the generated RNA products may support Cas12a recognition of the original ssDNA template, leading to collateral cleavage of fluorescent reporters and generating a detectable signal (Figure 5-1A). Building on this unique self-transcription mechanism, we developed two miR-21 sensing strategies by integrating toehold-mediated strand displacement (TMSD) reactions (Figure 5-1A). System 1 employs direct TMSD-mediated activation, in which the target miRNA displaces the cap strand and exposes the 3′ end of the ssDNA template, enabling self-transcription and switching the system from the OFF to the ON state. System 2 introduces a target recycling-enhanced TMSD strategy to potentially improve detection sensitivity. In this design, target miRNA binding opens the DNA hairpin through strand displacement, allowing the exposed 3′ end to fold back and initiate self-transcription. During RNA synthesis, the bound miRNA is proposed to be displaced and released from the hairpin, allowing it to participate in subsequent strand displacement reactions. This target recycling mechanism could enable repeated activation of additional hairpin templates, thereby enhancing signal generation.

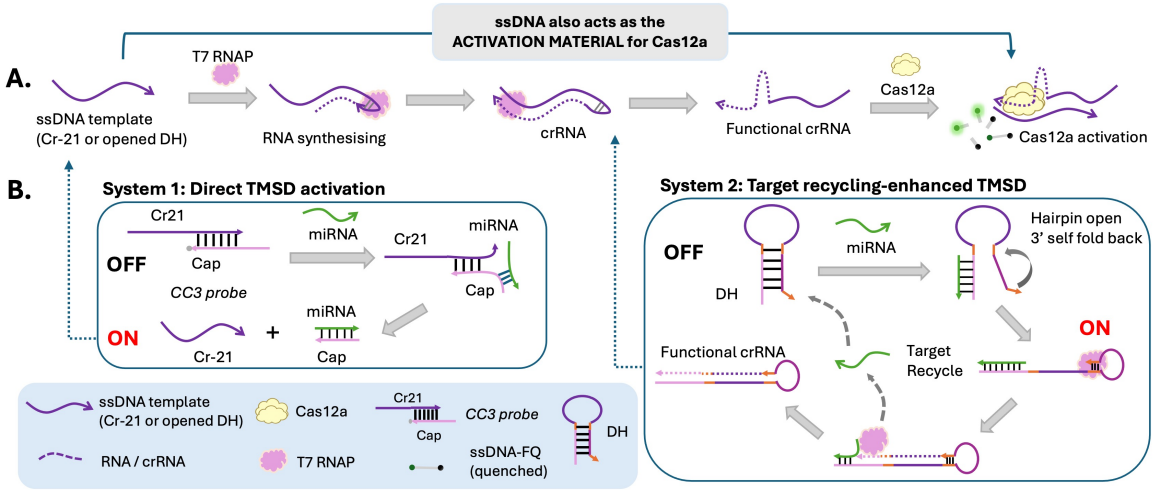


Figure 5-1: Overview of the STSR-CRISPR platform. (A) Schematic illustration of the self-transcription and self-recognition mechanism, where a single ssDNA template functions as both the transcription and Cas12a activation material. (B) miRNA sensing strategies based on direct TMSD activation (System 1) and target recycling-enhanced TMSD (System 2).

Based on the observations described in Chapter 4, 4.3.3, ssDNA template LRv was capable of activating the CRISPR reaction in the presence of T7 polymerase. We hypothesised that this activation was caused by the soft 3' terminal of LRv, where paired with another site in the sequence itself and extend with ribonucleotides to form a DNA/RNA chimeras[104,108]. In the previous study, this DNA/RNA hybrid product was termed "Dragon RNA"[14]. As the formation of Dragon RNA shares the basic principle of the RNA polymerisation process, the newly synthesised RNA is complementary to the 5' region of the LRv template. In the design, the 5' sequence of the LRv was pre-designed to correspond to the full-length crRNA sequence targeting the FQ probe. In this way, the newly synthesised Dragon RNA are capable of acting

as a functional crRNA-like molecule and activating the CRISPR, releasing the fluorescence through cis- cleavage of the FQ probe and trans- cleavage of the R1 probe. (Figure 5-2a) To further investigate the potential of LRv for sensing strategy, the Self-transcription CRISPR mechanism was tested by eliminating T7 polymerase and Cas12a, respectively (Figure 5-2b). In the presence of the LRv, T7 RNA polymerase and Cas12a, we observed strong fluorescence activation. In contrast, omission of either T7 RNA polymerase or Cas12a resulted in only a low fluorescence level, suggesting that both transcription and Cas12a-mediated activation are required for signal generation. We also observed LRv concentration-dependent fluorescence activation. Higher concentration of input LRv produced stronger fluorescence signals, whereas the signal in the no-template control remained close to the baseline.(Figure 5-2c)

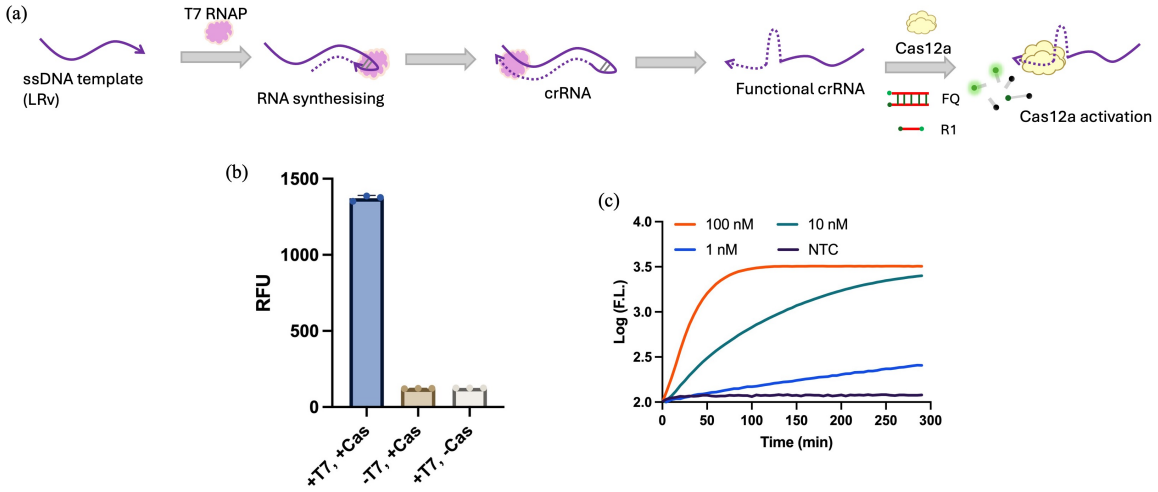


Figure 5-2: (a) Schematic illustration of self- transcription and self-recognition mechanism, where a single ssDNA template functions as both the transcription and Cas12a activation material. (b) Fluorescence signal under different reaction conditions. Signals were observed only in the presence of both T7 RNAP and Cas12a. ”+/-” indicates the presence or absence of polymerase. Mean ± SD (n = 3). (c) Real-time fluorescence signal at different template concentrations. Curves represent the mean of two replicate reactions (n=2).

To determine the optimal experimental conditions for the self-transcribing CRISPR assay. The fluorescent probe concentration and composition were tested (Figure 5-3a). The transcribed crRNA sequence was designed to recognise and target the FQ probe, leading to fluorescence release through cis-cleavage. In contrast, R1 acted as an auxiliary ssDNA probe which could be cleaved through trans- cleavage after CRISPR activation. With the increase of FQ concentration, the fluorescence kinetic curve also showed an increase in fluorescence intensity, indicating that sufficient crRNA-like product was generated to activate Cas12a and support FQ cleavage. The 5 nM FQ probe did not produce a detectable signal, likely because the fluorescence released from this low concentration was below the detection range of the plate reader. The addition of R1 further increased the fluorescence signal, particularly when lower concentrations of FQ were used. This is consistent with the role of R1 as an additional

probe that can enhance the final fluorescence readout[184]. However, when the FQ concentration was increased to 500 nM, the difference between reactions with and without R1 became relatively small. This may be because the high concentration of FQ already generated a strong cis-cleavage-dependent fluorescence signal, thereby reducing the relative contribution of the R1 reporter to the total fluorescence output. Another possibility is that the steric hindrance caused by the high concentration of cis-cleavage products may interfere with the access of R1 probe to the RuvC catalytic pocket for trans- cleavage[185]. The concentration of Cas12a was also investigated; the optimal concentration was 33 nM. Lower Cas12a concentrations may limit the formation of active RNP that causes the slow kinetics. However, excessive Cas12a did not further improve the signal and instead inhibited the CRISPR activity, potentially due to the imbalance between Cas12a and the available crRNA-like product[186,187].

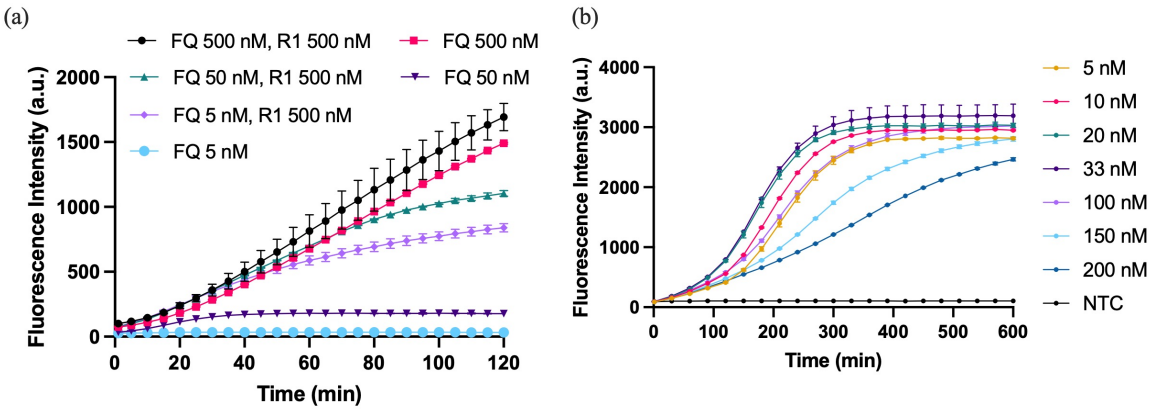


Figure 5-3: Optimisation of the self-transcribing CRISPR assay. (a) Effect of FQ and R1 reporter concentrations on fluorescence generation. (b) Effect of Cas12a concentration on fluorescence kinetics. The input ssDNA template concentration was 10 nM. Data represent the range of two technical replicates.

Target-triggered activation of the CRISPR system was designed based on miR-21. (Figure5-4a) In brief, the cap strand was annealed to the cr21 template to form a CC probe, leaving an 8 nt toehold for strand displacement. In the absence of miR-21, the cap strand was designed to block the 3′ region of cr21 and prevent the template from self-folding, thereby suppressing self-transcription and downstream CRISPR activation. In the presence of the target miR-21, miR-21 hybridises with the toehold region of the cap and displaces the cap from cr21. The exposed 3′ end of cr21 can then self-fold to initiate self-transcription and CRISPR activation. Two cr21 templates and two corresponding cap strands were designed. Compared with cr21-1, cr21-2 contained an additional two adenine residues at its 3′ end. Cap2 contained three additional nucleotides complementary to cr21 compared with cap1, increasing the length of the complementary region from 14 to 17 bp and the predicted melting temperature (Tm) from 44.7 to 48.6 °C.

Figure5-4b compared the blocking effects of different probes. The extra ”AA” tail did not

increase the fluorescence signal, suggesting that this modification did not improve cr21 transcription for more functional crRNA-like products. Cap 2 generally showed the strongest blocking ability in probes 2 and 4, which is likely due to the increased melting temperature and the greater number of base pairs. After overnight incubation, probe 4 still showed the lowest background fluorescence signal (Figure5-4c); therefore, probe 4 was selected for the strand displacement test. In the presence of miR-21, the fluorescence signal increased compared with the no-target condition, indicating that miR-21 successfully displaced the cap strand and restored the self-transcription/CRISPR activation process (Figure5-4d).

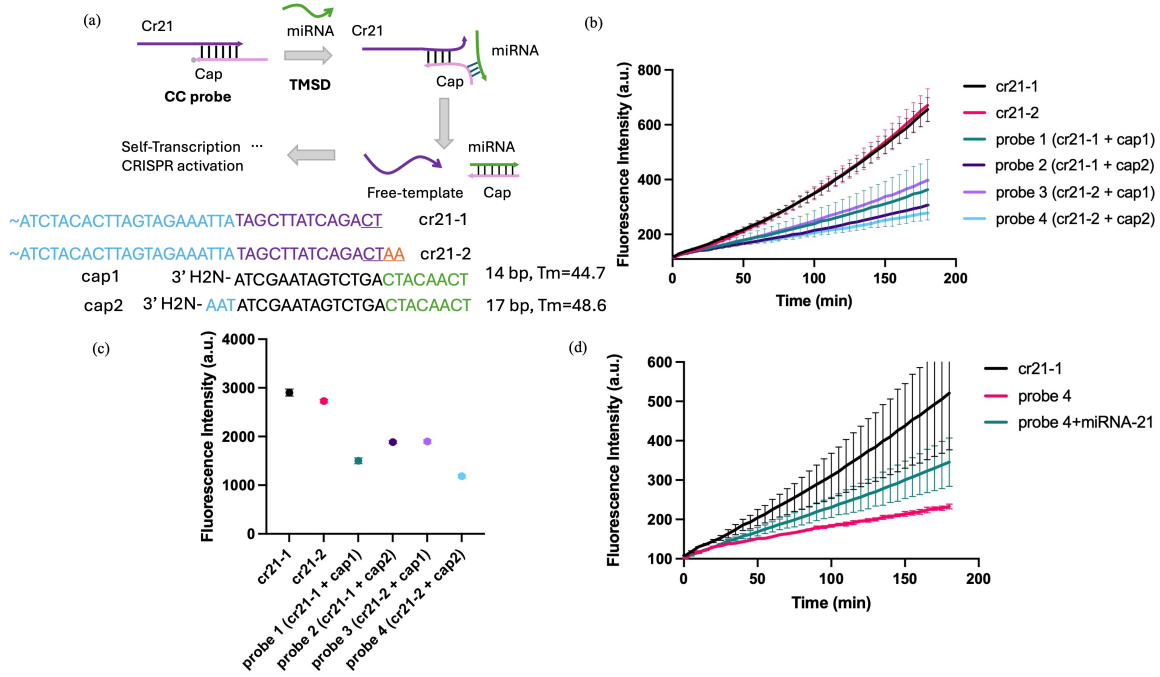


Figure 5-4: miRNA-triggered activation of the STSR-CRISPR system. (a) Schematic of miR-21-triggered TMSD and free-template release. (b) Fluorescence kinetics of cr21-1 and cr21-2 with or without different cap sequences. Cr21 and cap were both used at 10 nM. (c) Endpoint fluorescence intensity after overnight incubation. (d) Evaluation of miR-21-triggered strand displacement. Probe 4 and miR-21 were used at 100 nM. FQ and R1 were 500 nM. Data represent the mean and range of two replicates.

To further test the feasibility of the miR-21 triggered system, probes were tested with or without the miR-21 target and the fluorescence intensity was measured after 180 min. Probes 2 and 4, both containing cap2, showed lower background fluorescence in the absence of miR-21 than the corresponding probes containing cap1. This observation was consistent with the previous experiment, further supporting the improved blocking effect of cap2. (Figure 5-5a). To further compare the target response, the fluorescence ratio between the target and no-target reactions was calculated after overnight incubation (Figure 5-5b). Although probe 4 did not show the highest absolute fluorescence signal, it gave the highest target-to-background ratio, mainly due to its low no-target background. This suggested that probe 4 provided the best balance between target-triggered activation and low background, and therefore probe 4 was

selected for further experiments.

Universal crRNA was then used as a positive control to estimate the CRISPR activation level generated by the self-transcribed cr21 templates. As shown in Figure 5-5c, fluorescence increased with crRNA concentration, with clear activation observed at 30 and 300 nM. Endpoint fluorescence at 130 min was then plotted against crRNA concentration to generate a standard curve (Figure 5-5d). The fluorescence signals produced by 10 nM cr21-1 and cr21-2 were higher than the signal estimated for 10 nM universal crRNA from the fitted calibration curve, suggesting that self-transcription of the cr21 templates amplified the functional crRNA-like product to some extent before CRISPR activation. However, because the ssDNA templates and synthetic crRNA were not directly equivalent, this comparison should be interpreted as a fluorescence benchmark rather than a quantitative estimate of functional crRNA yield. Despite the presence of synthetic crRNA, the reaction showed relatively slow kinetics, with a pronounced increase in fluorescence occurring only after approximately 150 min.

Together, these results demonstrated that the self-transcribing CRISPR platform was successfully established. The ssDNA template was able to undergo T7 RNA polymerase-mediated self-transcription and generate crRNA-like products, which subsequently activated the Cas12a reaction and produced fluorescence signal. This system also showed the potential to achieve target-triggered detection through toehold-mediated strand displacement.

However, the overall performance of the system was still limited. The fluorescence response was relatively slow, and the target-triggered signal increase was not sufficiently strong for efficient detection. In addition, the amount of functional crRNA-like product generated from the ssDNA template appeared to be limited, suggesting that the transcription efficiency of the template itself may restrict the downstream CRISPR output. Therefore, further optimisation and mechanistic investigation were required to improve the efficiency of the system and to better understand how the self-transcribed products activate Cas12a.

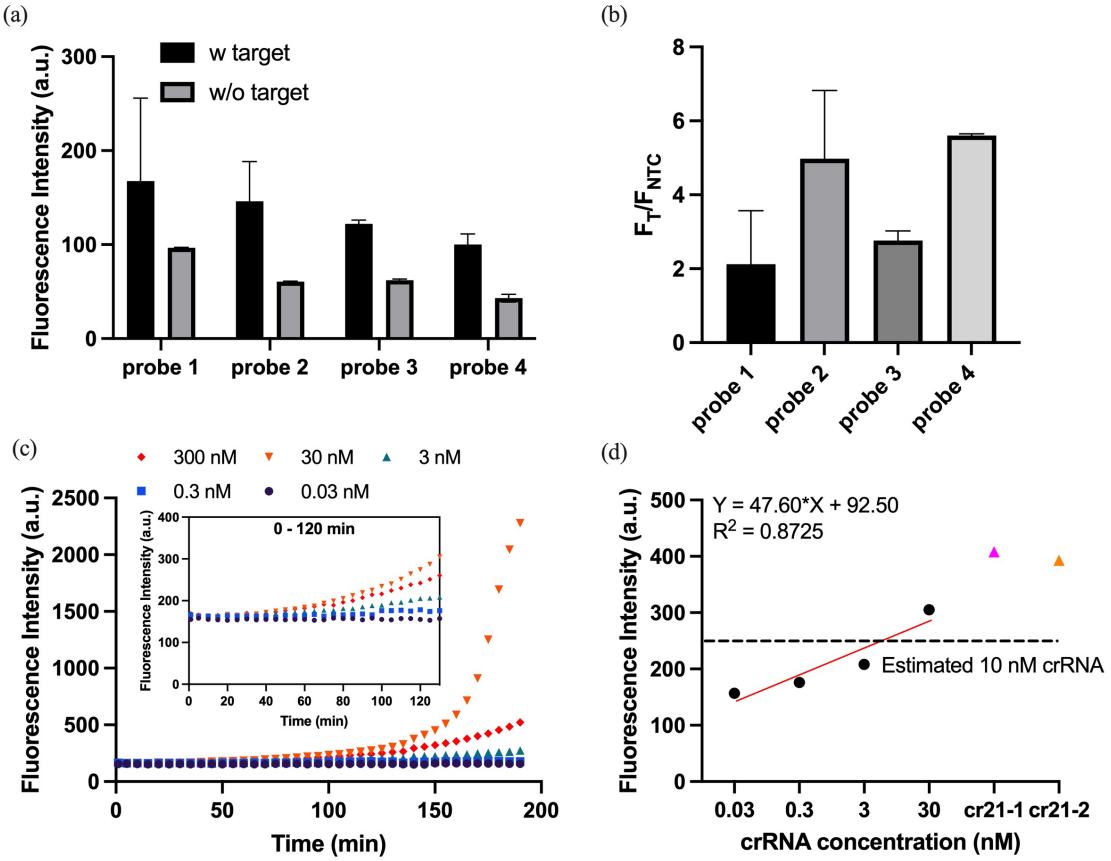


Figure 5-5: Evaluation of probe candidates for miR-21 detection and universal crRNA. (a) Fluorescence intensity of probes 1 – 4 (10 nM) at 180 min with or without miR-21 target (10 nM). (b) Overnight fluorescence ratio between the target and no-target reactions (FT/FNTC). FQ and R1 were 500 nM. Data are presented as mean with range, n = 2. (c) Fluorescence kinetics of universal crRNA at 0.03, 0.3, 3, 30, and 300 nM over 180 min. The inset shows the fluorescence response from 0 to 120 min. (d) Endpoint fluorescence intensity at 130 min for crRNA from 0.03 to 30 nM and for 10 nM cr21-1 and cr21-2. The red line represents the linear regression fitted using the crRNA standards. The dashed line indicates the estimated fluorescence intensity of 10 nM crRNA calculated from the regression equation. FQ and R1 were 500 nM. n=1.

5.3.2 Mechanistic investigation of STSR-CRISPR activation

Evaluation of split crRNA assembly and crRNA-like intermediates

According to Greenwald's work, shorter ssDNA templates are generally more likely to generate complete complementary RNA sequence during self-transcription. Therefore, we split the ssDNA template into two parts: a ss-spacer template and a ds-handle template (Figure 5-6a). The rationale for this design was that the correct handle configuration is important for Cas12a assembly and crRNA structural stability. Therefore, the handle region was transcribed using a conventional T7 promoter-based dsDNA template, while the spacer region

was generated from a shorter self-transcribing ssDNA template. The two parts were expected to assemble into a functional split crRNA and activate Cas12a. As shown in Figure 5-6b, both ss-spacer1 and ss-spacer2 produced strong fluorescence signals when combined with the ds-handle. However, the ds-handle alone also generated a relatively high fluorescence signal, indicating that the observed activation could not be specifically attributed to assembly of the intended split crRNA. Further testing showed that the fluorescence kinetics changed with ds-handle concentration; lower ds-handle concentrations generally produced weaker signals (Figure 5-6c). This suggests that the ds-handle itself contributed to the observed fluorescence, although the exact source of this signal requires further investigation.

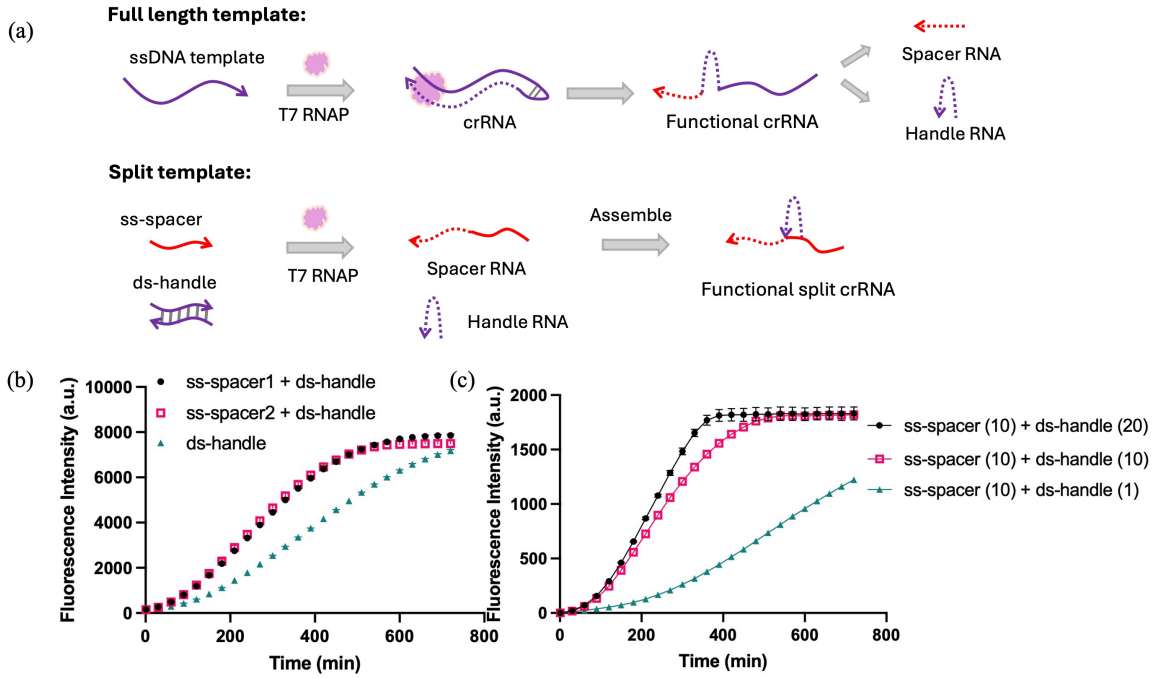


Figure 5-6: Design and evaluation of split crRNA system. (a) Schematic comparison of full-length crRNA generation and split crRNA assembly. For the split template design, spacer RNA is transcribed from spacer ssDNA and assembled with handle RNA generated from handle dsDNA to form functional split crRNA. (b) Fluorescence kinetics of handle dsDNA combined with different spacer templates. FQ and R1 reporter concentrations were both 500 nM. (c) Fluorescence kinetics using different handle dsDNA concentrations with 10 nM spacer template. FQ concentration was 500 nM. Data represent the mean and range of two replicates.

After comparison, the fluorescence signals generated by the split crRNA system (ss-spacer + ds-handle), the ds-handle template alone, and the full-length crRNA template (cr21-SE) were unexpectedly similar (Figure 5-7b). The split-template design was initially introduced to accelerate crRNA generation by producing the spacer and handle regions separately, with the expectation that the two RNA components could subsequently assemble into a functional crRNA. However, the split system did not produce a stronger or faster fluorescence response than the ds-handle template alone. The strong signal produced by the ds-handle template

indicated that the presence of the ss-spacer was not essential for Cas12a activation under these conditions. One possible reason is that the T7 polymerase may more favour the promoter-containing dsDNA template over the promoter-free ssDNA[14]. In this case, the ds-handle template could be transcribed into a large amount of handle RNA. One handle RNA may act as the handle region, while another handle RNA may act as a spacer-like RNA strand to target the ds-handle DNA template, thereby triggering Cas12a activation and trans-cleavage of the R1 reporter (Figure 5-7a). However, the cis-cleavage event in the ds-handle-only reaction is still uncertain. Although Cas12a has been reported to show off-target or non-canonical target cleavage activity[75,79], the fluorescence signal could not be differentiated between cis-cleavage and trans-cleavage because the same fluorophore was used for both probes.

We also noticed that the fluorescence kinetics changed when the annealing ratio between the F and Q strands was changed (Figure 5-7c). Theoretically, excess Q could block fluorescence leakage from the F strand more effectively.[188] However, because the crRNA was designed to target the F strand, excess Q may compete with the crRNA for the F strand once the FQ probe is partially unwound. This may delay Cas12a recognition and activation, explaining the slower fluorescence kinetics observed with the 1:1.5 FQ ratio. Therefore, 1:1 ratio of F and Q was selected for further experiments.

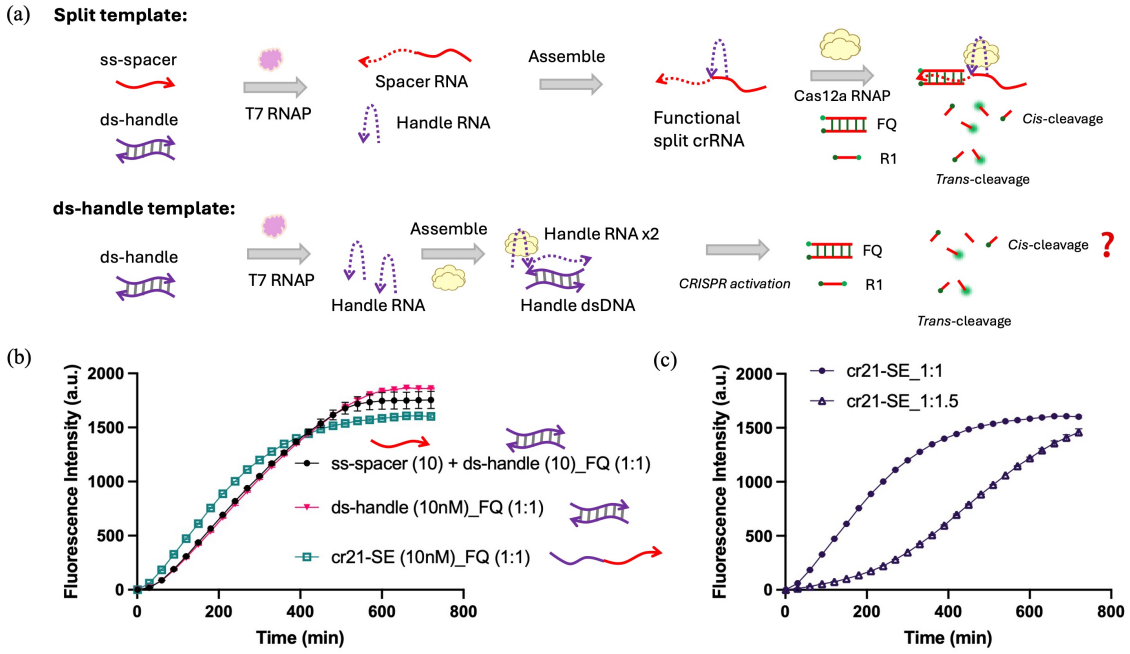


Figure 5-7: Comparison of split-template and ds-handle-mediated Cas12a activation. (a) Schematic of split crRNA assembly and ds-handle-mediated CRISPR activation. FQ serves as the cis-cleavage substrate, while R1 reports trans-cleavage activity. (b) Fluorescence validation of split template, ds-handle-only template, and full-length cr21-SE template at 10 nM with an FQ ratio of 1:1. (c) Effect of different FQ ratios on the fluorescence signal generated by the full-length cr21-SE template. Data represent the mean and range of two replicates.

Because the ds-handle alone generated a strong fluorescence signal, the spacer and handle

templates were switched in the redesigned split-template system. The full-length template was cr21-CG-3bp, while the split system was divided into an ssDNA Handle-CG-3bp template and a ds-spacer template (Figure 5-8a). In this new design, the ds-spacer was expected to generate a large amount of spacer RNA through conventional T7 promoter-based transcription, but the spacer RNA alone should not activate Cas12a without the correct handle structure. In contrast, Handle-CG-3bp was expected to self-transcribe into handle RNA, which could assemble with the spacer RNA generated from the ds-spacer template to form a functional split crRNA and activate the CRISPR/Cas12a reaction.

As shown in Figure 5-8b, the full-length ssDNA template cr21-CG-3bp still generated the highest fluorescence signal compared with the split crRNA system. This suggested that the full-length self-transcribing template was more effectively able to activate CRISPR under the tested conditions. Surprisingly, Handle-CG-3bp alone could also produce fluorescence signal, even in the absence of the ds-spacer. These results raised further questions about the mechanism of CRISPR activation in this system. If Handle-CG-3bp could generate fluorescence without a related PAM-containing dsDNA target, it suggested that the signal might not depend entirely on the designed FQ-mediated cis-cleavage pathway. To further examine this possibility, cr21-CG-3bp was tested with different FQ annealing ratios (Figure 5-8c), it shows a similar trend to the previous split crRNA system (Figure 5-7c). More importantly, when only the R1 reporter was added, fluorescence still exists. This indicated that the CRISPR reaction may be activated by the ssDNA template itself. In other words, the ssDNA may not only serve as a transcription template for generating crRNA-like products, but may also act as a CRISPR-recognised template that directly activates the CRISPR system.

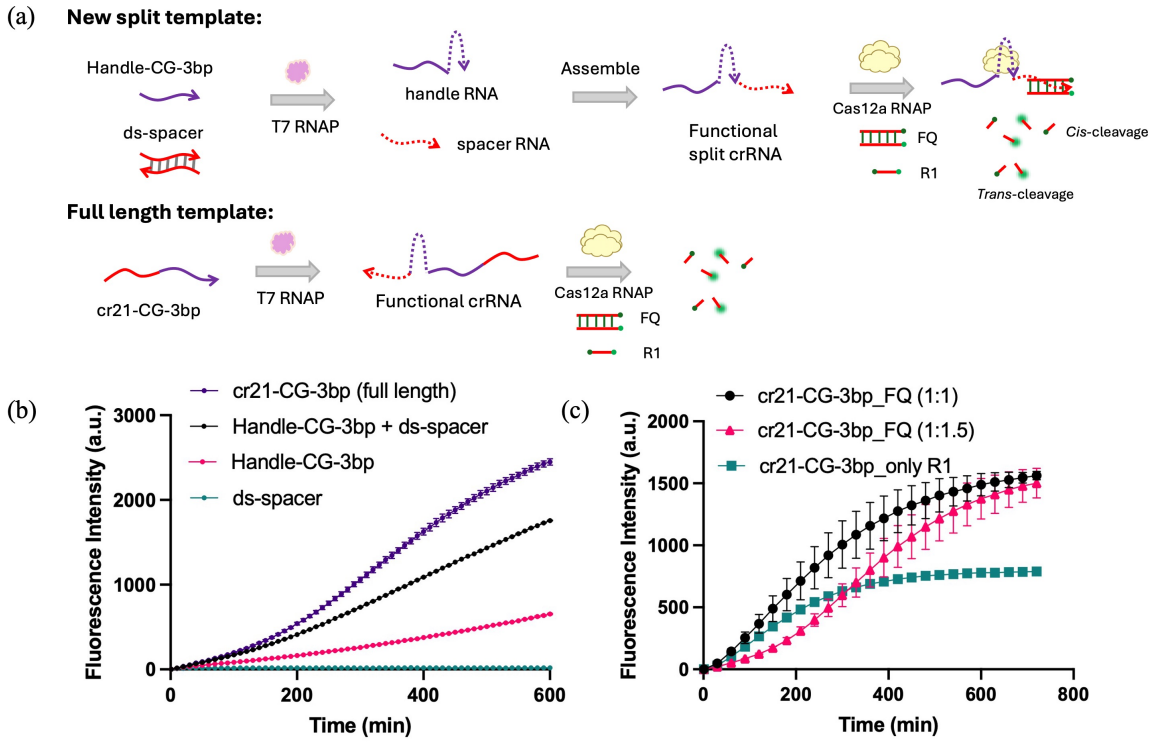


Figure 5-8: Comparison of split and full-length cr21-CG-3bp templates. (a) Schematic of the new split template and full-length template systems. FQ serves as the cis-cleavage substrate, and R1 reports trans-cleavage activity. (b) Fluorescence validation of full-length cr21-CG-3bp, split Handle-CG-3bp/ds-spacer, and individual template components. (c) Effect of different FQ ratios with R1, and R1-only condition on the full-length cr21-CG-3bp system. Data represent the mean and range of two replicates.

Reporter cleavage is not strictly limited to cognate FQ targets

To investigate whether cis-cleavage or trans-cleavage dominated the fluorescence response, FQ and R1 reporters were tested separately, and an unrelated double-stranded reporter, mir-FQ, was also introduced (Figure 5-9a). FQ served as the target-reporter designed to be recognised by the crRNA sequence, whereas R1 acted as a ssDNA trans-cleavage reporter after Cas12a activation. The mir-FQ probe contained an unrelated sequence and was used to test whether fluorescence release was restricted to the FQ target.

As shown in Figure 5-9b, both cr21-CG-3bp and Handle-CG-3bp generated increasing fluorescence with all three substrates, although the overall signal produced by cr21-CG-3bp was substantially higher than that produced by Handle-CG-3bp. For cr21-CG-3bp, FQ and R1 produced very similar fluorescence profiles and reached the highest signal intensities, whereas mir-FQ generated a lower but steadily increasing signal. In contrast, Handle-CG-3bp produced a weaker response overall, with R1 giving the highest fluorescence, followed by FQ and mir-FQ. Importantly, fluorescence was still observed when FQ was replaced by R1 or mir-FQ, indicating that the observed signal was not solely dependent on sequence-specific

cis-cleavage of FQ. Taken together, these results suggest that the ssDNA template may possess dual functions, serving both as a self-transcribing template and as a self-recognition element capable of activating Cas12a and promoting cleavage of other double-stranded DNA substrates.

To further investigate whether activated Cas12a could also induce fluorescence release from unrelated double-stranded DNA probes in other CRISPR systems, the unrelated mir-FQ probe was tested in HPV16 (Figure 5-9c) and HPV18 (Figure 5-9d) CRISPR reactions. In these systems, the HPV16- and HPV18-specific crRNAs were designed to recognise their corresponding HPV targets and should not interact with the mir-FQ probe. However, the fluorescence increased when the mir-FQ was included in the activated CRISPR reaction, and no fluorescence leakage was observed in the absence of Cas12a in our experiment (Data not shown), indicating that once Cas12a is activated by the ssDNA target, it may also cleave or open unrelated double-stranded FQ-type probes in a non-specific manner. The results in Figure 5-9c and d may also provide useful insight for assay development, as the addition of an unrelated fluorescent probe could potentially enhance the total fluorescence output and improve detection performance.

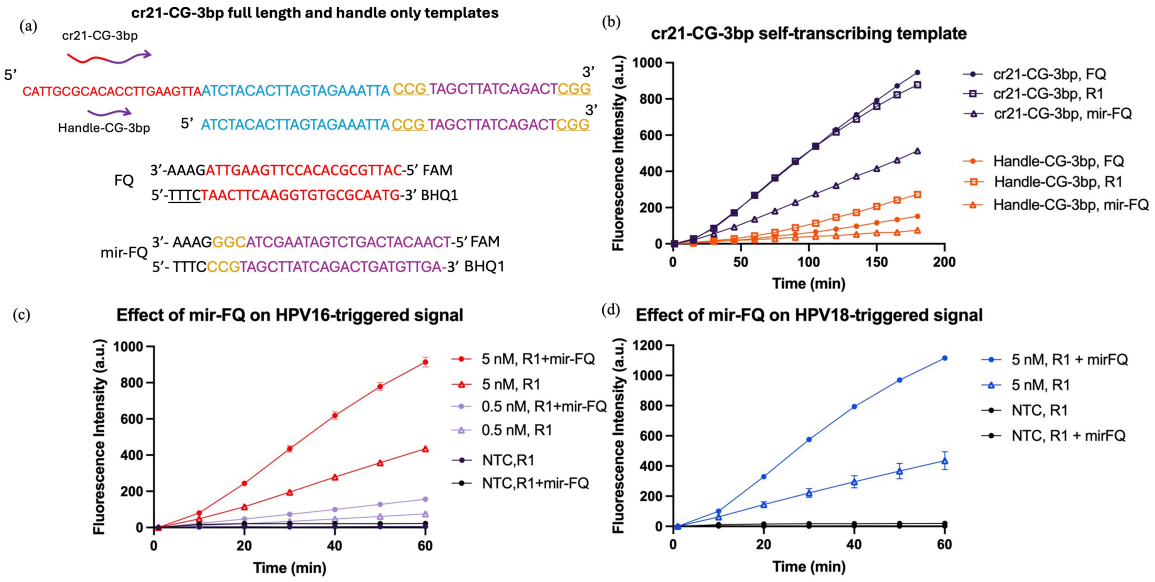


Figure 5-9: Evaluation of cr21-CG-3bp activity and mir-FQ-assisted HPV target detection.(a) Sequence design of the full-length cr21-CG-3bp and Handle-CG-3bp templates. Red letters represent the spacer region, and blue letters represent the handle region. (b) Fluorescence kinetics of the two templates with FQ, R1, or mir-FQ reporters. FQ and R1 were used at 500 nM. Data are shown as the mean of two independent experiments. (c,d) Detection of HPV16 (c) and HPV18 (d) targets using the corresponding crRNAs, comparing R1 alone with R1 plus mir-FQ. The indicated concentrations, such as 5 nM, refer to target concentrations. FQ and R1 were used at 500 nM. NTC reactions served as negative controls. Data are shown as mean ± SD, n=3.

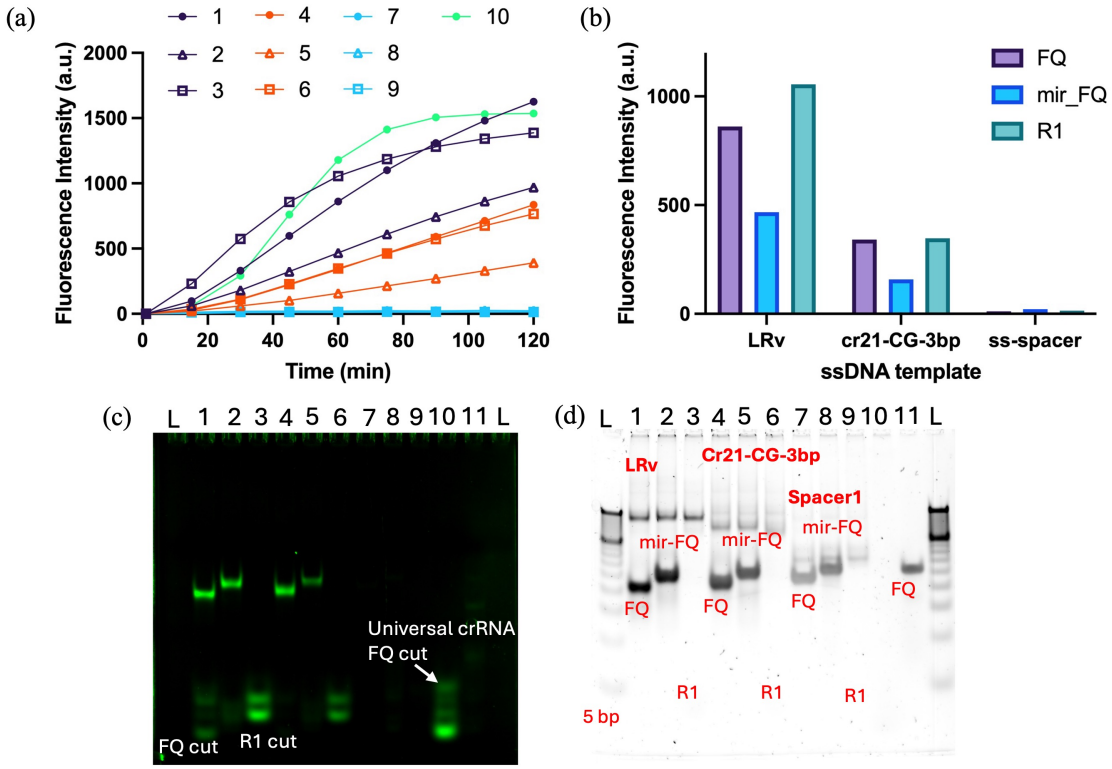
Although Cas12a activation is supposed to exclusively trigger non-specific ssDNA cleavage,

reports have demonstrated that the active RuvC domain can also degrade nonspecific dsDNA and ssRNA substrates[75,79]. Short dsDNA substrates have been reported to be used as fluorescent reporters in CRISPR/Cas12a systems. This is attributed to reduced double-stranded DNA stability under low-salt conditions, which may expose transient single-stranded regions to activated Cas12a[76,77]. However, the underlying mechanism was not investigated in detail, and it remains unclear whether fluorescence recovery results from direct trans-cleavage of the dsDNA reporter or from partial strand separation that increases the distance between the fluorophore and quencher. Long double-stranded λ DNA has also been used as a trans-cleavage substrate, possibly because of its intrinsic structural features, including locally accessible single-stranded regions[189]. More recent studies have shown that dsDNA degradation can be enhanced by introducing a short 3′ single-stranded overhang, although the proposed unidirectional trans-cleavage mechanism remains incompletely understood[78]. Therefore, gel electrophoresis was performed using the two major ssDNA templates, LRv and cr21-CG-3bp, to determine whether the observed fluorescence signal was associated with physical degradation of the dsDNA reporter. The ss-spacer template was included as a negative control, and the universal crRNA was a positive control.

Fluorescence kinetics were monitored for 120 min (Figure 5-10a) and the endpoint fluorescence intensities are shown in Figure 5-10b. For both LRv and cr21-CG-3bp, the FQ and R1 reporters produced stronger signals than the unrelated mir-FQ reporter. LRv generally generated higher fluorescence than cr21-CG-3bp, although further analysis, such as RNA sequencing, would be required to determine whether LRv produces more crRNA-like transcripts. In contrast, the ss-spacer template generated negligible fluorescence with all three reporters. Because ss-spacer contains only the spacer sequence and lacks the crRNA handle that cannot activate the CRISPR system.

Following fluorescence measurement, the reaction products were analysed by gel electrophoresis. In the FAM channel (Figure 5-10c), the LRv sample containing FQ showed a small fluorescent product near the bottom of the gel in lane 1, suggesting that part of the FAM-labelled strand was cleaved. Fluorescent cleavage products were also observed in the R1 samples in lanes 3 and 6, which is consistent with Cas12a trans-cleavage of the ssDNA reporter. However, the dsDNA reporters still showed fluorescent bands near the position of the intact probe, especially in the cr21-CG-3bp samples containing FQ and mir-FQ in lanes 4 and 5. A similar result was observed for LRv. In contrast, the ss-spacer samples showed no fluorescent signal, which agrees with the fluorescence curves. The universal crRNA positive control in lane 10 showed strong fluorescence release and a clear degraded product, indicating efficient reporter cleavage. In comparison, the LRv and cr21-CG-3bp samples still show fluorescent bands near the intact dsDNA reporter position. This suggests that the fluorescence signal was not caused only by complete cleavage of the dsDNA reporter. According to this observation, the fluorescence recovery was more likely caused by separation of the Q strand from the F

strand, while the F strand remained largely intact and therefore migrated close to the original dsDNA reporter position. This behaviour was different from the R1 reporter, which was clearly cleaved through Cas12a trans-cleavage.



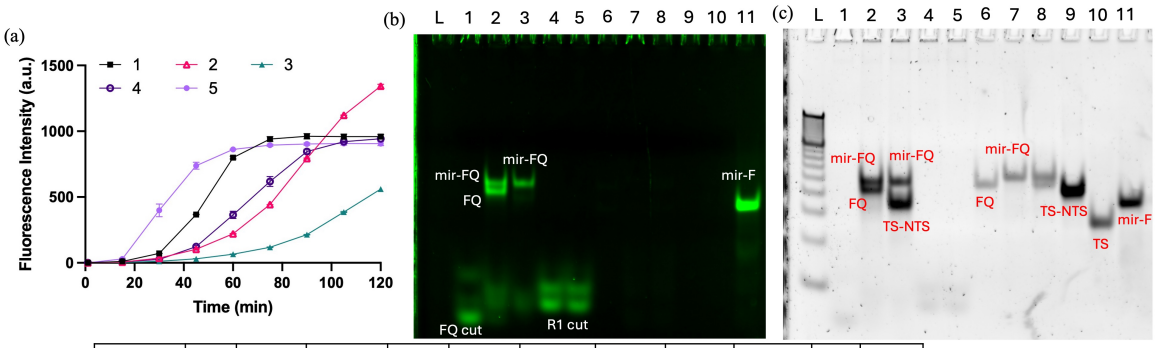
Lanes	1	2	3	4	5	6	7	8	9	10	11
Dragon Templates	LRv			cr21-CG-3bp			ss-spacer			/	/
Reporter	FQ	mir-FQ	R1	FQ	mir-FQ	R1	FQ	mir-FQ	R1	FQ	FQ
Universal crRNA	-									+	

Figure 5-10: Validation of template-generated crRNA activity and target-specific reporter cleavage. (a) Fluorescence kinetics of different template–reporter combinations. (b) End-point fluorescence comparison of LRv, cr21-CG-3bp, and ss-spacer templates with FQ, mir-FQ, or R1 reporters. FQ is the cognate F/Q-labelled target for all crRNAs, whereas mir-FQ is an unrelated F/Q-labelled target control. n=1. (c) FAM-channel gel image showing fluorescent reporter cleavage products. (d) Stained gel image showing total nucleic acid bands under the same conditions. Lanes 1–3: LRv with FQ, mir-FQ, or R1; lanes 4–6: cr21-CG-3bp with FQ, mir-FQ, or R1; lanes 7–9: ss-spacer with FQ, mir-FQ, or R1; lane 10: synthetic universal crRNA with FQ as a positive control; lane 11: FQ-only control.

To investigate whether fluorescence recovery from an unrelated dsDNA reporter—driven by double-strand unwinding/opening without cleavage of the fluorophore-labelled target strand—is a common phenomenon in conventional CRISPR-Cas12a systems, a synthetic universal crRNA was used as a model. A non-labelled TS-NTS target (sharing the same sequence as the FQ target but lacking fluorescent labels) was used. When FQ was used as both the target

and reporter, rapid fluorescence recovery was observed and reached a plateau within approximately 80 min (curve 1). Addition of the unrelated mir-FQ reporter produced slower initial kinetics but a continued increase in fluorescence after the FQ-only reaction had reached a plateau (curve 2), suggesting that activated Cas12a also acted on mir-FQ. This kinetic behaviour is supported by the gel analysis. In the FAM-channel gel (Figure 5-11b), FQ alone was fully digested as low molecular weight bands showed in lane 1 and the disappearance of the FQ band in the stained gel (Figure 5-11c, lane 1). In contrast, when the extra mir-FQ reporter was added (lane 2), fluorescent bands remained close to the positions of the intact FQ and mir-FQ duplexes. This is consistent with incomplete or strand-selective reporter processing in the presence of competing reporters, but does not distinguish duplex opening from limited or selective cleavage. Reporter competition may contribute to the slower initial kinetics, although the causal pathway was not established. Furthermore, to examine the mir-FQ fluorescence recovery independently, the non-labelled TS-NTS duplex was used as the target. This reaction produced the slowest kinetics, with remaining mir-FQ and TS-NTS bands still visible in lane 3. Finally, the trans-cleavage activity of the R1 reporter was compared using a single-stranded DNA target (TS, curve 5) and a double-stranded DNA target (TS-NTS, curve 4). The kinetics show that the ssDNA target (curve 5) has faster trans-cleavage kinetics, which is in line with the existed studies[190,191].

These results show that the FQ probe responds to Cas12a as both target and fluorescence reporter. When an additional unrelated dsDNA, mir-FQ, was present, the fluorescence kinetics became slower, suggesting competition of activated Cas12a between the two dsDNA substrates. Gel analysis showed extensive degradation of FQ when it was only used. In contrast, when FQ and mir-FQ were added together, fluorescence was detected from both probes while substantial fluorescent band remained close to the position of the intact duplex. This indicates that the duplex is not undergoing traditional, complete degradation.



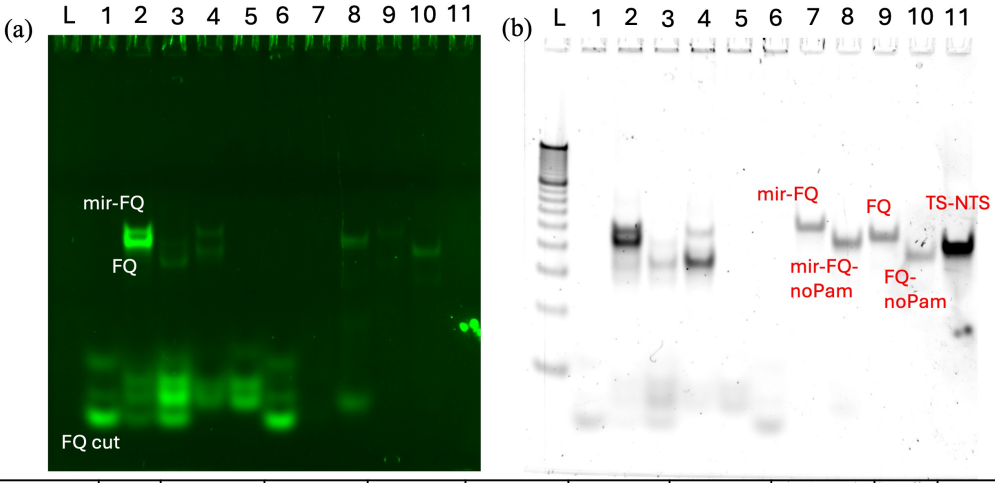
Lanes	1	2	3	4	5	6	7	8	9	10	11
Universal crRNA	+					-					
Template	FQ	FQ	TS-NTS	TS-NTS	TS	FQ	mir-FQ	mir-FQ FQ	TS-NTS	TS	mir-F
Reporter	FQ	FQ mir-FQ	mir-FQ	R1	R1						

Figure 5-11: Validation of target-dependent cis-cleavage and trans-cleavage using universal crRNA. (a) Fluorescence kinetics of different target–reporter combinations. n=1. (b) FAM-channel gel image showing fluorescent reporter and cleavage products. (c) Stained gel image showing total nucleic acid bands under the same conditions. Lanes 1–5 contain synthetic universal crRNA as the positive crRNA control: lane 1, FQ with FQ reporter; lane 2, FQ with FQ and mir-FQ reporters; lane 3, TS-NTS with mir-FQ reporter; lane 4, TS-NTS with R1 reporter; lane 5, TS with R1 reporter. Lanes 6–11 are no-crRNA controls containing FQ, mir-FQ, FQ/mir-FQ, TS-NTS, TS, or mir-F, respectively. FQ is the cognate F/Q-labelled target, mir-FQ is an unrelated F/Q-labelled target control, and R1 reports trans-cleavage activity.

Back to the CRISPR/Cas12a activation mechanism, the Cas12a/crRNA complex first binds a PAM-containing dsDNA and locally opens the duplex to test complementarity between the crRNA and the target strand (TS)[192]. Sufficient pairing within the seed region allows R-loop formation and activates the RuvC domain for cleavage[71]. Based on our findings, we speculate that Cas12a may transiently destabilise short, non-cognate PAM-containing duplexes during target searching. Given that the mir-FQ is only 29 bp in length, even localised unwinding could increase the separation between the fluorophore and quencher strand to restore fluorescence. The Q strand may then be separated or displaced, while the F strand remains largely intact. However, the gel results do not distinguish between strand displacement, limited nicking and selective cleavage of the Q strand.

To determine the role of the PAM sequence in mediating the transient unwinding of non-cognate duplexes, PAM-deficient reporters (mir-FQ-noPAM and FQ-noPAM) were evaluated (Figure 5-12a). When the reporter had a PAM sequence (Lane 2), it released fluorescence, but the duplex band was still at the same position, suggesting that near-intact labelled material remained, although this observation alone could not distinguish partial duplex opening from limited or strand-selective cleavage. However, when we removed the PAM sequence (Lane 3), the intact duplex band almost completely disappeared, and a lot of small cut pieces (FQ cut) showed up at the bottom. We saw the same thing when using the non-fluorescent TS-NTS

target: the reporter with a PAM sequence resisted the cutting (Lane 4), while the reporters without a PAM sequence were completely chopped up (Lanes 5 and 6). These observations suggest that the presence of a PAM-containing sequence may influence how short, non-cognate dsDNA reporters are processed by activated Cas12a. One possible explanation is that PAM-associated interactions alter duplex accessibility or cleavage behaviour. However, the present experiments do not establish a direct protective effect of PAM binding or distinguish local duplex opening from strand-selective cleavage. These results reveal a previously underexplored relationship between PAM-dependent DNA interrogation and the fluorescence response of a non-cognate dsDNA reporter. Unlike PAM-deficient reporters, which were extensively degraded, PAM-containing reporters retained near-intact FAM-labelled products despite fluorescence recovery. This suggests that PAM-dependent interaction with Cas12a may promote local duplex destabilisation or strand-selective processing rather than complete degradation of both reporter strands. However, deleting the PAM region also changes reporter length and sequence, so these results do not isolate a protective effect of PAM binding.



Lanes	1	2	3	4	5	6	7	8	9	10	11
Universal crRNA	+						-				
Template	FQ	FQ	FQ	TS-NTS	TS-NTS	TS-NTS					
Reporter	FQ	FQ, mir-FQ	FQ, mir-FQ-noPam	mir-FQ	mir-FQ-noPam	FQ-noPam	mir-FQ	mir-FQ-noPam	FQ	FQ-noPam	TS-NTS

Figure 5-12: Comparison of PAM-containing and PAM-deficient dsDNA reporters (a) FAM-channel gel image showing fluorescent reporter and cleavage products. (b) Stained gel image showing total nucleic acid bands under the same conditions. Lanes 1–6 contain synthetic universal crRNA: lanes 1–3, FQ target with FQ, FQ/mir-FQ, or FQ/mir-FQ-noPAM reporters; lanes 4–6, TS-NTS target with mir-FQ, mir-FQ-noPAM, or FQ-noPAM reporters. Lanes 7–11 are no-crRNA controls containing mir-FQ, mir-FQ-noPAM, FQ, FQ-noPAM, or TS-NTS, respectively. noPAM indicates the corresponding sequence lacking the PAM region.

Overall, these experiments were carried out to understand why unrelated dsDNA probes

could produce fluorescence after Cas12a activation. The results showed that this behaviour was not limited to the self-transcribing crRNA system, but could also be observed in conventional Cas12a reactions. Gel analysis further suggested that fluorescence recovery from dsDNA reporters was not always associated with complete reporter degradation, but could also involve partial duplex opening or strand-selective processing. The PAM-dependent experiments indicated that PAM recognition may influence how Cas12a interacts with these non-cognate dsDNA substrates. Together, these findings show that fluorescence from short dsDNA reporters should not be interpreted solely as sequence-specific cis-cleavage, and that non-cognate dsDNA interactions may also contribute to the observed signal.

Contribution of DNA template and transcription-associated intermediates

Another potential limitation of this design is that the crRNA sequence is generated by adding ribonucleotides from the 3' end of the template, the transcribed crRNA is highly likely to remain hybridised to its template, forming a DNA–RNA hybrid rather than being fully released into solution. This could reduce crRNA activity because the handle region must fold into its characteristic secondary structure to support stable Cas12a–crRNA complex formation[193]. If the handle remains partially base-paired with the DNA template, its correct folding and subsequent loading into Cas12a may be restricted, potentially becoming a rate-limiting step in the reaction[194].

To test this hypothesis, the transcription products were treated with DNase I to digest the residual ssDNA template and release the crRNA from the crRNA-DNA chimera (Figure 5-13a). It was expected that removal of the DNA template would allow the crRNA handle to fold more efficiently and increase the amount of functional crRNA available for Cas12a activation. Initially, physical and chemical methods (heat and EDTA-heat) were evaluated to inactivate DNase I before introducing the CRISPR components. However, these methods failed to completely inactivate the nuclease. In the control groups (no Cas), we observed substantial background fluorescence, indicating that residual DNase I was digesting our DNA probes during the CRISPR step.

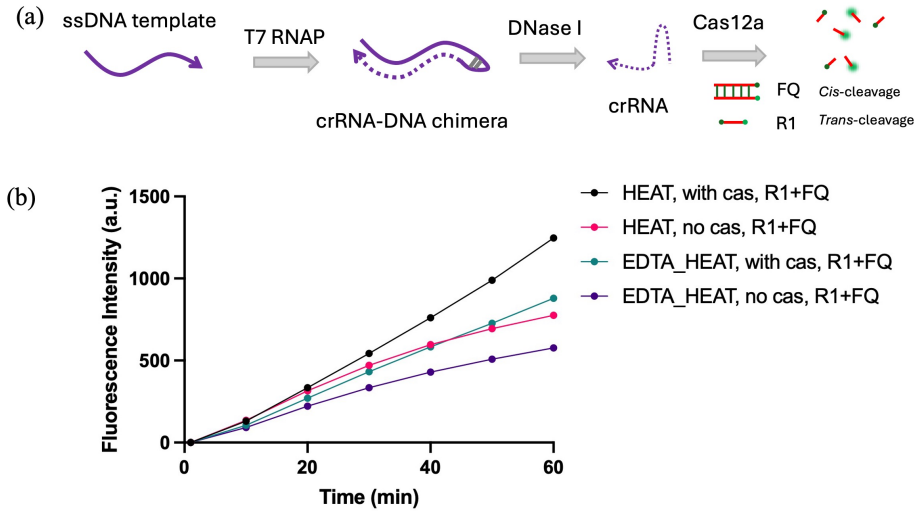


Figure 5-13: Evaluation of DNase I inactivation methods after crRNA transcription from ssDNA templates. (a) Schematic of DNase I-assisted crRNA preparation. After T7 RNAP transcription, DNase I was used to digest the DNA template, leaving crRNA for the subsequent Cas12a cleavage reaction with FQ and R1 reporters. (b) Comparison of different DNase I inactivation methods before Cas12a detection. DNase I was inactivated either by heat treatment alone or by EDTA followed by heat treatment, and reactions with or without Cas12a were included to evaluate background fluorescence. n=1.

To overcome this problem, column purification was subsequently introduced to physically remove DNase I and residual DNA fragments before the Cas12a reaction. After DNase I treatment and column purification, the fluorescence signal increased compared with the untreated sample (Figure 5-14a, b), suggesting that digestion of the DNA template improved crRNA release and activity. Importantly, column purification alone did not increase the signal and instead reduced it substantially (Figure 5-14c). The reduced signal after column purification alone may be caused by the loss of intact DNA–RNA hybrids or free crRNA during purification. The no-Cas12a controls remained near baseline after purification, confirming that the signal was mainly Cas12a-dependent (Figure 5-14d). Overall, DNase I treatment moderately improved crRNA activity, supporting the possibility that some crRNA remained associated with the DNA template. However, the improvement was limited and required additional digestion and purification steps. Therefore, this procedure was not included in the final assay workflow. The small differences among the FQ, R1, and FQ+R1 conditions suggest that fluorescence production was limited primarily by the amount of functional Cas12a–crRNA complex rather than reporter availability. The addition of a second reporter therefore did not produce a proportional increase in signal.

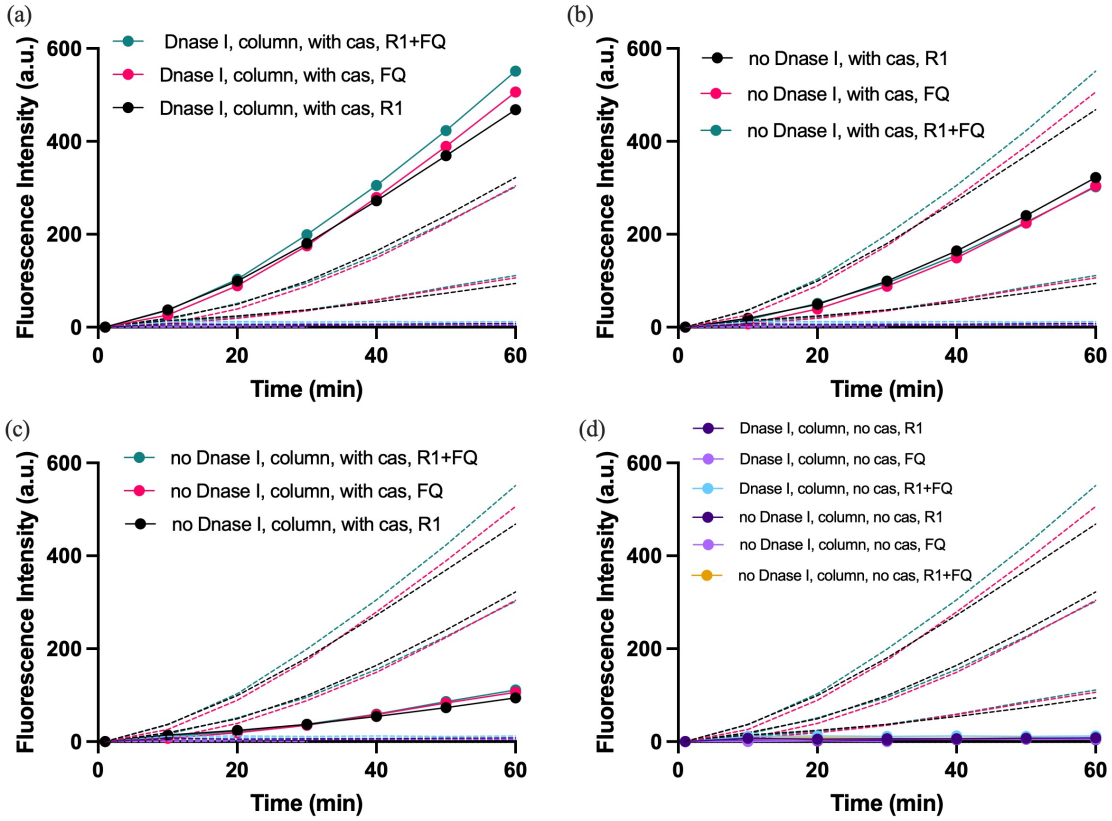
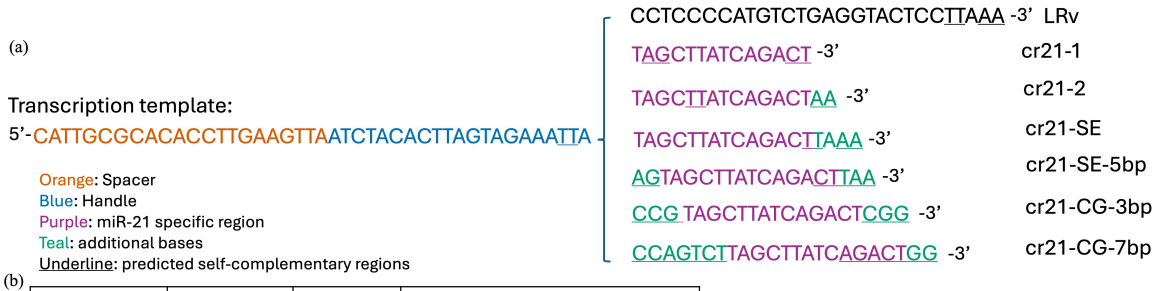


Figure 5-14: Evaluation of column purification after DNase I treatment. Fluorescence kinetics were measured under different DNase I, column purification, and Cas12a conditions.(a-c) Cas12a reactions using different reporter combinations after DNase I treatment and/or column purification.(d) No-Cas12a controls. Solid lines indicate the conditions highlighted in each panel legend, while dashed lines represent the other conditions from the same experiment for comparison. n=1.

5.3.3 Direct TMSD-gated STSR-CRISPR for miR-21 detection

To design ssDNA template facilitate both miR-21 recognition and self-transcription, several cr21 variant templates were designed. All templates contained the same 5' spacer, handle, and miR-21-specific region, but differed in the sequence added at the 3' end (Figure 5-15). These terminal sequences were introduced to test whether a short self-complementary domain could improve promoter-independent transcription. Greenwald et al. showed that T7 RNA polymerase could fold a 3′ end paired with an internal complementary region. They also observed greater consumption of GC-rich templates, suggesting that GC-rich complementary regions were more efficiently used in this reaction. Based on these findings, short complementary sequences with different lengths and GC contents were added to the 3′ end of the cr21 template. In comparison, cr21-CG-3bp showed a faster increase in fluorescence from the beginning of the reaction. Although cr21-SE-5bp and cr21-CG-7bp also contained manually added complementary sequences, both showed slower initial kinetics than cr21-CG-3bp. The

better performance of cr21-CG-3bp may result from its short GC-rich self-complementary region. At the same time, the 3 bp stem may remain sufficiently accessible for polymerase binding and extension. In contrast, the longer complementary regions in cr21-SE-5bp and cr21-CG-7bp may form more stable and compact structures. These structures may still support transcription and could potentially produce a greater amount of RNA, but the resulting transcripts may have different lengths or structures and may not function efficiently as crRNA. Therefore, the lower fluorescence of these templates may reflect reduced production of functional crRNA rather than reduced total RNA production. This remains a hypothesis and requires confirmation by sequencing the transcription products. All together, these results suggest that both the sequence and length of the self-complementary region affect the production of functional crRNA, and that increasing stem length alone does not necessarily improve the reaction.



(b)

Name	Self-priming stem (bp)	Additional bases (nt)	Design rationale
LRv	2		Soft end (TTAAA)
cr21-1	2	0	Minimal cr21 template
cr21-2	2	2	Adds a soft terminal end
cr21-SE	2	4	Mimic the 3' end of LRv
cr21-SE-5bp	5	5	Increases self-priming stem length
cr21-CG-3bp	3	3	Increases local terminal stability
cr21-CG-7bp	7	9	Strong GC/extended pairing

Figure 5-15: Design of LRv-based cr21 templates with different predicted self-priming strengths. (a) Sequence display of the parental LRv template and designed cr21 variants. (b) Summary of cr21 variants designed to tune 3′ self-priming stem length and self-folding efficiency.

The selected cr21-CG-3bp template was further compared with LRv and synthetic universal crRNA at different concentrations (Figure 5-16 b–d). At 10 nM, all three samples produced strong fluorescence signals. LRv showed a faster initial increase, while cr21-CG-3bp reached the highest fluorescence at the end of the reaction. The synthetic universal crRNA also produced a rapid signal increase but reached a plateau earlier. At 1 nM, all three samples remained active, although cr21-CG-3bp produced a slightly lower final signal than LRv and the universal crRNA. When the concentration was reduced to 0.1 nM, the universal crRNA produced the strongest signal, while both ssDNA templates showed weaker responses. These results confirmed that cr21-CG-3bp could be transcribed into a functional crRNA capa-

ble of activating Cas12a over a range of template concentrations. However, its performance was more affected at the lowest concentration, possibly because fewer template molecules were available to initiate transcription. It should also be noted that the ssDNA template and synthetic crRNA are not directly equivalent. In addition, one template molecule may generate more than one RNA transcript during the reaction. Therefore, the comparison mainly demonstrates the ability of cr21-CG-3bp to produce functional crRNA, rather than an equal activation efficiency at the same input concentration. Overall, these results supported the use of cr21-CG-3bp as the self-transcribing component for subsequent miR-21 sensing.

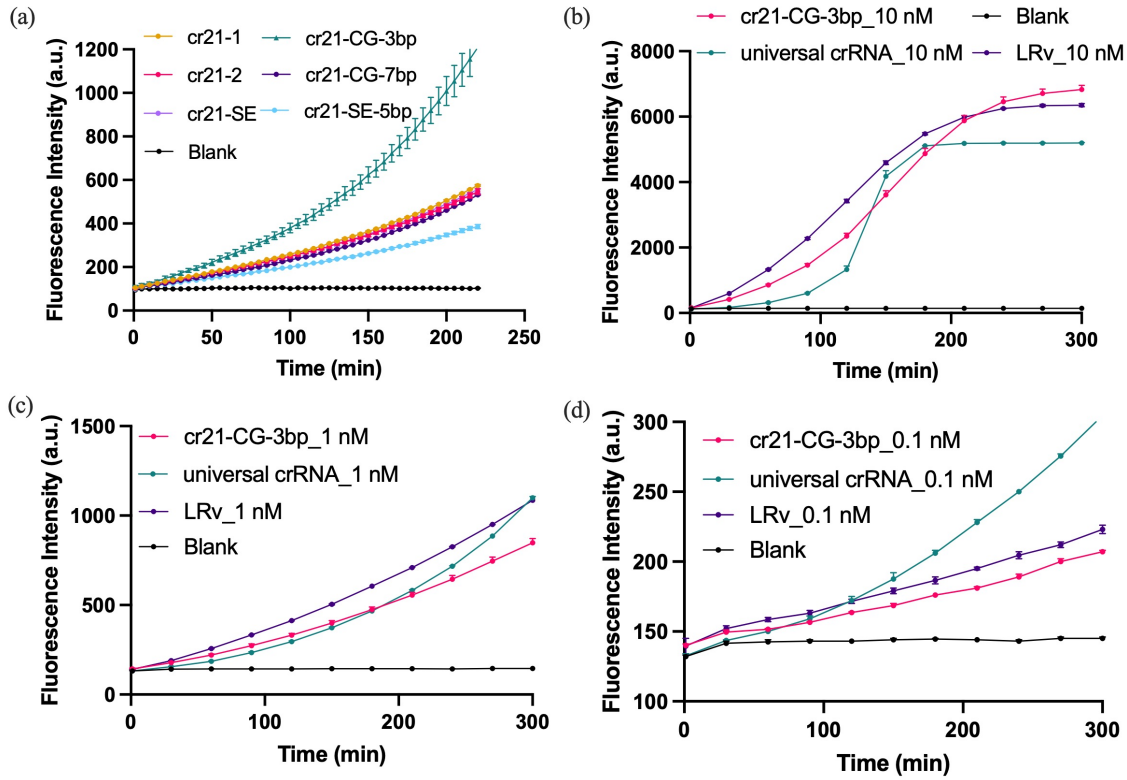


Figure 5-16: Validation of the screened cr21 template. (a) Fluorescence kinetics of different cr21 variants. cr21-CG-3bp showed the strongest signal and was selected for further validation. (b–d) Validation of the selected cr21-CG-3bp template by comparison with universal crRNA and LRv at 10 nM (b), 1 nM (c), and 0.1 nM (d). Fluorescence intensity was monitored over time to evaluate RNA-generation efficiency. Blank reactions were included as negative controls. Data represent the mean and range of two replicates.

A cap strand was designed to bind to the 3′ end of the cr21 template and block self-transcription in the absence of miR-21. When miR-21 was present, it was expected to bind to the cap through the toehold region and displace it from cr21. This would release the 3′ end of the template, allowing self-transcription and subsequent CRISPR/Cas12a activation. The strand-displacement process was first examined by native PAGE. The free cr21-1 and cr21-CG-3bp templates at around 70 nt in lanes 10 and 11. After hybridisation with the cap strands, slower-migrating bands appeared in lanes 5–8, indicating the formation of cr21–cap complexes. Af-

ter adding miR-21, additional faster-migrating bands were observed in lanes 1–4, together with an increase in bands close to the position of free cr21. These changes suggest that miR-21 interacted with the cap and promoted its displacement from the cr21 template. However, residual free-cr21 bands were still visible in some samples without miR-21, suggesting that the blocking efficiency of C1 and C2 was incomplete. In comparison, the CC3 probe showed a clearer shifted complex and less free cr21 before miR-21 addition, indicating more effective blocking of the cr21-CG-3bp template.

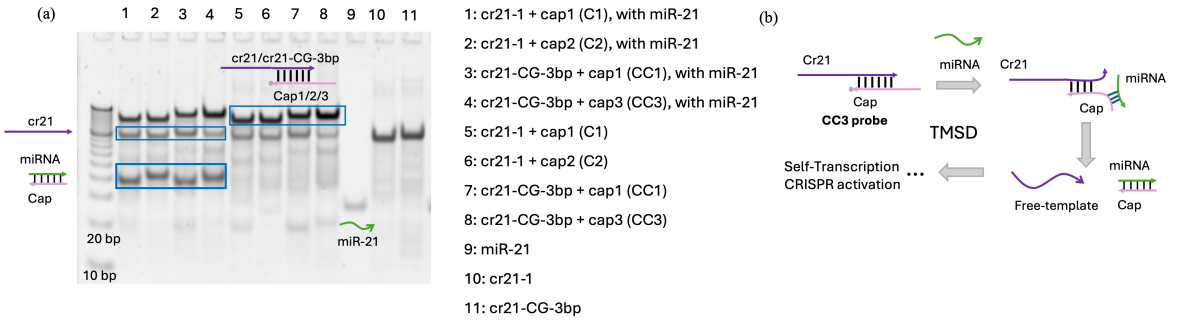


Figure 5-17: Validation of miR-21-mediated cap displacement from cr21 templates. (a) Native PAGE gel analysis of cr21/cap complexes in the presence or absence of miR-21. Lanes 1-4 show cr21-1 or cr21-CG-3bp complexed with different caps in the presence of miR-21; lanes 5–8 show the corresponding cr21/cap complexes without miR-21; lane 9 contains miR-21 alone; lanes 10–11 contain free cr21-1 and cr21-CG-3bp templates. (b) Schematic of miR-21-triggered toehold-mediated strand displacement (TMSD). miR-21 displaces the cap from the cr21 template to release the free template for downstream self-transcription and CRISPR activation.

For the selected cr21-CG-3bp template, cap1 and cap3 were compared for their ability to block the template and respond the miR-21. Cap3 contained an additional 3 bp sequence (CGG), which was expected to further stabilise the 3′ end of cr21-CG-3bp. In addition to the direct cr21–cap duplex, a three-strand probe containing the cr21 template, cap strand, and synthetic universal crRNA was also prepared (Figure 5-18b). This design was expected to form a more compact structure and reduce background transcription in the absence of miR-21[195]. It was further hypothesised that, after miR-21 displaced the cap, transcription of the released cr21 template could disrupt the remaining base-pairing interactions and promote release of the universal crRNA. This proposed mechanism was based on the strand-displacement-like behaviour associated with T7 RNA polymerase-mediated extension reported by Greenwald et al.

As shown in Figure 5-18c, CC1 and CC1U showed only small differences between the positive control (PC) and negative control (NC), indicating incomplete blocking and relatively high background leakage. In comparison, CC3 and CC3U showed lower NC signals, suggesting that the additional 3 bp sequence in cap3 improved the stability of the blocked structure. The CC3U triplex produced the lowest background signal, supporting the idea that the

three-strand structure provided stronger inhibition of the template. However, the PC signal of CC3U was not higher than that of CC3, as initially expected. This suggests that the universal crRNA mainly helped to stabilise the blocked complex rather than providing additional signal enhancement. Based on the clearer separation between the PC and NC groups, the CC3 probe was selected for further miR-21 detection. As shown in Figure 5-18d, both 6.6 nM and 66 pM miR-21 produced higher fluorescence signals than the NTC under the tested conditions. These results provide preliminary evidence of a response to picomolar miR-21, although additional concentrations and independent experiments are required to establish the analytical detection limit and concentration-dependent performance.

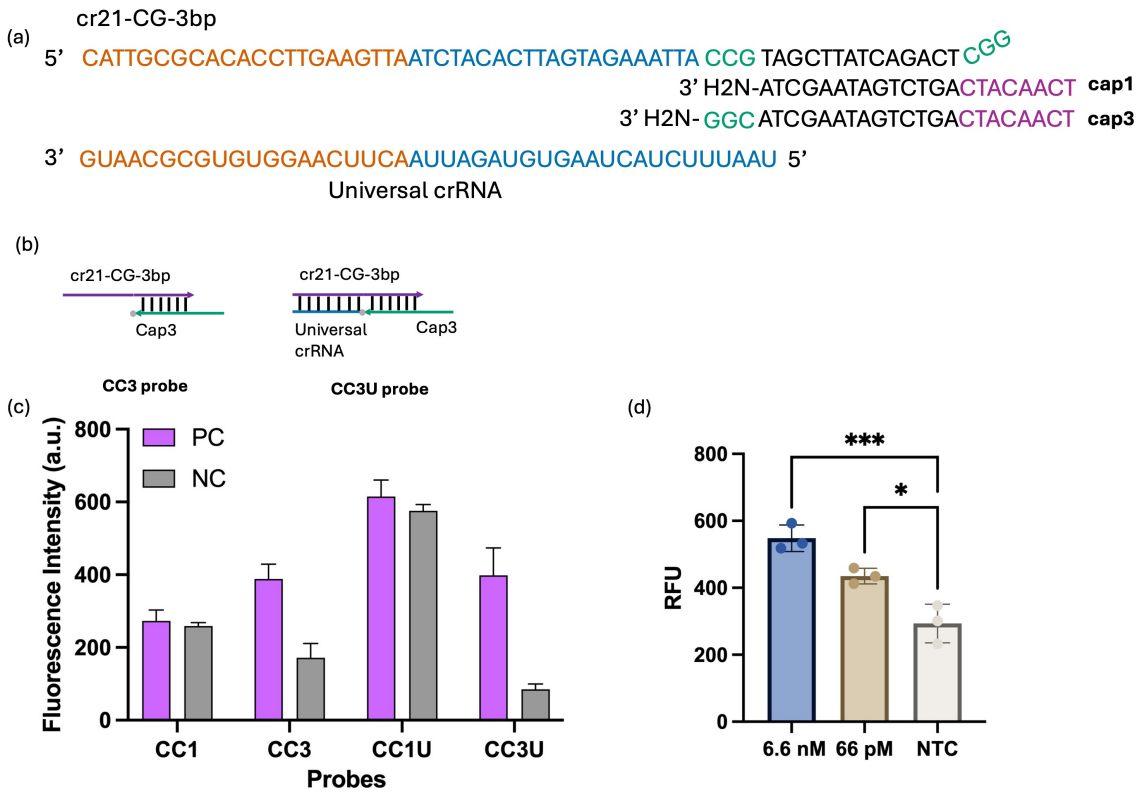


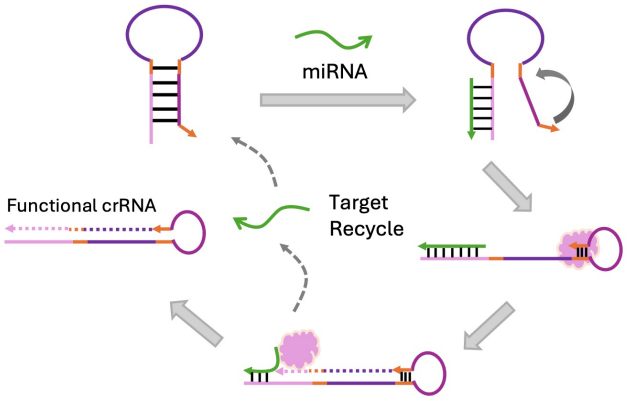
Figure 5-18: Probe screening and miR-21 detection using cr21-CG-3bp. (a) Sequence design of cr21-CG-3bp, universal crRNA, and cap1/cap3. (b) Schematic representation of the CC3 and CC3U probe designs. (c) Fluorescence intensities of CC1, CC3, CC1U, and CC3U probes using cr21-CG-3bp. PC represents reactions with 1 nM miR-21 target, and NC represents reactions without miR-21 target. (d) Fluorescence response of the CC3 probe to miR-21 at 6.6 nM and 66 pM, with NTC as the no-template control. Data are presented as mean ± SD (n = 3). Statistical significance was determined using an unpaired two-tailed Student's t-test between the indicated groups. *P < 0.05; ****P < 0.0001.

5.3.4 Dragon hairpin-mediated target recycling for enhanced miR-21 detection

A second strategy using a dragon hairpin (DH) was designed to achieve miR-21 recycling and improve signal generation. (Figure 5-19a) In the presence of miR-21, the target was expected to bind to the toehold region at the 5′ end of the DH probe and open the hairpin through toehold-mediated strand displacement. Opening the hairpin would expose the 3′ end of the template, allowing it to fold back and initiate self-transcription. During transcription, extension along the DH template was expected to disrupt the miR-21–DH duplex and release miR-21. The released miR-21 could then bind to another DH probe and start a new reaction cycle. In this way, one miR-21 molecule could potentially activate multiple templates and increase the production of functional crRNA.

Because the stability of the hairpin may affect both target-mediated opening and background transcription, DH probes with different stem lengths were designed and compared (Figure 5-19b). Increasing the stem length produced a more stable hairpin, as indicated by the more negative predicted free-energy values. However, an overly stable stem could make the hairpin more difficult for miR-21 to open. Therefore, the DH designs were selected to provide different balances between structural stability and target accessibility.

(a)



(b) Table 1. Structural and thermodynamic characterization of DNA hairpins

No.	Stem (bp)	Hairpin ΔG (kal/mol)	Hybridization with mir21
DH_12	12	-12.71	99.9%
DH_14	14	-13.48	99.2%
DH_15	15	-15.75	97.5%
DH_16	16	-18.42	82.2%

Figure 5-19: Target recycling-enhanced TMSD strategy and structural characterisation of DH probes. (a) Schematic illustration of miRNA-triggered target recycling of the STSR-CRISPR system. (b) Predicted secondary structure of the DH probe generated by NUPACK.

The opening of the different dragon hairpin probes by miR-21 was first examined using native PAGE (Figure 5-20a). For each DH design, the hairpin probe alone and the probe incubated with miR-21 showed different migration patterns. The appearance of additional slower-migrating bands after miR-21 addition suggested the formation of miR-21–DH complexes and partial opening of the hairpin structures. However, multiple bands were observed for some designs, indicating that more than one folded or hybridised structure may have been present.

The four DH probes were then compared in the self-transcription–CRISPR assay using 10 nM and 1 nM miR-21 (Figure 5-20b). DH_15 produced the highest fluorescence at both target concentrations, but it also showed a relatively high NTC signal, suggesting considerable background transcription in the absence of miR-21. DH_14 showed little difference between the target and NTC groups, indicating poor target-dependent activation. DH_16 gave a lower NTC signal, but its target signals were also relatively weak. In comparison, DH_12 showed a clear increase in fluorescence in the presence of miR-21 while maintaining a lower background signal.

These results show that increasing the stem length did not continuously improve the performance of the DH probe. A longer and more stable stem may reduce background opening, but it may also make target-mediated hairpin opening more difficult. In contrast, a less stable hairpin may be easier to open but may also undergo spontaneous self-transcription. Therefore, the performance of the DH probe depended on the balance between background suppression and accessibility to miR-21.

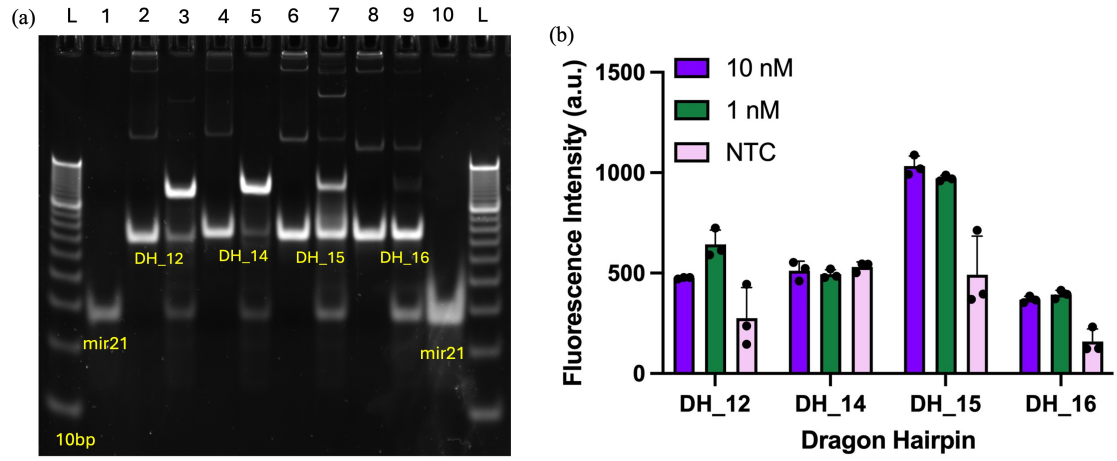


Figure 5-20: Evaluation of dragon hairpin designs for miR-21-responsive template release.(a) Native PAGE gel analysis of different dragon hairpin constructs in the presence of miR-21. DH_12, DH_14, DH_15, and DH_16 indicate different dragon hairpin designs, and miR-21-only controls are included. (b) Fluorescence comparison of DH_12, DH_14, DH_15, and DH_16 at 10 nM and 1 nM target concentrations. NTC reactions were included as negative controls. Data are shown as mean ± SD, n=3.

The DH assay was further tested using a range of miR-21 concentrations. (Figure 5-21) Although DH_12 provided a clearer target-to-background separation, DH_15 produced the highest absolute fluorescence at both target concentrations. DH_15 was therefore selected for the subsequent experiments. Higher fluorescence signals were generally observed in the presence of miR-21 than in the NTC, although considerable variation was seen between independent transcription reactions. Signals remained above the NTC at several low target concentrations, including the femtomolar range. However, the response was not strictly concentration-dependent, and some overlap was observed between concentrations. Although the technical replicates from the same transcription reaction showed similar fluorescence signals, considerable variation was observed between independent transcription reactions. This suggests that the main source of variation occurred during the transcription step rather than during the downstream CRISPR measurement. The signals from different transcription batches also appeared to separate into relatively high- and low-signal groups. One possible explanation is that two different reaction states were present in the system. For example, the DH template may form either a transcription-active structure that generates functional crRNA or an alternative structure that produces little or non-functional RNA. However, this remains a hypothesis, and further analysis of the transcription products would be required to determine whether different RNA products or reaction pathways were present. These results suggest that the DH design can respond to low concentrations of miR-21, but further optimisation and additional independent experiments are required to define the analytical detection limit.

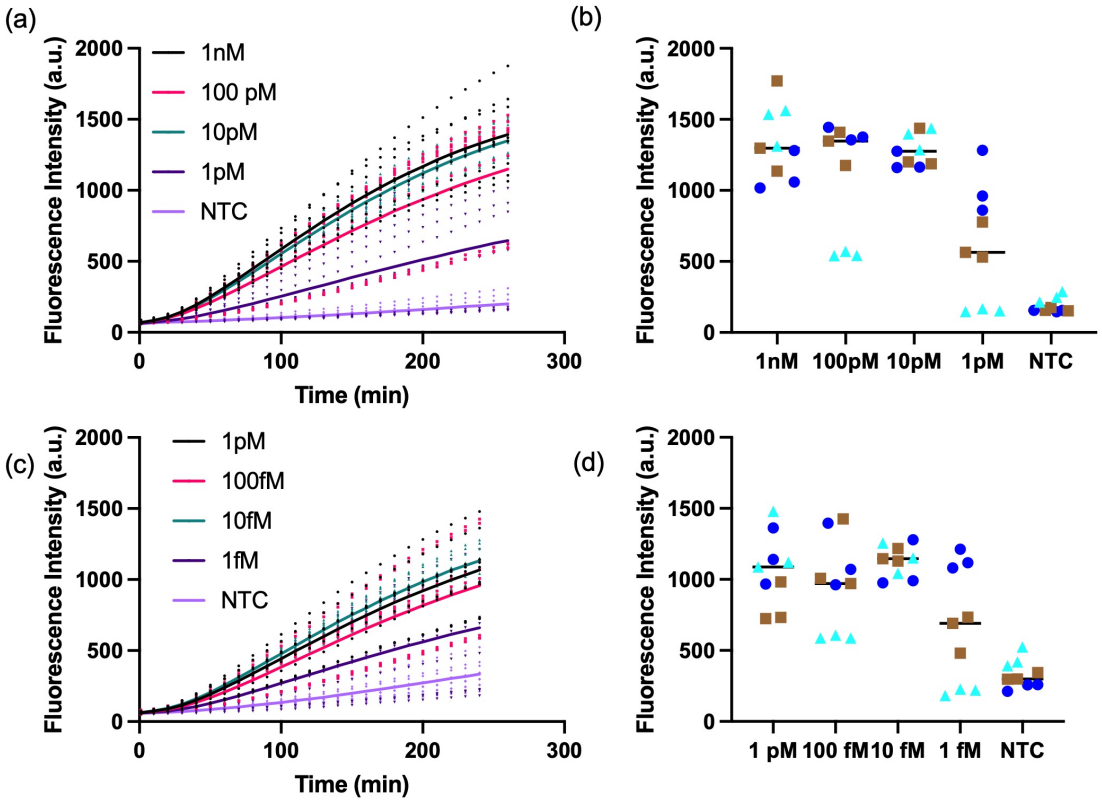


Figure 5-21: Sensitivity evaluation of the dragon hairpin-based miR-21 detection system. (a) Fluorescence kinetics of miR-21 detection from 1 nM to 1 pM. (b) Endpoint fluorescence comparison of the corresponding miR-21 concentrations in (a). (c) Fluorescence kinetics of low-concentration miR-21 detection from 1 pM to 1 fM. (d) Endpoint fluorescence comparison of the corresponding miR-21 concentrations in (c). NTC reactions served as negative controls. R1 probe was used at 500 nM. Each condition contains nine data points, with three same-colour points representing technical replicates from the same transcription product.

Compared with previously reported miRNA detection methods, the analytical performance of STSR-CRISPR remains preliminary. For example, Peng et al. reported a detection limit of 0.07 fM for miR-21 using a CRISPR-CHA system[181], while Yan et al. demonstrated single-digit femtomolar miRNA detection using a one-pot RCA–Cas12a assay[126]. Li et al. developed a polymerase strand recycling (PSR) system that uses non-canonical T7 RNA polymerase activity for signal amplification, achieving detection limits of 5–100 nM for three miRNA targets.[173]. Unlike their system, which uses transcription to recycle DNA strands in strand displacement circuits, STSR-CRISPR uses promoter-independent RNA generation from designed ssDNA templates to support Cas12a activation. Although fluorescence responses were observed at low miR-21 concentrations in the present study, considerable variation between independent transcription reactions prevented the establishment of a reliable detection limit. The main contribution of this work therefore lies in demonstrating the feasibility of coupling promoter-independent RNA generation with Cas12a activation, rather than achieving superior analytical sensitivity at this stage.

5.3.5 Bioanalyzer and RNA-seq

Although previous studies have provided evidence that in vitro transcription (IVT) products can activate the CRISPR system, the composition of these RNA transcripts remains unclear. In particular, evaluation of the LRv-based cr21 templates showed that the resulting fluorescence signal was highly dependent on template sequence composition, suggesting that different templates may generate distinct transcription products. Therefore, to better characterise the IVT products and further investigate promoter-independent transcription behaviour, Bioanalyzer analysis was used to examine the size distribution of the RNA products with improved separation and resolution, while RNA sequencing was performed to determine their sequence composition, length distribution, and relative abundance.

The Agilent 2100 Bioanalyzer uses a microfluidic electrophoresis system to separate nucleic acid samples based on their size[196]. The samples move through small channels filled with a gel-dye mixture, where smaller RNA fragments move faster than larger fragments. As the RNA fragments pass through the detection area, their fluorescence signals are recorded. The migration time of each RNA fragment is compared with the ladder and internal markers to estimate its size. The results are presented as an electropherogram, showing the fluorescence intensity against the estimated RNA length[197]. This method allows rapid analysis of RNA samples using a small sample volume and has previously been used to analyse in vitro transcription products[198]. In this study, Bioanalyzer analysis was used to examine the size and distribution of the RNA products generated by the promoter-independent transcription. This provided an initial view of the different RNA products generated from each template before further analysis by RNA sequencing. Three samples was performed including LRv, cr21-2, and cr21-CG-3bp.

The electropherograms showed the RNA product profiles generated by in vitro transcription. (Figure 5-22) All templates generated heterogeneous populations of small RNA fragments rather than a single full-length RNA transcript. The sharp peaks on the left were considered to represent the markers. Among these, LRv generated a broader distribution of RNA products, while cr21-2 and cr21-CG-3bp showed more distinct peaks, indicating that their transcripts were more enriched within particular length ranges. These differences suggest that template sequence composition may influence the size distribution of the transcription products. Meanwhile, the IVT products were tested for CRISPR-Cas12a activation using FQ as the reporter. LRv generally produced the highest fluorescence signal, followed by cr21-CG-3bp and cr21-2. Interestingly, this trend did not correspond to the total RNA concentrations measured by the Bioanalyzer, as cr21-CG-3bp (615 pg/µL) and cr21-2 (383 pg/µL) produced higher total RNA concentrations than LRv (348 pg/µL). This suggests that the total amount of RNA generated was not directly related to CRISPR activation. Although LRv produced less total RNA, its transcription products may have been functionally capable of forming active

crRNA-Cas12a complexes.

However, the Bioanalyzer results alone could not fully explain the differences in CRISPR activity among the three templates. Although the analysis provided information on the overall RNA yield and rough size distribution, it could not determine the sequence identity of the individual RNA products. In particular, a higher total RNA signal did not necessarily result in stronger CRISPR activation. Especially the broad RNA distribution observed for LRv suggested the presence of multiple RNA products of different lengths, but it remained unclear which of these products contained a complete or partial crRNA sequence and which could activate the Cas12a. Therefore, the functional activity of the transcription products may depend not only on the total amount of RNA generated, but also on their sequence composition and relative abundance. To further investigate this, RNA sequencing was performed to identify the major transcription products generated from each template and to determine their sequences, lengths, and relative abundance.

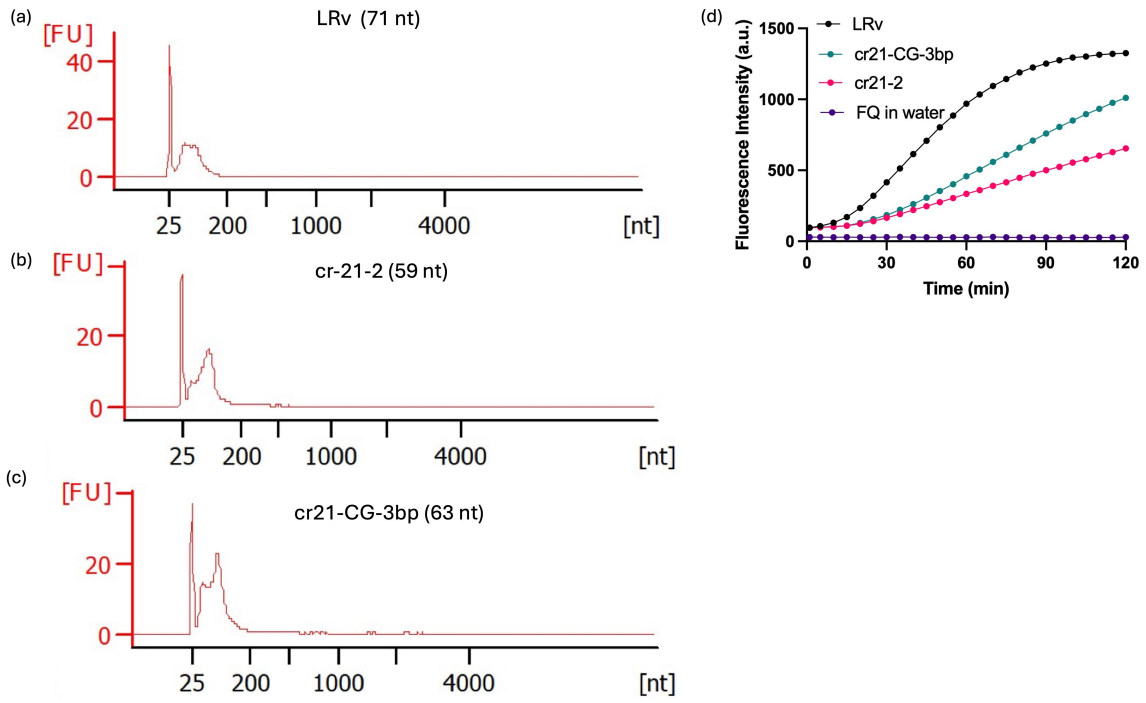


Figure 5-22: Characterisation of RNA products generated by promoter-independent transcription and their CRISPR activity. Bioanalyzer electropherograms of RNA products generated from (a) LRv, (b) cr21-2, and (c) cr21-CG-3bp templates. The LRv, cr21-2, and cr21-CG-3bp DNA templates were 71, 59, and 63 nt long, respectively. (d) CRISPR fluorescence generated by the corresponding transcription products using FQ as the reporter. FQ in water was included as the negative control. n=1.

RNA sequencing was performed by the MVLS Shared Research Facilities using an Illumina NextSeq 2000 platform, with a sequencing depth of ≥0.1 million reads per sample. The top 10 most abundant RNA products were extracted and aligned to the template sequence. For better visualisation and comparison, the sequences shown in the figure are presented as the

reverse complements of the original sequencing reads.

Based on the designed functional crRNA sequence, the RNA products can be divided into three categories: A, products containing the complete crRNA region (handle + spacer), positions 1–43; B, products containing an intact handle region, positions 23–43; and N, products containing neither the complete 1–43 crRNA region nor an intact 23–43 handle region. The designed crRNA consists of two functional components: a spacer region at positions 1–22 and a handle region at positions 23–43. In the canonical Cas12a–crRNA system, the handle mediates crRNA association with Cas12a, whereas the spacer for target recognition and subsequent activation of Cas12a trans-cleavage activity. However, in our previous observation, the fluorescence still showed up when only the handle-encoding template existed. This suggested that RNA products generated from handle-encoding templates may support Cas12a activation, although the specific active RNA species were not identified (Figure 5-7b, 5-8b). Therefore, in addition to investigating the full-length crRNA (position 1-43) products, particular attention was given to the complete handle region (position 23-43) in the subsequent analysis.

Among reads aligned to the corresponding DNA template, identical RNA sequences were grouped and ranked according to their read counts. The ten most abundant aligned RNA products for each template are presented in Figures 5-23, 5-24, 5-25. For the sample LRv, the ten most abundant products among the aligned reads varied in length, ranging from 17 to 66 nt; 4/10 contain the full-length crRNA, accounting for 3.82% of the trimmed reads. 9/10 contain the complete handle region, representing 7.43% of the total trimmed reads. The most abundant product, P1, is not related to the crRNA region. Notably, the complete functional crRNA sequence was predominantly present as part of longer transcripts rather than as a precisely 43-nt RNA product. This indicates that functional crRNA sequences could be generated despite imprecise transcription initiation and/or termination. This also provides a possible explanation for the CRISPR activity observed with the transcription products, suggesting that Cas12a may tolerate additional sequences at the 5′ and/or 3′ ends of the crRNA while retaining its activity. In fact, extended crRNA has previously been shown to retain Cas12a activity, and certain 3’ ssDNA or RNA extensions can even enhance LbCas12a-mediated trans-cleavage. It has also been shown that 5’-extended crRNA retains trans-cleavage activity[199]. However, this tolerance is dependent on the length of the extension, with certain extensions enhancing Cas12a activity whereas others may reduce it. Therefore, it can only be inferred that the additional sequences observed in these RNA products do not necessarily prevent them from supporting CRISPR activity.

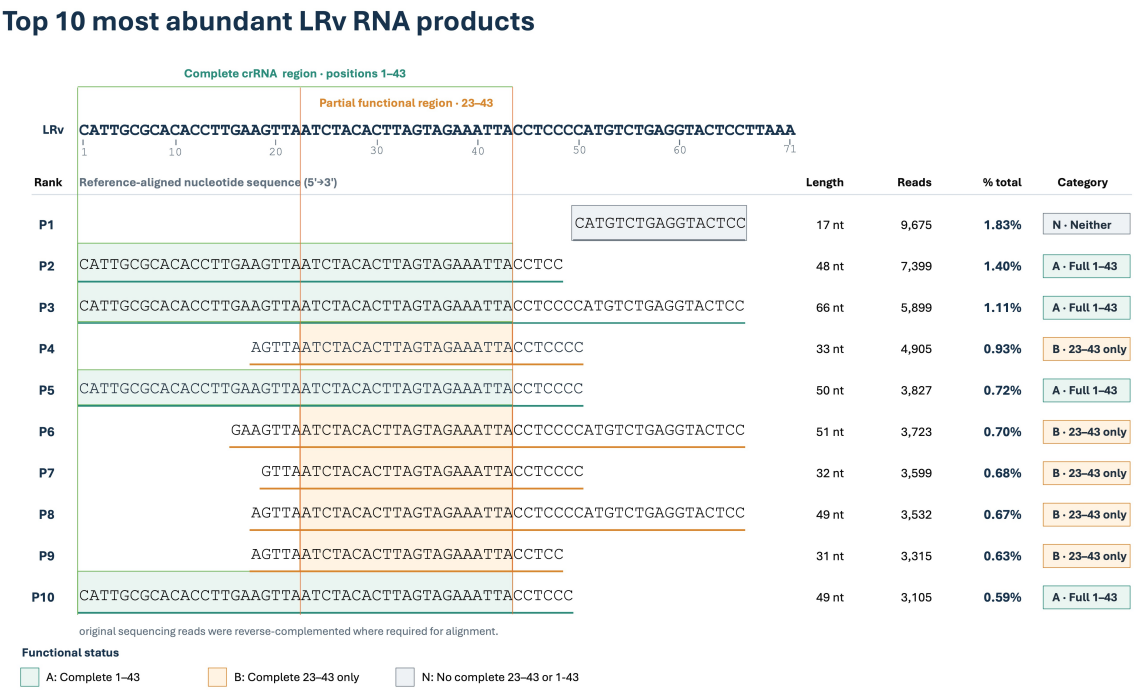


Figure 5-23: Top 10 most abundant RNA products generated from the LRv template. Identical sequencing reads aligned to the LRv template were grouped and ranked by read count. Sequences are shown in the reference-aligned orientation. The complete crRNA region (positions 1–43) consists of the spacer region (positions 1–22) and handle region (positions 23–43). Products were classified according to the presence of the complete crRNA region (A), complete handle region only (B), or neither complete region (N). Percentages indicate the proportion of each product among total sequencing reads.

For the cr21-2 template (Figure 5-24), only P9 contains the full-length crRNA among the top 10 products, accounting for 0.88% of the total trimmed reads. In contrast, most highly abundant products were truncated within the shared crRNA region, with P1–P8 starting in the middle of the handle region. The most abundant product, P1, accounted for 3.91% of the total reads but contained only positions 1–37 of the crRNA.

Top 10 most abundant cr21-2 RNA products

Complete crRNA-related region · positions 1–43

Shorter functional region · 23–43

cr21-2 CATTGCGCACACCTTGAAGTTAATCTACACTTAGTAGAAATTATAGCTTATCAGACTAA

1 10 20 30 40 50 59

Rank	Reference-aligned nucleotide sequence (5'→3')	Length	Reads	% total	Span
P1	CATTGCGCACACCTTGAAGTTAATCTACACTTAGTAG	37 nt	304,380	3.91%	1–37
P2	GCGCACACCTTGAAGTTAATCTACACTTAGTAG	33 nt	189,307	2.43%	5–37
P3	CATTGCGCACACCTTGAAGTTAATCTAC	28 nt	171,374	2.20%	1–28
P4	GCGCACACCTTGAAGTTAATCTAC	24 nt	119,751	1.54%	5–28
P5	CATTGCGCACACCTTGAAGTTAATCT	26 nt	100,009	1.28%	1–26
P6	CATTGCGCACACCTTGAAGTTAATC	25 nt	90,065	1.16%	1–25
P7	GCGCACACCTTGAAGTTAATCT	22 nt	80,837	1.04%	5–26
P8	GCATTGCGCACACCTTGAAGTTAATCTACACTTAGTAG	38 nt	78,547	1.01%	1–37
P9	CATTGCGCACACCTTGAAGTTAATCTACACTTAGTAGAAATTATAGCTTATCAGAC	56 nt	68,551	0.88%	A · Full 1–43
P10	GCGCACACCTTGAAGTTAATC	21 nt	62,195	0.80%	5–25

Figure 5-24: Top 10 most abundant RNA products generated from the cr21-2 template.

For cr21-CG-3bp (Figure 5-25), 7/10 products contained the complete 1–43 crRNA sequence, accounting for 9.66% of the total sequencing reads. One additional product (P7) contained the complete handle region. Notably, the most abundant product, P1, was 44 nt long and contained the complete crRNA sequence, only 1 nt longer than the designed 43-nt crRNA. The other complete crRNA products varied in length from 45 to 76 nt, again showing that the crRNA sequence could be present within longer transcripts.

Top 10 most abundant cr21-CG-3bp RNA products

Complete crRNA-related region · positions 1–43

Shorter functional region · 23–43

cr21-CG-3bp CATTGCGCACACCTTGAAGTTAATCTACACTTAGTAGAAATTACCGTAGCTTATCAGACTCGG

1 10 20 30 40 50 60 63

Rank	Reference-aligned nucleotide sequence (5'→3')	Length	Reads	% total	Category
P1	CATTGCGCACACCTTGAAGTTAATCTACACTTAGTAGAAATTAC	44 nt	160,510	2.06%	A · Full 1–43
P2	CATTGCGCACACCTTGAAGTTAATCTACACTTAGTAGAAATTACCGTAGCTTATCAGACTC	61 nt	145,121	1.87%	A · Full 1–43
P3	CATTGCGCACACCTTGAAGTTAATCTACACTTAGTAGAAATTACCGTAGCTTATCAGACT	60 nt	132,351	1.70%	A · Full 1–43
P4	CATTGCGCACACCTTGAAGTTAATCTACACTTAGTAGAAATTACC	45 nt	110,547	1.42%	A · Full 1–43
P5	CATTGCGCACACCTTGAAGTTAATCTACACTTAGTAGAAATTACCGTAGC	50 nt	82,512	1.06%	A · Full 1–43
P6	CATTGCGCACACCTTGAAGTTAATCTAC	28 nt	76,357	0.98%	1–28
P7	GCGCACACCTTGAAGTTAATCTACACTTAGTAGAAATTAC	40 nt	72,282	0.93%	B · 23–43 only
P8	CATTGCGCACACCTTGAAGTTAATCT	26 nt	63,842	0.82%	1–26
P9	CATTGCGCACACCTTGAAGTTAATCTACACTTAGTAGAAATTACCGTAGCTTATCAGACTCGGCATTGCGC	71 nt	62,095	0.80%	A · Full 1–43
P10	CATTGCGCACACCTTGAAGTTAATCTACACTTAGTAGAAATTACCGTAGCTTATCAGACTCGGCATTGCGCACACC	76 nt	58,187	0.75%	A · Full 1–43

original sequencing reads were reverse-complemented where required for alignment.

Figure 5-25: Top 10 most abundant RNA products generated from the cr21-CG-3bp template.

Despite the three templates sharing the identical 1–43 crRNA sequence, the sequence dis-

tribution of the main products is quite different. This suggests that sequences or structural features outside the shared crRNA region may influence the distribution and completeness of the generated RNA products. Potential priming sites based on 3′-end sequence complementarity are shown in Figure 5-26. Only potential priming sites located outside the crRNA region (green box) were considered relevant, as priming within this region would not generate crRNA-related sequence.

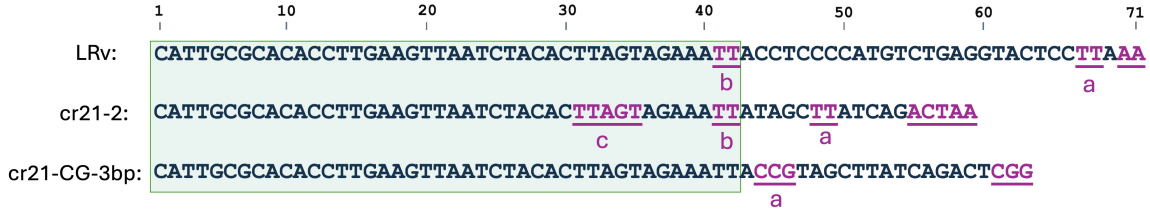


Figure 5-26: Comparison of the three ssDNA template sequences and their predicted priming sites for promoter-independent RNA extension. The shared crRNA region (positions 1–43) is shown for LRv, cr21-2, and cr21-CG-3bp. Potential priming sites (a–c) were predicted based on complementarity between the 3′-terminal sequence and internal regions of each template. The predicted sites were used to compare potential priming positions with the RNA product patterns observed by sequencing; however, these sites were not directly confirmed by the current sequencing analysis.

For LRv, the 3′ end terminates in AA; therefore, internal TT motifs were considered potential complementary priming sites. Two such sites were identified: site a, located close to the 3′ end of the template, and site b, located near the beginning of the crRNA handle region. Interestingly, the most abundant aligned LRv product, P1 (Figure 5-23), had a boundary immediately following site a. The same boundary was also observed for P3, P6, and P8, suggesting that site a may be associated with several abundant RNA products. In contrast, P2, P4, P7, P9, and P10 shared a second boundary around positions 49–50. This position did not correspond to the predicted site b, indicating that the observed product boundaries cannot be fully explained by the predicted 3′-end priming sites alone. The second group of products also did not contain the sequence before the boundary at positions 49–50. Therefore, they are unlikely to be produced simply by further extension of a P1-like product. If P1 was generated first and then further extended, the sequence already present in P1 should still remain in the longer product rather than disappear. These products may therefore be generated through a different priming or initiation event that was not predicted from the simple 3′-end complementarity. Interestingly, the first synthesised nucleotide at these secondary boundaries was always cytosine. This repeated occurrence of C suggests that the local sequence around these positions may also influence where the RNA products are generated. However, the alignment boundary cannot be directly interpreted as the original transcription initiation or priming position. RNA sequencing library preparation involves multiple processing steps, including adaptor ligation and subsequent adaptor trimming during data processing, which

may affect the recovered reads. Therefore, although the correspondence between P1 and the predicted site a is notable, the sequencing data alone do not provide sufficient evidence to identify site a as the actual transcription priming site.

cr21-2 has three predicted sites from the 3' end terminal. In addition to the two shorter TT-containing sites (sites a and b), a longer complementary sequence, TTAGT, was identified as site c. However, site c is located within the 1–43 crRNA region. Priming from this internal site maybe unlikely to produce complete crRNA sequence. Interestingly, most of the abundant cr21-2 products started from positions within the crRNA region. (Figure 5-24) This may be related to the additional internal site c, and could partly explain why many incomplete crRNA products were observed for cr21-2. However, the observed starting positions did not all exactly match the predicted site c. In addition, the sequencing data only show the final RNA products and cannot directly confirm the original priming position.

For cr21-CG-3bp, the predicted site was located outside the 1–43 crRNA region. 7/10 products contained the complete 1–43 crRNA sequence. This may partly explain why complete crRNA products were more frequently observed for cr21-CG-3bp than for cr21-2. However, P9 and P10 were 71 and 76 nt long, respectively, which were longer than the 63 nt original cr21-CG-3bp template. (Figure 5-27) In both products, the additional sequence following position 63 corresponded precisely to the sequence beginning at position 1 of the template, producing an apparent end-to-start junction. This is different from the observation reported in the DragonRNA study, where only 3' multiple extension was observed, suggesting that some other non-canonical extension might have happened in our system. However, the sequencing data cannot distinguish whether this extension occurs through intramolecular fold-back priming or intermolecular priming between different molecules.



Figure 5-27: AgniAlign sequence analysis of cr21-CG-3bp IVT products. P1, P9 and P10 were aligned to the original 63 nt cr21-CG-3bp template for visualisation. P9 and P10 were 71 and 76 nt long, and therefore extended beyond the expected sequence length. In both products, the sequence following the expected template boundary corresponded to the 5′ region of the cr21-CG-3bp template, forming an apparent end-to-start junction. Blue rectangles represent the input DNA template in the reference orientation, while red rectangles represent the corresponding antisense-oriented sequence used by AgniAlign for alignment. Red circles indicate RNA product nucleotides.

Overall, the three templates generated highly heterogeneous RNA products despite containing the same 1–43 crRNA sequence. Their product distributions were clearly different, with cr21-CG-3bp showing the highest representation of complete crRNA-containing products, while cr21-2 mainly generated incomplete products. LRv produced a mixture of complete crRNA- and handle-containing products. Notably, the designed 3-bp CGG terminal sequence in cr21-CG-3bp resulted in a higher proportion of complete crRNA-containing products than the original AA-ended cr21-2 template, suggesting that designed 3′-end complementarity may favour the generation of complete crRNA products. In contrast, the long internal priming site c in cr21-2 may contribute to the generation of incomplete crRNA products.

The observed product boundaries could only be partly explained by the predicted priming sites, and some longer products also suggested additional extension events. Together, these results indicate that sequences outside the crRNA region can strongly influence the RNA products generated during promoter-independent transcription.

The complete transcription of crRNA is highly related to Cas12a activation. Table 5-2 summarises the detailed results of the RNA abundance. Similar numbers of total reads were obtained for cr21-2 and cr21-CG-3bp, while LRv had a lower sequencing depth. The top 10 most abundant products accounted for 9.24%, 16.23% and 12.39% of the total reads for LRv, cr21-2 and cr21-CG-3bp, respectively, indicating that a large number of other less abundant RNA products were also present in all three samples. When all reads were considered, cr21-CG-3bp showed the highest product proportion with the complete 1-43 crRNA region (32.59%), compared with 17.71% for LRv and 12.97% for cr21-2. The proportion of reads containing the complete 23–43 handle region was similar for LRv (61.28%) and cr21-CG-3bp (60.83%), but lower for cr21-2 (30.40%). LRv had the highest proportion of handle-only products (43.57%), whereas this proportion decreased to 28.25% for cr21-CG-3bp and 17.43% for cr21-2.

Table 5-2: Summary of sequencing results for the three RNA products.

Metric	**LRv**	**cr21-2**	**cr21-CG-3bp**
Total reads	529,791	7,792,480	7,777,430
Top 10 cumulative	9.24%	16.23%	12.39%
Complete 1–43 (Handle + Spacer)	17.71%	12.97%	32.59%
Complete 23–43 total (Handle)	61.28%	30.40%	60.83%
23–43 only (Handle)	43.57%	17.43%	28.25%

In Figure 5-22d, we noticed that the fluorescence was in the order of LRv > cr21-CG-3bp > cr21-2. This trend was not fully consistent with the proportion of complete 1-43 crRNA products, which is cr21-CG-3bp > LRv > cr21-2. (Table 5-2) Therefore, the amount of com-

plete crRNA alone may not fully determine the observed CRISPR activity. Previous studies have shown that Cas12a activity is affected by spacer length, sequence and crRNA structure, and that truncated crRNAs can retain trans-cleavage activity even when only part of the spacer is present[200]. Interestingly, LRv and cr21-CG-3bp showed similar proportions of products containing the complete handle region (61.28% and 60.83%, respectively), while LRv contained a much higher proportion of handle-only products (43.57% versus 28.25%).

Beyond that, it is also interesting to see how much of the spacer sequence was retained in these complete-handle products. Therefore, the intact-handle products were further grouped according to the number of spacer nucleotides retained immediately downstream of the handle (Figure 5-28). LRv contained a larger proportion of products retaining only 1–15 nt of spacer, whereas cr21-CG-3bp contained more products with 16–21 nt of spacer or a complete 22-nt spacer. Interestingly, the abundance of intact-handle products containing 1–15 nt of spacer followed the same order as the fluorescence signal: LRv > cr21-CG-3bp > cr21-2. Previous studies have also shown that Cas12a cleavage activity can vary substantially with spacer length and guide structure, including truncated and split crRNAs[200],[201]. This is also consistent with our previous observation that the handle-only template could also generate CRISPR fluorescence, suggesting that some of these non-canonical handle-containing RNA products may contribute to the high fluorescence observed for LRv. However, their individual functionality cannot be determined from the sequencing data alone. In contrast, cr21-2 showed both the lowest proportion of complete crRNA products and a much lower proportion of complete handle-containing products, which is consistent with its lower CRISPR fluorescence. Together, these results suggest that, in the STSR system, CRISPR activity is related not only to the generation of complete crRNA, but also to the broader composition of the RNA product population.

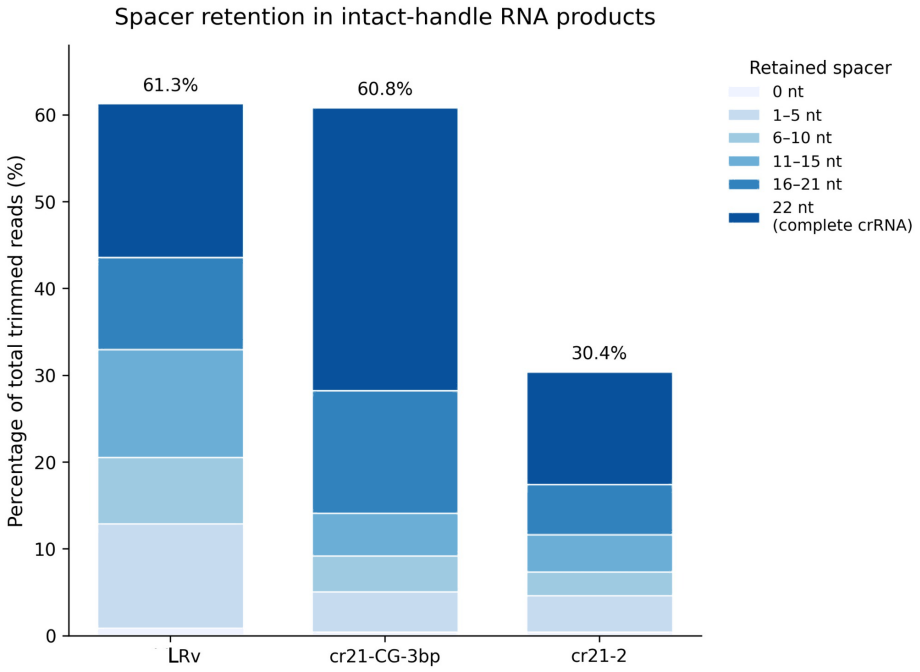


Figure 5-28: Spacer retention in RNA products containing a complete crRNA handle. RNA products containing the full handle region (positions 23–43) were grouped according to how many spacer nucleotides were retained immediately before the handle. The groups were 0, 1–5, 6–10, 11–15, 16–21, and 22 nt, where 22 nt represents a complete crRNA. Percentages were calculated from the total trimmed reads for each sample. The value above each bar shows the total percentage of reads containing a complete handle.

Overall, the Bioanalyzer and RNA sequencing results showed that promoter-independent transcription generated highly heterogeneous RNA products rather than uniform lengths. RNA sequencing provided more detailed information about these products and showed clear differences among the three templates, especially in the proportions of products containing the complete crRNA and handle regions. The designed 3-bp terminal complementarity in cr21-CG-3bp was associated with the highest proportion of reads containing the complete crRNA region.. This suggests that by regulating the 3' terminal sequence, it is possible to control the generation of functional RNA products. LRv generated the highest fluorescence even though it had a lower proportion of complete crRNA products than cr21-CG-3bp. This suggests that complete crRNA may not be the only RNA product contributing to CRISPR activation, and other RNA products may also play a role.

Further deep sequencing analysis is therefore needed to better understand how these different RNA products are generated. The current analysis mainly identified the most abundant RNA products and aligned them to the corresponding DNA template. A potentially useful next step would be to specifically identify reads containing both regions matching the original DNA template and newly synthesised RNA regions and then analyse the junction between these regions. Such junctions could provide stronger evidence for where priming and RNA extension occurred. However, this would be technically challenging because most of the

DNA template is removed during DNase treatment. Although a small fraction of ssDNA may remain protected through hybridisation with newly synthesised RNA, this small population is unlikely to represent the overall behaviour. If this problem can be solved, it would provide stronger evidence for where 3′-end priming and RNA extension occurred. It will also provide more information in designing template sequence, reducing unwanted RNA products, and achieving more controlled generation of functional RNA.

5.4 Conclusion

In this chapter, a Self-Transcribing Self-Recognition CRISPR platform, termed STSR-CRISPR, was developed from the unexpected LRv-derived fluorescence observed in Chapter 4. The system used designed ssDNA to generate crRNA-like products through T7 RNA polymerase-mediated transcription, followed by Cas12a activation and fluorescence generation. The main experimental findings are summarised below:

- Promoter-independent ssDNA transcription can be coupled with Cas12a activation. The results support that appropriately designed ssDNA templates can generate RNA-containing products that are able to support Cas12a activation without a conventional T7 promoter or externally synthesised crRNA. This establishes the basic feasibility of STSR-CRISPR as a new reaction concept.

- The reaction is strongly dependent on template structure, but the mechanism is more complex than initially expected. Short 3′ self-complementary regions improved the performance of some templates, while longer stems did not necessarily improve functional output. Split crRNA and DNase I experiments further suggested that the active species may include template-associated RNA products rather than only free, full-length crRNA.

- Cas12a activation in this system is not explained by the intended cognate FQ cleavage pathway alone. Fluorescence was also produced with R1-only and unrelated dsDNA reporters, indicating that once Cas12a is activated, additional reporter-processing pathways can contribute to the signal. The PAM-dependent behaviour of non-cognate dsDNA reporters further suggests that short duplex reporters can interact with activated Cas12a in a more complex manner than simple complete cis- or trans-cleavage.

- The self-transcribing template can be externally controlled by nucleic acid strand displacement. Using miR-21 as a model target, both the capped-template and dragon hairpin designs showed that access to the self-transcribing 3′ end could be regulated

through TMSD. This demonstrates the potential to convert the STSR reaction into a programmable target-responsive sensing platform, although the analytical performance and reproducibility still require further improvement.

- RNA sequencing revealed highly heterogeneous transcription products and showed that template design affected crRNA generation. Although the three templates shared the same crRNA sequence, they generated different RNA product distributions. The designed 3-bp terminal complementarity in cr21-CG-3bp produced a higher proportion of complete crRNA-containing products, suggesting that 3′-end design can influence functional RNA generation. Further analysis of RNA extension junctions will be required to identify the preferred priming sites and guide more precise template design.

Overall, this chapter establishes STSR-CRISPR as a proof-of-concept platform in which promoter-independent RNA extension from ssDNA can be linked to Cas12a activation and externally controlled by nucleic acid recognition. Importantly, the study also reveals that the reaction involves multiple interacting processes, including ssDNA structure, RNA generation, RNA–DNA association, Cas12a activation, and non-canonical reporter processing. These findings provide a basis for further mechanistic development of the platform rather than defining a fully optimised diagnostic assay at this stage.

Future work should focus on further characterising the transcription products, identifying their exact priming and extension pathways, and determining which RNAs are responsible for Cas12a activation. Template design should be further optimised to improve the yield and release of functional RNA product. For target detection, improving the stability of the OFF state and reducing variation between independent transcription reactions will be important for establishing reliable sensitivity performance. Once these mechanisms are better understood, the system could be further simplified towards an integrated one-pot sensing format.

Chapter 6

Summary and future perspective

6.1 Summary of key findings

Meeting the criteria of affordability, sensitivity, specificity, user-friendliness, rapidity, equipment-free operation, and deliverability (ASSURED) is essential for the development of effective point-of-care (POC) diagnostic tests[202]. Signal amplification strategies have substantially improved the sensitivity and efficiency of molecular diagnostics.[203] However, conventional INAATs still face several challenges, including non-specific amplification and complex primer design. Multiplex LAMP has been successfully demonstrated[151,152], although combining multiple primer sets can increase the complexity of primer design, optimisation and the assessment of competing interactions. The CRISPR/Cas system offers excellent molecular recognition and signal transduction capabilities. In recent years, isothermal nucleic acid amplification methods have been increasingly integrated with CRISPR/Cas systems, enabling highly sensitive and specific detection of a wide range of analytes[95]. However, many existing platforms rely on sequential amplification and CRISPR steps and externally synthesised crRNA, which increase reaction complexity and may limit their translation into simple POC formats. Therefore, this thesis explores the engineering of programmable isothermal amplification and CRISPR/Cas12a systems for nucleic acid detection. The work progresses from the development and optimisation of isothermal amplification strategies, through their integration with CRISPR/Cas12a, to the investigation of self-transcribing CRISPR systems in which nucleic acid templates can participate directly in crRNA generation and Cas12a activation. Collectively, these studies aim to reduce assay complexity while improving the programmability and integration of nucleic acid detection.

6.1.1 From programmable structure to controlled reaction initiation

The first study evaluated an abstract model-based (ABM) amplification strategy. (Chapter 2). Building on the previously published ABM principle from the group[5], this study evaluated its application to HPV16 rather than introducing a new ABM mechanism. This system used designed universal regions to help the formation of self-folding amplification intermediates for amplification. However, amplification was poorly reproducible and did not show dependence on target concentration. Optimisations did not eliminate amplification in the NTC group. Primer redesign also produced only temporary improvements. These findings suggested that the formation of the predicted structure alone was insufficient to ensure amplification specificity. The complementary domains required for self-folding could also participate in unintended interactions, and these competing reactions became the dominant amplification pathway, although their complete structures were not resolved. No evidence of target-specific amplification was obtained. Although the developed ABM assay was not sufficiently specific for HPV16 detection, the study established an important design constraint: programmable amplification must be evaluated according to the products that are experimentally generated, rather than only the intended reaction pathway.

A cleavage-assisted amplification strategy was subsequently investigated using CRISPR/Cas12a recognition and staggered cleavage to generate loop amplification substrate. (Chapter 3) This approach combined an existing loop region design[3] with the group's earlier strategy of placing CRISPR recognition before amplification[204], extending this concept to an isothermal workflow. In the proposed mechanism, Cas12a cleavage produced a 5′ overhang, allowing the extension product to fold back and enter an amplification cycle. This new concept enabled amplification using two core primers, reducing the primer requirements compared with conventional LAMP. The approach was developed for HPV16, HPV18 and HPV52. HPV16 and HPV18 produced different melting peaks when tested individually, whereas their mixed sample produced a broader intermediate peak rather than two clearly resolved peaks (Figure 3-26) In addition, HPV16, HPV18, and HPV52 were individually detected in the presence of all three primer sets under both two-step and one-pot triplex assay conditions. Distinct melting peaks were obtained for these individually tested targets in the two-step triplex assay; equivalent melt-based discrimination was not demonstrated for the one-pot triplex assay. This work investigated a direct role for CRISPR/Cas12a cleavage in generating an amplification-competent structure rather than acting only as a downstream reporter. It also demonstrated that a shared reaction principle could be adapted to several HPV genotypes.

6.1.2 Expanding the functional role of CRISPR/Cas12a

Although RPA provides rapid and sensitive nucleic acid amplification, its detection specificity is largely determined by specific primer amplification. (Chapter 4) To improve target-specific detection and less constrained of the integration with CRISPR/Cas12a, extended RPA primers were designed. RPA products served as templates for in vitro transcription, enabling crRNA generation directly after target amplification. A sequence-specific FQ probe was further introduced as both the Cas12a activator and fluorescence reporter. The three-step RPA-IVT-CRISPR assay detected 10 copies of HPV16 per reaction, while the simplified two-in-one format detected 100 copies per reaction. The three-step assay also distinguished HPV16 from the tested HPV18 and HPV52 targets under the experimental conditions. Importantly, the FQ probe enabled detection through sequence-specific cis-cleavage, while incorporation of the PAM into the probe removed the requirement for a suitable PAM in the original target and may provide potential for multiplex detection.

During assay development, unexpected fluorescence from primer-derived transcription products was observed during the RPA-IVT-CRISPR process, particularly from the LRv primer. Reducing the primer concentration suppressed this background while retaining RPA amplification. These findings demonstrated the feasibility of in situ crRNA generation from RPA products while revealing unintended transcriptional activity of extended primers in the integrated system. More importantly, it suggested that LRv could generate RNA products capable of supporting Cas12a activation. This unexpected observation became the starting point of the work in Chapter 5.

STSR-CRISPR was developed to investigate whether a designed ssDNA could perform two linked functions. First, its 3′ end could support promoter-independent RNA extension, generating products containing crRNA-related sequences. Second, the original ssDNA template could contribute to subsequent Cas12a activation. The template could therefore contribute to both RNA generation and Cas12a activation, giving rise to the terms self-transcribing and self-recognition. Unlike the RPA-IVT-CRISPR assay, this platform did not require target pre-amplification, a conventional T7 promoter or externally synthesised crRNA. Its main contribution was the coupling of promoter-independent RNA generation with Cas12a activation, rather than an established improvement in analytical sensitivity over existing miRNA detection methods.

These findings demonstrate that Cas12a does not need to be restricted to endpoint signal amplification. Cas12a cleavage was investigated as a possible means of facilitating amplification, amplified products can generate the guide RNA required for Cas12a, and a self-transcribing template can also act as a potential recognition target. Assigning additional functions to existing reaction components therefore provides several routes for reducing dependence on separately prepared primers, crRNA and reporter components.

6.1.3 Unintended reaction as a source of mechanistic discovery

A consistent finding throughout the thesis was that unintended reactions strongly influenced assay performance. Primer-derived amplification appeared to prevent reliable target discrimination in the ABM system. In the RPA-IVT-CRISPR assay, transcription products generated from the LRv primer caused Cas12a-dependent background. In STSR-CRISPR, heterogeneous transcription products and unexpected reporter responses made the activation mechanism more complex than the initially proposed pathway. This unexpected result provided the basis for STSR-CRISPR and converted an interfering reaction into a separate sensing concept.

Bioanalyzer and RNA-sequencing analyses showed that promoter-independent transcription generated heterogeneous RNA populations rather than a single defined crRNA. Templates containing the same crRNA-encoding region produced different product distributions. The cr21-CG-3bp template generated the highest proportion of complete crRNA-containing products, indicating that its designed 3′ terminal complementarity affected RNA formation. However, LRv produced the highest fluorescence despite containing a lower proportion of complete crRNA products. The proportion of complete crRNA-containing reads therefore did not directly predict fluorescence output. The strong LRv signal may also involve handle-containing or extended RNA products. Together with the fluorescence generated by handle-related templates, these results suggest that several RNA species may contribute to Cas12a activation. These results suggest that Cas12a activation may depend on the composition of the RNA product population rather than its total concentration alone.

Reporter behaviour provided a second example of an unintended reaction revealing additional molecular activity. Activated Cas12a generated fluorescence from non-cognate double-stranded reporters as well as from the intended FQ and R1 probes. PAGE analysis indicated that fluorescence recovery from these short duplexes did not always correspond to complete cleavage of the labelled strand. Local duplex opening, strand-selective processing or partial degradation may also have separated the fluorophore and quencher. Fluorescence output in these systems therefore needs to be interpreted cautiously as reporter dissociation or unintended cleavage rather than automatically as sequence-specific cleavage.

Taken together, these results establish mechanistic investigation as a central part of assay development. Non-specific amplification, primer-derived transcription and unexpected reporter fluorescence were not adequately explained by the intended reaction schemes. Characterising these signals revealed competing amplification pathways, promoter-independent RNA generation, self-recognition and non-canonical reporter processing. The work therefore demonstrates that unexpected signals can identify both limitations and previously unrecognised functions.

6.1.4 Progress towards programmable and multiplex detection

The developed strategies were evaluated using both DNA and RNA targets. The CRISPR/Cas12a-triggered loop amplification principle was adapted to HPV16, HPV18 and HPV52. Duplex detection of HPV16/18 mixtures was demonstrated in both two-step and one-pot formats, while the two-step triplex assay produced distinguishable melting peaks for individually tested HPV16, HPV18 and HPV52 targets. The one-pot triplex assay also supported amplification of each target, although reliable discrimination of all three genotypes in mixed samples was not established. This established the feasibility of applying a shared amplification principle to multiple targets, although performance remained dependent on the individual target and primer set.

The RPA-IVT-CRISPR assay provided HPV16 detection at low copy numbers and discrimination from the tested other HPV genotypes while generating crRNA within the workflow. Its sequence-specific activator-reporter design may also provide a basis for distinguishing multiple targets. However, this multiplexing potential was not experimentally established within the current assay.

Promoter-independent transcription was adapted to miR-21 detection by controlling access to the self-transcribing 3′ end. In the direct strategy, miR-21 displaced a blocking strand and released the template for RNA generation. The dragon hairpin strategy introduced a potential target-recycling mechanism. Signals above the no-target control were observed at low miR-21 concentrations. These results support the feasibility of target-responsive template activation; target recycling remains a proposed mechanism.

Overall, the work progressed from detecting HPV DNA through programmable amplification to controlling self-transcription using a short RNA target. This demonstrates the adaptability of nucleic acid structure as an interface between target recognition and signal generation. At the same time, differences among targets and templates show that programmable design does not remove the need for sequence-specific optimisation.

6.1.5 Overall contribution

The main contribution of this thesis is not a single assay combining every investigated technology. Instead, it is the development and mechanistic evaluation of a progression of nucleic acid reaction concepts.

Three general conclusions emerge from this work. First, nucleic acid components can perform more than one function: cleavage products can become amplification substrates, amplicons can become crRNA transcription templates, and ssDNA can support both RNA generation and CRISPR recognition. This multifunctionality can reduce the requirement for

additional assay components.

Second, increased functional coupling also creates new sources of background. Complementary primers can generate unintended amplification products, extended primers can undergo unexpected transcription, and activated Cas12a can process reporters through more than one pathway. Simplification at the component level does not therefore guarantee simplicity at the reaction level.

Third, the performance of a programmed nucleic acid system cannot be understood solely from its proposed reaction scheme. Product sequencing, electrophoretic analysis and targeted mechanistic controls are required to determine which structures and reaction pathways are actually present.

Together, the studies establish new approaches for CRISPR-triggered loop amplification, in situ crRNA generation and promoter-independent self-transcribing CRISPR. They also identify the design constraints that must be addressed before these concepts can be developed into reproducible analytical methods.

6.2 Limitations

Although this thesis demonstrated several approaches for integrating nucleic acid amplification and CRISPR/Cas12a, some limitations in assay design, analytical performance and mechanistic validation remain.

First, the amplification systems were not fully validated for reproducibility and multiplex detection. The ABM assay showed persistent non-specific amplification, which limited its application for HPV16 detection. For CRISPR/Cas12a-triggered loop amplification, although HPV16 and HPV18 produced distinct melting peaks when tested individually, their mixed samples generated a broader, intermediate melting peak rather than two clearly separated peaks. This limited the ability of melting-curve analysis to distinguish the two genotypes within the same reaction. The two-step triplex assay produced distinguishable melting peaks for individually tested HPV16, HPV18 and HPV52 targets, while the one-pot triplex format did not provide reliable subtype discrimination by melting-curve analysis. Simultaneous identification of all three genotypes in mixed samples was not established. The limited replicate numbers did not establish a detection rate of at least 95% at these inputs. Furthermore, direct comparisons with conventional LAMP under matched conditions were not performed, limiting conclusions about the benefits of the reduced primer design.

Second, although the RPA–IVT–CRISPR assay demonstrated sensitive HPV16 detection, its lowest detectable concentrations were determined using a limited number of replicates rather than a statistically validated detection limit. The assay also required multiple enzymes and reaction components, and the two/three-steps format involved additional handling. Further-

more, the sequence-specific reporter system was only evaluated for HPV16 detection, and its potential for multiplex detection was not experimentally demonstrated. A more systematic comparison with established amplification-assisted CRISPR assays would have provided a clearer assessment of its analytical performance and practical advantages.

Third, STSR-CRISPR remains a proof-of-concept platform. Several experiments were conducted with a limited number of replicates (n = 1 or 2), which restricted the assessment of reproducibility and the strength of the conclusions. Therefore, some of the mechanistic interpretations should be considered preliminary. Although target-dependent fluorescence responses were observed for miR-21, considerable variation between independent transcription reactions prevented the establishment of a reliable detection limit. The proposed target-recycling mechanism was also not directly demonstrated. In addition, RNA sequencing revealed heterogeneous transcription products, but the specific RNA species responsible for Cas12a activation and their exact formation pathways remain unclear.

Finally, the clinical and practical performance of the developed systems has not been fully established. Most experiments were performed using synthetic nucleic acid targets under controlled laboratory conditions. Their performance in complex biological samples, reagent requirements and compatibility with simplified detection formats therefore need further evaluation before their suitability for point-of-care applications can be determined.

6.3 Future work

6.3.1 Identification of amplification and transcription products

Future work should first identify the products responsible for intended and unintended signals. Individual ABM amplification products could be isolated by cloning and sequenced separately. High-throughput sequencing could then determine the relative abundance of target specific and primer-derived products and guide primer redesign. A positive control reproducing the published ABM chemistry[5] would also help distinguish limitations of the HPV16 implementation from failure to reproduce the original reaction.

For RPA-IVT-CRISPR, examining RNA products and FQ reporter cleavage at different time points could help explain the renewed fluorescence increase after the plateau in Figure 4-12.

For STSR-CRISPR, complete, extended, truncated and handle-only RNA sequences identified by RNA sequencing should be synthesised individually and tested for Cas12a activation. Transcription products could also be separated according to size before testing the activity of each fraction. These experiments would determine which components of the heterogeneous RNA population are functional.

The RNA-sequencing analysis should be extended to identify DNA-RNA extension junctions. Reads containing both template-derived and newly extended regions could provide stronger evidence for the positions at which self-priming and RNA extension occur. Independent transcription batches should also be sequenced to establish whether the observed products are reproducible. Different compositions of the crRNA should also be tested to support the STSR system working principle.

6.3.2 Development of generalisable design rules

The results indicate that secondary structure must balance stability with accessibility. This principle applies to amplification primers, self-transcribing 3′ ends, blocking strands and dragon hairpins. Future designs should therefore be evaluated both computationally and experimentally for intended folding, competing interactions and product identity. A systematic library of self-transcribing templates could be used to vary the length, sequence and GC content of the 3′ complementary region. Internal complementary sites should also be removed or repositioned. Measuring RNA composition and Cas12a activity separately would determine which structural features favour functional RNA generation rather than only increasing total transcription.

6.3.3 Analytical and multiplex validation

The CRISPR/Cas12a-triggered loop amplification assay should be evaluated using mixed HPV targets at unequal concentrations. Comparison with conventional LAMP under matched conditions should assess sensitivity, specificity, reaction time, primer requirements and background amplification. Further testing with extracted clinical samples would assess the effects of sequence variation and sample matrix.

The sequence-specific reporter principle of the RPA-IVT-CRISPR assay could be extended to additional HPV genotypes using orthogonal crRNA and reporter sequences. This would establish whether in situ crRNA generation can support distinguishable multiplex signals without increasing background. Benchmarking against established RPA-CRISPR methods should assess both analytical performance and workflow complexity.

For miR-21 detection, optimisation should first improve the stability of the OFF state and reproducibility of target-dependent activation. Both sensing strategies should be tested across a complete concentration range using independent transcription reactions. The direct capped-template assay should be tested across a complete concentration range using independent transcription reactions. The dragon hairpin system requires confirmation that transcription releases miR-21 and enables genuine target recycling. A detection limit should only be calculated after a reproducible concentration-response relationship has been established.

Across the assays, predefined positivity criteria and sufficient independent replicates would be required to establish analytical detection limits based on at least 95% detection. Subsequent evaluation with clinical samples would assess performance under more realistic diagnostic conditions.

Bibliography

[1] Léo Baldenweck, Noémie Berg, Mila Djisalov, Vitaly Efremov, Zorica Novakovic, Sandrine Auger, and Jasmina Vidic. Isothermal amplification techniques for rapid bacterial detection: alternatives to culturing and PCR-based methods. *Analytical Methods*, 18(27):5682–5712, 2026. ISSN 1759-9660, 1759-9679. doi: 10.1039/D6AY00756B. URL http://pubs.rsc.org/AY/article-lookup/doi/10.1039/D6AY00756B.

[2] Y.-P. Wong, S. Othman, Y.-L. Lau, S. Radu, and H.-Y. Chee. Loop-mediated isothermal amplification (LAMP): a versatile technique for detection of micro-organisms. *Journal of Applied Microbiology*, 124(3):626–643, March 2018. ISSN 13645072. doi: 10.1111/jam.13647. URL https://academic.oup.com/jambio/article/124/3/626/6714087.

[3] Rui Mao, Xinyao Wu, Qing Miao, and Ting Cai. Asymmetric stem-loop–mediated isothermal amplification of nucleic acids for DNA diagnostic assays by simple modification of canonical PCR primers. *Frontiers in Bioengineering and Biotechnology*, 10:931770, July 2022. ISSN 2296-4185. doi: 10.3389/fbioe.2022.931770.

[4] Gaolian Xu, Lin Hu, Huayan Zhong, Hongying Wang, Sei-ichi Yusa, Tristen C. Weiss, Paul J. Romaniuk, Sam Pickerill, and Qimin You. Cross Priming Amplification: Mechanism and Optimization for Isothermal DNA Amplification. *Scientific Reports*, 2(1):246, December 2012. ISSN 2045-2322. doi: 10.1038/srep00246.

[5] Gaolian Xu, Julien Reboud, Yunfei Guo, Hao Yang, Hongchen Gu, Chunhai Fan, Xiaohua Qian, and Jonathan M. Cooper. Programmable design of isothermal nucleic acid diagnostic assays through abstraction-based models. *Nature Communications*, 13(1):1635, December 2022. ISSN 2041-1723. doi: 10.1038/s41467-022-29101-1.

[6] Ivan Magriñá Lobato and Ciara K. O'Sullivan. Recombinase polymerase amplification: Basics, applications and recent advances. *TrAC Trends in Analytical Chemistry*, 98:19–35, January 2018. ISSN 01659936. doi: 10.1016/j.trac.2017.10.015.

[7] Beatriz Crego-Vicente, Manuel Diego Del Olmo, Antonio Muro, and Pedro Fernández-Soto. Multiplexing LAMP Assays: A Methodological Review and Diagnostic Application. *International Journal of Molecular Sciences*, 25(12):6374, June

2024. ISSN 1422-0067. doi: 10.3390/ijms25126374. URL https://www.mdpi.com/1422-0067/25/12/6374.

[8] Aakash Saha, Rodrigo Fregoso Ocampo, Jacquelyn T. Wright, David W. Taylor, and Giulia Palermo. Molecular mechanisms and biotechnology applications of CRISPR–Cas12a. *Nature Reviews Molecular Cell Biology*, 27(8):601–616, August 2026. ISSN 1471-0072, 1471-0080. doi: 10.1038/s41580-026-00969-x. URL https://www.nature.com/articles/s41580-026-00969-x.

[9] Janice S. Chen, Enbo Ma, Lucas B. Harrington, Maria Da Costa, Xinran Tian, Joel M. Palefsky, and Jennifer A. Doudna. CRISPR-Cas12a target binding unleashes indiscriminate single-stranded DNase activity. *Science*, 360(6387):436–439, April 2018. ISSN 0036-8075, 1095-9203. doi: 10.1126/science.aar6245.

[10] Xiong Ding, Kun Yin, Ziyue Li, Rajesh V. Lalla, Enrique Ballesteros, Maroun M. Sfeir, and Changchun Liu. Ultrasensitive and visual detection of SARS-CoV-2 using all-in-one dual CRISPR-Cas12a assay. *Nature Communications*, 11(1):4711, September 2020. ISSN 2041-1723. doi: 10.1038/s41467-020-18575-6. URL https://www.nature.com/articles/s41467-020-18575-6.

[11] Yalin Chen, Yicheng Chen, Cuijuan Zhang, Yongsheng Cai, Zhuoer Zeng, Julien Reboud, Jonathan M. Cooper, Hongbo Shan, Yang Wang, and Gaolian Xu. One-pot CRISPR-based point of care platform for rapid, specific and sensitive detection of HPV 16 without pre-amplification. *Microsystems & Nanoengineering*, 12(1):81, March 2026. ISSN 2055-7434. doi: 10.1038/s41378-025-01130-y.

[12] Max J. Kellner, Jeremy G. Koob, Jonathan S. Gootenberg, Omar O. Abudayyeh, and Feng Zhang. SHERLOCK: Nucleic acid detection with CRISPR nucleases. *Nature Protocols*, 14(10):2986–3012, October 2019. ISSN 1754-2189, 1750-2799. doi: 10.1038/s41596-019-0210-2.

[13] Jiongyu Zhang, Ziyue Li, Chong Guo, Xin Guan, Lori Avery, David Banach, and Changchun Liu. Intrinsic RNA Targeting Triggers Indiscriminate DNase Activity of CRISPR□Cas12a. *Angewandte Chemie International Edition*, 63(20):e202403123, May 2024. ISSN 1433-7851, 1521-3773. doi: 10.1002/anie.202403123. URL https://onlinelibrary.wiley.com/doi/10.1002/anie.202403123.

[14] Emily Greenwald, Drew Galls, Joon Park, Nimit Jain, Stephen B Montgomery, Bijoyita Roy, Y Whitney Yin, and Andrew Z Fire. DragonRNA: Generality of DNA-primed RNA-extension activities by DNA-directed RNA polymerases. *Nucleic Acids Research*, 53(6):gkaf236, March 2025. ISSN 0305-1048, 1362-4962. doi: 10.1093/nar/gkaf236.

[15] SJTU-QianLab. SJTUBME-QianLab/Machine_primer_design: The release with a DOI, January 2022. URL https://zenodo.org/record/5895944.

[16] Angelika Niemz, Tanya M. Ferguson, and David S. Boyle. Point-of-care nucleic acid testing for infectious diseases. *Trends in Biotechnology*, 29(5):240–250, May 2011. ISSN 01677799. doi: 10.1016/j.tibtech.2011.01.007. URL https://linkinghub.elsevier.com/retrieve/pii/S0167779911000187.

[17] Michael M. Kaminski, Omar O. Abudayyeh, Jonathan S. Gootenberg, Feng Zhang, and James J. Collins. CRISPR-based diagnostics. *Nature Biomedical Engineering*, 5 (7):643–656, July 2021. ISSN 2157-846X. doi: 10.1038/s41551-021-00760-7. URL https://www.nature.com/articles/s41551-021-00760-7.

[18] Tal Gilboa, Padric M. Garden, and Limor Cohen. Single-molecule analysis of nucleic acid biomarkers – A review. *Analytica Chimica Acta*, 1115:61–85, June 2020. ISSN 00032670. doi: 10.1016/j.aca.2020.03.001. URL https://linkinghub.elsevier.com/retrieve/pii/S0003267020303081.

[19] Pascal Craw and Wamadeva Balachandran. Isothermal nucleic acid amplification technologies for point-of-care diagnostics: a critical review. *Lab on a Chip*, 12 (14):2469, 2012. ISSN 1473-0197, 1473-0189. doi: 10.1039/c2lc40100b. URL https://pubs.rsc.org/lc/article/12/14/2469-2486/376072.

[20] K. Mullis, F. Faloona, S. Scharf, R. Saiki, G. Horn, and H. Erlich. Specific Enzymatic Amplification of DNA In Vitro: The Polymerase Chain Reaction. *Cold Spring Harbor Symposia on Quantitative Biology*, 51(0):263–273, January 1986. ISSN 0091-7451, 1943-4456. doi: 10.1101/SQB.1986.051.01.032. URL http://symposium.cshlp.org/cgi/doi/10.1101/SQB.1986.051.01.032.

[21] Pulkit Srivastava and Dinesh Prasad. Isothermal nucleic acid amplification and its uses in modern diagnostic technologies. *3 Biotech*, 13(6):200, June 2023. ISSN 2190-572X, 2190-5738. doi: 10.1007/s13205-023-03628-6. URL https://link.springer.com/10.1007/s13205-023-03628-6.

[22] Mei Lin, Zhiqiang Qiu, Mengen Hao, Weiwei Qi, Ting Zhang, Yuting Shen, Hongrui Xiao, Chaoyue Liang, Longxu Xie, Yongzhong Jiang, Meng Cheng, Tian Tian, and Xiaoming Zhou. Cas12a Cis-cleavage mediated lateral flow assay enables multiplex and ultra-specific nucleic acid detection. *Nature Communications*, 16(1):5597, July 2025. ISSN 2041-1723. doi: 10.1038/s41467-025-60917-9. URL https://www.nature.com/articles/s41467-025-60917-9.

[23] Xinggui Yang, Yaxing Xie, Yuting Zhong, Ying Li, Wen Bin, Lingbing Liao, Guorong Qi, Lei Zuo, Shijun Li, and Xiaolan Yang. Highly responsive push-orchestrated-

pull switching-enabled RNA-regulated Cas12a cis-cleavage: A universal one-pot multiplex-targeted detection platform with application to Mycobacterium tuberculosis complex. *Chemical Engineering Journal*, 523:168126, November 2025. ISSN 13858947. doi: 10.1016/j.cej.2025.168126. URL https://linkinghub.elsevier.com/retrieve/pii/S1385894725089685.

[24] Zhichen Xu, Dongjuan Chen, Tao Li, Jiayu Yan, Jiang Zhu, Ting He, Rui Hu, Ying Li, Yunhuang Yang, and Maili Liu. Microfluidic space coding for multiplexed nucleic acid detection via CRISPR-Cas12a and recombinase polymerase amplification. *Nature Communications*, 13(1):6480, October 2022. ISSN 2041-1723. doi: 10.1038/s41467-022-34086-y.

[25] Beatriz B. Oliveira, Bruno Veigas, and Pedro Viana Baptista. Isothermal Amplification of Nucleic Acids: The Race for the Next "Gold Standard". *Frontiers in Sensors*, 2: 752600, September 2021. ISSN 2673-5067. doi: 10.3389/fsens.2021.752600. URL https://www.frontiersin.org/articles/10.3389/fsens.2021.752600/full.

[26] Dana M. Nieuwkerk, Asja Korajkic, Erika L. Valdespino, Michael P. Herrmann, and Valerie J. Harwood. Critical review of methods for isothermal amplification of nucleic acids for environmental analysis. *Journal of Microbiological Methods*, 179:106099, December 2020. ISSN 01677012. doi: 10.1016/j.mimet.2020.106099. URL https://linkinghub.elsevier.com/retrieve/pii/S0167701220308150.

[27] Hanting Zhu, Zhitong Miao, Junfei Yuan, Wanying Xie, Qiaoqiao Zhang, and Kun Yang. The evolution of isothermal amplification technology: A bibliometric study (2013–2022). *Electronic Journal of Biotechnology*, 76:12–21, July 2025. ISSN 07173458. doi: 10.1016/j.ejbt.2025.03.003. URL https://linkinghub.elsevier.com/retrieve/pii/S0717345825000156.

[28] http://primerexplorer.jp/lampv5e/index.html.

[29] Yasuyoshi Mori, Kentaro Nagamine, Norihiro Tomita, and Tsugunori Notomi. Detection of Loop-Mediated Isothermal Amplification Reaction by Turbidity Derived from Magnesium Pyrophosphate Formation. *Biochemical and Biophysical Research Communications*, 289(1):150–154, November 2001. ISSN 0006291X. doi: 10.1006/bbrc.2001.5921. URL https://linkinghub.elsevier.com/retrieve/pii/S0006291X01959212.

[30] Nathan A. Tanner, Yinhua Zhang, and Thomas C. Evans. Visual Detection of Isothermal Nucleic Acid Amplification Using pH-Sensitive Dyes. *BioTechniques*, 58(2): 59–68, February 2015. ISSN 0736-6205, 1940-9818. doi: 10.2144/000114253. URL https://www.tandfonline.com/doi/full/10.2144/000114253.

[31] Jobie Budd, Benjamin S. Miller, Nicole E. Weckman, Dounia Cherkaoui, Da Huang, Alyssa Thomas Decruz, Noah Fongwen, Gyeo-Re Han, Marta Broto, Claudia S. Estcourt, Jo Gibbs, Deenan Pillay, Pam Sonnenberg, Robyn Meurant, Michael R. Thomas, Neil Keegan, Molly M. Stevens, Eleni Nastouli, Eric J. Topol, Anne M. Johnson, Maryam Shahmanesh, Aydogan Ozcan, James J. Collins, Marta Fernandez Suarez, Bill Rodriguez, Rosanna W. Peeling, and Rachel A. McKendry. Lateral flow test engineering and lessons learned from COVID-19. *Nature Reviews Bioengineering*, 1(1):13–31, January 2023. ISSN 2731-6092. doi: 10.1038/s44222-022-00007-3. URL https://www.nature.com/articles/s44222-022-00007-3.

[32] T. Notomi. Loop-mediated isothermal amplification of DNA. *Nucleic Acids Research*, 28(12):63e–63, June 2000. ISSN 13624962. doi: 10.1093/nar/28.12.e63.

[33] Olaf Piepenburg, Colin H Williams, Derek L Stemple, and Niall A Armes. DNA Detection Using Recombination Proteins. *PLoS Biology*, 4(7):e204, June 2006. ISSN 1545-7885. doi: 10.1371/journal.pbio.0040204.

[34] Paul M. Lizardi, Xiaohua Huang, Zhengrong Zhu, Patricia Bray-Ward, David C. Thomas, and David C. Ward. Mutation detection and single-molecule counting using isothermal rolling-circle amplification. *Nature Genetics*, 19(3):225–232, July 1998. ISSN 1061-4036, 1546-1718. doi: 10.1038/898. URL https://www.nature.com/articles/ng0798_225.

[35] Rozi Asadi and Hamidreza Mollasalehi. The mechanism and improvements to the isothermal amplification of nucleic acids, at a glance. *Analytical Biochemistry*, 631:114260, October 2021. ISSN 00032697. doi: 10.1016/j.ab.2021.114260. URL https://linkinghub.elsevier.com/retrieve/pii/S0003269721001615.

[36] J. Compton. Nucleic acid sequence-based amplification. *Nature*, 350(6313):91–92, March 1991. ISSN 0028-0836, 1476-4687. doi: 10.1038/350091a0. URL https://www.nature.com/articles/350091a0.

[37] Kenneth Morabito, Clay Wiske, and Anubhav Tripathi. Engineering Insights for Multiplexed Real-Time Nucleic Acid Sequence-Based Amplification (NASBA): Implications for Design of Point-of-Care Diagnostics. *Molecular Diagnosis & Therapy*, 17(3):185–192, June 2013. ISSN 1177-1062, 1179-2000. doi: 10.1007/s40291-013-0029-4. URL https://link.springer.com/10.1007/s40291-013-0029-4.

[38] Birgit Deiman, Pierre Van Aarle, and Peter Sillekens. Characteristics and Applications of Nucleic Acid Sequence-Based Amplification (NASBA). *Molecular Biotechnology*, 20(2):163–180, 2002. ISSN 1073-6085. doi: 10.1385/MB:20:2:163. URL http://link.springer.com/10.1385/MB:20:2:163.

[39] G. Terrance Walker, Melinda S. Fraiser, James L. Schram, Michael C. Little, James G. Nadeau, and Douglas P. Malinowski. Strand displacement amplification—an isothermal, *in vitro* DNA amplification technique. *Nucleic Acids Research*, 20(7):1691–1696, 1992. ISSN 0305-1048, 1362-4962. doi: 10.1093/nar/20.7.1691. URL https://academic.oup.com/nar/article-lookup/doi/10.1093/nar/20.7.1691.

[40] Qingshang Bi, Mengru Liu, Li Yan, Jun Cheng, Qingyang Sun, Yuzhu Dai, and Lingli Zou. Progress in the application of isothermal amplification technology in the diagnosis of infectious diseases. *Frontiers in Microbiology*, 16:1601644, July 2025. ISSN 1664-302X. doi: 10.3389/fmicb.2025.1601644. URL https://www.frontiersin.org/articles/10.3389/fmicb.2025.1601644/full.

[41] K. Nagamine, T. Hase, and T. Notomi. Accelerated reaction by loop-mediated isothermal amplification using loop primers. *Molecular and Cellular Probes*, 16(3):223–229, June 2002. ISSN 08908508. doi: 10.1006/mcpr.2002.0415.

[42] Olga Gandelman, Rebecca Jackson, Guy Kiddle, and Laurence Tisi. Loop-Mediated Amplification Accelerated by Stem Primers. *International Journal of Molecular Sciences*, 12(12):9108–9124, December 2011. ISSN 1422-0067. doi: 10.3390/ijms12129108. URL https://www.mdpi.com/1422-0067/12/12/9108.

[43] Rhett L. Martineau, Sarah A. Murray, Shufang Ci, Weimin Gao, Shih-hui Chao, and Deirdre R. Meldrum. Improved Performance of Loop-Mediated Isothermal Amplification Assays via Swarm Priming. *Analytical Chemistry*, 89(1):625–632, January 2017. ISSN 0003-2700, 1520-6882. doi: 10.1021/acs.analchem.6b02578. URL https://pubs.acs.org/doi/10.1021/acs.analchem.6b02578.

[44] Sheng Cai, Cheulhee Jung, Sanchita Bhadra, and Andrew D. Ellington. Phosphorothioated Primers Lead to Loop-Mediated Isothermal Amplification at Low Temperatures. *Analytical Chemistry*, 90(14):8290–8294, July 2018. ISSN 0003-2700, 1520-6882. doi: 10.1021/acs.analchem.8b02062. URL https://pubs.acs.org/doi/10.1021/acs.analchem.8b02062.

[45] Jinyi Shi, Sheng Ding, Chen Li, Gangyi Chen, Feng Du, Sifan Wang, Aiqin Yue, Kaiyuan Ren, Zhirong Yang, Pei Xu, Juan Dong, Jinzhong Zhao, and Zhuo Tang. Ultrafast DNA detection based on turn-back loop primer-accelerated LAMP (TLAMP). *Analytica Chimica Acta*, 1321:343041, September 2024. ISSN 00032670. doi: 10.1016/j.aca.2024.343041. URL https://linkinghub.elsevier.com/retrieve/pii/S0003267024008420.

[46] Rendong Fang, Xia Li, Lin Hu, Qimin You, Jing Li, Jie Wu, Peng Xu, Huayan Zhong, Ying Luo, Jian Mei, and Qian Gao. Cross-Priming Amplification for Rapid

Detection of *Mycobacterium tuberculosis* in Sputum Specimens. *Journal of Clinical Microbiology*, 47(3):845–847, March 2009. ISSN 0095-1137, 1098-660X. doi: 10.1128/JCM.01528-08. URL https://journals.asm.org/doi/10.1128/JCM.01528-08.

[47] Justin C. Rolando, Erik Jue, Nathan G. Schoepp, and Rustem F. Ismagilov. Real-Time, Digital LAMP with Commercial Microfluidic Chips Reveals the Interplay of Efficiency, Speed, and Background Amplification as a Function of Reaction Temperature and Time. *Analytical Chemistry*, 91(1):1034–1042, January 2019. ISSN 0003-2700, 1520-6882. doi: 10.1021/acs.analchem.8b04324.

[48] Olena Mayboroda, Ioanis Katakis, and Ciara K. O'Sullivan. Multiplexed isothermal nucleic acid amplification. *Analytical Biochemistry*, 545:20–30, March 2018. ISSN 00032697. doi: 10.1016/j.ab.2018.01.005. URL https://linkinghub.elsevier.com/retrieve/pii/S000326971830006X.

[49] Rana K Daher, Gale Stewart, Maurice Boissinot, and Michel G Bergeron. Recombinase Polymerase Amplification for Diagnostic Applications. *Clinical Chemistry*, 62 (7):947–958, July 2016. ISSN 0009-9147, 1530-8561. doi: 10.1373/clinchem.2015.245829.

[50] Jia Li, Joanne Macdonald, and Felix Von Stetten. Review: A comprehensive summary of a decade development of the recombinase polymerase amplification. *The Analyst*, 144(1):31–67, 2019. ISSN 0003-2654, 1364-5528. doi: 10.1039/C8AN01621F.

[51] Pranav Patel, Ahmed Abd El Wahed, Oumar Faye, Pauline Prüger, Marco Kaiser, Sasikanya Thaloengsok, Sukathida Ubol, Anavaj Sakuntabhai, Isabelle Leparc-Goffart, Frank T. Hufert, Amadou A. Sall, Manfred Weidmann, and Matthias Niedrig. A Field-Deployable Reverse Transcription Recombinase Polymerase Amplification Assay for Rapid Detection of the Chikungunya Virus. *PLOS Neglected Tropical Diseases*, 10(9):e0004953, September 2016. ISSN 1935-2735. doi: 10.1371/journal.pntd.0004953. URL https://dx.plos.org/10.1371/journal.pntd.0004953.

[52] Jonas A. Otoo and Travis S. Schlappi. REASSURED Multiplex Diagnostics: A Critical Review and Forecast. *Biosensors*, 12(2):124, February 2022. ISSN 2079-6374. doi: 10.3390/bios12020124.

[53] Robert J. Meagher, Aashish Priye, Yooli K. Light, Cheng Huang, and Eryu Wang. Impact of primer dimers and self-amplifying hairpins on reverse transcription loop-mediated isothermal amplification detection of viral RNA. *The Analyst*, 143(8):1924–1933, 2018. ISSN 0003-2654, 1364-5528. doi: 10.1039/C7AN01897E. URL https://xlink.rsc.org/?DOI=C7AN01897E.

[54] Nathan A. Tanner, Yinhua Zhang, and Thomas C. Evans. Simultaneous Multiple Target Detection in Real-Time Loop-Mediated Isothermal Amplification. *BioTechniques*, 53(2):81–89, August 2012. ISSN 0736-6205, 1940-9818. doi: 10.2144/0000113902. URL https://www.tandfonline.com/doi/full/10.2144/0000113902.

[55] Cameron S. Ball, Yooli K. Light, Chung-Yan Koh, Sarah S. Wheeler, Lark L. Coffey, and Robert J. Meagher. Quenching of Unincorporated Amplification Signal Reporters in Reverse-Transcription Loop-Mediated Isothermal Amplification Enabling Bright, Single-Step, Closed-Tube, and Multiplexed Detection of RNA Viruses. *Analytical Chemistry*, 88(7):3562–3568, April 2016. ISSN 0003-2700, 1520-6882. doi: 10.1021/acs.analchem.5b04054. URL https://pubs.acs.org/doi/10.1021/acs.analchem.5b04054.

[56] Padmavathy Bakthavathsalam, Guillaume Longatte, Slade O. Jensen, Mike Manefield, and J. Justin Gooding. Locked nucleic acid molecular beacon for multiplex detection of loop mediated isothermal amplification. *Sensors and Actuators B: Chemical*, 268: 255–263, September 2018. ISSN 09254005. doi: 10.1016/j.snb.2018.04.081. URL https://linkinghub.elsevier.com/retrieve/pii/S0925400518307858.

[57] Maksim A. Koryukov, Igor P. Oscorbin, Lidiya M. Novikova, Maria A. Gordukova, Irina E. Turina, Elena V. Galeeva, Dmitry A. Kudlay, and Maxim L. Filipenko. A Novel Multiplex LAMP Assay for the Detection of Respiratory Human Adenoviruses. *International Journal of Molecular Sciences*, 25(13):7215, June 2024. ISSN 1422-0067. doi: 10.3390/ijms25137215. URL https://www.mdpi.com/1422-0067/25/13/7215.

[58] Monika Singh, Deepa Pal, Raghavendra Aminedi, and Amit Kumar Singh. Multiplex Real-Time Loop-Mediated Isothermal Amplification (LAMP) Based on the Annealing Curve Analysis: Toward an On-Site Multiplex Detection of Transgenic Sequences in Seeds and Food Products. *Journal of Agricultural and Food Chemistry*, 72(31):17658–17665, August 2024. ISSN 0021-8561, 1520-5118. doi: 10.1021/acs.jafc.4c01803. URL https://pubs.acs.org/doi/10.1021/acs.jafc.4c01803.

[59] Yanchun Shao, Shengmei Zhu, Cuicui Jin, and Fusheng Chen. Development of multiplex loop-mediated isothermal amplification-RFLP (mLAMP-RFLP) to detect Salmonella spp. and Shigella spp. in milk. *International Journal of Food Microbiology*, 148(2):75–79, August 2011. ISSN 01681605. doi: 10.1016/j.ijfoodmicro.2011.05.004. URL https://linkinghub.elsevier.com/retrieve/pii/S0168160511002686.

[60] Jing□Wen Guo, Hsin□Ying Ho, Chia□Yen Dai, Yen□Hsu Chen, Ming□Lung Yu, and Ling□Shan Yu. Single□tube, single□strip lateral flow assays utilizing

loop□mediated isothermal amplification for simultaneous hepatitis B and C viral detection. *Journal of Medical Virology*, 96(6):e29721, June 2024. ISSN 0146-6615, 1096-9071. doi: 10.1002/jmv.29721. URL https://onlinelibrary.wiley.com/doi/10.1002/jmv.29721.

[61] Jinzhao Song, Changchun Liu, Michael G Mauk, Shelley C Rankin, James B Lok, Robert M Greenberg, and Haim H Bau. Two-Stage Isothermal Enzymatic Amplification for Concurrent Multiplex Molecular Detection. *Clinical Chemistry*, 63(3):714–722, March 2017. ISSN 0009-9147, 1530-8561. doi: 10.1373/clinchem.2016.263665. URL https://academic.oup.com/clinchem/article/63/3/714/5612881.

[62] So-Hee Kim, So-Young Lee, Unji Kim, and Se-Wook Oh. Diverse methods of reducing and confirming false-positive results of loop-mediated isothermal amplification assays: A review. *Analytica Chimica Acta*, 1280:341693, November 2023. ISSN 00032670. doi: 10.1016/j.aca.2023.341693.

[63] Feixue Wei, Damien Georges, Irene Man, Iacopo Baussano, and Gary M Clifford. Causal attribution of human papillomavirus genotypes to invasive cervical cancer worldwide: a systematic analysis of the global literature. *The Lancet*, 404(10451): 435–444, August 2024. ISSN 01406736. doi: 10.1016/S0140-6736(24)01097-3. URL https://linkinghub.elsevier.com/retrieve/pii/S0140673624010973.

[64] Le Cong, F. Ann Ran, David Cox, Shuailiang Lin, Robert Barretto, Naomi Habib, Patrick D. Hsu, Xuebing Wu, Wenyan Jiang, Luciano A. Marraffini, and Feng Zhang. Multiplex Genome Engineering Using CRISPR/Cas Systems. *Science*, 339(6121): 819–823, February 2013. ISSN 0036-8075, 1095-9203. doi: 10.1126/science.1231143. URL https://www.science.org/doi/10.1126/science.1231143.

[65] Yuxuan Wu, Dan Liang, Yinghua Wang, Meizhu Bai, Wei Tang, Shiming Bao, Zhiqiang Yan, Dangsheng Li, and Jinsong Li. Correction of a Genetic Disease in Mouse via Use of CRISPR-Cas9. *Cell Stem Cell*, 13(6):659–662, December 2013. ISSN 19345909. doi: 10.1016/j.stem.2013.10.016. URL https://linkinghub.elsevier.com/retrieve/pii/S1934590913004621.

[66] Bernd Zetsche, Jonathan S. Gootenberg, Omar O. Abudayyeh, Ian M. Slaymaker, Kira S. Makarova, Patrick Essletzbichler, Sara E. Volz, Julia Joung, John van der Oost, Aviv Regev, Eugene V. Koonin, and Feng Zhang. Cpf1 Is a Single RNA-Guided Endonuclease of a Class 2 CRISPR-Cas System. *Cell*, 163(3): 759–771, October 2015. ISSN 00928674. doi: 10.1016/j.cell.2015.09.038. URL https://linkinghub.elsevier.com/retrieve/pii/S0092867415012003.

[67] Zefeng Mao, Huang Lei, Ruipeng Chen, Shuyue Ren, Baolin Liu, and Zhixian Gao. CRISPR molecular detection techniques: Advances from single to multiple detection

methods. *TrAC Trends in Analytical Chemistry*, 166:117198, September 2023. ISSN 01659936. doi: 10.1016/j.trac.2023.117198.

[68] Shi-Yuan Li, Qiu-Xiang Cheng, Jing-Man Wang, Xiao-Yan Li, Zi-Long Zhang, Song Gao, Rui-Bing Cao, Guo-Ping Zhao, and Jin Wang. CRISPR-Cas12a-assisted nucleic acid detection. *Cell Discovery*, 4(1):20, April 2018. ISSN 2056-5968. doi: 10.1038/s41421-018-0028-z.

[69] Jonathan S. Gootenberg, Omar O. Abudayyeh, Jeong Wook Lee, Patrick Essletzbichler, Aaron J. Dy, Julia Joung, Vanessa Verdine, Nina Donghia, Nichole M. Daringer, Catherine A. Freije, Cameron Myhrvold, Roby P. Bhattacharyya, Jonathan Livny, Aviv Regev, Eugene V. Koonin, Deborah T. Hung, Pardis C. Sabeti, James J. Collins, and Feng Zhang. Nucleic acid detection with CRISPR-Cas13a/C2c2. *Science*, 356 (6336):438–442, April 2017. ISSN 0036-8075, 1095-9203. doi: 10.1126/science.aam9321. URL https://www.science.org/doi/10.1126/science.aam9321.

[70] Cia-Hin Lau, Siping Huang, and Haibao Zhu. Amplification-free nucleic acids detection with next-generation CRISPR/dx systems. *Critical Reviews in Biotechnology*, 45(4):859–886, May 2025. ISSN 0738-8551, 1549-7801. doi: 10.1080/07388551.2024.2399560. URL https://www.tandfonline.com/doi/full/10.1080/07388551.2024.2399560.

[71] Isabel Strohkendl, Aakash Saha, Catherine Moy, Alexander-Hoi Nguyen, Mohd Ahsan, Rick Russell, Giulia Palermo, and David W. Taylor. Cas12a domain flexibility guides R-loop formation and forces RuvC resetting. *Molecular Cell*, 84(14):2717–2731.e6, July 2024. ISSN 10972765. doi: 10.1016/j.molcel.2024.06.007. URL https://linkinghub.elsevier.com/retrieve/pii/S1097276524004854.

[72] Wei Zhang, Rui Shi, Kejun Dong, Hao Hu, Wan Shu, Yaoqin Mu, Bei Yan, Longjie Li, Xianjin Xiao, and Hongbo Wang. The Off-Target Effect of CRISPR-Cas12a System toward Insertions and Deletions between Target DNA and crRNA Sequences. *Analytical Chemistry*, 94(24):8596–8604, June 2022. ISSN 0003-2700, 1520-6882. doi: 10.1021/acs.analchem.1c05499. URL https://pubs.acs.org/doi/10.1021/acs.analchem.1c05499.

[73] Daan C. Swarts, John Van Der Oost, and Martin Jinek. Structural Basis for Guide RNA Processing and Seed-Dependent DNA Targeting by CRISPR-Cas12a. *Molecular Cell*, 66(2):221–233.e4, April 2017. ISSN 10972765. doi: 10.1016/j.molcel.2017.03.016. URL https://linkinghub.elsevier.com/retrieve/pii/S109727651730206X.

[74] Isabel Strohkendl, Fatema A. Saifuddin, James R. Rybarski, Ilya J. Finkelstein, and Rick Russell. Kinetic Basis for DNA Target Specificity of CRISPR-Cas12a. *Molecu-*

lar Cell, 71(5):816–824.e3, September 2018. ISSN 10972765. doi: 10.1016/j.molcel.2018.06.043. URL https://linkinghub.elsevier.com/retrieve/pii/S109727651830546X.

[75] Karthik Murugan, Arun S. Seetharam, Andrew J. Severin, and Dipali G. Sashital. CRISPR-Cas12a has widespread off-target and dsDNA-nicking effects. *Journal of Biological Chemistry*, 295(17):5538–5553, April 2020. ISSN 0021-9258, 1083-351X. doi: 10.1074/jbc.RA120.012933.

[76] Christopher W. Smith, Nidhi Nandu, Mahera J. Kachwala, Yu-Sheng Chen, Taha Bilal Uyar, and Mehmet V. Yigit. Probing CRISPR-Cas12a Nuclease Activity Using Double-Stranded DNA-Templated Fluorescent Substrates. *Biochemistry*, 59(15):1474–1481, April 2020. ISSN 0006-2960, 1520-4995. doi: 10.1021/acs.biochem.0c00140.

[77] Christopher W. Smith, Mahera J. Kachwala, Nidhi Nandu, and Mehmet V. Yigit. Recognition of DNA Target Formulations by CRISPR-Cas12a Using a dsDNA Reporter. *ACS Synthetic Biology*, 10(7):1785–1791, July 2021. ISSN 2161-5063, 2161-5063. doi: 10.1021/acssynbio.1c00204. URL https://pubs.acs.org/doi/10.1021/acssynbio.1c00204.

[78] Noor Mohammad, Logan Talton, Zach Hetzler, Megha Gongireddy, and Qingshan Wei. Unidirectional *trans* -cleaving behavior of CRISPR-Cas12a unlocks for an ultrasensitive assay using hybrid DNA reporters containing a 3′ toehold. *Nucleic Acids Research*, 51(18):9894–9904, October 2023. ISSN 0305-1048, 1362-4962. doi: 10.1093/nar/gkad715.

[79] Ryan T. Fuchs, Jennifer Curcuru, Megumu Mabuchi, Paul Yourik, and G. Brett Robb. Cas12a trans-cleavage can be modulated in vitro and is active on ssDNA, dsDNA, and RNA, April 2019.

[80] Ross Ka-Kit Leung, Qiu-Xiang Cheng, Zhi-Le Wu, Gulfaraz Khan, Yang Liu, Hai-Yang Xia, and Jin Wang. CRISPR-Cas12-based nucleic acids detection systems. *Methods*, 203:276–281, July 2022. ISSN 10462023. doi: 10.1016/j.ymeth.2021.02.018. URL https://linkinghub.elsevier.com/retrieve/pii/S1046202321000633.

[81] Kun Du, Qinlong Zeng, Mingjun Jiang, Zhiqing Hu, Miaojin Zhou, and Kun Xia. CRISPR/Cas12a-Based Biosensing: Advances in Mechanisms and Applications for Nucleic Acid Detection. *Biosensors*, 15(6):360, June 2025. ISSN 2079-6374. doi: 10.3390/bios15060360. URL https://www.mdpi.com/2079-6374/15/6/360.

[82] Yaoqiang Shi, Lan Kang, Rongrong Mu, Min Xu, Xiaoqiong Duan, Yujia Li, Chunhui Yang, Jia-Wei Ding, Qinghua Wang, and Shilin Li. CRISPR/Cas12a-Enhanced Loop-Mediated Isothermal Amplification for the Visual Detection of Shigella flexneri. *Fron-*

tiers in Bioengineering and Biotechnology, 10:845688, February 2022. ISSN 2296-4185. doi: 10.3389/fbioe.2022.845688. URL https://www.frontiersin.org/articles/10.3389/fbioe.2022.845688/full.

[83] Jinjoo Han, Seokhwan Kim, Seokjoon Kim, Eun Sung Lee, Byung Seok Cha, Jung Soo Park, Jiye Shin, Youngjun Jang, and Ki Soo Park. Cas12a-based primer production enables isothermal amplification for nucleic acid detection. *Sensors and Actuators B: Chemical*, 381:133401, April 2023. ISSN 09254005. doi: 10.1016/j.snb.2023.133401. URL https://linkinghub.elsevier.com/retrieve/pii/S0925400523001168.

[84] Koray Malcı, Laura E. Walls, and Leonardo Rios-Solis. Rational Design of CRISPR/Cas12a-RPA Based One-Pot COVID-19 Detection with Design of Experiments. *ACS Synthetic Biology*, 11(4):1555–1567, April 2022. ISSN 2161-5063, 2161-5063. doi: 10.1021/acssynbio.1c00617. URL https://pubs.acs.org/doi/10.1021/acssynbio.1c00617.

[85] Xueying Lei, Shengnan Cao, Tao Liu, Yongjun Wu, and Songcheng Yu. Non-canonical CRISPR/Cas12a-based technology: A novel horizon for biosensing in nucleic acid detection. *Talanta*, 271:125663, May 2024. ISSN 00399140. doi: 10.1016/j.talanta.2024.125663. URL https://linkinghub.elsevier.com/retrieve/pii/S0039914024000420.

[86] Caitlin H. Lamb, Brian Kang, and Cameron Myhrvold. Multiplexed CRISPR-based methods for pathogen nucleic acid detection. *Current Opinion in Biomedical Engineering*, 27:100471, September 2023. ISSN 24684511. doi: 10.1016/j.cobme.2023.100471. URL https://linkinghub.elsevier.com/retrieve/pii/S2468451123000272.

[87] Luyu Wei, Zhilong Wang, Yuanbin She, and Haiyan Fu. CRISPR/Cas Multiplexed Biosensing: Advances, Challenges, and Perspectives. *Analytical Chemistry*, 97(23):11943–11958, June 2025. ISSN 0003-2700, 1520-6882. doi: 10.1021/acs.analchem.4c04428.

[88] Jonathan S. Gootenberg, Omar O. Abudayyeh, Max J. Kellner, Julia Joung, James J. Collins, and Feng Zhang. Multiplexed and portable nucleic acid detection platform with Cas13, Cas12a, and Csm6. *Science*, 360(6387):439–444, April 2018. ISSN 0036-8075, 1095-9203. doi: 10.1126/science.aaq0179.

[89] Cheri M. Ackerman, Cameron Myhrvold, Sri Gowtham Thakku, Catherine A. Freije, Hayden C. Metsky, David K. Yang, Simon H. Ye, Chloe K. Boehm, Tinna-Sólveig F. Kosoko-Thoroddsen, Jared Kehe, Tien G. Nguyen, Amber Carter, Anthony Kulesa, John R. Barnes, Vivien G. Dugan, Deborah T. Hung, Paul C. Blainey, and Pardis C. Sabeti. Massively multiplexed nucleic acid detection with Cas13. *Nature*, 582(7811):277–282, June 2020. ISSN 0028-0836, 1476-4687. doi: 10.1038/s41586-020-2279-8. URL http://www.nature.com/articles/s41586-020-2279-8.

[90] L. Stewart Massad, Megan A. Clarke, Rebecca B. Perkins, Francisco Garcia, David Chelmow, Li C. Cheung, Teresa M. Darragh, Didem Egemen, Thomas S. Lorey, Ritu Nayar, Morgan Newman, Carolann Risley, Robert A. Smith, Nicolas Wentzensen, and Enduring Consensus Cervical Cancer Screening and Management Guidelines Committee. Applying Results of Extended Genotyping to Management of Positive Cervicovaginal Human Papillomavirus Test Results: Enduring Guidelines. *Journal of Lower Genital Tract Disease*, 29(2):134–143, April 2025. ISSN 1526-0976. doi: 10.1097/LGT.0000000000000865. URL https://journals.lww.com/10.1097/LGT.0000000000000865.

[91] Rebecca B. Perkins, Nicolas Wentzensen, Richard S. Guido, and Mark Schiffman. Cervical Cancer Screening: A Review. *JAMA*, 330(6):547, August 2023. ISSN 0098-7484. doi: 10.1001/jama.2023.13174. URL https://jamanetwork.com/journals/jama/fullarticle/2807981.

[92] D. A. M. Heideman, A. T. Hesselink, J. Berkhof, F. Van Kemenade, W. J. G. Melchers, N. Fransen Daalmeijer, M. Verkuijten, C. J. L. M. Meijer, and P. J. F. Snijders. Clinical Validation of the cobas 4800 HPV Test for Cervical Screening Purposes. *Journal of Clinical Microbiology*, 49(11):3983–3985, November 2011. ISSN 0095-1137, 1098-660X. doi: 10.1128/JCM.05552-11. URL https://journals.asm.org/doi/10.1128/JCM.05552-11.

[93] Spencer Seely, Jean-Marc Zingg, Pratibha Joshi, Brian Slomovitz, Matthew Schlumbrecht, Erin Kobetz, Sapna Deo, and Sylvia Daunert. Point-of-Care Molecular Test for the Detection of 14 High-Risk Genotypes of Human Papillomavirus in a Single Tube. *Analytical Chemistry*, 95(36):13488–13496, September 2023. ISSN 0003-2700, 1520-6882. doi: 10.1021/acs.analchem.3c01723. URL https://pubs.acs.org/doi/10.1021/acs.analchem.3c01723.

[94] Maria Barra, Megan Chang, Mila P. Salcedo, Kathleen Schmeler, Michael Scheurer, Mauricio Maza, Leticia Lopez, Karla Alfaro, and Rebecca Richards-Kortum. Single-tube four-target lateral flow assay detects human papillomavirus types associated with majority of cervical cancers. *Analytical Biochemistry*, 688:115480, May 2024. ISSN 00032697. doi: 10.1016/j.ab.2024.115480. URL https://linkinghub.elsevier.com/retrieve/pii/S0003269724000241.

[95] Yanan Tang, Lu Gao, Wei Feng, Chen Guo, Qianfan Yang, Feng Li, and X. Chris Le. The CRISPR–Cas toolbox for analytical and diagnostic assay development. *Chemical Society Reviews*, 50(21):11844–11869, 2021. ISSN 0306-0012, 1460-4744. doi: 10.1039/D1CS00098E. URL http://xlink.rsc.org/?DOI=D1CS00098E.

[96] Xue Zheng, Yuankun Li, Mingzhu Yuan, Yue Shen, Shuaiyin Chen, and Guangcai

Duan. Rapid detection of HPV16/18 based on a CRISPR-Cas13a/Cas12a dual-channel system. *Analytical Methods*, 14(48):5065–5075, 2022. ISSN 1759-9660, 1759-9679. doi: 10.1039/D2AY01536F. URL http://xlink.rsc.org/?DOI=D2AY01536F.

[97] Ahmed Ghouneimy, Zahir Ali, Rashid Aman, Wenjun Jiang, Mustapha Aouida, and Magdy Mahfouz. CRISPR-Based Multiplex Detection of Human Papillomaviruses for One-Pot Point-of-Care Diagnostics. *ACS Synthetic Biology*, 13(3):837–850, March 2024. ISSN 2161-5063, 2161-5063. doi: 10.1021/acssynbio.3c00655.

[98] Yan Liu, Zhujun Chao, Wei Ding, Tanfeng Fang, Xinxian Gu, Man Xue, Wei Wang, Rong Han, and Wanping Sun. A multiplex RPA-CRISPR/Cas12a-based POCT technique and its application in human papillomavirus (HPV) typing assay. *Cellular & Molecular Biology Letters*, 29(1):34, March 2024. ISSN 1689-1392. doi: 10.1186/s11658-024-00548-y. URL https://cmbl.biomedcentral.com/articles/10.1186/s11658-024-00548-y.

[99] John F. Milligan, Duncan R. Groebe, Gary W. Witherell, and Olke C. Uhlenbeck. Oligoribonucleotide synthesis using T7 RNA polymerase and synthetic DNA templates. *Nucleic Acids Research*, 15(21):8783–8798, 1987. ISSN 0305-1048, 1362-4962. doi: 10.1093/nar/15.21.8783.

[100] Graham M. T. Cheetham and And Thomas A. Steitz. Structure of a Transcribing T7 RNA Polymerase Initiation Complex. *Science*, 286(5448):2305–2309, December 1999. ISSN 0036-8075, 1095-9203. doi: 10.1126/science.286.5448.2305. URL https://www.science.org/doi/10.1126/science.286.5448.2305.

[101] David Septian Sumanto Marpaung, Ayu Oshin Yap Sinaga, Damayanti Damayanti, Taharuddin Taharuddin, and Setyadi Gumaran. Current biosensing strategies based on in vitro T7 RNA polymerase reaction. *Biotechnology Notes*, 6:59–66, 2025. ISSN 26659069. doi: 10.1016/j.biotno.2025.01.002. URL https://linkinghub.elsevier.com/retrieve/pii/S2665906925000029.

[102] Zheng Li, Liyan Hua, Liming Xie, Dou Wang, and Xingyu Jiang. Automated Microfluidic Nucleic Acid Detection Platform-Integrated RPA-T7-Cas13a for Pathogen Diagnosis. *Analytical Chemistry*, 95(17):6940–6947, May 2023. ISSN 0003-2700, 1520-6882. doi: 10.1021/acs.analchem.3c00242. URL https://pubs.acs.org/doi/10.1021/acs.analchem.3c00242.

[103] Tianchi Zhuang, Chang Gao, Wenwu Zhao, Hairong Yu, Yun Liu, Ning Zhang, Ning Li, and Minghui Ji. A minimal transcription template-based amplification-free CRISPR-Cas13a strategy for DNA detection. *Biosensors and Bioelectronics*, 270:116918, February 2025. ISSN 09565663. doi: 10.1016/j.bios.2024.116918. URL https://linkinghub.elsevier.com/retrieve/pii/S0956566324009254.

[104] Xin Mu, Emily Greenwald, Sadeem Ahmad, and Sun Hur. An origin of the immunogenicity of in vitro transcribed RNA. *Nucleic Acids Research*, 46(10):5239–5249, June 2018. ISSN 0305-1048, 1362-4962. doi: 10.1093/nar/gky177.

[105] Bingbing Yu, Yifan Chen, Yan Yan, Xueling Lu, and Bin Zhu. DNA-terminus-dependent transcription by T7 RNA polymerase and its C-helix mutants. *Nucleic Acids Research*, 52(14):8443–8453, August 2024. ISSN 0305-1048, 1362-4962. doi: 10.1093/nar/gkae593. URL https://academic.oup.com/nar/article/52/14/8443/7709539.

[106] Hani S. Zaher and Peter J. Unrau. T7 RNA Polymerase Mediates Fast Promoter-Independent Extension of Unstable Nucleic Acid Complexes. *Biochemistry*, 43(24):7873–7880, June 2004. ISSN 0006-2960, 1520-4995. doi: 10.1021/bi0497300.

[107] Yasaman Gholamalipour, William C Johnson, and Craig T Martin. Efficient inhibition of RNA self-primed extension by addition of competing 3′-capture DNA-improved RNA synthesis by T7 RNA polymerase. *Nucleic Acids Research*, 47(19):e118–e118, November 2019. ISSN 0305-1048, 1362-4962. doi: 10.1093/nar/gkz700.

[108] Nimit Jain, Lucas R. Blauch, Michal R. Szymanski, Rhiju Das, Sindy K. Y. Tang, Y. Whitney Yin, and Andrew Z. Fire. Transcription polymerase–catalyzed emergence of novel RNA replicons. *Science*, 368(6487):eaay0688, April 2020. ISSN 0036-8075, 1095-9203. doi: 10.1126/science.aay0688.

[109] Gaoting Wang, Weimin Tian, Xiaoling Liu, Wei Ren, and Chenghui Liu. New CRISPR-Derived microRNA Sensing Mechanism Based on Cas12a Self-Powered and Rolling Circle Transcription-Unleashed Real-Time crRNA Recruiting. *Analytical Chemistry*, 92(9):6702–6708, May 2020. ISSN 0003-2700, 1520-6882. doi: 10.1021/acs.analchem.0c00680. URL https://pubs.acs.org/doi/10.1021/acs.analchem.0c00680.

[110] Yang Song, Ke Gao, Xiaoying Cai, Wei Cheng, Shijia Ding, Decai Zhang, and Shixiong Deng. Controllable crRNA Self-Transcription Aided Dual-Amplified CRISPR-Cas12a Strategy for Highly Sensitive Biosensing of FEN1 Activity. *ACS Synthetic Biology*, 11(11):3847–3854, November 2022. ISSN 2161-5063, 2161-5063. doi: 10.1021/acssynbio.2c00420. URL https://pubs.acs.org/doi/10.1021/acssynbio.2c00420.

[111] Xiuhua Yuan, Hui Yuan, Bingxin Liu, and Yeling Liu. Self-Supplying Guide RNA-Mediated CRISPR/Cas12a Fluorescence System for Sensitive Detection of T4 PNKP. *Molecules*, 27(24):9019, December 2022. ISSN 1420-3049. doi: 10.3390/molecules27249019. URL https://www.mdpi.com/1420-3049/27/24/9019.

[112] Yong-Li Song, Xiang-Lan He, Yong Li, Ming Wang, Ming Jiang, Li Xu, and Xu Yu. Homogeneous detection of viral nucleic acid via selective recognition proximity

ligation and signal amplification with T7 transcription and CRISPR/Cas12a system. *Analytica Chimica Acta*, 1280:341881, November 2023. ISSN 00032670. doi: 10.1016/j.aca.2023.341881. URL https://linkinghub.elsevier.com/retrieve/pii/S0003267023011029.

[113] Jiangbo Dong, Shiying Zhou, Yin Liu, Liyuan Deng, Zhen Huang, Jian Chen, Jiawei Li, Changjun Hou, and Danqun Huo. A self-supply crRNA-mediated CRISPR/Cas12a-driven controlled-release homogeneous biosensor for ultrasensitive detection of microRNA. *Chemical Engineering Journal*, 471:144507, September 2023. ISSN 13858947. doi: 10.1016/j.cej.2023.144507. URL https://linkinghub.elsevier.com/retrieve/pii/S1385894723032382.

[114] Margot Karlikow, Evan Amalfitano, Xiaolong Yang, Jennifer Doucet, Abigail Chapman, Peivand Sadat Mousavi, Paige Homme, Polina Sutyrina, Winston Chan, Sofia Lemak, Alexander F. Yakunin, Adam G. Dolezal, Shana Kelley, Leonard J. Foster, Brock A. Harpur, and Keith Pardee. CRISPR-induced DNA reorganization for multiplexed nucleic acid detection. *Nature Communications*, 14(1):1505, March 2023. ISSN 2041-1723. doi: 10.1038/s41467-023-36874-6.

[115] Tianchi Zhuang, Shuyi Jia, Pengfei Gu, Haokun Mei, Chang Gao, Xinyi Zhao, Muyi Yang, Jiemiao Shen, and Minghui Ji. Online synthesis of crRNA for One-Step RPA-CRISPR-Cas12 assay of Group b Streptococcus. *Microchemical Journal*, 213: 113745, June 2025. ISSN 0026265X. doi: 10.1016/j.microc.2025.113745. URL https://linkinghub.elsevier.com/retrieve/pii/S0026265X25010999.

[116] Xiaofan Zhu, Jingran Jiao, Qun Ni, Li Yao, Yule Zhang, Kaiyong Liu, Lin Huang, Qingli Bo, and Panzhu Qin. Development of a universal one-pot CRISPR assay based on multifunctional tagged primer eliminating unstable crRNA input and PAM dependency for point-of-care detection of bacterial infections. *Biosensors and Bioelectronics*, 287:117718, November 2025. ISSN 09565663. doi: 10.1016/j.bios.2025.117718.

[117] Xiaoning Xu, Ke Tang, Liu Yang, Yunhua Wu, Yiping Gu, and Yong Li. Split crRNA-Mediated Regulation of CRISPR-Cas12a Enables Construction of Biochemical Circuits for Sensitive Molecular Diagnostics. *Analytical Chemistry*, 97(30):16645–16651, August 2025. ISSN 0003-2700, 1520-6882. doi: 10.1021/acs.analchem.5c03196.

[118] Patrick Wakaba, Akira Muramatsu, Toshifumi Imagawa, Yuki Furuse, Nobuo Saito, and Naoki Uno. CRISPR-Cas12a biosensing via transcription of crRNA from PCR or LAMP products for pathogen detection. *Biosensors and Bioelectronics*, 310: 118860, October 2026. ISSN 09565663. doi: 10.1016/j.bios.2026.118860. URL https://linkinghub.elsevier.com/retrieve/pii/S0956566326004926.

[119] David P. Bartel. Metazoan MicroRNAs. *Cell*, 173(1):20–51, March 2018. ISSN 00928674. doi: 10.1016/j.cell.2018.03.006. URL https://linkinghub.elsevier.com/retrieve/pii/S0092867418302861.

[120] Vivek Priy Dave, Tien Anh Ngo, Anna-Karin Pernestig, Diana Tilevik, Krishna Kant, Trieu Nguyen, Anders Wolff, and Dang Duong Bang. MicroRNA amplification and detection technologies: opportunities and challenges for point of care diagnostics. *Laboratory Investigation*, 99(4):452–469, April 2019. ISSN 00236837. doi: 10.1038/s41374-018-0143-3. URL https://linkinghub.elsevier.com/retrieve/pii/S0023683722006602.

[121] Tinglan Ouyang, Zhiyu Liu, Zhiyi Han, and Qinyu Ge. MicroRNA Detection Specificity: Recent Advances and Future Perspective. *Analytical Chemistry*, 91(5):3179–3186, March 2019. ISSN 0003-2700, 1520-6882. doi: 10.1021/acs.analchem.8b05909. URL https://pubs.acs.org/doi/10.1021/acs.analchem.8b05909.

[122] C. Chen. Real-time quantification of microRNAs by stem-loop RT-PCR. *Nucleic Acids Research*, 33(20):e179–e179, November 2005. ISSN 0305-1048, 1362-4962. doi: 10.1093/nar/gni178. URL https://academic.oup.com/nar/article-lookup/doi/10.1093/nar/gni178.

[123] Ruijie Deng, Kaixiang Zhang, and Jinghong Li. Isothermal Amplification for MicroRNA Detection: From the Test Tube to the Cell. *Accounts of Chemical Research*, 50(4):1059–1068, April 2017. ISSN 0001-4842, 1520-4898. doi: 10.1021/acs.accounts.7b00040. URL https://pubs.acs.org/doi/10.1021/acs.accounts.7b00040.

[124] Jingmin Jin, Sophie Vaud, Alexander M. Zhelkovsky, Janos Posfai, and Larry A. McReynolds. Sensitive and specific miRNA detection method using SplintR Ligase. *Nucleic Acids Research*, 44(13):e116–e116, July 2016. ISSN 0305-1048, 1362-4962. doi: 10.1093/nar/gkw399. URL https://academic.oup.com/nar/article-lookup/doi/10.1093/nar/gkw399.

[125] Mai Zhang, Honghong Wang, Hui Wang, Fangfang Wang, and Zhengping Li. CRISPR/Cas12a-Assisted Ligation-Initiated Loop-Mediated Isothermal Amplification (CAL-LAMP) for Highly Specific Detection of microRNAs. *Analytical Chemistry*, 93(22):7942–7948, June 2021. ISSN 0003-2700, 1520-6882. doi: 10.1021/acs.analchem.1c00686. URL https://pubs.acs.org/doi/10.1021/acs.analchem.1c00686.

[126] He Yan, Yunjie Wen, Zimu Tian, Nathan Hart, Song Han, Steven J. Hughes, and Yong Zeng. A one-pot isothermal Cas12-based assay for the sensitive detection of microRNAs. *Nature Biomedical Engineering*, April 2023. ISSN 2157-846X. doi: 10.1038/s41551-023-01033-1. URL https://www.nature.com/articles/s41551-023-01033-1.

[127] Yuanyue Shan, Xiaoming Zhou, Ru Huang, and Da Xing. High-Fidelity and Rapid Quantification of miRNA Combining crRNA Programmability and CRISPR/Cas13a *trans* -Cleavage Activity. *Analytical Chemistry*, 91(8):5278–5285, April 2019. ISSN 0003-2700, 1520-6882. doi: 10.1021/acs.analchem.9b00073. URL https://pubs.acs.org/doi/10.1021/acs.analchem.9b00073.

[128] Xi Long, Tong Luo, Panpan Yuan, Yuqing Gan, Hui Liu, Zhiwei Deng, Jiacheng Ding, Zan Gong, Yanjing Yang, and Shian Zhong. Hairpin Switches-Based Isothermal Transcription Amplification for Simple, Sensitivity Detection of MicroRNA. *Analytical Chemistry*, 95(37):13872–13879, September 2023. ISSN 0003-2700, 1520-6882. doi: 10.1021/acs.analchem.3c02051.

[129] Hyogu Han, Hyo Won Jeon, Jieun Yang, Chang Yeol Lee, and Jun Ki Ahn. Label-free and isothermal multiplex detection of miRNAs using self-priming hairpin probes and light-up aptamer transcription. *Analytica Chimica Acta*, 1400:345310, May 2026. ISSN 00032670. doi: 10.1016/j.aca.2026.345310.

[130] Stephen A Bustin, Jan M Ruijter, Maurice J B Van Den Hoff, Mikael Kubista, Michael W Pfaffl, Gregory L Shipley, Nham Tran, Stefan Rödiger, Andreas Untergasser, Reinhold Mueller, Tania Nolan, Mojca Milavec, Malcolm J Burns, Jim F Huggett, Jo Vandesompele, and Carl T Wittwer. MIQE 2.0: Revision of the Minimum Information for Publication of Quantitative Real-Time PCR Experiments Guidelines. *Clinical Chemistry*, 71(6):634–651, June 2025. ISSN 0009-9147, 1530-8561. doi: 10.1093/clinchem/hvaf043. URL https://academic.oup.com/clinchem/article/71/6/634/8119148.

[131] Ravil R. Garafutdinov, Aidar R. Gilvanov, and Assol R. Sakhabutdinova. The Influence of Reaction Conditions on DNA Multimerization During Isothermal Amplification with Bst exo− DNA Polymerase. *Applied Biochemistry and Biotechnology*, 190(2):758–771, February 2020. ISSN 0273-2289, 1559-0291. doi: 10.1007/s12010-019-03127-6. URL http://link.springer.com/10.1007/s12010-019-03127-6.

[132] Patrice Francois, Manuela Tangomo, Jonathan Hibbs, Eve-Julie Bonetti, Catharina C. Boehme, Tsugunori Notomi, Mark D. Perkins, and Jacques Schrenzel. Robustness of a loop-mediated isothermal amplification reaction for diagnostic applications. *FEMS Immunology & Medical Microbiology*, 62(1):41–48, June 2011. ISSN 0928-8244, 1574-695X. doi: 10.1111/j.1574-695X.2011.00785.x. URL https://academic.oup.com/femspd/article-lookup/doi/10.1111/j.1574-695X.2011.00785.x.

[133] Maud Savonnet, Mathilde Aubret, Patricia Laurent, Yoann Roupioz, Myriam Cubizolles, and Arnaud Buhot. Kinetics of Isothermal Dumbbell Exponential Amplification: Effects of Mix Composition on LAMP and Its Derivatives. *Biosen-*

sors, 12(5):346, May 2022. ISSN 2079-6374. doi: 10.3390/bios12050346. URL https://www.mdpi.com/2079-6374/12/5/346.

[134] MinJu Jang and Sanghyo Kim. Inhibition of Non-specific Amplification in Loop-Mediated Isothermal Amplification via Tetramethylammonium Chloride. *BioChip Journal*, 16(3):326–333, September 2022. ISSN 1976-0280, 2092-7843. doi: 10.1007/s13206-022-00070-3.

[135] Dua Mohammad Ghaith and Robin Abu Ghazaleh. Carboxamide and N-alkylcarboxamide additives can greatly reduce non specific amplification in Loop-Mediated Isothermal Amplification for Foot-and-Mouth disease Virus (FMDV) using Bst 3.0 polymerase. *Journal of Virological Methods*, 298:114284, December 2021. ISSN 01660934. doi: 10.1016/j.jviromet.2021.114284.

[136] Xueqin Gao, Bingqi Sun, and Yifu Guan. Pullulan reduces the non-specific amplification of loop-mediated isothermal amplification (LAMP). *Analytical and Bioanalytical Chemistry*, 411(6):1211–1218, February 2019. ISSN 1618-2642, 1618-2650. doi: 10.1007/s00216-018-1552-2.

[137] Yinhua Zhang, Guoping Ren, Jackson Buss, Andrew J Barry, Gregory C Patton, and Nathan A Tanner. Enhancing colorimetric loop-mediated isothermal amplification speed and sensitivity with guanidine chloride. *BioTechniques*, 69(3):178–185, September 2020. ISSN 0736-6205, 1940-9818. doi: 10.2144/btn-2020-0078.

[138] Inyup Paik, Phuoc H. T. Ngo, Raghav Shroff, Daniel J. Diaz, Andre C. Maranhao, David J.F. Walker, Sanchita Bhadra, and Andrew D. Ellington. Improved Bst DNA Polymerase Variants Derived *via* a Machine Learning Approach. *Biochemistry*, 62 (2):410–418, January 2023. ISSN 0006-2960, 1520-4995. doi: 10.1021/acs.biochem.1c00451. URL https://pubs.acs.org/doi/10.1021/acs.biochem.1c00451.

[139] Bingling Li, Andrew D. Ellington, and Xi Chen. Rational, modular adaptation of enzyme-free DNA circuits to multiple detection methods. *Nucleic Acids Research*, 39 (16):e110–e110, September 2011. ISSN 1362-4962, 0305-1048. doi: 10.1093/nar/gkr504. URL https://academic.oup.com/nar/article-lookup/doi/10.1093/nar/gkr504.

[140] Yu Sherry Jiang, Sanchita Bhadra, Bingling Li, and Andrew D. Ellington. Mismatches Improve the Performance of Strand□Displacement Nucleic Acid Circuits. *Angewandte Chemie International Edition*, 53(7):1845–1848, February 2014. ISSN 1433-7851, 1521-3773. doi: 10.1002/anie.201307418. URL https://onlinelibrary.wiley.com/doi/10.1002/anie.201307418.

[141] H. Allawi. Thermodynamics of internal C.T mismatches in DNA. *Nucleic Acids*

Research, 26(11):2694–2701, June 1998. ISSN 13624962. doi: 10.1093/nar/26.11.2694. URL https://academic.oup.com/nar/article-lookup/doi/10.1093/nar/26.11.2694.

[142] Zilan Yuan, Xinmiao Liu, Sha Deng, Guiping He, Jiaqi Zhang, Qiang He, Yuanlong Chi, Xiue Jiang, Xuhan Xia, and Ruijie Deng. Single-Cell Genotyping of Single-Nucleotide Mutations Using *In Situ* Allele-Specific Loop-Mediated Isothermal Amplification. *ACS Sensors*, 8(11):4315–4322, November 2023. ISSN 2379-3694, 2379-3694. doi: 10.1021/acssensors.3c01679. URL https://pubs.acs.org/doi/10.1021/acssensors.3c01679.

[143] Andreas Untergasser, Ioana Cutcutache, Triinu Koressaar, Jian Ye, Brant C. Faircloth, Maido Remm, and Steven G. Rozen. Primer3—new capabilities and interfaces. *Nucleic Acids Research*, 40(15):e115–e115, August 2012. ISSN 1362-4962, 0305-1048. doi: 10.1093/nar/gks596. URL https://academic.oup.com/nar/article-lookup/doi/10.1093/nar/gks596.

[144] Guojun Cao, Jilie Kong, Zhifang Xing, Yigui Tang, Xinju Zhang, Xiao Xu, Zhihua Kang, Xueen Fang, and Ming Guan. Rapid detection of CALR type 1 and type 2 mutations using PNA-LNA clamping loop-mediated isothermal amplification on a CD-like microfluidic chip. *Analytica Chimica Acta*, 1024:123–135, September 2018. ISSN 00032670. doi: 10.1016/j.aca.2018.04.022.

[145] Pasquale Luca Curci and Gabriella Sonnante. How a Small Double-Stranded Trick Can Mislead Sanger Sequencing. *Journal of Biomolecular Techniques : JBT*, 26(3):80–82, September 2015. ISSN 1524-0215, 1943-4731. doi: 10.7171/jbt.15-2603-004. URL https://www.ncbi.nlm.nih.gov/pmc/articles/PMC4502656/.

[146] Beate M. Crossley, Jianfa Bai, Amy Glaser, Roger Maes, Elizabeth Porter, Mary Lea Killian, Travis Clement, and Kathy Toohey-Kurth. Guidelines for Sanger sequencing and molecular assay monitoring. *Journal of Veterinary Diagnostic Investigation*, 32(6):767–775, November 2020. ISSN 1040-6387, 1943-4936. doi: 10.1177/1040638720905833.

[147] Mohammed Baqur S. Al-Shuhaib and Hayder O. Hashim. Mastering DNA chromatogram analysis in Sanger sequencing for reliable clinical analysis. *Journal of Genetic Engineering and Biotechnology*, 21(1):115, December 2023. ISSN 1687157X. doi: 10.1186/s43141-023-00587-6.

[148] Jian Huang and Lan Zhao. A high-throughput strategy for COVID-19 testing based on next-generation sequencing, June 2020.

[149] Kerstin U. Ludwig, Ricarda M. Schmithausen, David Li, Max L. Jacobs, Ronja Hollstein, Katja Blumenstock, Jana Liebing, Mikołaj Słabicki, Amir Ben-Shmuel, Ofir

Israeli, Shay Weiss, Thomas S. Ebert, Nir Paran, Wibke Rüdiger, Gero Wilbring, David Feldman, Bärbel Lippke, Nina Ishorst, Lara M. Hochfeld, Eva C. Beins, Ines H. Kaltheuner, Maximilian Schmitz, Aliona Wöhler, Manuel Döhla, Esther Sib, Marius Jentzsch, Eva-Maria C. Moench, Jacob D. Borrajo, Jonathan Strecker, Julia Reinhardt, Brian Cleary, Matthias Geyer, Michael Hölzel, Rhiannon Macrae, Markus M. Nöthen, Per Hoffmann, Martin Exner, Aviv Regev, Feng Zhang, and Jonathan L. Schmid-Burgk. LAMP-Seq enables sensitive, multiplexed COVID-19 diagnostics using molecular barcoding. *Nature Biotechnology*, 39(12):1556–1562, December 2021. ISSN 1087-0156, 1546-1696. doi: 10.1038/s41587-021-00966-9.

[150] Xin Huang, Gongyu Tang, Nahed Ismail, and Xiaowei Wang. Developing RT-LAMP assays for rapid diagnosis of SARS-CoV-2 in saliva. *eBioMedicine*, 75:103736, January 2022. ISSN 23523964. doi: 10.1016/j.ebiom.2021.103736.

[151] Phiaw Chong Foo, Yean Yean Chan, Maizan Mohamed, Weng Kin Wong, A.B. Nurul Najian, and Boon Huat Lim. Development of a thermostabilised triplex LAMP assay with dry-reagent four target lateral flow dipstick for detection of Entamoeba histolytica and non-pathogenic Entamoeba spp. *Analytica Chimica Acta*, 966:71–80, May 2017. ISSN 00032670. doi: 10.1016/j.aca.2017.02.019.

[152] Kenny Malpartida-Cardenas, Luca Miglietta, Tianyi Peng, Ahmad Moniri, Alison Holmes, Pantelis Georgiou, and Jesus Rodriguez-Manzano. Single-channel digital LAMP multiplexing using amplification curve analysis. *Sensors & Diagnostics*, 1(3):465–468, 2022. ISSN 2635-0998. doi: 10.1039/D2SD00038E. URL https://pubs.rsc.org/sd/article/1/3/465-468/787439.

[153] Yi Hong, Biao Ma, Jiali Li, Jiangbing Shuai, Xiaofeng Zhang, Hanyue Xu, and Mingzhou Zhang. Triplex-Loop-Mediated Isothermal Amplification Combined with a Lateral Flow Immunoassay for the Simultaneous Detection of Three Pathogens of Porcine Viral Diarrhea Syndrome in Swine. *Animals*, 13(12):1910, June 2023. ISSN 2076-2615. doi: 10.3390/ani13121910.

[154] Lisa Becherer, Nadine Borst, Mohammed Bakheit, Sieghard Frischmann, Roland Zengerle, and Felix Von Stetten. Loop-mediated isothermal amplification (LAMP) – review and classification of methods for sequence-specific detection. *Analytical Methods*, 12(6):717–746, 2020. ISSN 1759-9660, 1759-9679. doi: 10.1039/C9AY02246E.

[155] Rui Mao, Tianzuo Wang, Yue Zhao, Xinyao Wu, Shun Zhang, and Ting Cai. Closed dumbbell mediated isothermal amplification of nucleic acids for DNA diagnostic assays. *Talanta*, 240:123217, April 2022. ISSN 00399140. doi: 10.1016/j.talanta.2022.123217.

[156] Poramin Boonbanjong, Kiatnida Treerattrakoon, Wassa Waiwinya, Piyawat Pitikultham, and Deanpen Japrung. Isothermal Amplification Technology for Disease Diagnosis. *Biosensors*, 12(9):677, August 2022. ISSN 2079-6374. doi: 10.3390/bios12090677.

[157] Cheulhee Jung and Andrew D. Ellington. A primerless molecular diagnostic: Phosphorothioated-terminal hairpin formation and self-priming extension (PS-THSP). *Analytical and Bioanalytical Chemistry*, 408(30):8583–8591, December 2016. ISSN 1618-2642, 1618-2650. doi: 10.1007/s00216-016-9479-y.

[158] Dayong Li, Yanheng Yao, Wenting Cheng, Zhiqiang Hou, Zhongyun Wang, and Yang Xiang. Self-Priming Cyclic Amplification Accelerating CRISPR Sensor for Sensitive and Specific MicroRNA Analysis with No Background. *Analytical Chemistry*, 96(4): 1717–1724, January 2024. ISSN 0003-2700, 1520-6882. doi: 10.1021/acs.analchem.3c04866.

[159] Siyuan S. Wang, Erhu Xiong, Sanchita Bhadra, and Andrew D. Ellington. Developing predictive hybridization models for phosphorothioate oligonucleotides using high-resolution melting. *PLOS ONE*, 17(5):e0268575, May 2022. ISSN 1932-6203. doi: 10.1371/journal.pone.0268575.

[160] Hecheng Wang, Jiatong Liu, Yanyan Fang, Xudan Shen, Hui Liu, Lushan Yu, Su Zeng, Sheng Cai, Jingjing Zhou, and Zheyong Li. Design and analysis of self-priming extension DNA hairpin probe for miRNA detection based on a unified dynamic programming framework. *Analytica Chimica Acta*, 1303:342530, May 2024. ISSN 00032670. doi: 10.1016/j.aca.2024.342530.

[161] Nan Yang, Han Zhang, Xiu Han, Zhifeng Liu, and Yan Lu. Advancements and applications of loop-mediated isothermal amplification technology: A comprehensive overview. *Frontiers in Microbiology*, 15:1406632, July 2024. ISSN 1664-302X. doi: 10.3389/fmicb.2024.1406632.

[162] Nathan A. Tanner and Thomas C. Evans. Loop-Mediated Isothermal Amplification for Detection of Nucleic Acids. *Current Protocols in Molecular Biology*, 105(1), January 2014. ISSN 1934-3639, 1934-3647. doi: 10.1002/0471142727.mb1514s105.

[163] Liang Zhang, Mengfan Zhang, Xingxing Liu, Jia Wei, Caihong Yin, Nan Wang, Beibei Fan, Yanli Fu, Yanwen Liu, Liangyun Bu, Zhenyue Su, Bo Pang, Jinhua Li, and Xiuling Song. Portable DNA extraction integrated with LAMP-CRISPR/Cas12a technology for on-site detection of Salmonella Typhimurium. *npj Science of Food*, 9(1):39, March 2025. ISSN 2396-8370. doi: 10.1038/s41538-025-00401-2.

[164] Dohwan Lee, Yong Shin, Seok Chung, Kyo Seon Hwang, Dae Sung Yoon, and Jeong Hoon Lee. Simple and Highly Sensitive Molecular Diagnosis of Zika Virus by Lateral Flow Assays. *Analytical Chemistry*, 88(24):12272–12278, December 2016. ISSN 0003-2700, 1520-6882. doi: 10.1021/acs.analchem.6b03460.

[165] W. Henke, K. Herdel, K. Jung, D. Schnorr, and S. A. Loening. Betaine Improves the PCR Amplification of GC-Rich DNA Sequences. *Nucleic Acids Research*, 25(19): 3957–3958, October 1997. ISSN 0305-1048, 1362-4962. doi: 10.1093/nar/25.19.3957.

[166] Cuiping Ma, Yifan Wang, Pansong Zhang, and Chao Shi. Accelerated isothermal nucleic acid amplification in betaine-free reaction. *Analytical Biochemistry*, 530:1–4, August 2017. ISSN 00032697. doi: 10.1016/j.ab.2017.04.017.

[167] Heyjin Son, Jaeil Park, Injoo Hwang, Youngri Jung, Sangsu Bae, and Sanghwa Lee. Mg^{2+} -dependent conformational rearrangements of CRISPR-Cas12a R-loop complex are mandatory for complete double-stranded DNA cleavage. *Proceedings of the National Academy of Sciences*, 118(49):e2113747118, December 2021. ISSN 0027-8424, 1091-6490. doi: 10.1073/pnas.2113747118.

[168] Hao Bai, Yuqing Liu, Linbo Gao, Tao Wang, Xiaoli Zhang, Jie Hu, Lisha Ding, Yueting Zhang, Qian Wang, Lei Wang, Jianlong Li, Zhifeng Zhang, Yang Wang, Chenlan Shen, Binwu Ying, Xiaoyu Niu, and Wenchuang Hu. A portable all-in-one microfluidic device with real-time colorimetric LAMP for HPV16 and HPV18 DNA point-of-care testing. *Biosensors and Bioelectronics*, 248:115968, March 2024. ISSN 09565663. doi: 10.1016/j.bios.2023.115968.

[169] Kathryn A. Kundrod, Maria Barra, Alexis Wilkinson, Chelsey A. Smith, Mary E. Natoli, Megan M. Chang, Jackson B. Coole, Akshaya Santhanaraj, Cesaltina Lorenzoni, Celda Mavume, Hira Atif, Jane Richards Montealegre, Michael E. Scheurer, Philip E. Castle, Kathleen M. Schmeler, and Rebecca R. Richards-Kortum. An integrated isothermal nucleic acid amplification test to detect HPV16 and HPV18 DNA in resource-limited settings. *Science Translational Medicine*, 15(701):eabn4768, June 2023. ISSN 1946-6234, 1946-6242. doi: 10.1126/scitranslmed.abn4768.

[170] Hao Liu, Meng-Mei Lv, Xiang Li, Mei Su, Yin-Gang Nie, and Zhan-Ming Ying. Ligation-recognition triggered RPA-Cas12a cis-cleavage fluorogenic RNA aptamer for one-pot and label-free detection of MicroRNA in breast cancer. *Biosensors and Bioelectronics*, 272:117106, March 2025. ISSN 0956-5663. doi: 10.1016/j.bios.2024.117106.

[171] Samuel W. Schaffter, Eli Kengmana, Joshua Fern, Shane R. Byrne, and Rebecca Schulman. Strategies to Reduce Promoter-Independent Transcription of DNA Nanos-

tructures and Strand Displacement Complexes. *ACS Synthetic Biology*, 13(7):1964–1977, July 2024. ISSN 2161-5063, 2161-5063. doi: 10.1021/acssynbio.3c00726.

[172] Goeun Lee, Junhyung Ryu, Jinmin Jang, Wooseong Noh, and Dong-Eun Kim. Template nicking suppresses promoter-independent antisense transcription in IVT via R-loop-mediated strand displacement. *Nucleic Acids Research*, 54(2):gkaf1536, January 2026. ISSN 0305-1048, 1362-4962. doi: 10.1093/nar/gkaf1536.

[173] Yueyi Li, Tyler Lucci, Matias Villarruel Dujovne, Jaeyoung Kirsten Jung, Daiana A. Capdevila, and Julius B. Lucks. A cell-free biosensor signal amplification circuit with polymerase strand recycling. *Nature Chemical Biology*, 21(6):949–958, June 2025. ISSN 1552-4450, 1552-4469. doi: 10.1038/s41589-024-01816-w.

[174] Cameron P. Bracken, Hamish S. Scott, and Gregory J. Goodall. A network-biology perspective of microRNA function and dysfunction in cancer. *Nature Reviews Genetics*, 17(12):719–732, December 2016. ISSN 1471-0056, 1471-0064. doi: 10.1038/nrg.2016.134.

[175] Victor Ambros. The functions of animal microRNAs. *Nature*, 431(7006):350–355, September 2004. ISSN 0028-0836, 1476-4687. doi: 10.1038/nature02871.

[176] Lin He and Gregory J. Hannon. MicroRNAs: Small RNAs with a big role in gene regulation. *Nature Reviews Genetics*, 5(7):522–531, July 2004. ISSN 1471-0056, 1471-0064. doi: 10.1038/nrg1379.

[177] Ae Erson and Em Petty. MicroRNAs in development and disease. *Clinical Genetics*, 74(4):296–306, October 2008. ISSN 0009-9163, 1399-0004. doi: 10.1111/j.1399-0004.2008.01076.x.

[178] Songcheng Yu, Xueying Lei, and Chenling Qu. MicroRNA Sensors Based on CRISPR/Cas12a Technologies: Evolution From Indirect to Direct Detection. *Critical Reviews in Analytical Chemistry*, 55(5):968–984, July 2025. ISSN 1040-8347, 1547-6510. doi: 10.1080/10408347.2024.2329229.

[179] Xin-Yuan Qiu, Lv-Yun Zhu, Chu-Shu Zhu, Jia-Xin Ma, Tao Hou, Xiao-Min Wu, Si-Si Xie, Lu Min, De-An Tan, Dong-Yi Zhang, and Lingyun Zhu. Highly Effective and Low-Cost MicroRNA Detection with CRISPR-Cas9. *ACS Synthetic Biology*, 7 (3):807–813, March 2018. ISSN 2161-5063, 2161-5063. doi: 10.1021/acssynbio.7b00446.

[180] Ting Zhou, Ru Huang, Mengqi Huang, Jinjin Shen, Yuanyue Shan, and Da Xing. CRISPR/Cas13a Powered Portable Electrochemiluminescence Chip for Ultrasensitive and Specific MiRNA Detection. *Advanced Science*, 7(13):1903661, July 2020. ISSN 2198-3844, 2198-3844. doi: 10.1002/advs.201903661.

[181] Shuang Peng, Zhen Tan, Siyu Chen, Chunyang Lei, and Zhou Nie. Integrating CRISPR-Cas12a with a DNA circuit as a generic sensing platform for amplified detection of microRNA. *Chemical Science*, 11(28):7362–7368, 2020. ISSN 2041-6520, 2041-6539. doi: 10.1039/D0SC03084H.

[182] Emily Greenwald. Dragonrna: Code used for analysis of dragonrna paper. https://github.com/emilygreenwald/DragonRNA, 2025. GitHub repository, accessed 16 September 2026.

[183] Fire Lab. Firelabsoftware. https://github.com/FireLabSoftware. GitHub repository, Stanford University School of Medicine. Accessed 16 September 2026.

[184] Xinyi Xia, Zhigang Liang, Guanhong Xu, Fangdi Wei, Jing Yang, Xiaolei Zhu, Chenglin Zhou, Jun Ye, Qin Hu, Zheng Zhao, Ben Zhong Tang, and Yao Cen. Split crRNA Precisely Assisted Cas12a Expansion Strategy for Simultaneous, Discriminative, and Low-Threshold Determination of Two miRNAs Associated with Multiple Sclerosis. *Analytical Chemistry*, 97(5):2873–2882, February 2025. ISSN 0003-2700, 1520-6882. doi: 10.1021/acs.analchem.4c05388.

[185] Injoo Hwang, Yo Han Song, and Sanghwa Lee. Enhanced trans-cleavage activity using CRISPR-Cas12a variant designed to reduce steric inhibition by cis-cleavage products. *Biosensors and Bioelectronics*, 267:116859, January 2025. ISSN 09565663. doi: 10.1016/j.bios.2024.116859.

[186] XuRan Fu, JiaDi Sun, Bingqian Yu, Yongli Ye, Lina Sheng, Jian Ji, Jiayu Zheng, Minghong Fan, Jingdong Shao, and XiuLan Sun. Investigating enzyme kinetics and fluorescence sensing strategy of CRISPR/Cas12a for foodborne pathogenic bacteria. *Analytica Chimica Acta*, 1290:342203, February 2024. ISSN 00032670. doi: 10.1016/j.aca.2024.342203.

[187] Jinlong Ai, Jinhai Deng, Jingjing Hu, Xingxiang Pu, Tongyan Yuan, Yuling Teng, Han Li, Bojie Chen, Jinlian Du, Ling Jiang, Xiaoyan Chen, Erhu Xiong, and Ronghua Yang. PAM-Independent CRISPR-Cas12a System for Specific Assays of Single Nucleotide Variants. *JACS Au*, 5(3):1392–1401, March 2025. ISSN 2691-3704, 2691-3704. doi: 10.1021/jacsau.5c00011.

[188] Feng Xuan and I-Ming Hsing. Triggering Hairpin-Free Chain-Branching Growth of Fluorescent DNA Dendrimers for Nonlinear Hybridization Chain Reaction. *J. Am. Chem. Soc.*, page 4, 2014.

[189] Noor Mohammad, Shrinivas S. Katkam, and Qingshan Wei. A Sensitive and Nonoptical CRISPR Detection Mechanism by Sizing Double□Stranded λ DNA Reporter. *Angewandte Chemie International Edition*, 61(50):e202213920, December

2022. ISSN 1433-7851, 1521-3773. doi: 10.1002/anie.202213920. URL https://onlinelibrary.wiley.com/doi/10.1002/anie.202213920.

[190] Yichuan Chen, Xinping Wang, Junqi Zhang, Qingyuan Jiang, Bin Qiao, Baoxia He, Wenhao Yin, Jie Qiao, and Yi Liu. Split crRNA with CRISPR-Cas12a enabling highly sensitive and multiplexed detection of RNA and DNA. *Nature Communications*, 15 (1):8342, September 2024. ISSN 2041-1723. doi: 10.1038/s41467-024-52691-x.

[191] Diego A. Huyke, Ashwin Ramachandran, Vladimir I. Bashkirov, Efthalia K. Kotseroglou, Theofilos Kotseroglou, and Juan G. Santiago. Enzyme Kinetics and Detector Sensitivity Determine Limits of Detection of Amplification-Free CRISPR-Cas12 and CRISPR-Cas13 Diagnostics. *Analytical Chemistry*, 94(27):9826–9834, July 2022. ISSN 0003-2700. doi: 10.1021/acs.analchem.2c01670.

[192] Daan C. Swarts and Martin Jinek. Mechanistic Insights into the cis- and trans-Acting DNase Activities of Cas12a. *Molecular Cell*, 73(3):589–600.e4, February 2019. ISSN 10972765. doi: 10.1016/j.molcel.2018.11.021.

[193] Sruthi Sudhakar, Christopher L. Barkau, Ramadevi Chilamkurthy, Halle M. Barber, Adrian A. Pater, Sean D. Moran, Masad J. Damha, P.I. Pradeepkumar, and Keith T. Gagnon. Binding to the conserved and stably folded guide RNA pseudoknot induces Cas12a conformational changes during ribonucleoprotein assembly. *Journal of Biological Chemistry*, 299(5):104700, May 2023. ISSN 00219258. doi: 10.1016/j.jbc.2023.104700. URL https://linkinghub.elsevier.com/retrieve/pii/S0021925823003423.

[194] Eman A. Ageely, Ramadevi Chilamkurthy, Sunit Jana, Leonora Abdullahu, Daniel O'Reilly, Philip J. Jensik, Masad J. Damha, and Keith T. Gagnon. Gene editing with CRISPR-Cas12a guides possessing ribose-modified pseudoknot handles. *Nature Communications*, 12(1):6591, November 2021. ISSN 2041-1723. doi: 10.1038/s41467-021-26989-z. URL https://www.nature.com/articles/s41467-021-26989-z.

[195] M. Lane. The thermodynamic advantage of DNA oligonucleotide 'stacking hybridization' reactions: energetics of a DNA nick. *Nucleic Acids Research*, 25(3): 611–617, February 1997. ISSN 13624962. doi: 10.1093/nar/25.3.611. URL https://academic.oup.com/nar/article-lookup/doi/10.1093/nar/25.3.611.

[196] Nicholas J Panaro, Po K I Yuen, Taku Sakazume, Paolo Fortina, Larry J Kricka, and Peter Wilding. Evaluation of DNA Fragment Sizing and Quantification by the Agilent 2100 Bioanalyzer. *Clinical Chemistry*, 46(11):1851–1853, November 2000. ISSN 0009-9147, 1530-8561. doi: 10.1093/clinchem/46.11.1851. URL https://academic.oup.com/clinchem/article/46/11/1851/5641424.

[197] Bruce I. Sodowich, Irini Fadl, and Craig Burns. Method validation of ***in vitro*** RNA transcript analysis on the Agilent 2100 Bioanalyzer. *ELECTROPHORESIS*, 28(14):2368–2378, July 2007. ISSN 0173-0835, 1522-2683. doi: 10.1002/elps.200600673. URL https://analyticalsciencejournals.onlinelibrary.wiley.com/doi/10.1002/elps.200600673.

[198] Andrea Masotti and Tobias Preckel. Analysis of small RNAs with the Agilent 2100 Bioanalyzer. *Nature Methods*, 3(8):658–658, August 2006. ISSN 1548-7091, 1548-7105. doi: 10.1038/nmeth908. URL https://www.nature.com/articles/nmeth908.

[199] Long T. Nguyen, Brianna M. Smith, and Piyush K. Jain. Enhancement of trans-cleavage activity of Cas12a with engineered crRNA enables amplified nucleic acid detection. *Nature Communications*, 11(1):4906, September 2020. ISSN 2041-1723. doi: 10.1038/s41467-020-18615-1. URL https://www.nature.com/articles/s41467-020-18615-1.

[200] Wei Zhang, Ziwen Zhou, Xiaohuan Feng, Tingting Feng, Xiaojing Liu, Qiang Lin, Weiwen Fan, and Chaoxing Liu. crRNA Truncation Minimizes *cis* -Cleavage for Universal One-Pot RPA-CRISPR-Cas12a Detection with Attomolar Sensitivity. *JACS Au*, 6(4):2591–2602, April 2026. ISSN 2691-3704, 2691-3704. doi: 10.1021/jacsau.6c00235. URL https://pubs.acs.org/doi/10.1021/jacsau.6c00235.

[201] Xinrui Fei, Chao Lei, Wei Ren, and Chenghui Liu. 'Splice-at-will' Cas12a crRNA engineering enabled direct quantification of ultrashort RNAs. *Nucleic Acids Research*, 53 (2):gkaf002, January 2025. ISSN 0305-1048, 1362-4962. doi: 10.1093/nar/gkaf002.

[202] Frank X. Liu, Johnson Q. Cui, Zhihao Wu, and Shuhuai Yao. Recent progress in nucleic acid detection with CRISPR. *Lab on a Chip*, 23(6):1467–1492, 2023. ISSN 1473-0197, 1473-0189. doi: 10.1039/D2LC00928E. URL http://xlink.rsc.org/?DOI=D2LC00928E.

[203] Ijaz Gul, Muhammad Akmal Raheem, Md. Reyad-ul Ferdous, Xi Yuan, Zhenglin Chen, Chenying Lv, Minjiang Chen, Jiansong Ji, Duanpo Wu, Qiang Zhao, Chenggang Yan, and Dongmei Yu. State-of-the-art signal amplification strategies for nucleic acid and non-nucleic acid biosensors. *Sensors and Actuators Reports*, 9:100268, June 2025. ISSN 26660539. doi: 10.1016/j.snr.2024.100268. URL https://linkinghub.elsevier.com/retrieve/pii/S2666053924000845.

[204] Yalin Chen, Yicheng Chen, Cuijuan Zhang, Yongsheng Cai, Zhuoer Zeng, Julien Reboud, Jonathan M. Cooper, Hongbo Shan, Yang Wang, and Gaolian Xu. One-pot CRISPR-based point of care platform for rapid, specific and sensitive detection of HPV 16 without pre-amplification. *Microsystems & Nanoengineering*, 12

(1):81, March 2026. ISSN 2055-7434. doi: 10.1038/s41378-025-01130-y. URL https://www.nature.com/articles/s41378-025-01130-y.

Appendix A. Python scripts for RNA sequencing analysis

A.1 Identification and ranking of the top 10 RNA products

```
input_file = "Old_Rv_R1_001.fastq"

F = open(input_file, mode="rt").read().splitlines()
Sequences1 = F[1::4]

print("Total reads:", len(Sequences1))
print("First read:", Sequences1[0])
print("First read length:", len(Sequences1[0]))

from collections import Counter

StartDNA1 = "CATTGCGCACACCTTGAAGTTAATCTACACTTAGTAGAAATTACCTCCCCATGTCTGAGGTACTCCTTAAA
    "

def complement(s):
    return (
        s.upper()
        .replace("A", "t")
        .replace("T", "a")
        .replace("G", "c")
        .replace("C", "g")
        .upper()
    )

StartDNAComplement1 = complement(StartDNA1)[::-1]

print("Template length:", len(StartDNA1))
print("Template:")
print(StartDNA1)

print("\nReverse complement:")
```

```
print(StartDNAComplement1)

klen1 = 10
tlen1 = len(StartDNAComplement1)

WordsInStartDNA1 = Counter(
    [StartDNA1[i:i+klen1] for i in range(tlen1-klen1+1)]
)

WordsInStartComplement1 = Counter(
    [StartDNAComplement1[i:i+klen1] for i in range(tlen1-klen1+1)]
)

DNAWords1 = WordsInStartDNA1 + WordsInStartComplement1

print("Template 10-mers:", len(WordsInStartDNA1))
print("Reverse-complement 10-mers:", len(WordsInStartComplement1))
print("Combined unique 10-mers:", len(DNAWords1))

rawCounter1 = Counter(Sequences1)
filteredCounter1 = Counter()

for seq1 in rawCounter1:
    OM1 = False

    for i1 in range(len(seq1) - klen1 + 1):
        w1 = seq1[i1:i1+klen1]

        if w1 in DNAWords1:
            OM1 = True
            break

    if OM1:
        filteredCounter1[seq1] = rawCounter1[seq1]

print("Total reads:", len(Sequences1))
print("Unique read sequences:", len(rawCounter1))
print("Unique sequences passing template filter:", len(filteredCounter1))
print("Total reads represented after filtering:", sum(filteredCounter1.values()))

for i1, (s1, c1) in enumerate(filteredCounter1.most_common(10), start=1):
    print(f">Old_Rv_MostCommon_{i1}_Counts:{c1}")
    print(s1)
    print("Length:", len(s1))
    print()

    total_reads = len(Sequences1)
```

```
filtered_reads = sum(filteredCounter1.values())

print(
    f"{'Rank':<6}"
    f"{'Count':<10}"
    f"{'% total':<12}"
    f"{'% filtered':<14}"
    f"{'Length':<8}"
    f"Sequence"
)

print("-" * 120)

for rank, (seq, count) in enumerate(filteredCounter1.most_common(10), start=1):

    pct_total = count / total_reads * 100
    pct_filtered = count / filtered_reads * 100

    print(
        f"{rank:<6}"
        f"{count:<10}"
        f"{pct_total:<12.3f}"
        f"{pct_filtered:<14.3f}"
        f"{len(seq):<8}"
        f"{seq}"
    )
```

A.2 Classification of RNA products

```
import numpy as np
import matplotlib.pyplot as plt

# Categories
categories = [
    "Complete crRNA\n-(143)",
    "Complete spacer\n-(122)",
    "Complete handle\n-(2343)",

]

# Percentages calculated from the trimmed FASTQ reads
oldrv_values = [
    oldrv_results["Complete crRNA"],
    oldrv_results["Complete spacer"],
    oldrv_results["Complete handle"],
```

```
17
18 ]
19
20 cr21_2_values = [
21     cr21_2_results["Complete crRNA"],
22     cr21_2_results["Complete spacer"],
23     cr21_2_results["Complete handle"],
24
25 ]
26
27 cg3bp_values = [
28     cg3bp_results["Complete crRNA"],
29     cg3bp_results["Complete spacer"],
30     cg3bp_results["Complete handle"],
31 ]
32
33 # X-axis positions
34 x = np.arange(len(categories))
35 width = 0.25
36
37 # Create figure
38 fig, ax = plt.subplots(figsize=(12, 6))
39
40 bars1 = ax.bar(x - width, oldrv_values, width, label="Old_Rv", color="#4C78A8")
41 bars2 = ax.bar(x, cr21_2_values, width, label="cr21-2", color="#F2A541")
42 bars3 = ax.bar(x + width, cg3bp_values, width, label="cr21-CG-3bp", color="#B0B0B0")
43
44
45 # Axis labels and title
46 ax.set_ylabel("Percentage of total trimmed reads (%)")
47 ax.set_title("Prevalence of crRNA-related regions in RNA products")
48
49 ax.set_xticks(x)
50 ax.set_xticklabels(categories)
51
52 ax.set_ylim(0, 70)
53
54 ax.legend()
55
56 # Add percentage labels above each bar
57 for bars in [bars1, bars2, bars3]:
58     for bar in bars:
59         height = bar.get_height()
60         ax.text(
61             bar.get_x() + bar.get_width() / 2,
62             height + 1,
63             f"{height:.2f}%",
```

```
            ha="center",
            va="bottom",
            fontsize=8
        )

plt.tight_layout()
plt.savefig(
    "crRNA_region_comparison.png",
    dpi=300,
    bbox_inches="tight"
)
plt.show()

# ============================================================
# Classify intact-handle reads by retained spacer length
# ============================================================

from collections import defaultdict


def classify_handle_spacer_retention(
    template,
    raw_counter,
    total_reads
):
    # Define spacer and handle
    spacer = template[0:22]
    handle = template[22:43]

    # Store counts for exact retained spacer lengths: -022 nt
    retained_counts = defaultdict(int)

    for seq, count in raw_counter.items():

        # Find the maximum number of contiguous spacer nucleotides
        # retained immediately adjacent to the complete handle
        max_retained = None

        # Test from 22 nt down to 0 nt
        # The first match is therefore the longest retained spacer
        for k in range(22, -1, -1):

            if k == 0:
                motif = handle
            else:
                motif = spacer[-k:] + handle

```

```
            motif_rc = reverse_complement(motif)

            # Check both sequencing orientations
            if motif in seq or motif_rc in seq:
                max_retained = k
                break

        if max_retained is not None:
            retained_counts[max_retained] += count

    # Convert exact retained lengths into broader groups
    grouped_counts = {
        "0 nt": retained_counts[0],
        "-15 nt": sum(retained_counts[k] for k in range(1, 6)),
        "-610 nt": sum(retained_counts[k] for k in range(6, 11)),
        "-1115 nt": sum(retained_counts[k] for k in range(11, 16)),
        "-1621 nt": sum(retained_counts[k] for k in range(16, 22)),
        "22 nt\n(complete crRNA)": retained_counts[22]
    }

    grouped_percentages = {
        key: value / total_reads * 100
        for key, value in grouped_counts.items()
    }

    return retained_counts, grouped_counts, grouped_percentages

    # Old_Rv
oldrv_retained_exact, oldrv_retained_grouped, oldrv_retained_pct = (
    classify_handle_spacer_retention(
        oldrv_StartDNA,
        oldrv_rawCounter,
        oldrv_total_reads
    )
)

# cr21-2
cr21_2_retained_exact, cr21_2_retained_grouped, cr21_2_retained_pct = (
    classify_handle_spacer_retention(
        cr21_2_StartDNA,
        cr21_2_rawCounter,
        cr21_2_total_reads
    )
)

# cr21-CG-3bp
cg3bp_retained_exact, cg3bp_retained_grouped, cg3bp_retained_pct = (
```

```
    classify_handle_spacer_retention(
        cg3bp_StartDNA,
        cg3bp_rawCounter,
        cg3bp_total_reads
    )
)

def print_retention_results(sample_name, results):

    print(f"\n{sample_name}")

    for category, value in results.items():
        print(f"{category}: {value:.2f}%")


print_retention_results(
    "Old_Rv",
    oldrv_retained_pct
)

print_retention_results(
    "cr21-2",
    cr21_2_retained_pct
)

print_retention_results(
    "cr21-CG-3bp",
    cg3bp_retained_pct
)
```

A.3 AgniAlign visualisation

```
# ============================================================
# 1. Template and P10 sequences
# ============================================================
cg3bp_template = (
    "CATTGCGCACACCTTGAAGTTAATCTACACTTAGTAGAAATTACCGTAGCTTATCAGACTCGG"
)

cg3bp_p10 = (
    "GGTGTGCGCAATGCCGAGTCTGATAAGCTACGGTAATTTCTACTAAGTGTAGATTAACTTCAAGGTGTGCGCAATG"
)

print("Template length:", len(cg3bp_template))
print("P10 length:", len(cg3bp_p10))
```

```
14
15 # ============================================================
16 # 2. Create FASTA files
17 # ============================================================
18
19 with open("cr21_CG_3bp_template.fa", "w") as f:
20     f.write(">cr21_CG_3bp_template\n")
21     f.write(cg3bp_template + "\n")
22
23 with open("cr21_CG_3bp_P10.fa", "w") as f:
24     f.write(">cr21_CG_3bp_P10\n")
25     f.write(cg3bp_p10 + "\n")
26
27 # ============================================================
28 # 3. Download AgniAlign if the folder is missing
29 # ============================================================
30 if not os.path.exists("AgniAlign"):
31     subprocess.run(
32         [
33             "git",
34             "clone",
35             "https://github.com/FireLabSoftware/AgniAlign.git"
36         ],
37         check=True
38     )
39
40
41 # ============================================================
42 # 4. Run AgniAlign
43 # ============================================================
44
45 subprocess.run(
46     [
47         sys.executable,
48         "AgniAlign/AgniAlign_ah01_100123.py",
49         "Template=cr21_CG_3bp_template.fa",
50         "Product=cr21_CG_3bp_P10.fa",
51         "outputfile=cr21_CG_3bp_P10_AgniAlign.svg"
52     ],
53     check=True
54 )
55
56 print("SVG generated successfully.")
57 # ============================================================
58 # 5. Install CairoSVG for SVG-to-PNG conversion
59 # ============================================================
60
```

```
subprocess.run(
    [
        sys.executable,
        "-m",
        "pip",
        "install",
        "-q",
        "cairosvg"
    ],
    check=True
)
# ============================================================
# 6. Convert SVG to high-resolution PNG
# ============================================================

import cairosvg

cairosvg.svg2png(
    url="cr21_CG_3bp_P10_AgniAlign.svg",
    write_to="cr21_CG_3bp_P10_AgniAlign.png",
    scale=3
)

print("PNG generated successfully:")
print("cr21_CG_3bp_P10_AgniAlign.png")
```